Molecular mechanism of regulation of the cellular protein levels of endonuclease III homologue (NTH1) in response to DNA damage

Thesis submitted in accordance with the requirements of the University of Liverpool for the degree of Doctor in Philosophy by Sarah Williams.

Date: 04-May 2018

ACKNOWLEDGEMENTS

To family, friends and my own stubborn determination…

Still I Rise – Maya Angelou

ABSTRACT

Deoxyribonucleic acid (DNA) is the store of genetic material, needed for cellular survival and replication. Cellular DNA is under constant attack from genotoxic agents, arising endogenously or exogenously in relation to the cell. Maintaining the stability of the genome is imperative to ensure accurate inheritance of the genetic code for future progeny and ensures that crucial biological processes are undisturbed. To uphold the integrity of the genome, cells have developed numerous DNA surveillance and repair mechanisms. The base excision repair (BER) pathway is one of the pathways that has evolved to remove minor types of DNA damage. The main sub-pathway of BER involves recognition and removal of the oxidised DNA base lesion, incision of the phosphodiester backbone, followed by insertion of the correct complementary nucleotide, before the nick in the DNA backbone is restored.

During BER, the recognition of damaged bases relies on DNA glycosylase enzymes. Human endonuclease III (NTH1) is a DNA glycosylase enzyme which specifically recognises oxidised base lesions, caused by reactive oxygen species (ROS). Crucially, NTH1 excises thymine glycol (Tg), which is a particularly mutagenic base lesion.

Regulation of enzymes implicated in the BER pathway is important to prevent excessive DNA damage. Reports have demonstrated the importance of post translational modifications (PTMs) in controlling the levels, activity and interactivity of BER proteins. Ubiquitylation is a PTM that has been implicated in the regulation of several BER enzymes. Ubiquitylation is completed by the ubiquitin proteasome pathway (UPP); whereby E3 ligase enzymes attach of moieties of ubiquitin to lysine residues of substrate proteins. The attachment of multiple moieties of ubiquitin (polyubiquitylation) is associated with the regulation of protein levels, whereas, the attachment of singular subunits of ubiquitin (monoubiquitylation) can have variable consequences.

Despite this understanding, evidence of PTMs that target human NTH1 are deficient. A proteomic study demonstrated that NTH1 is subject to ubiquitylation dependent regulation, but the specific UPP enzymes involved were not identified. The overarching aim of this project was to understand the molecular mechanisms employed by human cells to regulate levels of NTH1 via ubiquitylation, with specific emphasis on discovering the E3 ligase enzymes involved.

Using a well refined purification technique, human cell extracts were fractionated using a series of column chromatography columns. Candidate E3 ligase activity was examined using *in vitro* ubiquitylation assays of chromatography fractions, with recombinant NTH1 as the substrate protein. Eventually, mass spectrometry analysis of an isolated ubiquitylated fraction, identified tripartite motif containing 26 (TRIM26) as the only candidate E3 ligase enzyme present in the active fraction. We strengthened this finding by repeating ubiquitylation assays using recombinant TRIM26. Together, these findings identify TRIM26 as the major E3 in human cell extracts that catalyses the ubiquitylation of NTH1. Following this, site directed mutagenesis identified lysine 67 as the major site of TRIM26 dependent ubiquitylation of NTH1.

Aside to this, the cellular implications of TRIM26 dependent regulation of NTH1 were investigated. Elevated levels of cellular NTH1 following proteasome inhibition confirmed that NTH1 levels may be regulated in cells by ubiquitylation dependent degradation. However, depletion of cellular TRIM26 via siRNA had no significant impact on the steady state levels of the glycosylase. Fractionation of cellular extracts confirmed that cellular NTH1 is located primarily in the nucleus and may be associated with chromatin. Depletion of TRIM26 resulted in no alteration in the cellular distribution of the glycosylase.

Since TRIM26 dependent ubiquitylation did not appear to regulate the steady state levels of NTH1, further examination using hydrogen peroxide as a DNA damaging agent showed that DNA damage responsive levels of NTH1 protein expression increased following TRIM26 depletion. The clonogenic assay demonstrated that cells had increased survival capacity in the absence of TRIM26. Importantly, this observation was recapitulated with a partial overexpression of NTH1. Similarly, the alkaline single gel electrophoresis (comet) assay, in combination with an siRNA mediated depletion of TRIM26, concluded that cells with reduced TRIM26 levels have improved ability to manage oxidative stress. Once more, a similar level of improved DNA repair kinetics could be achieved by partially overexpressing NTH1.

Overall, I successfully purified and identified TRIM26 as the major E3 ligase that ubiquitylates NTH1. The major site of TRIM26 dependent ubiquitylation is lysine 67; as substitution of this residue substantially impeded *in vitro* ubiquitylation via TRIM26. Cellular studies confirmed that levels of NTH1 may be regulated by ubiquitylation dependent degradation, although, TRIM26 dependent ubiquitylation was not implicated in the regulation of steady state levels of NTH1. Rather, it appears that

TRIM26 may be implicated in the regulation of DNA damage responsive levels of NTH1. Interestingly, a separate investigation in our laboratory previously identified TRIM26 as one of the major E3 ligase enzymes involved in regulation of the steady state levels of another BER glycosylase, endonuclease VIII-like protein 1 (NEIL1).

Excitingly, the outcomes of this work have now been peer-reviewed and accepted for publication in the Molecular and Cellular Biology scientific journal (see appendix).

In summary, an increasingly dynamic role of TRIM26 is now becoming apparent; whereby, the E3 ligase is involved in the regulation of multiple BER glycosylases with different effects in relation to the DNA damage response. Despite this increased perception, the cellular mechanism which dictates the outcome of ubiquitylation of either glycosylase under the regulation of TRIM26 remains to be fully understood and demands further inspection.

CONTENTS

SUMMARY OF TABLES

SUMMARY OF FIGURES

CHAPTER 1 – INTRODUCTION

1.1. The cellular genome

Cells are described as the smallest functional unit of every organism. Cells consist of a viscous aqueous material encapsulated within a cellular membrane. The majority of organisms exist as single cells, however, other organisms consist of multiple cells that are differentiated and grouped together to achieve specialised functions. The structures of different cell types are often related to their function. It is estimated that the human body is made up of more than 10^{13} cells. Remarkably, every cell within a multicellular organism originates from cellular divisions from one original embryonic cell. To achieve this, every single cell contains the hereditary instructions and materials needed to construct a complete copy of itself during cellular divisions.

The hereditary information of all living cells is stored as strands of deoxyribonucleic acid (DNA). Each DNA molecule is composed of a double helix formed from two complementary antiparallel strands of repeating units of nucleotide monomers called bases (**Figure 1**). There are four types of bases; adenine (A), thymine (T), cytosine (C) and guanine (G) (**Figure 2**). The two strands of DNA are held together by hydrogen bonds between these bases, which exhibit base pairing specificity; G-C and A-T (**Figure 3**). The order in which these bases are arranged dictates the genetic code of the cell. Autonomous cellular divisions are dependent on the duplication of the genetic information encoded by DNA, which relies on one of the DNA strands acting as a template to generate an identical complementary strand.

The genetic information encoded by DNA not only enables cellular replication, but it also contains the instructions needed for the cell to synthesise the fundamental proteins required for survival. The sequence of nucleotides on the DNA strands determines the sequence of the protein; three DNA bases encode one amino acid, which are the monomeric units of proteins. Sections of DNA, termed genes, encode the instructions for the manufacture of one or a few cellular proteins.

Proteins are linear molecules consisting of repeating units of amino acids; of which there are 20, joined together by peptide bonds to create a polypeptide chain. The sequence of the polypeptide chain dictates the final three-dimensional structure of the protein, which ultimately determines protein function. Reactive sites on the surface of proteins enable them to bind with high specificity to other molecules, so that they may act as enzymes to direct biochemical reactions within the cell. In addition, cellular

proteins play vital roles in maintaining structures, enabling movement or sensing signals.

The survival and maintenance of an organism is dependent on the ability of cells to store, replicate and express the genetic code. To survive and perform their designated function, every cell must respond to stimuli. Cellular responses are primarily dependent on the regulation of the levels, activity, localisation or interactions of proteins within the cell. Protein interactions are mostly grouped together to form protein cascades. There is a substantial amount of cross-talk between protein pathways, generating a complex and dynamic cellular protein network. It is estimated that at any given time, a human cell may exhibit 130 000 binary protein interactions (160).

Despite the importance of DNA, the molecule is not exempt from spontaneous changes or attack by reactive molecules generated within the cell. DNA is also subject to damage by thermal disruption, chemical insults or radiation exposure. The survival of a cell is dependent on preventing changes to the nucleotide sequence of DNA. A permanent change or mutation in the sequence of DNA bases of a gene can have detrimental consequences depending on its position on the DNA sequence. Ultimately, a genetic mutation can disrupt the composition of a polypeptide chain that the gene encodes. Changes in the sequence of amino acids generated may influence the tertiary structure of the affected protein, resulting in altered activity, regulation or ability to interact effectively with other cellular components. The impact the genetic mutation has on the cell, largely depends on the role of the mutated protein. Due to the complexity of the proteome, the impact of an abnormal protein may be exaggerated by affecting multiple biochemical cascades.

Cancer is a familiar example of the impact genetic mutations can induce in somatic cells. Mutations in genes encoding proteins involved in cell growth, proliferation or programmed cell death can give cells a selective advantage over the surrounding tissue. This leads to uncontrolled cellular growth and division, resulting in the development of malignant tumours. Cells with cancerous mutations may demonstrate increased invasive potential and ability to spread to other areas of the body via metastasis. Cancer continues to be a major source of human morbidity and mortality worldwide. In 2012 alone, it was estimated that 14.1 million new cases of cancer occurred, with 8.2 million related deaths (155). With this being considered, a substantial amount of scientific research remains focused on improving our understanding of cancer and seeking better treatments. Current non-invasive curative

treatments, such as chemotherapy or radiotherapy, eradicate cancerous cells by inducing detrimental DNA damage to highly proliferative cancer cells. The objective of current treatments highlights the importance of research related to DNA damage and its effects.

1.2. The structure of DNA

In 1953, the structure of DNA was characterised by Watson and Crick (172). The monomeric building blocks of DNA are nucleotides, which consist of a ribose sugar, phosphate group and a nitrogen containing nucleobase (**Figure 1**). There are a total of four DNA nucleobases: A, T, C and G (**Figure 2**). The nucleobases are all cyclical compounds that are characterised according to the number of cyclical rings in their structure. For instance, C and T are pyrimidines with one cyclical ring, whereas, A and G are purines with two cyclical rings (**Figure 2**). The cyclical bases attach to the first carbon atom on the deoxyribose sugar by an *N*-glycosidic bond. A phosphate group attaches to the sugar molecule in place of the –OH group on the 5' atom via a phosphoester bond (**Figure 1**). In basic terms, a DNA strand is simply a string of nucleotides. The nucleotides covalently attach to each other by a phosphodiester bond between the 5'-phosphate group of one nucleotide and the 3'-hydroxyl group on the sugar of the adjacent nucleotide. This gives rise to a sugar-phosphate backbone from which the bases protrude (**Figure 3**). The order in which the nucleotides are arranged dictates the genetic code.

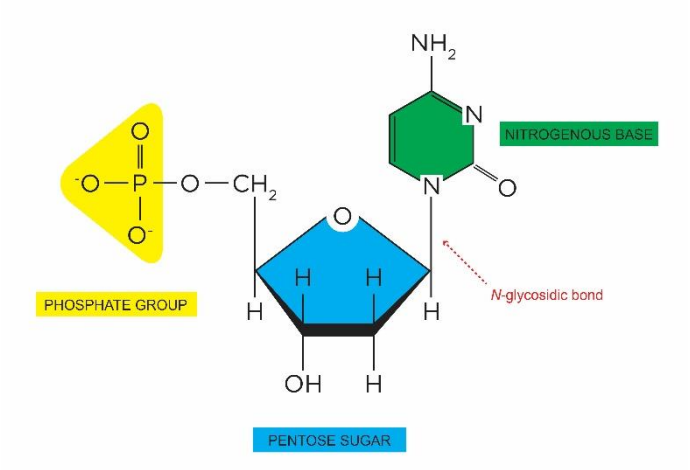

Figure 1. Schematic representing the composition of a nucleotide. Nucleotides are composed of a five-carbon deoxyribose sugar, from which a nitrogenous base (adenine, thymine, cytosine or guanine) is attached to the first carbon via an *N*-glycosidic bond. A phosphate group is attached to the fifth carbon via an ester bond. Repeating units of nucleotides are the building blocks of DNA strands. The order that they are arranged dictates the genetic code.

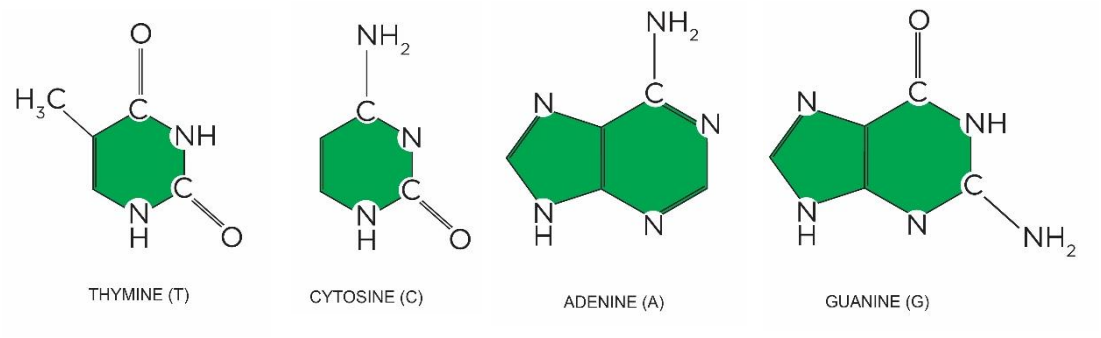

Figure 2. Schematic of the four nitrogenous bases which compose DNA. The pyrimidine bases, cytosine (C) and thymine (T), each have a single six-member ring, whereas, the purine bases, guanine (G) and adenine (A) consist of a five-atom ring attached to a six-atom ring.

DNA molecules are made up of two antiparallel strands of nucleotides that run in opposite directions. The two DNA strands are arranged in an energetically favourable manner, whereby the hydrophilic sugar-phosphate backbones reside on the outside with the hydrophobic bases located within the interior. The two opposite strands of DNA are held together via hydrogen bonds between the nucleobases (**Figure 3**). To maintain consistent distance between the two nucleotide strands and ensure maximum stability, the nucleobases demonstrate base pairing specificity. A two-ring purine base always bonds with a single-ring pyrimidine base. In this way, A binds to T using two hydrogen bonds and C pairs with G by three hydrogen bonds (**Figure 3**). Base pairing specificity aids the fidelity of the DNA molecule and ensures that the nucleotide sequences of partner strands of DNA are complementary.

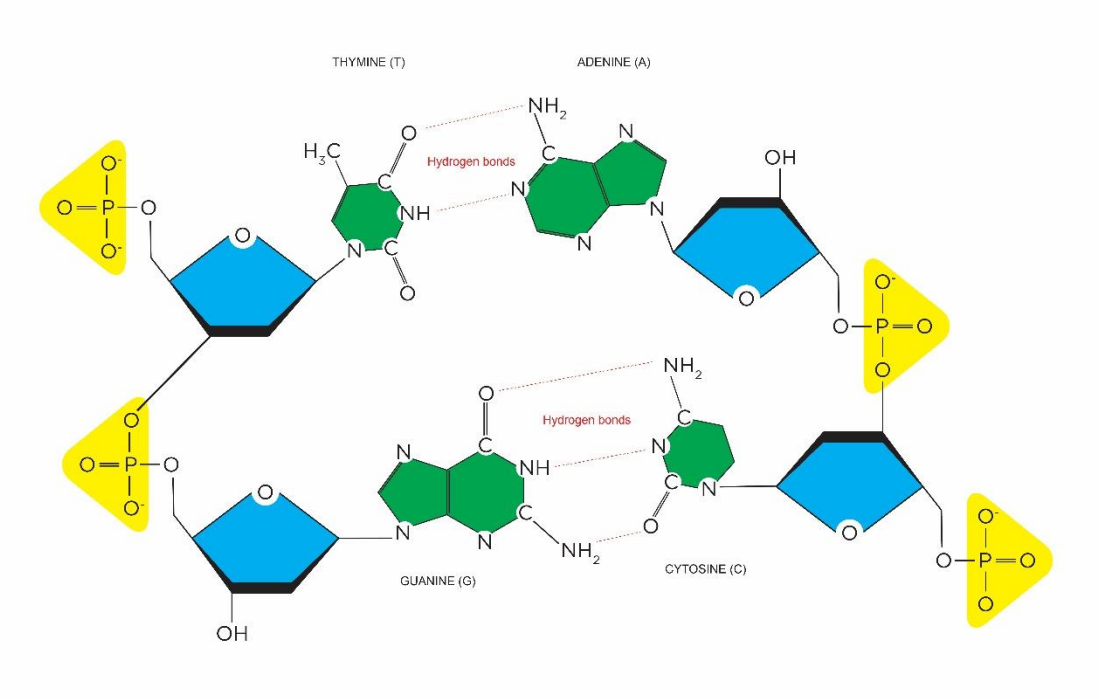

Figure 3. The chemical structure of duplex DNA. Repeating units of nucleotides attached via phosphodiester bonds make up strands of DNA (only two nucleotides each shown). Molecules of DNA consist of two strands of nucleotides arranged with the bases protruding from sugar-phosphate backbones. The two strands of nucleotides are held together by hydrogen bonds between the protruding bases. The bases demonstrate base pairing specificity; adenine (A) binds to thymine (T) using two hydrogen bonds, whereas, cytosine (C) binds to guanine (G) via three hydrogen bonds.

To ensure efficient packing of the base pairs, the DNA molecule winds around itself every ten base pairs, giving rise to the iconic double helix structure. The chemical polarity of the DNA strands is dictated by the orientation of the deoxyribose sugar located at each terminus, giving rise to so called 5' and 3' ends. This orientation is particularly important during events such as replication or transcription which always run from the 5' end to the 3' end of the DNA strand. Stacking between adjacent bases is primarily responsible for the stability of the DNA molecule at this level (183).

To package the long, linear strands of DNA into each cell, it is condensed into chromatin consisting of DNA in complex with organisational proteins. To form chromatin, DNA is tightly wound around positively charged proteins called histones. Double stranded DNA wraps around an octamer of 8 histone 1.65 times to form a nucleosome. Coils of nucleosomes then further arrange themselves to give rise to a 30 nm chromatin fibre that forms loops averaging 300 nm in diameter. The fibres are compressed and bundled to form chromosomes. Principally, this level of organisation

safeguards the integrity of the DNA by reducing the exposure of the surface area of the DNA molecule to the physiological environment, providing a certain level of physical protection from genotoxic agents. Furthermore, accessibility of specific regions of DNA can be more tightly regulated with respect to cellular function. The total number of chromosomes containing all of the genetic material required for the survival of an organism is referred to as its genome. The human genome consists of approximately 3.2×10^9 DNA nucleotide pairs arranged between 23 pairs of chromosomes.

Sections of DNA encoding heritable traits are termed genes. It is worth noting that somatic cells contain two complete sets (diploid state) of chromosomes; with one set inherited from each parent. For this reason, gamete cells contain only one set of chromosomes (haploid state). Since one set of chromosomes is inherited from each parent, every individual inherits two different versions of each gene, which are termed alleles. Alleles may be recessive or dominant which contribute to which observable phenotype the progeny exhibits.

1.3. DNA DAMAGE

Maintaining the stability of the genome is imperative to ensure accurate inheritance of the genetic code for future progeny and ensures that crucial biological processes are undisturbed. However, like any biological molecule, DNA is susceptible to spontaneous chemical reactions arising from endogenous reaction products or exogenous elements in the environment. Examples of forms of DNA damage include sugar or base modifications, single strand breaks, double strand breaks, abasic sites or cross-linking. The bases in DNA are extremely susceptible to chemical modification, which results in the formation of DNA base lesions. DNA base lesions can be transformed into mutations via replication errors or faulty DNA repair. Genomic mutations are permanent alterations to the DNA code and may continually influence biological function. The impact of a genetic mutation is dictated by the type of DNA lesion and the gene it affects. For instance, mutations causing the activation of oncogene function or loss of tumor-supressor genes can trigger unregulated cellular proliferation and malignant growth. In this way, DNA lesions can induce mutations related to cancer.

1.3.1 Endogenous DNA damage

Cellular DNA is susceptible to damage from genotoxic agents within the cell or following exposure to external sources. Genotoxic sources within the cell are referred to as endogenous sources of DNA damaging agents. Endogenous genotoxic sources include reactive biological molecules, such as ROS, which are discussed in the following sections.

1.3.1.1 Hydrolysis

The majority of endogenous DNA damage arises from spontaneous hydrolysis. The *N*-glycosidic bond, connecting DNA bases to the deoxyribose sugar, is particularly labile and susceptible to acid-catalysed hydrolysis, resulting in the loss of DNA bases and the generation of abasic sites. The reaction occurs more readily at purine bases; resulting in the loss of 2,000 to 10,000 purine DNA bases per cell, per day, under normal physiological conditions (88). Another study using liver cells, proposed that in fact 50,000 abasic sites occur per cell, per day, at steady state levels (110). Comparing the rates of depurination of ssDNA to dsDNA suggests that the double helix structure protects against hydrolytic release of bases. The velocity of depurination is four times faster in single stranded DNA, compared to duplex DNA (87)**.** Abasic sites are cytotoxic and have the potential to block transcription and DNA replication. Likewise, abasic sites are noncoding lesions with mutagenic potential and can facilitate the incorporation of an incorrect nucleotide by DNA polymerases. Due to its frequency, hydrolytic loss of DNA bases can be thought of as one of the most important mutagenic events endangering the stability of the genome.

In addition to the inherent lability of the glyosidic bonds, DNA bases themselves are subject to spontaneous hydrolytic deamination events. Cytosine most frequently undergoes hydrolytic deamination, yielding uracil residues. Hydrolytic conversion of cytosine to uracil residues involves direct deamination, followed by an acid catalysed attack by water on the protonated base (143). Interestingly, the epigenetically methylated form of cytosine, 5-methylcytosine, which accounts for approximately 1 % of total human DNA, is deaminated to form thymine residues four times more rapidly than its cytosine precursor (87, 144). Deamination of adenine to hypoxanthine and thymine to xanthine is much less frequent, occurring at only 3 % of the rate of cytosine deamination (77). However, hypoxanthine is a highly mutagenic lesion as it preferentially pairs with cytosine, resulting in a post-replicative transversion mutation (77).

1.3.1.2 Oxidation

Oxygen is an element needed for many cellular processes, including cellular metabolism, cellular signalling and the immune response. Though, constant exposure to molecular oxygen creates an unavoidable source of genotoxic molecules in the form of reactive oxygen species (ROS), generated by oxygen reduction. Types of ROS include the superoxide anion ($O_2^{\bullet-}$), hydrogen peroxide (H_2O_2) and hydroxyl radicals ($^{\bullet}OH$). The superoxide anion, can further react with cellular molecules to form secondary types of ROS. For instance, the superoxide anion can be reduced to hydrogen peroxide. Further to this, hydrogen peroxide is converted to hydroxyl radicals, via a transition metal catalysed Fenton reaction.

All ROS are highly reactive and can induce oxidative damage to cellular molecules, including; lipids, proteins, RNA and DNA. Unrepaired ROS induced damage to cellular macromolecules can result in cell death, genetic mutation, changes in gene expression and chromosome instability.

Sources of ROS can be either endogenous or exogenous. Endogenous sources of ROS originate from normal cellular metabolism, peroxisomes and inflammatory cells. During cellular oxidative metabolism, approximately 4-5 % of oxygen escapes reduction to water via the mitochondrial electron transport chain. Instead, it is converted to ROS (mainly the superoxide anion). Inflammatory cells are major contributors to cellular ROS levels. For example, in response to stimuli, phagocytes undergo respiratory bursts to release ROS. It is believed that the ROS released by this process support the destruction of the microbial insult by generating ROS induced damage to the bacterial biomolecules. Undesirably, the ROS from this mechanism can diffuse to other localised areas and induce damage to non-bacterial molecules. The association between chronic inflammation and carcinogenesis is well acknowledged (59). Peroxisomes are also an endogenous contributor of cellular ROS. Rodent studies demonstrated that peroxisomes account for nearly 35 % of hydrogen peroxide production (139). Other studies have highlighted that administration of therapeutics instigating increased peroxisome proliferation result in carcinogenesis (45). In addition, exogenous sources of DNA damaging agents, such as ionizing or ultraviolet radiation, can generate ROS as by-products. For example, ionising radiation rapidly generates ROS through radiolysis of water molecules. Most of the harmful effects of ionising radiation are mediated through ROS, which diffuse through the cell and cause persistent damage (135, 158).

With regards to DNA, all ROS have the potential to cause over 20 distinctive oxidised DNA adducts (32), although hydroxyl radicals are the primary ROS that damages DNA (93). ROS can directly oxidise DNA components; leading to base modifications, deoxyribose sugar alterations, cross-linking or strand breaks. It is estimated that every human cell endures 10^4 oxidised base lesions per day (4). A frequent oxidised DNA base lesion that features in the top 10 most common endogenous DNA damage insults, is 8-oxo-7,8-dihydrogaunine (8-oxoG; **Figure 6**) (148). The lesion is formed via the addition of a hydroxyl radical at the C8 position of the guanine ring, which is then reduced. The 8-oxoG lesion has high mutagenic potential and preferentially pairs with A (instead of C). Incorrect base pairing with A results in a transversion mutation, if 8-oxoG is not repaired prior to DNA replication (28). Unsurprisingly, elevated levels of 8-oxoG have been documented in numerous cancers (37, 105, 150). Measuring levels of 8-oxoG has been a useful biomarker to estimate oxidative burden (159). Another common base lesion used to estimate oxidative stress is 5, 6-dihydroxy-5,6-dihydrothymine (thymine glycol, Tg; **Figure 6**), which is caused by the interaction of the hydroxyl radical with thymine. Tg lowers the thermal stability of DNA and induces large structural changes, which blocks the action of replicative polymerases (76).

1.3.1.3 Alkylation

Alkylation is another type of DNA damage induced due to the presence of endogenous reactive molecules. Alkylation is a process whereby an alkyl group is transferred from a reactive molecule to regions of the DNA molecule. The primary sites of alkylation are the oxygen and nitrogen atoms of the nucleobases. The addition of bulky alkyl adducts to the DNA nucleobases can disrupt base pairing specificity. One of the most abundant alkylating agents is S-adenosylmethionine (SAM). It is well known that SAM is used as a cofactor in most cellular transmethylation reactions. All DNA methyltransferase enzymes use SAM as the methyl donor during regulation of gene expression, via DNA methylation. Still, non-enzymatic methylation of DNA by SAM can cause two major DNA base lesions; 7-methylguanine and 3-methyladenine (**Figure 4**). It is expected that SAM generates 600 3-methyladenine residues and up to 4,000 7-methylguanine base lesions, per mammalian cell, each day (136). The 7-methylguanine lesion is not immediately harmful, as it does not affect base pairing specificity and the N-methylpurine DNA glycosylase (MPG) is dedicated to the removal of 7-methylguanine. However, 7-methylguanine can influence the lability of the *N*-glycosidic bond, leading to abasic sites. In comparison, 3-methyladenine is highly cytotoxic and blocks cellular replication. Due to this, MPG is also dedicated to

the excision of 3-methyladenine lesions. Interestingly, it has been suggested that the effectiveness of MPG decreases with age in human cells (8). To a lesser extent, SAM can generate alkylated pyrimidine lesions, such as 3-methylthymine or 3-methylcytosine, which have the capacity to prevent DNA replication. Other alkylated DNA base lesions from endogenous origin include; O^6-methylguanine, O^4-methylthymine and O^4-ethylthymine. Base lesions formed from methylation of oxygen molecules are notoriously difficult to examine due to low frequency and rapid repair rate (86). Despite this, it has been established that they are associated with transition mutations during DNA replication (111, 131).

1.3.1.4 Single strand breaks

Single strand breaks (SSBs) are one of the most frequent types of DNA damage and can arise from endogenous agents (such as ROS or other intracellular metabolites), exposure to exogenous agents (such as ionising radiation), or due to miscellaneous activity of particular enzymes (for example, DNA topoisomerases) (**Figure 4**). Furthermore, SSBs can be spontaneously generated through miscellaneous DNA repair. SSBs are an unavoidable intermediate following incision of the abasic site during the BER pathway (24). Likewise, SSBs can occur due to collapsed DNA replication forks, leading to excessive protein poly-ADP-ribose polymerase 1 (PARP1) activation (24).

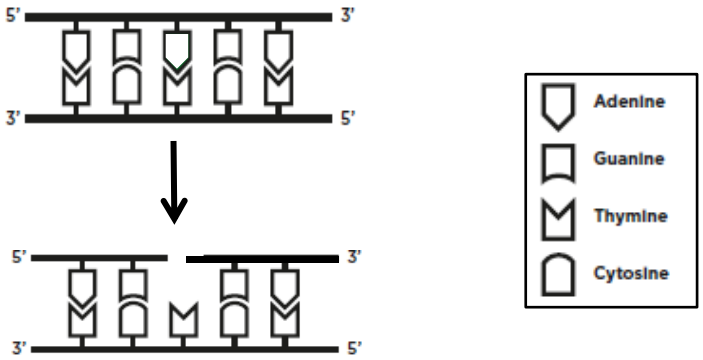

Figure 4. Single strand breaks (SSBs). A schematic showing the formation of a DNA SSB. Bases are represented by four different shapes and the DNA backbone is represented by a thick black line. A single strand break is formed on one side of the DNA backbone, which is normally associated with the loss of a DNA base and damage to the 5' and 3' terminal ends of the DNA strand.

1.3.1.5 Double strand breaks

Double strand breaks (DSBs) are one of the most lethal forms of genomic damage associated with genomic instability and cellular transformation. DSBs arise when the phosphate backbones of the two complementary DNA strands are broken simultaneously, in close (within 0-20 base pairs) proximity (**Figure 5**). Base-pairing and chromatin structure are unable to keep the two DNA ends connected (70). As a consequence, the two DNA ends are liable to become physically dissociated from one another, hindering repair processes and increasing the opportunity for inappropriate recombination (**Figure 5**). Therefore, DSBs are particularly cytotoxic or mutagenic and are associated with chromosomal relocations. Alike to other types of DNA damage, DSBs arise pathologically following exposure to exogenous genotoxic agents, such as ionising radiation or due to intracellular metabolites. The major endogenous source arises when DNA replication forks collapse. Due to the lethality of DSBs, cells have evolved important repair mechanisms; homologous recombination (HR) and nonhomologous end-joining (NHEJ) (70).

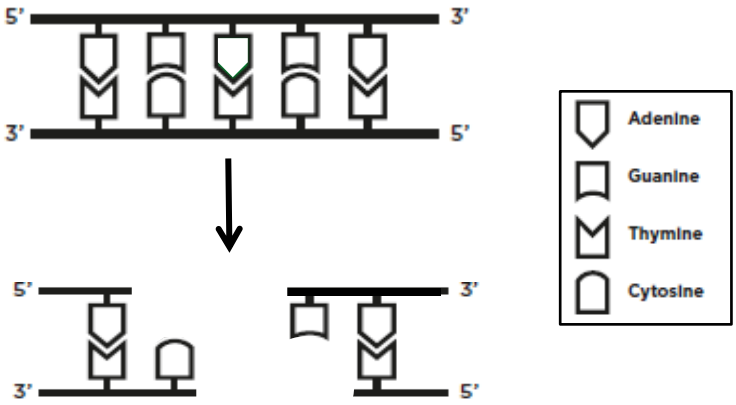

Figure 5: DNA Double Strand Breaks (DSBs). A schematic showing the formation of a DNA SSB. Bases are represented by four different shapes and the DNA backbone is represented by a thick black line. A DSB is formed when the phosphodiester backbone is broken simultaneously on both strands of DNA. Base-pairing and chromatin structure are insufficient to keep the two DNA ends juxtaposed.

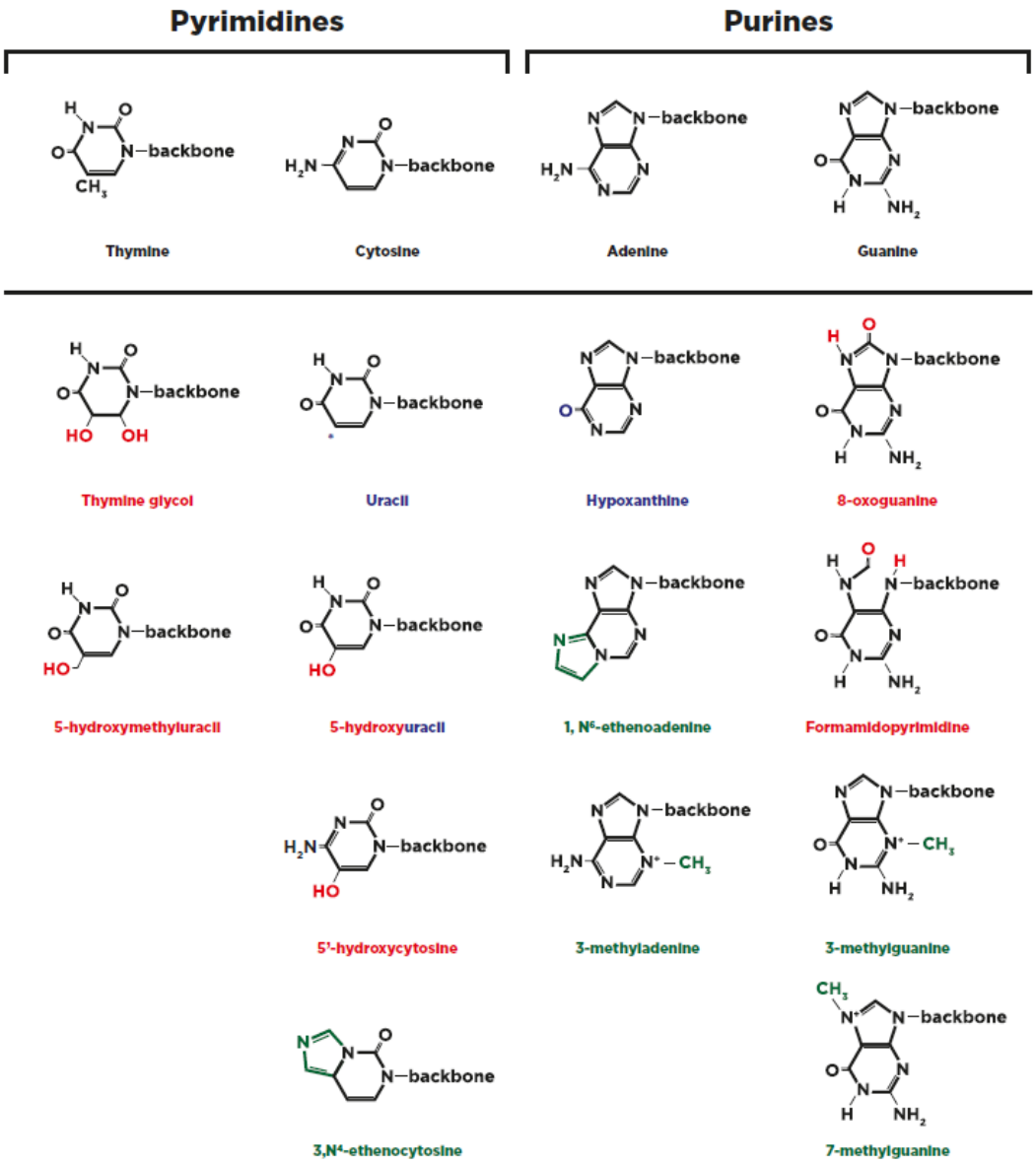

Figure 6. Schematic of DNA base lesions. The chemical structures of the four undamaged nucleotides are featured above with some of the damaged derivatives of each nucleotide represented below. The colours utilised represents the type of damage encountered; red represents oxidative damage, blue represents deamination and green for alkylation.

1.3.2 Exogenous DNA damage

Cellular DNA is under constant attack from genotoxic agents. Reactive molecules that damage the genome can arise from exposure to exogenous sources, such as ionising radiation. Different types of exogenous agents and the DNA damage they induce are discussed in the proceeding sections.

1.3.2.1 Ultraviolet light exposure

Ultraviolet light (UV) is an unavoidable DNA damaging agent arising from exposure to the sun. Direct damage to the DNA macromolecule is predominantly induced by highly reactive UV-B wavelengths of radiation (134). UV-A radiation interacts poorly with DNA, but can still induce genomic damage by indirect photosensitising reactions, via singlet oxygen molecules.

Two of the most abundant types of DNA lesions, cyclobutane pyrimidine dimers (CPD's) and 6–4 pyrimidine photoproducts, are induced by UV exposure. Both pyrimidine adducts are defined by the formation of atypical covalent bonds between adjacent pyrimidine bases. Areas consisting of adjacent pyridines, particularly two cytosine residues, are prone to UV-induced damage. CPD's occur up to 3 times more frequently than 6-4 photoproducts, but both types of dimers are equally pre-mutagenic and potentially cytotoxic by significantly distorting the double-helix (134). Due to the disproportion in frequency, CPD's are believed to have the greatest mutagenic effect. Related to this, 6-4 photoproducts are more rapidly repaired by DNA repair pathways, compared to CPD's (100). The formation of modified purine bases in response to UV radiation has also been acknowledged, but these occur infrequently (17, 56).

If UV-induced lesions are not repaired, they result in permanent mutations within the genome following replication of the DNA strand. The cumulative effects of DNA damage following recurrent exposure to UV contributes to photoaging, immunosuppression and the development of skin cancers (100).

1.3.2.2 Ionising radiation

Ionising radiation arises from environmental sources, such as cosmic radiation, or from man-made sources, including X-rays. When tracks of ionisation pass through cells, they can interact with biomolecules. The most significant effects of ionising radiation are observed when tracks of radiation interact with genomic DNA. It is now understood that radiation can cause a spectrum of DNA damage, including base lesions, SSBs and DSBs. It is estimated that one gray (Gy) of ionising radiation with low linear energy transfer (LET) can induce 1,300 DNA base lesions, 1,000 SSBs, and up to 40 DSBs per cell (92). Of all of the DNA aberrations caused by ionising radiation, DSBs are considered to be the major mutagenic risk to the genome (**Section 1.3.1.5**). This is due to one of the DSB repair pathways being particularly

error prone, risking chromosomal aberrations. As the dose of radiation exposure increases so does the yield of DSBs (92).

A distinctive feature of genomic damage following exposure to a single radiation track, is the formation of two or more DNA lesions that are clustered within 1-2 helical turns of DNA. The number of lesions contributing to a site of clustered (complex) DNA damage is related to the LET of the radiation. Approximately 90 % of the energy deposited by radiation with high LET induces clustered (complex) DNA damage, whereas 30 % of the energy deposited by radiation tracks with low LET is associated with the formation of these lesions (92). Importantly, sites of complex DNA damage, including DSBs, are less readily repaired. Complex DNA lesions are believed to persist 8 times longer than single base lesions (91). As the LET of radiation increases, so does the complexity of the DNA lesions (113).

In addition to directly interacting with cellular structures, ionising radiation can indirectly cause biological changes through by-products created when the track of radiation interacts with other cellular biomolecules. Ionising radiation can interact with water molecules within the cell, to generate ROS. The hydroxyl radicals produced can diffuse through the cell and damage proteins or DNA (135). The indirect effects of radiation are particularly relevant to ionising radiation with low LET.

It has now been established that the biological effects of ionising radiation are further amplified by the radiation-induced bystander effect (9). Studies identified that neighbouring cells, not exposed to tracks of radiation, also experience levels of damage resulting in chromosomal breakages and tumour formation. It is believed that the bystander effects of radiation are attributed to the release of signalling molecules by irradiated cells. These signalling molecules include inflammatory cytokines, that stimulate production of nitric oxide and ROS, which can diffuse to neighbouring cells and induce DNA damage (65). Likewise, damage to mitochondria results in increased production of hydrogen peroxide, which can diffuse across cellular membranes (65).

1.4. DNA damage repair

To ensure survival, organisms must preserve the stability of the genome against the DNA lesions which form every day. Indeed, most DNA lesions are repaired immediately via specialised repair mechanisms, meaning only a small proportion of them accumulate as permanent mutations propagated within cell progeny. The importance of repairing DNA lesions is highlighted by the cellular investment made to maintain numerous DNA repair enzymes. The importance of each DNA repair enzyme

is evident by increased mutation rates following its inactivation. The association of inactivation of DNA repair proteins and human diseases has been well characterised.

Coincidentally, the structure of DNA is well suited to enable accurate repair due to the preservation of two copies of the genetic information on separate strands. In this way, the complementary strand can act as a template during DNA repair and directs the insertion of correct complementary nucleotides onto the damaged DNA strand. The advantage of storing genetic information in this way is emphasised by the preservation of the double-stranded helix structure of DNA in most organisms.

Cells have developed several processes to deal with different types of DNA lesions. Two of the most common pathways are the base excision repair (BER) pathway, which eliminates minor examples of damaged base lesions (118), and the nucleotide excision repair (NER) pathway, which removes larger lesions to genomic DNA (84). In both repair pathways, the damaged nucleotides are excised then polymerases use the complementary strand of DNA as a template to insert the correct nucleotide on the damaged DNA strand. Then DNA ligase enzymes seal the break in the sugar-phosphate backbone and restore the double-helix (**Figure 7**).

Of course, when DNA is exceptionally damaged, it is not always possible to use the undamaged DNA strand as a template. In this circumstance, cells have developed alternative repair strategies that rely on translesion polymerases to bypass the DNA damage and enable cell survival. Translesion polymerases are less accurate, as they estimate which nucleotide to incorporate into the damaged site (170). In this respect, translesion polymerases compromise the integrity of the genome and contribute to the accumulation of base-substitutions or deletion mutations.

Likewise, a template strand of DNA is understandably unavailable when both strands of the DNA helix are broken. This makes DSBs particularly destructive to the integrity of the genome, often leading to cell death. To process DSBs, cells have developed a NHEJ strategy, which essentially ligates the two ends of DNA together, usually resulting in the deletion of one or several nucleotides (35). Further inaccuracy of this pathway arises from the fact that it has no mechanism to ensure the ends of the DNA strands it ligates together were formerly adjacent to each other. This means NHEJ can cause entire rearrangements of the genome. In contrast, HR is employed to process DSBs with better accuracy. HR is critical in recovering faulty replication forks or inter-strand cross links. However, HR is only applied to newly replicated DNA (in the S and G_2 phases of the cell cycle), as it relies on the use of sister chromatids as

template DNA (138). HR avoids creating deletions, but can still pose the threat of chromosomal rearrangements or loss of heterozygosity via gene conversion.

To minimise the probability of permanent mutations being inherited by future cell progeny during cellular divisions, most cells initiate a transient delay in cell cycle progression when DNA damage is incurred. This allocates time to enable DNA repair before the cell divides. Throughout the cell cycle (G_1, S, G_2, M) there are many checkpoints, which the cell utilises to monitor status. The G_1 checkpoint monitors DNA integrity and dictates whether the cell will initiate DNA replication in S-phase, before undergoing mitosis. If DNA damage is detected, then either DNA repair mechanisms will be initiated or the cell will undergo apoptosis.

1.4.1 Nucleotide excision repair

NER is a DNA repair mechanism which counteracts a diverse spectrum of DNA lesions. Although, lesions which significantly distort the DNA helix appear particularly relevant to NER, such as bulky CPDs or (6-4) photoproducts. For this reason, patients with defects in genes implicated with NER exhibit photosensitivity and susceptibility to skin cancer. In fact, studies based upon patients with these clinical manifestations formed the basis of identification of many factors of NER. NER can also remove bulky chemical adducts, intra-strand cross-links, inter-strand cross-links and different types of oxidative damage (**Figure 7**).

In general, two sub-pathways of NER can be distinguished; global genome repair (GGR), targets lesions across the entire genome, whereas, transcription-coupled repair (TCR) targets transcriptionally active regions of DNA (41). Due to their different repair targets, the two modes of NER differ in the way that the DNA lesions are recognised, but the subsequent stages are shared (**Figure 7**). Remarkably, it has been shown that the components needed for NER can assemble and eliminate genomic damage within 4 minutes (66).

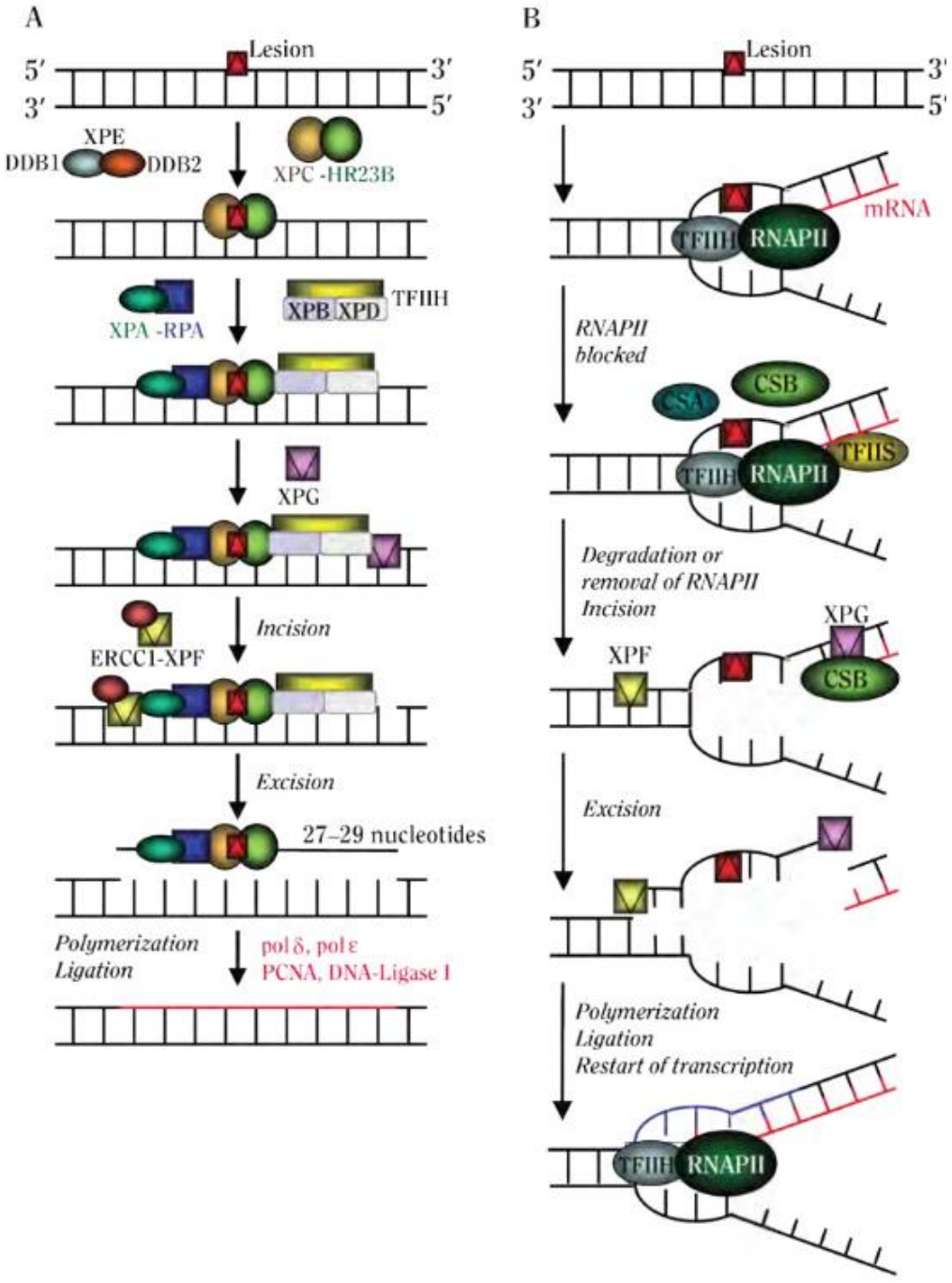

Figure 7. The mechanism of nucleotide excision repair (NER). Schematic representation of the two sub-pathways of NER; (**A**) global genomic repair (GGR) and (**B**) transcription-coupled repair (TCR). In GGR, damage is recognised by the XP-C and XP-E complex; XP-A recruits the transcription factor IIH (TFIIH) complex that contains the XP-B and XP-D ATPase-dependent helicases, which unwind approximately 30 nucleotides surrounding the genomic damage. The XPG endonuclease cleaves the DNA backbone 3' to the lesion, whilst the XPF-ERCC1 endonuclease heterodimer cleaves the DNA backbone 5' to the lesion. Nucleotides are inserted by replicative polymerases delta and epsilon (Pol δ and Pol ε). The nick in the DNA backbone is repaired by DNA ligase I or III. Whereas, TCR recognises a stalled replication fork via CSA and CSB proteins. The TFIIH complex is recruited and completion of repair continues as per GGR. Following repair, the RNA polymerase can continue to transcribe RNA. Figure is adapted from (31).

CSA = Cockayne syndrome complementation group A; CSB = Cockayne syndrome complementation group B; DDB = DNA binding protein; ERCC1 = excision repair cross-complementation group 1; HR23B = homologous recombinational repair group 23B; mRNA = messenger RNA; PCNA = proliferating cell nuclear antigen; pol = polymerase; RNAPII = RNA polymerase II; RPA = replication protein A; TFIIH = transcription initiation factor IIH; TFIIS = transcription initiation factor IIS; XP = xeroderma pigmentosum (groups A–G).

In GGR, damage recognition is instigated by the XP-C and XP-E complex, which continually scans the DNA for obvious structural distortions. In response to damage recognition, XP-A recruits the TFIIH complex that contains the XP-B and XP-D ATPase-dependent helicases, which unwind approximately 30 nucleotides surrounding the genomic damage (**Figure 7**). The XPG endonuclease cleaves the DNA backbone 3' to the lesion, whilst the XPF-ERCC1 endonuclease heterodimer cleaves the DNA backbone 5' to the lesion. The excised nucleotides are replaced by the action of replicative Pol δ and Pol ε. Finally, the nick in the DNA backbone is restored via the action of DNA ligase I or III (41). In contrast, identification of a stalled replication fork by TCR, is achieved by CSA and CSB proteins. After this, the TFIIH complex is recruited and completion of repair continues as per GGR (**Figure 7**). Following repair, the RNA polymerase can continue to transcribe RNA (41).

1.4.2 Mismatch repair

The mismatch repair pathway (MMR) corrects mismatched bases incorporated during DNA synthesis or caused by agents which disturb base binding affinities. Mutation rates are up to 1000 times greater in MMR deficient tumour cells (137). The significance of MMR in preventing the accumulation of mutations is highlighted by patients with Lynch syndrome, caused by heritable defects in multiple MMR genes. The disease is associated with early onset of hereditary non-polyposis colorectal carcinoma (HNPCC).

The action of MMR is instigated by two heterodimers; the MutL heterodimers (MutLα, MutLβ and MutLγ) and the MutS heterodimers (MutSα and MutSβ). MutS is present in two forms; MutSα and MutSβ. The MutSα heterodimer, is primarily involved in the repair of base substitutions, whereas, the MutSβ has been shown to repair larger types of mismatch damage, including insertion-deletion loops that are up to 10 nucleotides (137). Following recognition of mismatches, multiple MutL heterodimers are recruited. The MutL heterodimer possesses inherent endonuclease activity and incises the DNA backbone. Following this, exonuclease 1, removes a region of nucleotides containing the mismatch and stops upon encountering the start of an

Okazaki fragment generated during replication. Repair is completed by replicative polymerases and ligases. The replication protein A protects the exposed single stranded DNA until repair is finalised.

1.4.3 Double strand break repair

DSBs are one of the most biologically cytotoxic forms of DNA damage induced by intracellular ROS or following exposure to ionising radiation. Repair of DSBs is imperative to cellular survival; if left unresolved DSBs can induce genomic rearrangements, chromosomal aberrations, cellular apoptosis or promote mutagenesis. Regrettably, the generation of DSBs is inevitable during biological processes dependent on genomic rearrangements, such as meiosis. To counteract the potentially lethal effects of DSBs, two repair pathways have evolved; NHEJ and HR.

Of the two pathways, NHEJ is mechanistically the simplest and consists of direct re-ligation of the broken ends of DNA regardless of sequence homology. In this way, NHEJ is particularly error prone, but is predominant throughout most stages of the cell cycle. The first step of NHEJ is recognition of the DSB by the Ku heterodimer; which consists of two proteins, Ku70 and Ku80 (**Figure 8**). The binding of Ku facilitates the formation of a ring structure that is threaded onto the end of the DNA. The attachment of Ku also attracts the DNA protein kinase catalytic subunit (DNA-PKcs) to bridge the two ends of DNA and phosphorylates X-ray cross complementing protein 4 (XRCC4) to stimulate DNA end ligation and resolution (71).

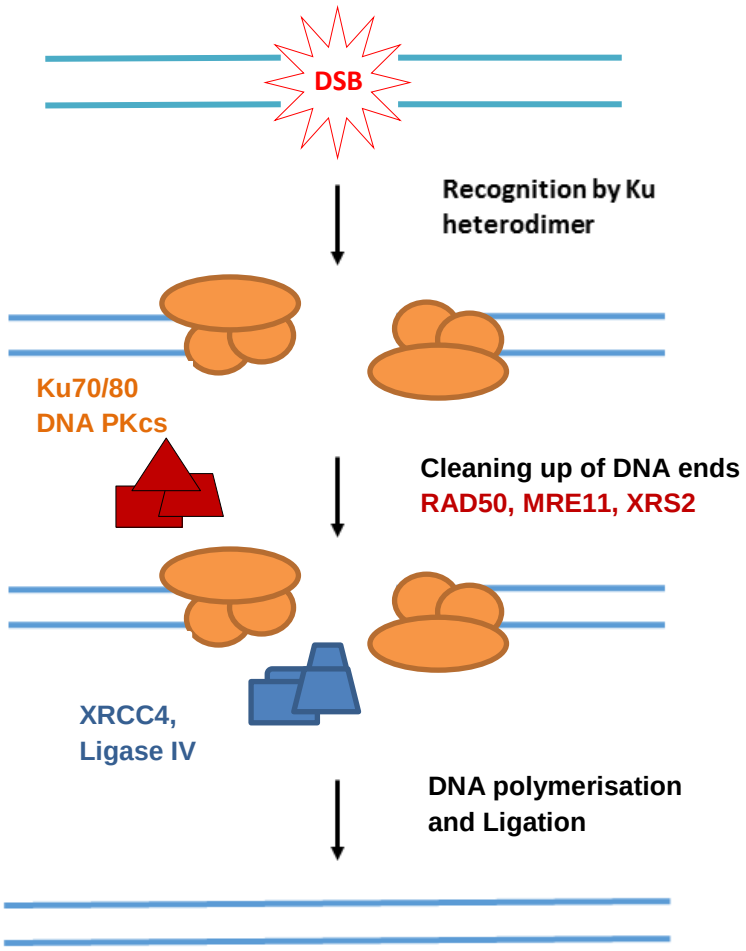

Figure 8: Non-homologous end joining (NHEJ). Double strand breaks are recognised by a heterodimer of Ku70 and Ku80 which form a ring structure that threads onto the DNA strands. Presence of Ku70/80 attracts DNA-PKcs which bridge the terminal ends and initiates phosphorylation of XRCC4 to stimulate DNA ligation and restoration of two intact strands of DNA Figure adapted from (70).

Conversely, HR is only active during late S-G_2 phases of the cell cycle, as it relies on the presence of a sister chromatid as a repair template. However, this method of action means that HR results in accurate and non-mutagenic repair. The events of HR are complex and based on studies in multiple organisms, under different biological circumstances. Therefore, the mechanistic details of HR are still debated. In general terms, HR is initiated when the MRN complex recognises DSBs and resects the DNA to form 3' single strand overhangs (**Figure 6**), which are coated with RPA (71, 96).

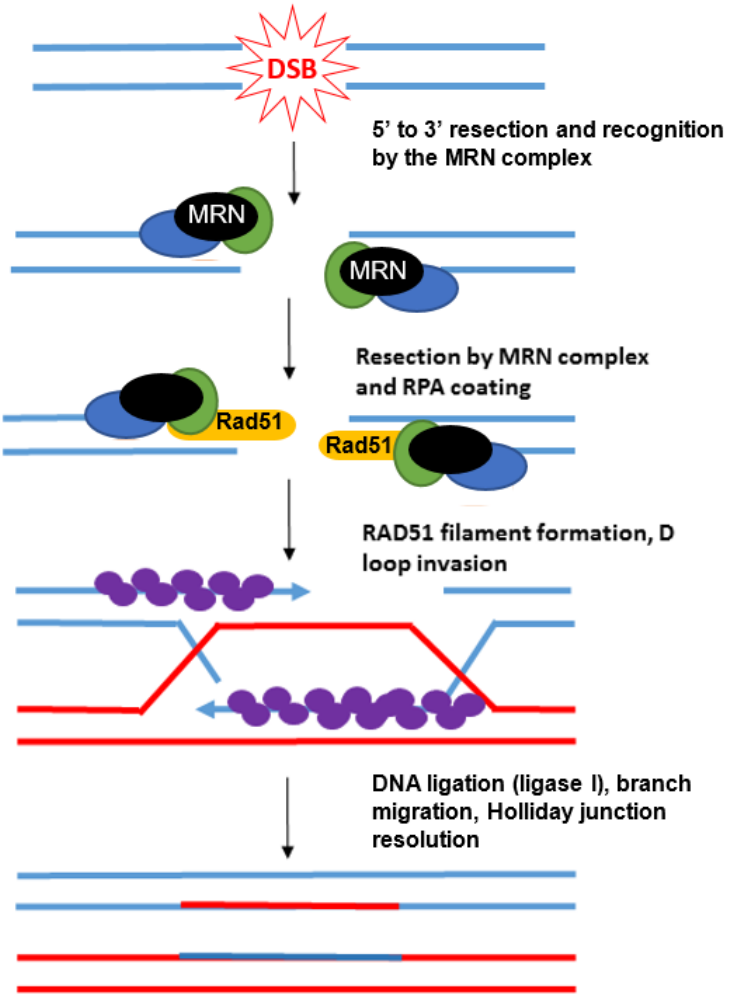

Figure 9: Homologous recombination (HR). Double strand breaks are recognised by the MRN complex which resects DNA to form 3' single strand overhangs which are coated by RPA. Afterwards, RPA is replaced by RAD51 which invades the sister chromatid, to form a D-loop, so that the sister chromatid can be utilised as a template for repair. After DNA crossovers, the Holliday junctions are resolved and cleaved DNA is ligated to restore two intact strands of genomic DNA. Figure adapted from (70).

Following this, HR involves the generation of a Holliday junction. During this, RAD51 replaces RPA and initiates the invasion of the sister chromatid to be utilised as template. After DNA crossovers, the Holliday junctions are resolved by cleavage and ligation to restore two intact DNA molecules. Recent work has demonstrated strong correlations between HR and the breast susceptibility proteins, BRCA1 and BRCA2 (129). It is not yet apparent how these effects occur, although they might reflect potential binding of BRCA1/2 to RAD51 (129). Loss of HR results in a cellular inability to successfully enter S-phase, due to the inability to restart collapsed replication forks.

As expected, inactivation of HR genes such as RAD51, BRAC1 and BRCA2 leads to embryonic lethality in animal models and non-viable cells in culture (129).

1.4.4 Base excision Repair

As mentioned earlier, BER is one of the major DNA repair pathways applied to managing small, non-distorting DNA base lesions created by deamination, alkylation or oxidation. Likewise, the latter stages of BER are also employed to manage abasic sites formed by spontaneous reactions, such as hydrolysis.

In 1974, the initial stages of BER were discovered by Dr. Thomas Lindahl (85). Lindahl was the first to identify a DNA glycosylase implicated in the removal of uracil (U) residues from DNA. Following excision of the base lesion, Lindahl further recognised that endonuclease, polymerase and ligase enzymes restore the DNA. This discovery ultimately led to the outline of the fundamental stages of BER that are acknowledged in the present day. Since this discovery, the function of numerous enzymes implicated in BER have been characterised.

The first stage of BER consists of recognition and removal of the damaged nucleotide by 11 damage-specific glycosylase enzymes, which scan along the DNA molecule and cleave the *N*-glycosidic bond upon detection of damage (**Figure 10**). Each BER glycosylase enzyme exhibits specificity towards certain types of DNA base damage and utilise a “base-flipping” mechanism to identify and remove base lesions. Generally, there are two types of BER DNA glycosylases; monofunctional glycosylases possess DNA glycosylase activity only, or bifunctional glycosylases cleave the DNA strand as well as excising the damaged DNA base (25). Generally, excision of DNA base lesions via monofunctional glycosylases enzymes results in the formation of an abasic site which is recognised by AP endonuclease 1 (APE1). APE1 then cleaves the phosphodiester backbone resulting in the formation of a nucleotide gap flanked by 3’-hydroxyl and 5’-deoxyribosephosphate (5’dRP) terminal ends (25). Alternatively, removal of base lesions via bifunctional glycosylases with inherent lyase activity, results in the formation of a single nucleotide gap flanked by either a 5’-phosphate and a 3’-α,β-unsaturated aldehyde (following β-elimination) or 5’-phosphate and 3’-phosphate terminal groups (following β,δ-elimination). Glycosylase enzymes known to possess β-elimination activities include; NTH1 and 8-OxoG DNA glycosylase 1 (OGG1) (**Table 1**). After their actions, the 3’-α, β-unsaturated aldehyde is processed by APE1, to generate a 3’-hydroxyl group. Due to the low efficiency of β-elimination, APE1 generally bypasses this stage and cleaves the AP site (163).

Bifunctional enzymes, which excise DNA base lesions via β, δ-elimination are the endonuclease VIII-like proteins 1 to 3 (NEIL1-3) (**Table 1**). The 3'-phosphate terminal group generated by their activity is removed by polynucleotide kinase phosphatase (PNKP) (176). Regardless of if BER is initiated by mono-/bi-functional glycosylase activities, a single nucleotide gap with a 3'-hydroxyl end is always the final product formed, owing to subsequent terminal end processing by APE1 or PNKP. This terminal end is required as a suitable substrate for DNA polymerase activity. The major DNA polymerase employed in BER is Pol β, which acts to remove 5'-dRP terminal ends and inserts the correct undamaged nucleotide. The remaining nick in the DNA backbone is sealed by a complex of Lig IIIα and XRCC1. SSBs to the phosphodiester backbone are protected via binding by the poly (ADP-ribose) polymerase, PARP-1. It has been shown that PARP-1 acts in combination with XRCC1 to stabilise the abasic site and secure it for processing by BER enzymes downstream in the pathway (19).

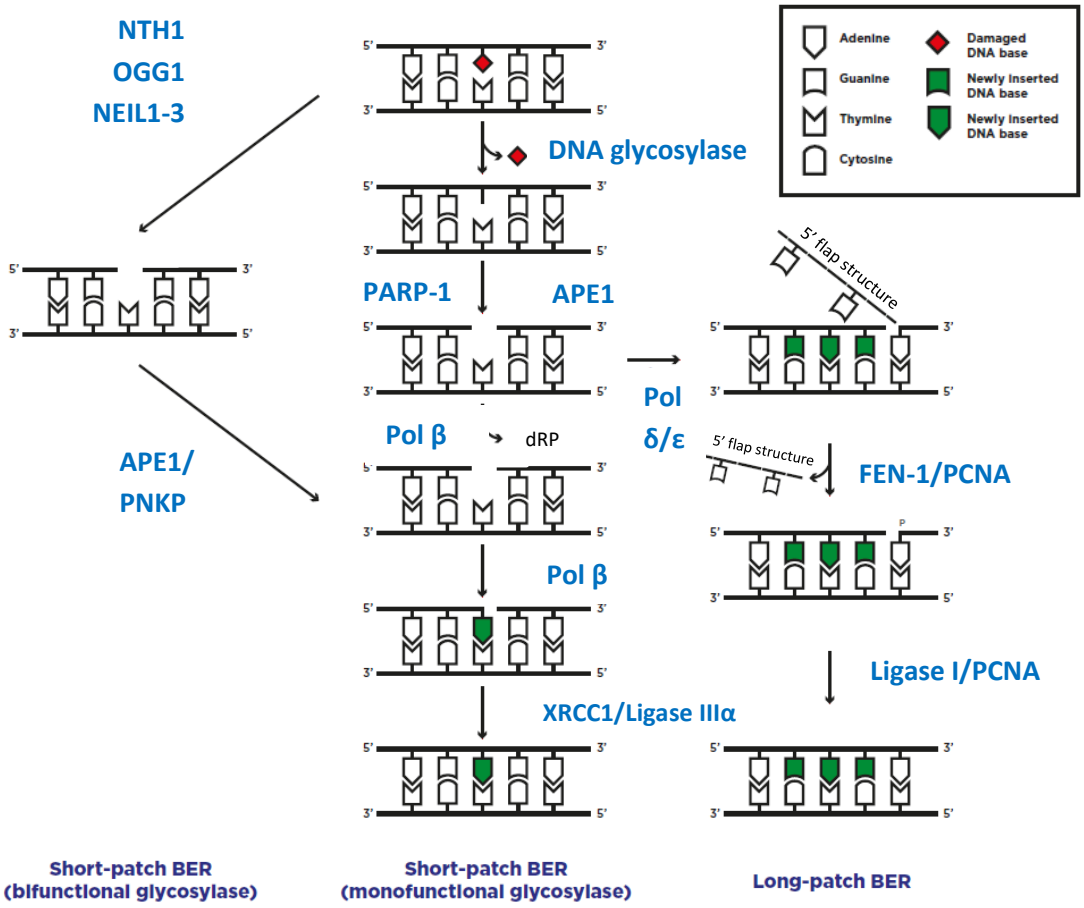

Figure 10. Base excision repair (BER). Monofunctional, damage-specific DNA glycosylases recognise and excise the damaged base by cleavage of the *N*-glycosidic bond leaving an abasic site. This is incised by APE1 to generate a single stranded break, containing a 5'-dRP moiety. PARP-1 binds to the incised phosphodiester backbone to protect the single strand break from further damage and stabilises it for further processing. The 5'-dRP moiety is removed by the d-RP lyase activity of DNA Pol β, which inserts the correct complementary nucleotide (**Short-patch BER, monofunctional glycosylase**). Bifunctional, damage-specific DNA glycosylases (such as NTH1, OGG1 and NEIL1-3), possess inherent lyase activity and can simultaneously remove the damaged DNA base lesion whilst incising the DNA backbone. The terminal ends require processing by APE1 or PNKP, before nucleotide insertion by Pol β (**Short-patch BER, bifunctional glycosylase**). Finally, the nick in the phosphodiester backbone is restored by a complex of DNA Ligase IIIα and XRCC1. If the terminal ends of the DNA backbone generated by APE1 incision are resistant to Pol β processing then long-patch BER occurs, whereby, up to 13 nucleotides are inserted into the repair gap by the action of DNA Pol δ/ε (**Long-patch BER**). This generates a 5' flap of displaces nucleotides which is removed by the action of flap endonuclease (FEN1) in the presence of proliferating cell nuclear antigen (PCNA). The gap in the DNA backbone is subsequently repaired by a complex of DNA Ligase I (Lig I) and PCNA. Adapted from (25).

These stages, termed short-patch BER, detail the preferred mechanism used to repair up to 80 % of damaged nucleotides (38). In some instances, the terminal groups are

not compliant to the latter stages of BER. For example, if the 5'-dRP residue is oxidised or reduced, it becomes resistant to Pol β excision. In this situation, a changeover to replicative enzyme Pol δ or Pol ε ensues (128) and long-patch BER occurs. The two BER sub-pathways differ in the BER enzymes used and the number of nucleotides inserted within the damaged region. Long-patch BER results in the replacement of at least 2 nucleotide monomers; Pol δ/ε typically adds 2-8 nucleotides into the single nucleotide gap, resulting in a 5'-flap structure, which is removed via the action of flap endonuclease (FEN1) in a proliferating cell nuclear antigen (PCNA) dependent manner. The resulting nick in the DNA backbone is subsequently repaired by Lig I in association with PCNA (25).

1.4.4.1. Enzymes of BER

The following sections concentrate on the specific enzymes implicated in each stage of the BER pathway in more detail, with specific reference to enzymes involved in short-patch BER since the majority of damage (80%) is repaired via this sub-pathway (37).

1.4.4.1.i DNA Glycosylases

The initial stage of BER relies on recognition and removal of the damaged DNA nucleotide via DNA glycosylase enzymes. There are 11 distinct mammalian DNA glycosylase enzymes that are specific to the type of DNA lesion they excise (**Table 1**). The DNA glycosylases are subdivided into 4 distinct families, elected by structural characteristics. These are the Uracil DNA glycosylases (UDG), Helix-hairpin-helix glycosylases (HhH), 3-methyl-purine glycosylase (MPG) and the NEIL glycosylases (**Table 1**). The enzymatic core between glycosylases is well conserved, but compared to prokaryotic counterparts, mammalian glycosylases display additional disordered terminal extensions that function in protein interactions, PTMs, DNA recognition and determining subcellular localisation (64).

The nucleophile each DNA glycosylase uses to cleave the *N*-glycosidic bond subdivides them into either monofunctional or bifunctional enzymes. Monofunctional glycosylases utilise activated water molecules, whereas, bifunctional glycosylases possess inherent AP lyase activity and incise the DNA sugar-phosphate backbone, as well as removing the base lesion (147). Bifunctional glycosylases utilise the amino group of a lysine side chain for nucleophilic attack of the *N*-glycosidic bond, forming a covalent Schiff-base intermediate with the damaged nucleobase. Resolution of the

Schiff base (by β or δ elimination) results in incision of the DNA backbone. Data suggests that the incision of the DNA backbone by mammalian glycosylases does not always occur simultaneously, but the rate of cleavage of the DNA backbone may be slower than the removal of the damaged nucleotide (98, 190).

The glycosylase enzymes involved in BER all face a similar problem; how to efficiently identify minor changes to damaged bases that do not significantly distort the DNA helix. Interestingly, the glycosylases share a unified mechanism for detecting DNA base damage. The enzymes rotate nucleobases out of the DNA helix into a selective catalytic pocket that increases the surface area for molecular interactions. This facilitates analysis of aromaticity and detection of small base irregularities. To some extent, the selectivity of each glycosylase is dictated by steric exclusion from the base binding pocket; if the damaged base fits within the catalytic pocket then the *N*-glycosidic bond can be cleaved (10, 54). Conserved residues positioned around the entry of the catalytic pocket often enable selection of damaged substrates without full insertion of the nucleotide into the cavity, thus improving the time taken for recognizing damaged nucleobases (10, 54).

The methods used by DNA glycosylases to scan genomic DNA are still debated. Biochemical evidence suggests that non-specific interactions enable DNA glycosylases to slide along the DNA helix. However, due to the functional diversity of glycosylases this is unlikely to be utilised by every member (54). It has been proposed that glycosylases containing iron-sulphur clusters could co-operatively locate DNA lesions through redox signalling mechanisms (15). This concept was first speculated based on observations that the oxidation state of the iron-sulphur clusters change upon contact with DNA (16).

Another trait that appears synonymous with BER glycosylases is bending of the DNA helix following binding to the base lesion. Indeed, UNG induces a 45° bend to the DNA, plus a bend of 70° has been reported following association of OGG1 (21, 117). It is suggested that bending of the DNA molecule may serve as a structural signal to coordinate initiation of the next stages of BER.

Following the removal of the DNA lesion, DNA glycosylases generally remain bound to the abasic site. In fact, a number of glycosylases demonstrate increased binding affinity to abasic sites compared to their respective DNA substrates (117, 171). Some studies have suggested that the release of abasic sites by glycosylases is a rate limiting step within the BER pathway. Although, this is debateable as other rate limiting steps could be inflicted by Pol β activity or DNA ligation stages. Since abasic sites are

unstable and potentially mutagenic, it is reasonable to assume that the binding of the glycosylase may have a protective effect. As expected, the recruitment of downstream proteins involved in BER stimulates removal of the glycosylase (117, 171). Superior to this, PTMs have also been shown to regulate the dissociation of glycosylases (25, 62).

Cells lacking DNA glycosylase expression exhibit increased levels of DNA damage, elevated mutations and hypersensitivity to DNA damaging agents. Surprisingly, animal models of glycosylase knockouts are viable, with relatively unaffected phenotype and slight increased mutation frequency. This is largely due to redundancy between different glycosylase members (123, 149). Although, an exception to this is knockout murine models of thymine DNA glycosylase (TDG), which is embryonically lethal. This is potentially due to the epigenetic function of TDG (33).

Table 1. A comprehensive list of mammalian glycosylases and their modes of action as well as their physiological substrates. There are eleven distinct mammalian glycosylases which demonstrate specificity to particular physiological substrates. Their mode of action is either monofunctional (M) or bifunctional (B) depending on the nucleophile utilised to disrupt the *N*-glycosidic bond of damaged DNA bases. Adapted from (72).

Type of base lesion	Glycosylase	Mono (M) or bi (B) functional	Physiological substrates
Uracil in ssDNA or dsDNA	Uracil-N glycosylase **(UNG)**	M	U, 5-FU, ss and dsDNA
	Single-strand-specific monofunctional uracil DNA glycosylase 1 **(SMUG1)**	M	U, 5--hmU, 5-FU, ss and dsDNA
Pyrimidine derivates in mismatches	Methyl-binding domain glycosylase 4 **(MBD4)**	M	T, U, 5-FU, εC, opposite G, dsDNA
	Thymine DNA glycosylase **(TDG)**	M	T, U, 5-FU, εC, 5-hmU, 5-fC, 5-caC; opposite G, dsDNA
Oxidative purine base damage	8-OxoG DNA glycosylase 1 **(OGG1)**	B	8-oxoG, FaPy, opposite C, dsDNA
	MutY homolog DNA glycosylase **(MYH)**	M	A opposite 8-oxoG, C or G, 2-hA opposite G, dsDNA
Alkylated purines	Methylpurine glycosylase **(MPG)**	M	3-meA, 7-meG, 3-meG, hypoxanthine, **ε**A, ss and dsDNA
Oxidized, ring-fragmented or -saturated pyrimidines	Endonuclease III-like 1 **(NTH1)**	B	Tg, FaPyG, 5-hC, 5-hU, dsDNA
	Endonuclease VIII-like glycosylase 1 **(NEIL1)**	B	Tg, FaPyG, FaPyA, 8-oxoG, 5-hU, 5-hC, ss and dsDNA
	Endonuclease VIII-like glycosylase 2 **(NEIL2)**	B	As NTHL1 and NEIL1
	Endonuclease VIII-like glycosylase 3 **(NEIL3)**		FaPyG, FaPyA, prefers ssDNA

U, uracil; *A*, adenine; *T*, thymine; *C*, cytosine; *G*, guanine; *ss,* single stranded; *ds*, double stranded; *5-hm*, 5-hydroxymethyl; *5-FU*, 5-fluorouracil; *ε*, etheno; *5-fC*, 5-formylcytosine; *5-caC*, 5-carboxylcytosine; *8-oxoG*, 8-oxo-7,8-dihydroguanine; *Tg*, thymine glycol; *FaPy*, 2,6-diamino-4-hydroxy-5-*N*-methylformamidopyrimidine; *me*, methyl; *h*, hydroxyl

1.4.4.1.ii APE1

Following removal of the damaged nucleotide, an endonuclease enzyme incises the DNA backbone 5' to the abasic site. This generates a strand break to enable a DNA polymerase to insert the correct complementary nucleotide. The major endonuclease implicated in BER; accounting for over 95 % of the total DNA incising activity within the cell, is APE1 (177). APE1 promotes a hydrolytic reaction to incise the phosphodiester bonds within the DNA backbone. This hydrolytic mechanism is believed to be stabilized by Mg^{2+} ions (106). Knockout rodent models have demonstrated that APE1 expression is essential for survival (94).

Besides its primary endonuclease activity, APE1 also has several other functions. For example, APE1 processes 3'-blocking terminal groups generated by bifunctional glycosylases to enable the progression of BER. Furthermore, APE1 is the major enzyme which removes 3'-phosphoglycolate ends of DSBs (122). Similarly, the 3' to 5' exonuclease activity of APE1 may proofread for insertion of damaged nucleotides or mismatches, during the synthesis stages of the BER pathway (30). Aside to this, APE1 has been shown to act as a redox co-activator of several transcription factors, including p53 and nuclear factor κB (NF-κB), although the precise mechanism of this activity has yet to be resolved (152). It is speculated that APE1 regulates the reduction state of cysteine residues located within regulatory or DNA binding domains of the transcription factors. These two functionalities of APE1 are believed to occur on two distinct domains; a cysteine residue on the N-terminal region of APE1 acts as the redox co-activator of different transcription factors. Whereas, the C-terminal region is largely devoted to incision of the DNA backbone at abasic sites (152, 180).

1.4.4.1.iii End processors

Since the functionality of the glycosylase dictates the chemical groups located on the ends of the incised DNA backbone, this impacts the subsequent stages of BER. For successful insertion of an incoming nucleotide into the abasic site, the terminal groups required are 3'-hydroxyl and a 5'-phosphate. To ensure these groups are present, the terminal ends of the DNA break are subject to processing.

If the damaged nucleotide is removed by a glycosylase with monofunctional activity, then the DNA backbone is incised 3' to the abasic site by APE1. Incision by APE1 generates a 3'-hydroxyl and 5'-deoxyribose phosphate (dRP) terminal group. The 5'-dRP group prevents ligation of the break in the DNA backbone, before the correct

nucleotide has been inserted. The amino terminus of Pol β possesses AP lyase activity, which primarily removes the 5'-dRP blocking group, whilst inserting the complementary nucleotide into the abasic site (99). Both DNA Pol λ and Pol ι can remove the 5'-dRP; although, Pol β is believed to be the dominant polymerase in BER; Pol λ and Pol ι participation may be lesion specific. Removal of the damaged base by a bifunctional glycosylase, results in the formation of a 3'phospho-α, β-unsaturated aldehyde and a 5'-phosphate. The 3'phospho-α, β-unsaturated aldehyde is processed by APE1, to create a 3'-hydroxyl group compatible with insertion of the correct nucleotide.

Alternatively, incision of the DNA backbone during β, δ-elimination of the damaged nucleotide by NEIL glycosylases, results in the formation of a 3'-phosphate and 5'-phosphate groups. The 3'-terminus groups created are not compatible substrates for Pol β and ligation. The 3'-phosphate is processed by PNKP (173). Human PNKP is an enzyme with phosphatase and kinase activity that can be considered as a putative DNA repair enzyme. PNKP can phosphorylate DNA at 5'-hydroxyl termini and dephosphorylate 3'-phosphate termini (173). Unsurprisingly, PNKP is implicated in several DNA repair pathways and interacts with numerous DNA repair enzymes, notably XRCC1 and XRCC4 (173). Through its two catalytic activities, PNKP ensures that DNA termini are compatible with extension and ligation by either removing 3'-phosphates, or by phosphorylating 5'-hydroxyl groups as necessary.

1.4.4.1.iv Polymerase β

A single abasic site flanked by a 5'-phosphate end and 3'-hydroxyl end acts as a substrate for DNA polymerase activity. The major DNA polymerase in BER is Pol β (146), which belongs to the X family of polymerases. Pol β acts as a replicative polymerase to insert the correct nucleotide using the undamaged DNA strand as a template. Upon reaction between the incoming nucleotide and the 3'-hydroxyl group, energy is released in the form of pyrophosphate. As mentioned earlier, Pol β also plays another key role in BER; processing 5'-dRP groups on the ends of DNA strand breaks. In addition, it has been shown that the amino terminal region of Pol β is implicated in binding regions of single stranded DNA. This can direct the polymerase to gaps within DNA and facilitates the synthesis of short regions (1-6 nucleotides long) of DNA (67, 89).

1.4.4.1.v Nick sealing

The final stage of BER relies on sealing the nick inflicted on the DNA backbone. DNA ligase enzymes generate a covalent phosphodiester bond between the 3'-OH end of the upstream nucleotide and the 5'-phosphate end of the downstream nucleotide. To do this, DNA ligases utilise energy of phosphoanhydride hydrolysis to catalyse the formation of the phosphodiester bond, in an ATP or NAD+ dependent manner. The ligases involved in the final stage of BER are Lig I and Lig IIIα. DNA Lig I is an ATP-dependent enzyme and is mainly active in long-patch BER. Whereas, the final stage of short patch BER is completed by the ATP-dependent DNA ligase IIIα. The activity of DNA Lig IIIα is dependent on the presence of the non-enzymatic, scaffolding protein, XRCC1. Indeed, cells deficient in XRCC1 exhibit reduced levels of DNA Lig IIIα, resulting in inadequate repair of SSBs and increased sensitivity to DNA modifying agents (19). It has been suggested that Pol β enhances recruitment of the Lig IIIα-XRCC1 complex, by interacting with XRCC1. Indeed, the activity of Pol β is enhanced by the presence of the Lig IIIα-XRCC1 complex (40, 119).

1.5.1.3. Poly (ADP-ribose) polymerases

Poly (ADP-ribose) polymerases (PARPs) are a family of enzymes that catalyse the transfer of ADP-ribose to target proteins. There are at least 18 members of the PARP family, encoded by different genes. PARPS play key roles in regulating cellular processes including; proliferation, apoptosis and modulation of chromatin structure (108). However, particular PARP isoforms (PARP-1 and PARP-2) are best known for their involvement in DNA repair processes. Evidence for the involvement of PARP enzymes in DNA repair, arises from findings that exposure to DNA damaging agents results in increased PARP activity (108).

Although not directly an end processor, PARP-1 activity has been implicated in BER by stimulating the recruitment of BER proteins to sites of DNA damage (179). Indeed, PARP-1 deficient mice were shown to be increasingly sensitive to carcinogenic agents (157). It is acknowledged that during BER, PARP-1 binds to the abasic site following APE1 incision of the phosphodiester backbone. This is since PARP-1 possesses high affinity for SSBs. It is understood that PARP-1 modulates DNA repair capacity by preserving SSBs and preventing their conversion into DSBs (120, 179), whilst regulating the access of repair proteins (such as Pol β). In this way, PARP-1 is thought to be fundamental to the repair of acute DNA damage. Interestingly, studies advocate that PARP-1 does not inflict a catalytic advantage on the stimulation of BER,

but rather slows down the repair reaction (3). Further to this, it has been shown that PARP-1 is implicated in the latter stages of the BER pathway. It is acknowledged that PARP-1 recruits the Ligase IIIα-XRCC1 complex to SSBs (39). It is believed that PNKP and XRCC1 act to stabilise SSBs whilst the terminal ends are processed (19, 24).

Mechanistic studies have shown that PARP-1 binds to DNA strand breaks as a homodimer which activates its catalytic activity. Interestingly, PARP-1 auto modifies itself via poly ADP-ribosylation, resulting in the accumulation of a negative charge, subsequently leading to PARP-1 dissociation from the DNA. Following PARP-1 dissociation, BER enzymes can then bind to the preserved SSBs (179).

1.4.4.2 Co-ordination of BER

Earlier predictions suggested that the steps of BER progressed via a 'passing the baton' mechanism, whereby, each BER protein would interact with the next BER protein required for the subsequent stage (178). These predictions were based on studies demonstrating that APE1 interacts with Pol β (12), then Pol β interacts with Lig IIIα-XRCC1 complex (119). However, this model does not account for the incorporation of different damage specific glycosylases or end processors. The model was also contradicted by the binding of PARP-1 to SSBs prior to any other BER protein (120). Similarly, XRCC1 was shown to interact with multiple BER proteins irrespective of their order in the pathway (162). The discovery of XRCC1 as a binding protein for multiple BER components provoked the idea of the formation of multi-protein repair complexes. Although, it was anticipated that numerous complexes would need to form in order to manage different types of damage. It is now recognised that removal of DNA damage may be co-ordinated by interactions between damage specific glycosylases and APE1 at the repair site. Following incision of the DNA backbone, the necessary end processors (APE1, Pol β or PNKP) are then recruited. This stimulates the recruitment of a complex of Pol β, Lig IIIα- XRCC1, which complete the BER process (118).

1.4.4.3 BER and cancer

The roles of BER proteins in maintaining genome stability and in the aetiology of human diseases, have largely been examined using knockout models. The models have revealed a correlation between the inactivation of BER proteins and embryonic lethality. For example, deletion of APE1 (181), Pol β (146), FEN1 (82), DNA Lig IIIα

(132) and XRCC1 (151) are fatal to embryonic development. Likewise, haploinsufficiency models of BER proteins APE1, Pol β or XRCC1 showed increased sensitivity to DNA damaging agents and spontaneous tumour formation (23).

Surprisingly, knockout models of individual DNA glycosylase enzymes involved in BER are well tolerated, with only slight increases in mutation frequency (123). This mild phenotypic effect is largely due to redundancy between BER glycosylases and other DNA repair pathways (123). For example, NEIL1 has been shown to act as a back-up glycosylase for the removal of Tg residues in NTH1 knockout mice (78, 149), with deletion of the genes encoding both NTH1 and NEIL1 resulting in increased incidence of tumours compared to the single knockout models (26). Indeed, these results are understandable given the overlapping substrate specificities of the BER glycosylases and highlight the importance of regulating BER within the cell.

Inherited defects of BER have not been associated with any human genetic disorders, although some mutations of BER glycosylases are associated with genomic instability in small scale studies. For instance, a small scale study focused on tumours from individuals affected with multiple colorectal adenomas, without an inherited mutation of the adenomatous polyposis coli gene, contained somatic inactivating mutations of adenomatous polyposis coli, comprising of G:C to A:T transversions. Analysis of MYH, showed that individuals were compound heterozygotes for non-conservative missense variants, resulting in reduced activity of the glycosylase. These observations link the inherited variants in MYH to the pattern of somatic adenomatous polyposis coli mutations and implicate defective BER in predisposition to tumours in humans (2). Similar to this, small-scale studies have shown that nearly 30 % of human tumours express variant DNA Pol β (148). Moreover, a small scale tumour analysis suggested that mutations affecting OGG1 may be associated with lung and kidney tumours (29).

1.5 Human endonuclease III homologue (NTH1)

NTH1 is a bifunctional glycosylase that initiates BER. The enzyme was first discovered in *E.coli*, but is well conserved throughout phylogeny. The human NTH1 glycosylase has broad substrate specificity excising oxidised pyrimidines such as 5-hydroxycytosine, 5-hydroxy-6-hydrothymine, 5-hydroxyuracil and 5-formyluracil (42, 104). Crucially, NTH1 excises Tg (42) which significantly distorts the structural double helix arrangement of DNA strands and blocks the action of replicative polymerases

(76, 165). Unlike its bacterial homologues, human NTH1 also targets ring fragmented purines, or oxidised pyrimidines such as formamidopyrimidine (FaPy) (95).

Characteristic of bifunctional glycosylases, NTH1 possesses inherent AP lyase activity. Alike to other bifunctional DNA glycosylases, the AP lyase activity of NTH1 does not always occur at the same rate as removal of the damaged nucleotide (190). In fact, the rate of the glycosylase activity versus the AP lyase activity is dependent on the nucleobase opposite the damaged nucleobase. With regards to NTH1, the incision of the DNA backbone is 7 times slower than the glycosylase activity when the Tg substrate is opposite an A residue, compared to if the Tg is opposite a G residue (98). Another study, also demonstrated that NTH1 preferentially acts on 5-hydroxycytosine and abasic sites when they are opposite G residues (49). The delayed AP lyase activity of NTH1 may have a protective effect to postpone the formation of DNA strand breaks until suitable downstream processors of the BER pathway are recruited. This is supported by studies showing APE1 circumvents the AP lyase activity of NTH1, increasing its glycosylase activity and dissociation from the abasic site (97).

The efficiency of NTH1 in removing Tg in different orientations on mononucleosomes, that more closely mimic chromatin structure rather than naked DNA, has been examined. Studies show that residues of Tg facing outward from the histone octamer were processed with comparable efficiency to naked DNA, using low concentrations of NTH1, whereas, Tg lesions facing inwards on the nucleosome were removed at a 10-fold decreased rate than free DNA. However, increasing NTH1 concentrations to near physiological concentrations progressively increased Tg excision at inward facing sites (130). Indeed, increasing the concentration of NTH1 to physiological relevance caused Tg excision to reach 48 % relative to that of free DNA (130). This is concurrent with other studies examining processing of alternative substrates in different orientations on nucleosomes by other glycosylases (11).

1.5.1 NTH1 structure, localisation and cell cycle regulation

Elucidation of the crystal structure of the bacterial homologue of NTH1, endonuclease III, using NMR spectroscopy and X-ray crystallography, combined with mutational analysis has provided the structural basis to characterise the DNA binding and catalytic activity of the enzyme (**Figure 11**). It has been determined that the enzyme consists of two α-helical domains which contain five DNA binding motifs, including a Helix-hairpin-helix (HhH) domain and an iron-sulphur 4[Fe-4S] cluster loop (153).

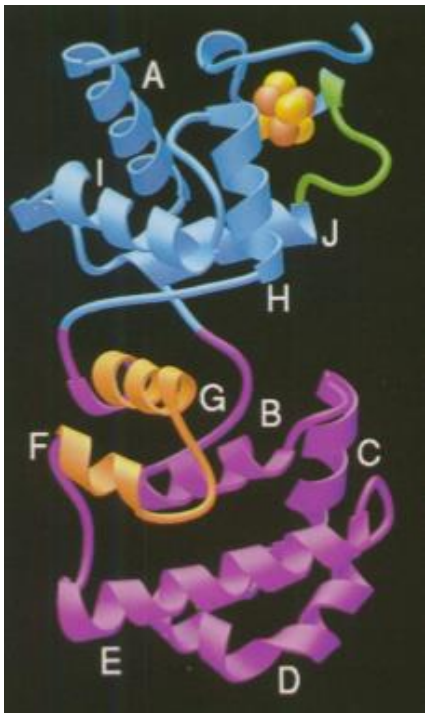

Figure 11. Schematic of the domains and DNA binding motifs of endonuclease III. The bacterial homologue of the human NTH1 enzyme consists of a 6-helix barrel domain (pink), which is made up of antiparallel helices connected in a +1 topology which contains the HhH motif (orange). Helices etA and aHcHzJ and the 4[Fe-4S] cluster (yellow spheres) comprise the 4[Fe-4S] cluster domain (blue) containing the FCL motif (green). Adapted from (Thayer et al. 1995).

These binding motifs are well conserved between bacterial, mouse and human counterparts. Furthermore, structural studies based on sequence conservation between human and bacterial homologues have suggested that Lys-212 is the catalytic residue of human NTH1. Substitution of Lys-212 with Gln-212 inactivated NTH1, although it does not impact its DNA binding ability. Likewise, substitution of Lys-212 with Arg-212 resulted in reduction of the catalytic specificity of NTH1 (68). Despite sharing conserved catalytic residues and DNA binding motifs, human NTH1 differs to its bacterial counterparts, by an extended N-terminal tail of 95 amino acid residues (90) (**Figure 12**). Controlled proteolysis experiments have revealed that the extended N-terminal tail may play an inhibitory role on NTH1 activity. In fact, recombinant NTH1 truncations lacking 55 residues from the N-terminus were 5 times more active than the wild type protein (90). The rate limiting step of most glycosylase enzymes is their dissociation from the abasic site (97). Interestingly, kinetic studies have shown that the activity of human homologues of a number of glycosylase enzymes, including NTH1, is 100 times reduced compared to bacterial enzymes. It has now been considered that the N-terminal extension of human NTH1 may be

responsible for this discrepancy (90). Other kinetic studies using truncations of NTH1 have confirmed that the N-terminal residues are not essential to enzymatic activity, but speculated that they are involved in putative targeting signals or protein interactions (68). These kinetic studies have also revealed other factors regarding NTH1 activity, for example experiments utilising Tg containing substrates show that NTH1 has optimal activity at pH 8 and in 75 mM NaCl. Furthermore, NTH1 is impeded by the presence of divalent cations (68).

The gene encoding human NTH1 has been recognised as *OCTS3* on chromosome 16 (7). There are 3 isoforms of human NTH1, generated by the presence of three start codons within the first 16 amino acids. It is unclear which isoform is transcribed in cells. Studies using HeLa cells confirmed that all NTH1 isoforms are sorted to the nucleus (69, 95) with some levels of cytoplasmic NTH1 believed to be primarily localised to the mitochondria (68). The nuclear localisation of NTH1 is believed to be dependent on the presence of two nuclear localisation signals (69) (**Figure 12**). The cell cycle regulation of NTH1 has been investigated using synchronised cell studies, which noted increased transcription of NTH1 during early and mid S-phase (95). Furthermore, despite recognition of the cell cycle regulation of NTH1, the PTM regulation of NTH1 has not been identified.

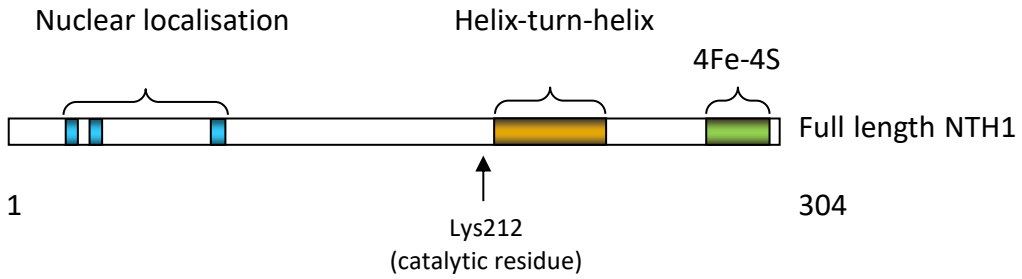

Figure 12. Schematic representation of the proposed structural domains of human NTH1. Based on conserved similarities between bacterial, mouse and human counterparts of the glycosylase enzyme the proposed structural domains of human NTH1 are represented. Compared to the bacterial counterpart, endonuclease III, human NTH1 demonstrates an extended N-terminal region of 95 amino acids. The N-terminal region contains regions signalling for nuclear localisation (blue). Furthermore, NTH1 contains a helix-turn-helix domain (orange) and an iron-sulphur 4[Fe-4S] cluster (green) instigated in DNA binding. Studies based on sequence conservation suggest that Lys-212 is the catalytic residue of human NTH1 (arrow).

1.5.2. NTH1 interactions

Several proteins have been identified that modulate the catalytic activity of NTH1. An *in vitro* yeast-two hybrid screen, identified that the addition of a damage-inducible pluripotent transcription factor, Y-box-binding protein 1 (YB-1), stimulated NTH1 activity. Further analysis suggested that YB-1 stimulated the β-elimination activity of NTH1 by increasing Schiff base intermediate formation (98). The relationship between YB-1 modulating NTH1 activities may suggest a tentative link between the coordination of BER with other cellular processes, including transcription. Likewise, APE1 has also been shown to stimulate NTH1 by circumventing the AP lyase activity of NTH1, increasing its glycosylase activity and dissociation from the abasic site (97). Similarly, direct association of the endonuclease XPG with NTH1 has been shown to promote the binding of NTH1 to base lesion substrates as well as doubling its rate of activity (13). These studies were founded upon the observations that cells from Cockayne syndrome patients with mutations in the XPG gene demonstrate a reduction in repair of Tg (13). Interestingly, XPG is an endonuclease enzyme which plays a critical role in DNA strand cleavage during the NER pathway. With this in mind, the way in which XPG interacts with NTH1 is not fully understood and why it would impact the rate of activity of NTH1 has not been fully comprehended. Similarly, another study investigating this novel interaction also suggested that XPG may serve as a co-factor which promotes the binding of NTH1 to the damaged DNA (80). The fact that this interaction has been observed in multiple studies advances the credibility

that the interaction is relevant. The concept of cross-talk between DNA repair pathways is not entirely irrational as it would make sense for all of the DNA repair pathways to work collaboratively to maintain the genome with optimum efficiency. However, the exact mechanisms behind these interactions need to be fully resolved in order to gain a full insight into the cross-communication between DNA repair pathways.

1.5.3. NTH1 and cancer

As with most BER proteins, the role of NTH1 in relation to human disease, including cancer, has been examined through the use of animal models. As mentioned earlier, murine knockout models of NTH1 display no overt abnormalities, presumably due to compensation by other back up enzymes, such as the NEIL glycosylases (149). It has been suggested that NTH1 and NEIL1 glycosylases display isomer specificity towards Tg substrates (78). In fact, the concept of redundancy between glycosylases is supported by double knockout models (26). Strains of mice lacking both NTH1 and NEIL1 expression ($NTH1^{-/-}NEIL1^{-/-}$) displayed a higher incidence of pulmonary and hepatocellular tumours, compared to single knockouts of NTH1 or NEIL1 alone (26). These results suggest that there is redundancy between BER glycosylases to ensure the accurate repair of base lesions. This is alike to a number of glycosylase deficient mouse models which have proved surprisingly resilient to the loss of the major DNA glycosylase activities (123).

Interestingly, a single nucleotide polymorphism (D239Y) of NTH1 has been identified within 6.2 % of the global population, with 0.6 % of people being homozygous (55). The D239Y variant arises from the substitution of Asp for a Tyr residue within the suspected active site of human NTH1. It is suspected that the Asp residue acts as the active nucleophile enabling the glycosylase activity of NTH1. In agreement with this, studies using oligonucleotides containing oxidised nucleobase substrates demonstrated that the D239Y NTH1 variant lacks glycosylase or inherent lyase capability. This loss of activity has the expected effect when the D239Y NTH1 variant is expressed in cells; resulting in genomic instability, accumulation of DSBs and chromosomal aberrations (55). Expression of the D239Y polymorphism also results in increased sensitivity to damaging agents, such as hydrogen peroxide. Further to this, cells expressing the D239Y variant display increased invasive potential, with increased foci formation and anchorage independent growth (55).

More specifically, another NTH1 germline mutation has been linked to predisposition to familial adenomatous polyposis and colorectal cancer. A whole exome sequencing study using peripheral blood derived DNA revealed a germ line mutation in NTH1 may lead to susceptibility to multiple adenomatous adenomas; precursors of colorectal cancer (175). Of 51 individuals screened, 7 individuals recessively inherited the mutation (encoding Gln 90) resulting in nonsense mediated decay of NTH1. All of the subjects that were homozygous for the NTH1 mutation developed multiple colonic adenomas and 4 individuals had colorectal carcinomas (175). All of the women affected also developed endometrial lesions. Database studies predicted that homozygous inheritance of this trait is likely to occur once in every 75,076 individuals (175).

Altered NTH1 expression has furthermore been linked to development of gastric cancer. A causative factor of gastric cancer is believed to be the accumulation of oxidatively damaged DNA in gastric epithelium. Based on this, NTH1 levels were investigated in 8 gastric cancer cells lines, which revealed reduced NTH1 expression. Furthermore, NTH1 was abnormally localised to the cytoplasm in over 20 % of the primary gastric cancers (58).

1.5.4 Post translational regulation of NTH1

It is well acknowledged that PTMs such as ubiquitylation, phosphorylation, methylation, acetylation or SUMOylation are important mechanisms in the regulation of the BER pathway. It has been shown that PTMs are implicated in the regulation of the levels, localisation, activity and interactivity of BER proteins. The PTM dependent regulation of a number of BER glycosylase enzymes including OGG1, MutY, NEIL2 and MPG have been examined; reviewed in (25). Despite this, PTMs implicated in the regulation of NTH1 have not yet been reported. The only evidence of PTM dependent regulation of NTH1 has arisen from a proteomic screen which documents that NTH1 is subject to intracellular ubiquitylation. However, the biological effect of ubiquitylation of NTH1 protein were not examined further (34).

1.6. The Ubiquitin Proteasome Pathway (UPP)

Ubiquitylation is an essential modification used to modulate the activity of intracellular proteins implicated in nearly all vital cellular processes including the cell cycle, cell signalling, cell survival and DNA repair (127). Ubiquitin, a small 8 kDa protein, composed of 76 amino acids, is used to modify substrate proteins through covalent

attachment to specific lysine residues via an isopeptide bond. In humans, ubiquitin is encoded by 4 genes; two of which *UbB* and *UbC,* encode ubiquitin chains composed of 3-9 repeats of ubiquitin. Free ubiquitin is generated from these gene products by peptidases belonging to family of enzymes termed deubiquitylases (DUBS), of which there are more than 90, which also act to reverse the attachment of ubiquitin on substrate proteins (107).

In general terms, cellular ubiquitin inhabits three different forms; free ubiquitin, activated ubiquitin linked to enzymes involved in the ubiquitylation process and finally conjugated ubiquitin attached to substrate proteins. In mammalian cell lines, most of the ubiquitin is conjugated to substrate proteins (monoubiquitylation; **Figure 13**). Single ubiquitin moieties can also be added to multiple lysine residues (multi-monoubiquitylation). Indeed, in human embryonic kidney HEK293 cells, more than 60 % of the total cellular ubiquitin is conjugated via monoubiquitylation, with approximately half associated with a histone-enriched fraction (75). More than likely, most of this fraction consists of ubiquitylated histone H2A, which is one of the most abundant cellular proteins. In a number of mammalian cell lines, approximately 15 % of all H2A is monoubiquitylated, except during mitosis when the ubiquitin is removed via a highly co-ordinated process using the DUB, USP16 (74).

Further intricacy of ubiquitylation arises from the fact that ubiquitin itself contains seven internal lysine residues (Lys^{6}, Lys^{11}, Lys^{27}, Lys^{29}, Lys^{33}, Lys^{48}, and Lys^{63}), which can themselves be utilised for the attachment of other ubiquitin moieties (**Figure 14**). This leads to the generation of ubiquitin chains (polyubiquitylation; **Figure 13**). Chains of ubiquitin moieties can be linear, composed of the same repeating linkages, or branched ubiquitin chains made up of different linkages, creating different topologies (81). Similarly, a small fraction of linear ubiquitin chains (typically <0.5 % of totally polyubiquitylation), may also be generated by the conjugation of the C-terminal glycine of one ubiquitin to the N-terminal methionine of another ubiquitin moiety (M1-linked) (164). The array of possible combinations of linkages between ubiquitin moieties creates variability in the exposed surfaces available to ubiquitin binding proteins. This permits processing enzymes to demonstrate specificity towards particular linkage types. Thus, distinct chain types are associated with specific biological outcomes and regulation of certain cellular processes. The proportions of possible linkages between ubiquitin chains may vary significantly depending on the cell cycle and following differentiation.

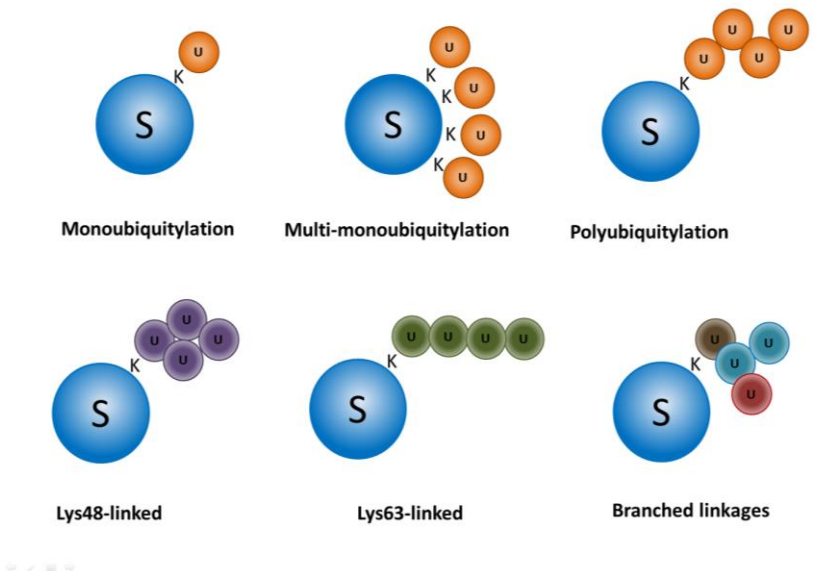

Figure 13. A schematic representation of different topologies of ubiquitylation of a typical substrate protein. Blue spheres represent substrate proteins (S) with attached ubiquitin moieties (U) to specific lysine residues (K). Single moieties of ubiquitin can be added to lysine residues of substrate proteins, which generally influence the localisation, activity or interactivity of the substrate protein. Multi-monoubiquitylation events can also occur whereby individual ubiquitin moieties are attached to multiple lysine residues of substrates. Alternatively, ubiquitin itself also possesses several lysine residues which can attach subsequent ubiquitin molecules, creating chains of ubiquitin moieties, termed polyubiquitylation. Homotypic chains of more than four K48-linked ubiquitin moieties targets substrate proteins for degradation by the 26S proteasome. Homotypic K63-linked ubiquitin chains have been implicated in the formation of complexes with effector proteins. Heterotypic ubiquitin chains composed of multiple linkage types can also be generated which can give rise to branched ubiquitin chains. Heterotypic ubiquitin chains are believed to have multiple biological effects including signal co-ordination. Adapted from (186)

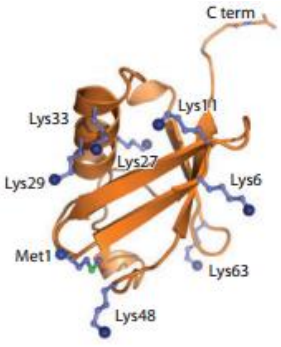

Figure 14. The structure of ubiquitin showing the position of the methionine 1 residue and seven lysine residues (6, 11, 27, 29, 33, 48, 63). Blue spheres represent amino groups implicated in the formation of chains of ubiquitin molecules (81).

Monoubiquitylation events are typically associated with regulation of molecular interactions that affect the localisation, interaction or activity of modified proteins. Generally, this impacts diverse cellular functions such as cell growth, cell division, genomic repair and gene expression. Monoubiquitylation can have opposing effects depending on the substrate protein. For example, monoubiquitylation of PCNA at stalled replication forks promotes its interaction with translesion synthesis DNA polymerases and regulates the translesion synthesis pathway (14). Whereas, monoubiquitylation of a transcription factor termed SMAD4, prevents its interaction with its signalling partner; meaning that monoubiquitylation acts as a regulative step in managing the transforming growth factor β (TGFβ) signalling pathway (44). The TGFβ signalling pathway is implicated in several cellular processes including cell growth, cell division and programmed cell death (44).

Polyubiquitylation of substrate proteins results in a range of outcomes, although one of the major effects is the regulation of protein levels, through ubiquitin signalled degradation. Proteasomal degradation is a crucial mechanism for protein homeostasis and is necessary for the removal of misfolded or damaged proteins. Homotypic linear chains of 4 or more ubiquitin moieties, linked through their Lys^{48} residues, targets proteins for degradation via the 26S proteasome (154). The 26S proteasome consists of a hollow cylinder deemed the 20S protein subunit which is flanked by two 19S regulatory caps. Ubiquitin receptors featured on the 19S subunits recognise and bind to ubiquitylated proteins, which they then unfold in an ATP-dependent manner. Removal of the bulky polyubiquitin chains on tagged proteins is necessary to permit entry of the peptide into the 20S catalytic core. To aid the removal of ubiquitin chains, three DUBS are associated with the 19S subunit of the proteasome; POH1, UCHL5 and USP14. It has been shown that USP14 and UCHL5 activity results in progressive shortening of ubiquitin chains. UCHL5 can cleave both Lys^{48} and Lys^{63} linkage types, whereas USP14 is selective for Lys^{48} linked ubiquitin only (142). Interestingly, UCHL5 or USP14 dependent trimming of ubiquitin chains, appears to delay degradation, resulting in prolonged binding of substrate proteins to the 19S subunit, offering potential exclusion from degradation (142). It has been suggested that this mechanism may act as an important proof-reading mechanism to ensure accurate degradation of cellular proteins. The amino acids and free ubiquitin formed as a result of proteasomal degradation are recycled within the cellular milieu.

Alternatively, homotypic polyubiquitin chains, linked through different lysine residues are associated with non-proteolytic functions. Linear chains of M1-linked ubiquitin moieties have been implicated in the regulation of several innate and adaptive

immune signalling pathways (57, 60). Likewise, it is acknowledged that Lys^{63} linked polyubiquitin chains regulate DNA repair, protein sorting and the innate immune response. In particular, Lys^{63} ubiquitylation has been implicated in the activation of the NF-κB transcription factor which regulate genes involved in immunity, inflammation and cell survival (36, 61). For example, a chain of 3 ubiquitin molecules linked through their Lys^{63} residues are required for the activation of the retinoic acid inducible gene 1 (RIG-1) in response to invading viral RNA, which in turn activates NF-κB (189). Interestingly, unanchored Lys^{63} linked chains can also possess activity and may act as signalling molecules in innate immunity (189). Homotypic polyubiquitin chains connected by Lys^{11} linkages are generally associated with signalling for proteasomal degradation. Although Lys^{11} linkages in the context of mixed ubiquitin chains are associated with regulation of proteins involved in membrane trafficking events, DNA repair and cell signalling (20). It is known that the formation of ubiquitin chains with mixed linkages is dependent on the co-ordination between E2 enzymes, with different linkage specificities. The role of mixed, branched chains of ubiquitin is now beginning to be explored in more detail, however, there is no consensus regarding the cellular effects branched ubiquitin chains induce. For example, it was reported that the addition of Lys^{11} linked branched chains onto particular target proteins by the anaphase-promoting complex, promoted the degradation of cell-cycle regulators during early mitosis quicker than homotypic polyubiquitin chains (103). Whereas, a separate study suggested that substrates tagged with branched ubiquitin chains were degraded slower than those tagged with linear polyubiquitin chain. This suggests that mixed, branched ubiquitin conjugates may impede proteasomal degradation (79).

1.6.1. The ubiquitylation cascade

Ubiquitylation of substrate proteins is implemented by a cascade of enzymes, collectively termed the ubiquitin proteasome pathway (UPP; **Figure 12**). The cascade consists of three main steps accomplished by three types of enzymes; E1 activating enzymes (2 members), E2 conjugating enzymes (approximately 40 members) and E3 ligase enzymes (>600 members). The number of members in each step is not representative of the copy numbers associated with each stage of the UPP cascade; in fact it is estimated that the ratio of E1: E2: E3 enzymes is around 1:3:2 in HeLa cells (83). In HeLa cells the total aggregate of proteins involved in ubiquitylation represents approximately 1.3 % of the total global proteins (83).

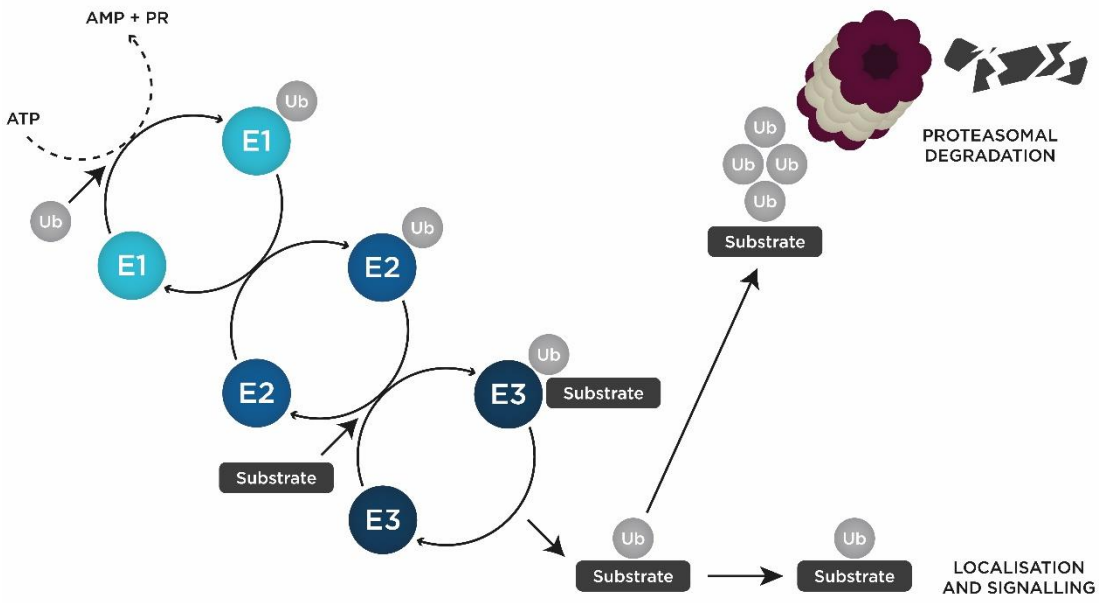

Figure 15. The ubiquitin proteasome pathway (UPP). Ubiquitin (Ub) is activated by E1 activating enzymes (E1) before being transferred to E2 conjugating enzymes (E2), which carries the activated Ub to an E3 ubiquitin ligase enzyme (E3), which facilitates the transfer of Ub from the E2 to a specific lysine residue on the target substrate protein (S). The attachment of one Ub moiety generally impacts signalling or localisation events, whereas, the addition of multiple Ub moieties in certain topologies, can signal for protein degradation by the 26S proteasome.

The first stage of the conjugation of ubiquitin to substrate proteins is instigated by E1 activating enzymes, which utilise ATP in a series of reactions to generate the formation of a thioester bond between the C-terminus of ubiquitin and the catalytic cysteine residue of the E1. In humans, there are two E1 enzymes, UBA1 and UBA6. It is worth noting that UBA1 features in the top 2 % of most abundant proteins in HeLa cells. In proliferating mammalian cells, nearly all UBA1 has ubiquitin bound to its active cysteine (73). Following the attachment of ubiquitin to the E1 enzyme, subsequent structural rearrangements lead to increased affinity for E2 conjugating enzymes, thus, facilitating the transfer of the ubiquitin moiety to the catalytic cysteine residue of an E2 enzyme via a thioesterification reaction. Finally, E3 ligase enzymes assist the transfer of the ubiquitin from the E2 enzyme to the ε-amino group of a lysine residue of a substrate protein via an isopeptide bond (127).

Of the 40 members of the E2 family present in the human genome, 35 of them are dedicated to ubiquitylation. The characteristics that dictate whether the E2 enzyme is confined to monoubiquitylation or polyubiquitylation are not well defined. It has been noted that some E2 enzymes are solely dedicated to building chains of ubiquitin

moieties with specific linkage types, whereas other E2 enzymes demonstrate flexibility in the substrates they are able to interact with. Members of the E2 enzyme family have been subdivided into different classes depending on structural appendages present either side of their catalytic site. These attachments may dictate the activity of the E2 enzymes; for instance, a number of E2 enzymes belonging to the class II category are restricted to monoubiquitylation, potentially because extensions of their N-terminal domains prevent ubiquitin binding (141). Furthermore, a subset of E2 enzymes have demonstrated that they are unable to attach ubiquitin to anything besides other ubiquitin moieties; therefore they are solely dedicated to the extension of ubiquitin chains (187).

There are three main families of E3 ligase enzymes which transfer the ubiquitin moieties onto substrate proteins using different mechanisms. Alike to E2 conjugating enzymes, homologous to E6-AP carboxyl terminus (HECT) and RING between RING (RBR) E3 ligases also possess an active site cysteine residue that binds to the ubiquitin moiety before transferring it to the substrate protein. On the other hand, the most abundant family of E3 ligases lack a catalytic cysteine residue and instead act as adaptor proteins to align the E2 conjugating enzyme with the substrate protein (22). To facilitate this, these E3 ligases feature a type of zinc-finger domain, termed a really interesting new gene (RING) domain, although a few have a U-box domain which is structurally similar to the RING motif but does not coordinate zinc ions. As expected, E2 enzymes bind to a conserved surface of the RING/U-box domains to initiate ubiquitin transfer. Several studies have suggested that dimerization of some RING domains is essential to enable E2 enzyme binding (22). It has also been proposed that RING E3 ligases may act to allosterically activate the E2 enzyme assisting the destabilisation of the thioester bond (116). In most cases, the ubiquitin is transferred from the E2 directly to the amino group of the target lysine, thus in scenarios involving RING E3 ligases the E2 enzyme largely dictates the substrate specificity (5). To some extent, the type of E3 ligase required for ubiquitylation of substrate proteins is dictated by the E2 enzyme, for example UBCH7 (UBE2L3) lacks reactivity to lysine, therefore, is reliant on transfer of ubiquitin via a transthiolation reaction utilising HECT E3 ligases (174).

1.6.2. Ubiquitylation and BER

Over the last few years, there has been increasing evidence demonstrating that ubiquitylation plays a vital role in regulating several DNA repair pathways, including

BER. The specific UPP enzymes involved in the regulation of a number of key BER proteins have been identified and their effects have been examined (25, 48).

Firstly, it is well known that levels of APE1 are regulated through polyubiquitylation of the N-terminal residues of the protein. The major E3 ligase enzyme that instigates this is the ubiquitin protein ligase E3 component n-recognin 3 (UBR3) (102). Initially, the regulation of APE1 via UBR3 was established through the use of *in vitro* assays using APE1 as a substrate with fractionated whole cell extracts which purified candidate E3 ligase enzymes specific to APE1. Then in cells evidence arose from studies demonstrating that mouse embryonic fibroblasts lacking the *Ubr3* gene exhibit amplified levels of APE1, with increased DSB formation as a result (102).

Employment of *in vitro* ubiquitylation assays using cell extracts fractionated via column chromatography has been a key technique to elucidate other E3 ligase enzymes specific to BER enzymes. For example, using Pol β as a substrate, this technique identified carboxyl terminus of Hsc70 interacting protein (CHIP) as the major E3 ligase responsible for polyubiquitylation of Pol β (125). Likewise, using the same technique ARF-BP1/HectH9 (Mule) was also defined as another E3 ubiquitin ligase for Pol β. Although, Mule activity was primarily associated with monoubiquitylation of Pol β at lysines 41, 61 and 81 (126). Interestingly, monoubiquitylation of Pol β retains it in the cytoplasmic compartment of the cell and further acts as a prerequisite for polyubiquitylation via CHIP, which targets it for proteasomal degradation (126). Crucially, this suggests a complex mechanism where monoubiquitylation acts as a cellular marker signalling degradation of excessive BER proteins. In this way, monoubiquitylation enables discrimination between proteins relocating to sites of damage or those suitable for degradation and serves as a fine-tuning mechanism to closely regulate BER protein levels in relation to DNA damage levels. In support of this, it is known that Mule activity is tightly regulated by the tumour suppressor, ARF (27), which upon DNA damage detection translocates from the nucleoli to the cytoplasm, where it inhibits Mule activity. Consequently, monoubiquitylation of Pol β ceases, resulting in reduced CHIP-dependent degradation and ultimately the accumulation of Pol β levels in response to DNA damage (126). The use of *in vitro* assays with chromatography fractions has additionally been utilised to investigate the UPP enzymes involved in reversing ubiquitylation of BER proteins. In this way, the ubiquitin-specific protease 47 was purified as the major DUB activity for Pol β; further expanding our understanding of regulation of key BER components to respond appropriately to genomic damage

levels and prevent instability (121). Currently, USP47 is recognised as the only DUB that has been characterised in controlling the efficiency of BER.

Further investigations have suggested crosstalk between different post translational modifications and ubiquitylation. An example of this is the stabilisation of levels of the end processor, PNKP, due to inhibition of ubiquitylation through phosphorylation of serine residues 114 and 126 by the protein kinase ataxia telangiectasia mutated (124). Phosphorylation of PNKP inhibits ubiquitin dependent proteasomal degradation of PNKP in response to oxidative DNA stress, enabling accumulation of levels of the end processor needed for DNA repair. The candidate E3 ligase was identified as a complex of Cul4a with DNA damage binding protein 1 (DDB1). Specificity of the ubiquitylation reaction was reliant on the presence of serine-threonine kinase receptor associated protein (STRAP) as an adaptor for the Cul4A-DDB1 complex (124). Embryonic murine fibroblasts deficient in STRAP consequently show elevated PNKP levels and resistance to oxidative damage (124).

Despite accumulating evidence of regulation of BER via ubiquitylation, investigations regarding the ubiquitylation dependent regulation of proteins present relatively upstream in the BER process are lacking in comparison to more well characterised BER proteins (25). For instance, ubiquitylation of some glycosylase enzymes (NTH1, MBD4, TDG, NEIL2, and NEIL3) has only been suggested via proteome-wide ubiquitylation screens and not explored further (34). The limitations of such screens resulting in false positives and even undetected candidates should not be overlooked. For instance, proteomic screens did not suggest that OGG1 was subject to ubiquitylation, however, other studies later confirmed that OGG1 is in fact ubiquitylated by the E3 ubiquitin ligase CHIP. Interestingly, mild hyperthermia induced rapid inactivation of OGG1 by relocalisation followed by degradation instigated by CHIP dependent ubiquitylation (52). Another HhH glycosylase, MutYH, has been shown to be ubiquitylated between residues 475-535 by Mule. Experimentation using MutYH with mutated lysine residues demonstrated that ubiquitylation regulates MutYH localisation as well as its degradation (43).

Despite proteome-wide ubiquitylation screens recurrently demonstrating that all members of the uracil DNA glycosylases are potentially regulated by the UPP, candidate E3 ligase enzymes have only been revealed for two members; UNG and SMUG1. Ubiquitylation and subsequent proteasomal degradation of UNG and SMUG1 is instigated by the E3 ligases cullin 1 (Cul 1) and cullin 4 (Cul 4) which is stimulated by binding to the human immunodeficiency virus (HIV) accessory protein

Vpr. This process is hypothesised to facilitate virus replication by reducing the frequency of abasic sites in viral reverse transcripts due to UNG and SMUG1 activity on uracil residues generated by the apolipoprotein B mRNA editing enzyme-3 (140).

Most recently, colleagues within our laboratory successfully purified and identified two E3 ligase enzymes, Mule and TRIM26, instigated in the regulation of the DNA glycosylase, NEIL1 (46). The candidate E3 ligase enzymes were purified from HeLa whole cell extract fractionation using a typical column chromatography approach in combination with *in vitro* ubiquitylation assays. Using this approach two NEIL1 specific ubiquitylation activities were observed and the E3 ligases responsible were identified via nano LC–MS/MS tandem mass spectrometry. Using purified recombinant versions of each E3 ligase it was determined using *in vitro* ubiquitylation assays that Mule activity required the H5 class of E2 enzymes as well as H7. Likewise, recombinant TRIM26 ubiquitylation was dependent on the H5 class of E2 enzymes and on H6. Site-directed mutagenesis of NEIL1, to create mutant NEIL-1 containing sequential lysine to arginine mutations determined that NEIL1 is ubiquitylated at the same seven lysine residues (between 319 and 376) by both Mule and TRIM26 (46). Consistent with observations that both E3 ligases were catalysing the polyubiquitylation of NEIL1, siRNA mediated knockdown of Mule or TRIM26 individually in cells resulted in increased NEIL1 stability. The same experiment was utilised in the presence of increasing levels of DNA-damage induced by ionising radiation to investigate the effects of the E3 ligases in regulating DNA-damage responsive levels of NEIL-1. It was found that decreased expression of TRIM26 had no significant effect on NEIL-1 levels post-irradiation, whereas, knockdown of Mule supressed NEIL1 elevation, demonstrating that Mule activity may indirectly co-ordinate DNA-damage induced levels of NEIL1. Consistent with this result, the radiosensitivity of cells was examined using clonogenic assays and which demonstrated no difference in response to Mule siRNA treatment, whereas, cells with reduced TRIM26 expression were radioresistant. The use of alkaline single cell gel electrophoresis (comet) assays to examine levels of single-stranded DNA breaks post-DNA damage induced by ionising radiation demonstrated no difference upon the siRNA mediated knockdown of TRIM26 expression; suggesting that the increase in NEIL1 levels caused by depletion of TRIM26 do not contribute greatly to the general repair of damaged DNA but may be involved in the repair of specific DNA damage substrates. Overall, it was established that both E3 ligase enzymes purified in this study were important in regulating both the cellular state and DNA damage responsive levels of NEIL1 (46). Despite accumulating knowledge, the regulation of other BER proteins via

ubiquitylation, particularly a number of DNA glycosylases, including NTH1, is unknown.

CHAPTER 2 – PROJECT AIMS

BER is a key DNA repair pathway involved in the maintenance of genome stability, which prevents the development of human diseases including; premature ageing, neurodegenerative diseases and cancer. Observations have documented altered BER protein levels in cells extracted from patients suffering from these diseases. Interestingly, accumulating evidence suggests that PTMs, such as ubiquitylation, can regulate BER protein activity. Investigations regarding understanding the regulation of components of the BER pathway, particularly DNA glycosylases, by ubiquitylation are still limited and the specific UPP enzymes involved remain unclear. As previously stated, proteomic screens have identified that NTH1 is ubiquitylated, but the E3 ligase enzyme(s) implicated in this process have not been examined. Expanding our understanding of the enzymes involved in the ubiquitylation dependent regulation of NTH1, and other BER proteins, may help us to identify particular E3 ligases that control specific classes of BER enzymes, or reveal if each BER protein is regulated by its own unique complement of UPP enzymes. Maximising our knowledge may help to select novel drug targets or small molecule inhibitors, which could be combined with other treatments, such as radiotherapy or chemotherapy, to improve current management of patients with diseases associated with irregular BER protein expression.

The overarching aim of this project is to understand the molecular mechanisms employed by human cells to regulate the steady-state and DNA-damage induced levels of the BER glycosylase, NTH1. Particular emphasis will be focused on the role of ubiquitylation and the ubiquitin E3 ligase enzyme(s) involved. Specifically, the main objectives of the study were to;

1. Purify, identify and characterise the E3 ubiquitin ligase enzyme(s) that ubiquitylate NTH1
2. Elucidate the site-specific lysine residues of NTH1 that are ubiquitylated by the E3 ubiquitin ligase enzyme(s)
3. Determine the role of the identified E3 ubiquitin ligase enzyme(s) in controlling the cellular steady state and DNA-damage responsive protein levels of NTH1.
4. Understand the impact of the ubiquitylation dependent regulation of NTH1 on DNA damage repair kinetics and sensitivity to oxidative stress.

CHAPTER 3 – MATERIALS AND METHODS

3.1. Materials

3.1.1. Reagents

General laboratory reagents were obtained from either Bio-Rad Laboratories Ltd (Hertfordshire, UK), Fisher Scientific (Loughborough, UK) or Sigma Aldrich (Poole, UK) as stated. Chromatography columns were obtained from GE Healthcare (Little Chafont, UK). The CHT ceramic hydroxyapatite was obtained from Bio-Rad (Hertfordshire, UK).

3.1.2. Plasmids and proteins

Histidine tagged recombinant NTH1 was generated from the pET28a plasmid (**Figure 16**) containing the coding sequence for *NTH1* (starting at Met9, since the consensus in the literature is that this represents the translational start) that was kindly provided by Dr. Sarah Allinson (Lancaster University). Mutant NTH1 was generated from this by creating truncated versions of NTH1 using cloning techniques, or via site directed mutagenesis. The mammalian expression plasmid for TRIM26 was kindly provided by Prof A. Garcia-Sastre (The Icahn School of Medicine at Mount Sinai, USA). The full-length cDNA for *TRIM26* was re-cloned from this into a pET28a bacterial expression plasmid by ligation-independent cloning (LIC) (46). Full length *NTH1* cDNA was also re-cloned from the bacterial expression vector using the same approach into a pCMV-Tag3a vector for mammalian expression. A partial intracellular expression of human influenza hemagglutinin (HA) tagged ubiquitin was generated from the mammalian expression plasmid PMT-HA-Ub.

His-tagged recombinant NTH1 and TRIM26 were overexpressed in Rosetta (DE3) pLysS bacterial cells (Merck-Millipore, Watford, UK) and the proteins purified using HisTrap column chromatography (GE healthcare, Little Chafont, UK). TRIM26 was additionally purified using ion exchange (Mono Q 5/5 GL) chromatography (GE Healthcare, Little Chalfont, UK).

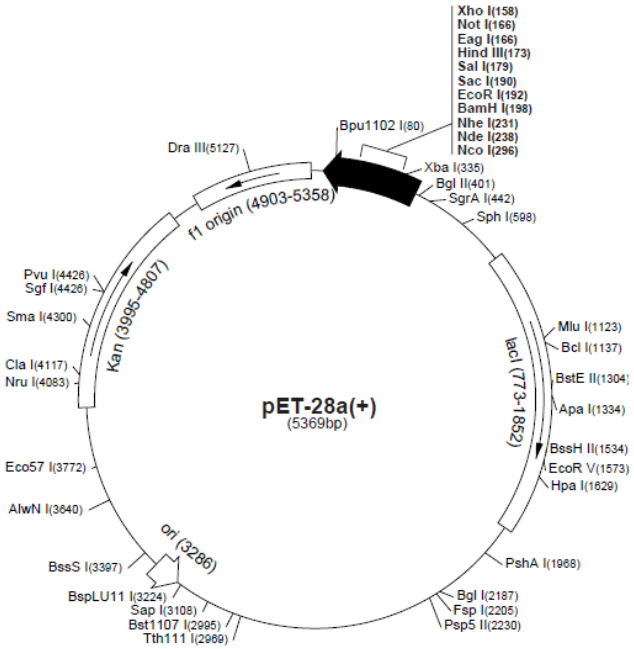

Figure 16. Schematic of the pET28a bacterial expression vector used for recombinant protein expression. The pET28a bacterial expression vector was obtained from Novagen (Middlesex, UK). Target genes are cloned into pET plasmids under control of strong bacteriophage T7 transcription and expression induced by providing a strong source of T7 RNA polymerase in the host cell. The pET28 vector carries an N-terminal Histidine tag/thrombin/T7 tag configuration.

3.1.3. Antibodies

The reactivity and source of the primary antibodies used throughout this study are summarised in **Table 2**. Antibodies were used to probe for the presence and expression levels of specific proteins analysed via Western blotting. The dilutions of each antibody for Western blotting are also detailed in **Table 2.**

Table 2. A summary of the primary antibodies used. The reactivity, dilution and molecular weight of each primary antibody used throughout are detailed below. The source of each primary antibody is also provided.

Antibody	Reactivity and clonality	Dilution	Source
Actin	Mouse monoclonal	1:20,000	Sigma Aldrich
Histidine-tag	Mouse monoclonal	1:1000	Millipore
Mule	Rabbit polyclonal	1:2000	Bethyl Labs
HA Tag	Rabbit polyclonal	1: 10,000	Abcam
Lamin A/C	Mouse monoclonal	1:1000	Santa Cruz
NTH1	Mouse monoclonal	1:1000	Abcam
NTH1	Rabbit polyclonal	1:1000	Santa Cruz
TRIM26	Mouse polyclonal	1:500	Abcam
TRIM26 - N-terminal	Rabbit polyclonal	1:250	Abcam
Tubulin	Mouse monoclonal	1:10,000	Sigma
Ubiquitin	Mouse monoclonal	1:5,000	Abcam
Ubiquitin	Rabbit polyclonal	1:1000	Santa Cruz

The secondary antibodies used throughout this study are summarised in **Table 3.** Fluorescently tagged secondary antibodies were applied to Western blotting membranes (Sigma Aldrich, St. Louis, Missouri, USA) after primary antibody incubation. The corresponding reactivity was selected so that the secondary antibody bound to the primary antibody.

Table 3. A summary of the secondary antibodies used. The reactivity, source and dilutions used for Western blotting are detailed below.

Antibody	Dilution	Source
Alexafluor 680 goat anti-mouse IgG	1:10 000	Invitrogen
Alexafluor 680 goat anti-rabbit IgG	1:10 000	Invitrogen
IR dye 800 goat anti-mouse IgG	1:10 000	Li-Cor
IR dye 800 goat anti-rabbit IgG	1:10 000	Li-Cor

3.1.4. Cells

HeLa, human colon carcinoma (HCT116$^{p53\ +/+}$) cells and human female osteosarcoma (U2OS) cells were cultured as a monolayer in Dulbeccos Modified Eagle Medium (DMEM) with HEPES modification, 4500 mg/L glucose, 25 mM HEPES and sodium bicarbonate further supplemented with 10% fetal bovine serum (FBS, non-USA origin, sterile filtered), 2 mM L-glutamine, 100 U penicillin, 0.1 mg streptomycin and 1 %

MEM non-essential amino acid solution (all tissue culture reagents obtained from Sigma Aldrich St. Louis, Missouri, USA). All cell culture work was performed using aseptic technique in a class II hood with laminar flow, cleaned with 70 % ethanol before each use. All plastics used were of tissue culture grade. Other cell culture reagents include; Dulbecco's PBS and Trypsin -EDTA solution 0.25 % (2.5 g porcine trypsin and 0.2 g EDTA. 4Na /L of Hank balanced salt solution with phenol red). All cell culture solutions were warmed at 37°C in a water bath prior to use. All cells were stored in a humidified cell culture incubator at 5 % CO_2 at 37°C.

3.1.5. Primers

3.1.5.1. Ligase independent cloning (LIC) primer sequences

LIC primers were used to produce bacterial expression plasmids for TRIM26, full-length NTH1 and truncated versions of NTH1 in a pET28a backbone (**Table 4**). They were also used to generate mammalian expression plasmid, pCMV3Tag3A, containing TRIM26 and full-length NTH1, which were used to induce a partial overexpression of these proteins in cells (**Figure 17**). A summary of the LIC cloning primers used is provided in **Table 3**. All primers were obtained from Eurogentec (Seraing, Belgium).

Table 4. A summary of the custom ligase independent cloning (LIC) oligonucleotides used throughout this study. The target gene, primer sequence for both forward and reverse are shown in the table. All primers were obtained from Eurogentec (Seraing, Belgium).

Mutant	Forward LIC oligonucleotide sequence (5'-3')	Reverse LIC oligonucleotide sequence (5'-3')
TRIM26	TACTTCCAATCCATGGCCAC GTCAGCCCCACTAC	TATCCACCTTTACTGGGGGTCTTA GCAGGAGGCGTGTTC
pET28a	AGTAAAGGTGGATACCCCGA ATTCGAGCTCCGTCGAC	ATGGATTGGAAGTACCCGCTGCT GCCCATGGTATATCTCC
pCM3Tag3A	AGTAAAGGTGGATACCATCG ATACCGTCGACCTCGAGGAT	ATGGATTGGAAGTACCCGTGGAG CTCCAGCTTTTGTTCCC
NTH1	TACTTCCAATCCATGTGTAGT CCGCAGGAGTCCG	TATCCACCTTTACTGGGAGACCCT GGGCGGCCG
9-93	TACTTCCAATCCATGTGTAGT CCGCAGGAGTCCG	TATCCACCTTTACTGGTCAGGCAC GGATGTTGACCAGCTG
9-174	TACTTCCAATCCATGTGTAGT CCGCAGGAGTCCG	TATCCACCTTTACTGGTCACCAGA AACCGACGG-GGTAGATGAG
185-305	TACTTCCAATCCATGGCCATC CTGCAGCAGCACTAC	TATCCACCTTTACTGGGAGACCCT GGGCGGCCG
99-305	TACTTCCAATCCATGGCACCT GTGGACCATCTGGGG	TATCCACCTTTACTGGGAGACCCT GGGCGGCCG

3.1.5.2. Site-directed mutagenesis primers

Site-directed mutagenesis primers were used to generate pET28NTH1 containing point mutations at specific lysine residues. Lysine residues were replaced with arginine residues. The pET28NTH1 plasmid was kindly provided by Dr. Sarah Allinson (Lancaster University). All primers were obtained from Eurogentec (Seraing, Belgium). A summary of the site-directed mutagenesis primers used throughout this study is provided in **Table 5**.

Table 5. A summary of the custom site directed mutagenesis oligonucleotides used throughout this study. The target gene, primer sequence for both forward and reverse are shown in the table. All primers were obtained from Eurogentec (Seraing, Belgium).

Mutant	Forward oligonucleotide sequence (5'-3')	Reverse oligonucleotide sequence (5'-3')
K42R	CAGAAGCGAGGAGAAGCCACAGCCCC	GGGGCTGTGGCTTCTCCTCGCTTCTGC
K48R	ACAGCCCCGTGAGGCGTCCGCGG	CCGCGGACGCCTCACGGGGC
K52R	GCGTCCGCGGAGAGCACAGAGACTGC	GCAGTCTCTGTGCTCTCCGCGGACGC
K48, 52R	GCCCCGTGAGGCGTCCGCGGAGAGCACAG	CTGTGCTCTCCGCGGACGCCTCACGGGGC
K67R	GGGCTCGGACAGTGAGAGAGGTGAGGG	CCCTCACCTCTCTCACTGTCCGAGCCC
K245, 246R	CTGAGGTGGACCAGGAGGGCAACCAAGTCCC	GACTTGGTTGCCCTCCTGGTCCACCTCAGCC
D239Y	CAGGCATTGCAGTGTACACGCATGTGCACAG	CTGTGCACATGCGTGTACACTGCAATGCCTG

3.1.5.3. Real-time PCR primer sequences

Real time PCR primers were employed to measure the efficiency of an siRNA mediated knockdown of TRIM26 in HCT116$^{p53+/+}$ human colon carcinoma cells. Actin was used as an expression control and all results were normalised to this CT value. The primer sequences are in **Table 6**.

Table 6. Real-time primer sequences used for target gene. The target gene, primer sequence for both forward and reverse and the length of the target sequence of gene are shown in the table. All primers were obtained from Eurogentec (Seraing, Belgium).

Gene	RT-PCR primer sequence	Amplicon (bp)	Source
TRIM26	Forward. 5'-CCA-TGG-ATC-TAT-AGG-AGA-GCA-AG-3' Reverse. 5'- CAG-CTC-CAG-CAC-TCA-GTC-AA-3'	71	Eurogentec
Actin	Forward.5'-AGGCACCAGGGCGTGAT-3' Reverse.5'-CGCCCACATAGGAATCCTTCT-3'	52	Eurogentec

3.2. Methods

3.2.1. Measuring protein and DNA concentration

Protein concentrations were measured by the Bradford Assay using Bio-Rad Protein assay reagent (Bio-Rad, Hertfordshire, UK) for measurement at an optical density (OD) of 595 nm using a UV spectrophotometer (Cecil CE 2021 2000 series). A standard BSA protein sample (0.2 mg/ml) was used as a reference to calculate the protein concentration using the following calculation:

$BSA = 0.2/Ab_{BSA} = V$
Samples concentration = V X Ab_{sample} x dilution factor

Where applicable, protein or DNA concentration of samples was measured using the Nanodrop ND-1000 spectrometer (software version V3.7.1) purchased from Thermo-Scientific (Massachusetts, USA).

3.2.2. Sodium dodecyl sulphate polyacrylamide gel electrophoresis (SDS-PAGE) and Western blotting

3.2.2.1. SDS-PAGE

Proteins extracts (typically 40 µg) or *in vitro* ubiquitylation reactions were separated via sodium dodecyl sulphate polyacrylamide gel electrophoresis (SDS-PAGE). The separating portion of SDS-PAGE gels was prepared by mixing 377 mM Tris HCl (pH 8.8), 0.2 % SDS, 2 mM EDTA, 6 % or 10% or 16% acrylamide/bis solution (30:0.8) from Bio-Rad Laboratories (UK), 1 % APS and 0.1% TEMED, made up to a final volume with distilled water. Three quarters of a 1.5 mm gel cassette (Fisher Scientific, Loughborough, UK) was filled with the separating solution. A volume of 100 % ethanol

was layered on top whilst the gel set. The acrylamide percentage (6 %, 10 % or 16 %) was selected depending on the molecular weight (kDa) of protein being analysed. The ethanol was removed by washing with distilled water before the 5 % stacking gel consisting of; 62.5 mM Tris HCl (pH 6.8), 0.2 % SDS, 2 mM EDTA, 5 % acrylamide/bis solution (30:0.8), 10 % APS, 1 % TEMED, made up to final volume with distilled water, was added to the remaining quarter of the gel cassette and either a 10-well or 15-well comb added before setting.

Protein samples, extracts or reactions were diluted in SDS-PAGE loading buffer (25 mM Tris pH 6.8, 1 % SDS, 10 % glycerol, 2.5 % mercaptoethanol, 0.5 mg/ml bromophenol blue and 1 mM EDTA) and proteins were denatured by heating at 95°C for 5 mins before being loaded onto the polyacrylamide gel. Electrophoresis was performed at 125 V for 2 h in 1x Tris-glycine SDS running buffer (0.025 M Tris, 0.192 M glycine, and 0.1 % SDS, pH 8.3) (Fisher Scientific UK, Loughborough, UK). The Precision Plus Protein All Blue Pre-Stained Protein Standards (Bio-Rad, Laboratories Ltd) were used as standard markers ranging from 10 kDa to 250 kDa. Following SDS-PAGE, protein levels were analysed via protein staining or Western blotting.

3.2.2.2. SDS-PAGE gel protein staining

The SDS-PAGE gel was rinsed in distilled water and incubated in Instant Blue (Expedeon, San Diego, California, USA) on a rotating platform for 1 h. The gel was then washed in 1x PBS until the background intensity was reduced. The gel was imaged using the Odyssey image analysis system (Li-Cor Biosciences, Cambridge, UK).

3.2.2.3. Western blotting

Proteins were transferred from an SDS-PAGE gel onto an activated Immobilon-FL polyvinylidene diflouride (PVDF) membrane (Millipore, Watford, UK). The PVDF membrane was activated by washing in 100 % methanol for 15 sec, distilled water for 2 min followed by SDS-transfer buffer (25 mM Tris pH 8.3, 192 mM glycine, 20 % methanol). Electrophoresis was carried out at 25 V for 90 min in SDS-transfer buffer. The PVDF membrane was blocked in Odyssey blocking buffer (Li-Cor Biosciences, Cambridge, UK) diluted 1:1 in PBS for 1 h at room temperature. Blocking buffer was removed and the membrane was probed with the relevant primary antibody diluted to the recommended concentration (See **Table 2**) in Odyssey blocking buffer and PBS (1:1), 0.1 % Tween-20 and incubated on a rotating platform overnight at 4°C. The

membrane was washed thrice for 5 min in PBS containing 0.1 % Tween-20 solution. The membrane was probed for 1 h at room temperature with the appropriate secondary antibody diluted in Odyssey blocking buffer and PBS (1:1) containing 0.1% Tween-20 to the recommended concentration (See **Table 3**). The membrane was washed twice for 5 min in PBS containing 0.1 % Tween-20 solution with an additional 5 min wash in PBS to finish. Proteins were visualized and quantified using the Odyssey image analysis system (Li-cor Biosciences, Cambridge, UK).

3.2.3 Transformation of competent cells

DH5α cells (Invitrogen, Waltham, Massachusetts, USA) or Rosetta2 (DE3) pLysS (Merck-Millipore, Watford, UK), were thawed on ice and mixed gently using a pipette tip. DH5α cells were transfected with 1 ng of purified plasmid (or one tenth of a PCR reaction) and incubated on ice for 30 min. The cells were then heat shocked at 42°C for 20 s then returned to ice for a further 2 min. To this, pre-warmed (to 37°C) lysogeny broth (LB) (2.5 % w/v LB granule, 0.5 % (w/v) NaOH, pH 7.2) (Fisher Scientific UK, Loughborough, UK) was added and cells incubated at 37°C in a shaking incubator for 1 h. From this, 100 µl was removed and spread onto LB agar plates (2.5 % w/v LB granules, 1.5 % w/v agar, 0.5 % NaOH) containing the correct selective antibiotic; 50 µg/ml ampicillin or 34 µg/ml kanamycin (Fisher Scientific UK, Loughborough, UK). These plates were inverted and incubated at 37°C for 12 h. Colonies were selected and grown overnight in 5 ml LB containing 50 µg/ml ampicillin or 34 µg/ml at 37°C on a shaking platform, at 225 rpm, overnight.

3.2.4. Site-directed mutagenesis

DNA was prepared by PCR reactions containing 250 pg/µl of the plasmid of interest incubated with 0.3 µM of forward primer, 0.3 µM of reverse primer, 1x Phusion buffer, 200 µM dNTPs and 0.02 U/ µl high fidelity Phusion polymerase. PCR reactions were performed by 1 cycle at 98°C for 2 mins, followed by 18 cycles of; 98°C for 2 mins, 55°C for 1 min, 72°C for 5 min, followed by a final extension 72°C for 20 min.

The PCR products were transformed into DH5α cells (**Section 3.2.3**) and selected for by growth on LB agar plates containing the correct selective antibiotic; 50 µg/ml ampicillin or 34 µg/ml kanamycin. These plates were inverted and incubated at 37°C for 12 h. Colonies were selected and grown overnight in 5 ml LB containing 50 µg/ml ampicillin or 34 µg/ml at 37°C on a shaking platform, at 225 rpm, overnight. Plasmid DNA was then extracted from bacterial contaminants by mini-prepping (**Section**

3.2.9). The success of the site directed mutagenesis reaction was confirmed by sequencing the purified plasmid using the Sanger Sequencing Service provided by Source Bioscience (Nottingham, UK).

3.2.5. Analysis of PCR products using agarose gels

Broad range agarose was prepared at 1 % in Tris-acetate-EDTA (TAE) buffer. Samples were diluted in 6x DNA loading dye, loaded onto the gel and electrophoresed at 75 V for 1 h in a Mini Gel Tank. All reagents and Mini Gel Tanks were obtained from Thermo Fisher Scientific (Cheshire, UK, WA7 1TA).

3.2.6. Purifying DNA from bacterial cultures

The overnight cultures were then centrifuged at 5000 x g for 5 min and supernatant removed. The DNA was purified using the QIAprep® Spin Miniprep Kit, manufacturer's protocol (Qiagen, Manchester, UK) and eluted in TE buffer. The concentration of the DNA was measured using a Nanodrop ND-1000 spectrometer (software version V3.7.1), (Thermo Scientific, Runcorn, UK) at a wavelength of OD_{230}

3.2.7. Preparation of purified NTH1

3.2.7.1. Overexpression of histidine-tagged NTH1

Histidine-tagged pET28a NTH1 plasmid (provided by Dr Sarah Allinson, The University of Lancaster) was transformed into Rosetta2(DE3) pLysS bacterial cells and plated onto LB agar plates containing 30 µg/ml kanamycin and 34 µg/ml chloramphenicol. A colony was selected and cultured overnight with 5 ml LB, composed of 10 g/L Tryptone, 5 g/L yeast extract and 10 g/L sodium chloride (Fisher Scientific UK, Loughborough, UK). To this, 30 µg/ml kanamycin and 34 µg/ml chloramphenicol were added to select for resistant NTH1 plasmid amplification only. If the culture appeared turbid 300 µl culture was transferred to 30 ml LB with 30 µg/ml kanamycin and 0.1 % glucose added and grown at 37°C at 225 rpm shaking until turbid (OD_{600} ~ 0.6 to 0.8). The entire culture was expanded to 300 ml with LB containing antibiotic plus glucose, then incubated with shaking until turbid (OD_{600} 0.6 to 0.8). Protein expression was induced with 1 mM IPTG and incubated at 30°C with shaking for 3 h. The culture was centrifuged at 5000 x g for 2 mins, the supernatant aspirated, and pellets were then stored at -80°C.

3.2.7.2. Purification of histidine-tagged NTH1

The bacterial cell pellet containing overexpressed His-tagged NTH1 was resuspended in lysis buffer [(25 mM Tris-HCl (pH 8), 0.5 M NaCl, 5 % glycerol, 5 mM imidazole, pH 8 (Sigma Aldrich St. Louis, Missouri, USA), 1 mM PMSF and 1 µg/ml of each protease inhibitor; leupeptin, chemostatin, pepstatin and aprotinin)]. Then, 2 mg lysozyme was added and the cells were incubated on ice for 15 min. Cells were lysed by sonication for 3x15 sec pulses with 30 sec intervals on ice. Lysates were transferred to 50 ml Oakridge tubes and centrifuged at 23,000 x g for 20 min at 4^{O}C. The supernatant was collected and filtered through a 1 µM syringe pre-filter, and then a 0.45 µM syringe filter. A 1 ml HisTrap column (GE Healthcare, Little Chalfont, UK) was attached to the AKTA purifier FPLC and the column washed in the same lysis buffer as above with 0.1 mM PMSF added. The lysate was added to the column and washed thoroughly until no more protein eluted. Bound proteins were collected by 20 ml gradient elution using elution buffer (25 mM Tris-HCl pH 8, 0.5 M NaCl, 5 % glycerol, 500 mM imidazole and 0.1 mM PMSF) collecting 0.5 ml fractions. Fractions were subject to analysis by SDS-PAGE and Western blotting with anti-NTH1 antibodies to select fractions containing purified his-tagged NTH1. Fractions containing NTH1 were concentrated using Amicon Ultra 15 ml centrifugal concentrators (10 kDa MWCO) in a swinging bucket rotor at 4000 x g at 4^{O}C until the volume reached approximately 500 µl. This volume was then made up to 1 mL in JPDB buffer (50 mM Tris HCl pH8, 50 mM KCl, 1mM EDTA, 10 % glycerol) and concentrated once more at 4000 x g at 4^{O}C. This process was repeated twice more to buffer exchange the fractions.

3.2.8 Preparation of purified recombinant histidine-tagged TRIM26

3.2.8.1. Generation of a pET28TRIM26 bacterial expression plasmid

A LIC strategy (6) was employed to generate an expression construct for histidine-tagged recombinant TRIM26 in a pET28a bacterial expression vector (Novagen). During LIC cloning, the vector DNA and inserts are PCR amplified separately using custom primers designed with flanking LIC sequences (**Figure 14**). LIC cloning then employs the 3’ to 5’ exonuclease activity of T4 DNA polymerase to create specific complementary overhangs, typically of 10-15 bases, between the insert and expression vector (**Figure 17**). The annealing of the insert and the vector is then performed by simply mixing the DNA fragments at different ratios and does not require

the need for a ligase enzyme (**Figure 17**). The process is typically very effective as only the desired product can form.

An empty pET28a vector (from Novagen), was amplified using relevant oligonucleotides flanked by corresponding LIC sequences (**Table 4**). Aside to this, an insert of histidine-tagged TRIM26 was PCR amplified from a mammalian expression plasmid containing a TRIM26 insert (kindly provided by Prof A. Garcia-Sastre, The Icahn School of Medicine at Mount Sinai, USA) using relevant oligonucleotides flanked by corresponding LIC sequences (**Table 4**).

PCR amplification of each component was performed by incubation of 5 ng of template DNA with 200 µM of each dNTP (A, T, G and C) and 1x HF Phusion buffer (1.5 mM $MgCl_2$, F-518L, Thermo Fisher Scientific, Runcorn, UK) or 1x GC Phusion buffer (1.5 mM $MgCl_2$, F-519L, Thermo Fisher Scientific, Runcorn, UK), with 0.02 U/µl Phusion High-fidelity DNA Polymerase. These were mixed with 0.5 µM of custom forward and reverse primers in a final reaction volume of 50 µl which was made up with nuclease-free water. The Phusion High-fidelity DNA Polymerase and corresponding Phusion buffers were obtained from Thermo Fisher Scientific (Runcorn, UK). Custom primers were obtained from Eurogentec (Southampton, UK). Reactions were mixed briefly on a vortex shaker before being incubated at 98°C for 2 min, followed by 30 cycles of; 98 °C for 30 s, 57°C for 30 s and 72°C for 30 s per kb of DNA. The reactions were then finished with a final incubation at 72°C for 5 min.

The size of the amplified DNA products was analysed using agarose gels before methylated template DNA was then removed via incubation with 0.1 µl of the restriction enzyme DpnI (10 U/ µl, Thermo Fisher Scientific, Runcorn, UK) for 1 h at 37°C. Cohesive ends were then formed by exploiting the 3' to 5' exonuclease activity of T4 DNA Polymerase. To each PCR reaction, 0.5 µl of T4 DNA Polymerase (5 U/µl, Thermo Fisher Scientific, Runcorn, UK) was added with 1 mM DTT, 1.5 mM BSA and 5 µl DNA sample. For vector DNA 0.5 mM dGTPs were added to this reaction, whereas 0.5 mM dCTPs were incubated with insert DNA. This enabled the polymerase activity of T4 DNA polymerase to be engaged whilst retaining complementary overhangs. The T4 DNA polymerase reactions were heated at 22°C for 30 min, then 80°C for 30 min. The complementary overhangs were used to anneal the vector and insert DNA by incubation at 22°C for 10 mins at a ratio of 1:1 or 1:3 (vector: insert).

The pET28TRIM26 plasmid from the LIC reaction was then transformed into library efficient DH5α cells according to manufacturer's instructions (Thermo Fisher

Scientific, Runcorn, UK) and grown on antibiotic containing agar plates overnight at 37°C. Colonies were inoculated into 5 ml of LB media containing selective antibiotic. Plasmid DNA (ranging from 70 bp to 10 kb), was then purified using the QIAquick PCR Purification Kit (250) obtained from Qiagen Ltd (Manchester, UK) to remove excess primers, enzymes and other impurities. Plasmid DNA was sequenced via the Sanger Sequencing Service provided by Source Bioscience (Nottingham, UK). Chromatographs were analysed using the BioEdit Sequence Alignment Editor and the sequence checked via alignments using the multiple sequence alignment tool, Clustal Omega (101).

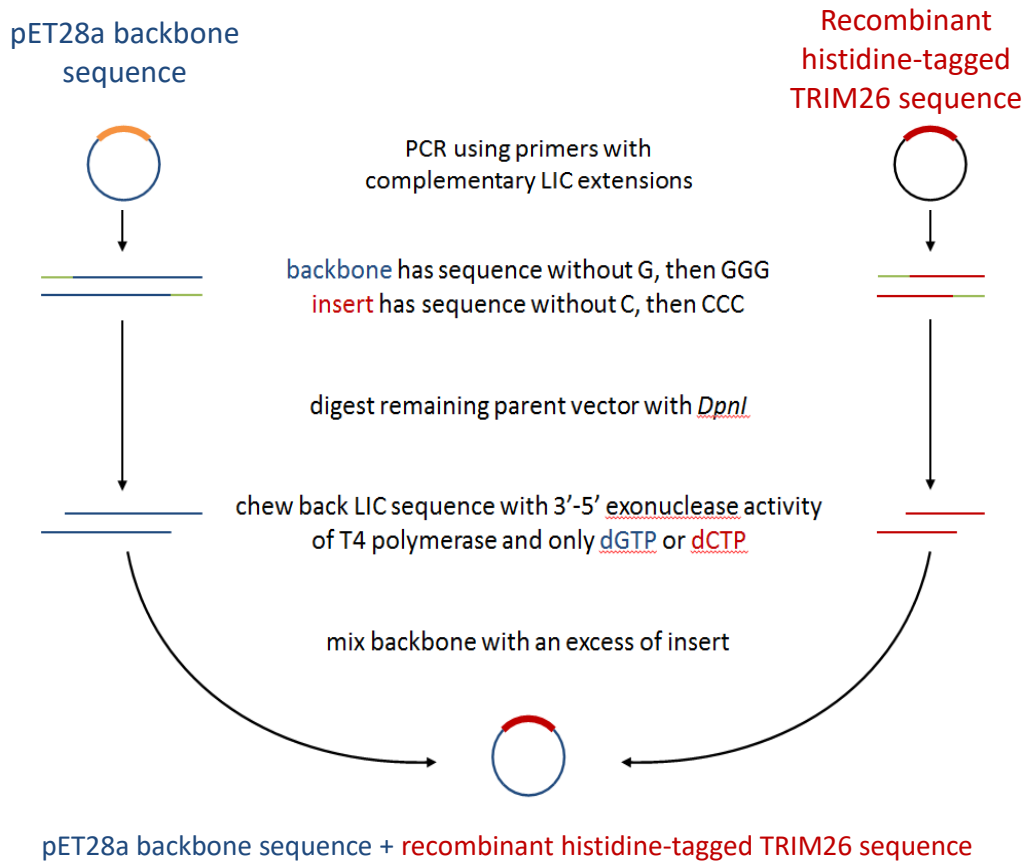

Figure 17. Schematic of Ligase Independent Cloning (LIC). LIC cloning is a technique used to generate expression constructs of interest. The process exploits the 3' to 5' exonuclease activity of T4 DNA polymerase. The vector sequence and the insert of interest are PCR amplified separately using oligonucleotides with flanking complimentary sequences. The parental DNA is then removed via digestion using DPN1. The 3' to 5' activity of T4 polymerase is then utilised to create complementary overhangs between the two components. These complementary overhangs are maintained when the polymerase activity of the T4 polymerase is engaged by incubating them in the presence of one DNA base group only. For vector DNA 0.5 mM dGTPs were added to the reaction, whereas 0.5 mM dCTPs were incubated with

insert DNA. The two amplification products are then annealed by simply mixing and incubating different ratios of the two components. The process is generally effective due to the specific overhangs generated, meaning only one product can form.

3.2.8.2. Test overexpression of histidine-tagged TRIM26

Initially a test expression was performed to establish the bacterial cells which gave the maximal recombinant TRIM26 expression. The pET28TRIM26 construct was transformed into a range of Rosetta cells; Rosetta 2(DE3) pLysS cells, Rosetta 2 cells, Rosetta-blue cells, Rosetta-gami cells and Origami 2 (DE3) cells. These were then grown in a 5 mL culture of LB media containing the following selective antibiotics; 50 µg ampillin, 30 µg kanamycin, 34 µg chloramphenicol, and grown overnight at 37°C and 250 rpm. Following this, a 40 mL culture was generated in the presence of 150 µg selective antibiotic incubated at 37°C and 250 rpm, until the OD_{600nm} was approximately 0.6. An aliquot of the cell suspension was removed before protein expression was induced via 1 mM IPTG for 3 h at 37°C and 250 rpm. An aliquot of the induced cell suspension was then removed. The aliquots of cell suspension before and after IPTG induction were re-suspended in SDS loading buffer and loaded onto a 10% SDS-PAGE gel for analysis of cellular proteins. Samples pre-IPTG and post-IPTG were analysed in tandem.

3.2.8.3. Overexpression of histidine-tagged TRIM26

His-tagged pET28a TRIM26 plasmid was transformed into Rosetta2(DE3) pLysS bacterial cells and plated onto LB agar plates containing 30 µg/ml kanamycin and 34 µg/ml chloramphenicol. A colony was selected and cultured overnight with 5 ml LB composed of 10g/L Tryptone, 5g/L Yeast extract and 10g/L Sodium Chloride (Fisher Scientific UK, Loughborough, UK). To this, 30 µg/ml kanamycin and 34 µg/ml chloramphenicol were added, to select for resistant TRIM26 plasmid amplification only. If the culture appeared turbid 300 µl culture was transferred to three 30 ml LB cultures with 30 µg/ml kanamycin, and 0.1 % glucose and grown at 37°C at 225 rpm shaking until turbid (OD_{600} ~ 0.6 to 0.8). The three cultures were expanded to three separate 300 ml LB cultures with antibiotic plus glucose added, then incubated with shaking until turbid (OD_{600} ~ 0.6 to 0.8). Protein expression was induced with 1 mM IPTG and incubated at 30°C with shaking for 3 h. The culture was centrifuged at 5000 x g for 2 min, the supernatant aspirated, and pellets were then stored at -80°C.

3.2.8.4. Purification of histidine-tagged TRIM26 via affinity chromatography

The bacterial cell pellet containing overexpressed his-tagged TRIM26 was resuspended in lysis buffer (25 mM Tris-HCl (pH8), 0.5 M NaCl, 5 % glycerol, 5 mM imidazole, pH 8 [(Sigma Aldrich St. Louis, Missouri, USA), 100 mM PMSF and 1 µg/ml of each protease inhibitor; leupeptin, chemostatin, pepstatin and aprototin)]. Then, 2 mg lysozyme was added and the cells were incubated on ice for 15 min. Cells were lysed by sonication for 3x15 sec pulses with 30 sec intervals on ice. Lysates were transferred to 50 ml Oakridge tubes and centrifuged at 23,000 x g for 20 min at 4^{O}C. The supernatant was collected and filtered through a 1 µM syringe pre-filter, and then a 0.45 µM syringe filter. A 1 ml HisTrap column (GE Healthcare, Little Chalfont, UK) was attached to the AKTA purifier FPLC and the column washed in the same lysis buffer as above with 0.1 mM PMSF added. The lysate was added to the column and washed thoroughly until no more protein eluted. Bound proteins were collected by a 20 ml gradient elution using elution buffer (25 mM Tris-HCl pH8, 0.5 M NaCl, 5 % glycerol, 500 mM imidazole and 0.1 mM PMSF) collecting 0.5 ml fractions. Fractions were subject to analysis by SDS-PAGE and Western blotting with anti-histidine antibodies to select fractions with purified his-tagged TRIM26. Fractions containing TRIM26 were selected, pooled and concentrated using Amicon Ultra 15 ml centrifugal concentrators (10 kDa MWCO) in a swinging bucket rotor at 4000 x g to generate a concentrated TRIM26 stock for further purification via ion exchange.

3.2.8.5. Purification of histidine-tagged TRIM26 via ion exchange chromatography

Concentrated affinity chromatography fractions containing his-tagged TRIM26 were further separated using a 1 ml ion exchange (MonoQ) chromatography Q 5/50 GL column (GE Healthcare, Little Chalfont, UK) pre-equilibrated with MonoQ buffer I (50 mM KCl, 50 mM Tris HCl pH 8, 1 mM EDTA, 5 % glycerol, 1 mM DTT and 0.1 mM PMSF) using an AKTA-FPLC in a cold cabinet at 4°C. Pooled fractions were concentrated using 10 kDa MWCO centrifuge filters and were diluted 10-fold in JPDB buffer to minimise NaCl levels. Following this, the sample was added onto the column and proteins eluted using a linear gradient of 50–1000 mM KCl using MonoQ buffer II (50 mM Tris HCl pH 8, 1 M KCl, 1 mM EDTA, 5 % glycerol, 1 mM DTT, 0.1 mM PMSF) over 20 min. Fractions of 0.5 ml were collected using an automated fraction collector until the UV signal stabilised. Collected fractions with peaks of protein presence were

subject to 14 % SDS-PAGE separation and Western blotting with TRIM26 specific antibodies. Fractions containing TRIM26 were selected, pooled and concentrated using Amicon Ultra 15 ml centrifugal concentrators (10 kDa MWCO) in a swinging bucket rotor at 4000 x g to generate a concentrated TRIM26 stock for subsequent assays. To improve preservation of the activity of the concentrated stock of the recombinant ligase, it was stabilised by the addition of a 50 % glycerol solution (1:1), aliquoted and stored at -80°C.

3.2.9. Purification of E3 ligase activity for NTH1

3.2.9.1 Preparation of HeLa whole cell extract

Commercially obtained 20 g HeLa whole cell pellets (Cilbiotech, Mons, Belgium) were thawed on ice and re-suspended in one packed cell volume (PCV) of buffer I containing 10 mM Tris HCl (pH 7.8), 200 mM KCl (Sigma Aldrich St. Louis, Missouri, USA), 1 µg/ml of each protease inhibitor; pepstatin, aprotinin, chymostatin and leupeptin (Sigma Aldrich St. Louis, Missouri, USA), 0.1 mM PMSF and 1 mM DTT. Following this, the extract was further suspended in two PCVs of buffer II containing 10 mM Tris–HCl (pH 7.8), 600 mM KCl, 40 % glycerol, 2 mM EDTA, 0.2 % IGEPAL CA-630, 1 µg/ml of each protease inhibitor (as stated), 0.1 mM PMSF and mixed thoroughly by rotation for 30 min at 4°C. Following this, the suspension was spun at 23 000 x g at 4°C for 20 min in pre-cooled Oakridge tubes. The supernatant was collected and dialysed to minimise NP-40 and KCl concentrations, using Snakeskin dialysis tubing (10 kDa MWCO, 35 mm Dry ID) in 3 L of 150 mM KCl buffer with the addition of 1 mM DTT and 0.1 mM of PMSF for 12 h at 4°C. After this, the dialysed solution was spun at 23 000 x g at 4°C in pre-cooled Oakridge tubes to remove precipitated proteins. The supernatant was filtered through 1 µM syringe pre-filters and 0.45 µM filters using a pre-cooled syringe. The filtered extract was then subject to separation via column chromatography.

3.2.9.2. Phosphocellulose Chromatography

A 250 ml P-11 phosphocellulose column (GE Healthcare Little Chalfont, UK), was equilibrated by washing in PC150 buffer (50 mM Tris-HCl pH 8, 150 mM KCl, 1 mM EDTA, 5 % glycerol, 1 mM DTT, 0.1 mM PMSF) using an AKTA-prime FPLC in a cold room at 4°C at ~2 ml/min. HeLa whole cell extract (~2 g protein) was loaded onto the equilibrated column. Unbound proteins were eluted and collected (PC150 fraction) until the UV signal stabilised. Bound proteins were then eluted and collected (PC1000

fraction) by washing the column in PC1000 buffer (1 M KCl, 50 mM Tris-HCl pH8, 1 mM EDTA, 5% glycerol, 1 mM DTT, 0.1 mM PMSF).

3.2.9.3. Ion exchange chromatography

A 20 ml HiLoad 16/10 sepharose high performance column (GE Healthcare, Little Chalfont, UK) was equilibrated in MonoQ buffer I (50 mM KCl, 50 mM Tris HCl pH 8, 1 mM EDTA, 5 % glycerol, 1 mM DTT and 0.1 mM PMSF) using an AKTA-purifier FPLC in a cold cabinet at 4°C. Following this, the PC150 fraction (obtained from Phosphocellulose chromatography) was diluted 1:1 in no salt buffer (50 mM Tri HCl pH 8, 1 mM EDTA, 5 % glycerol) and added to the column at a flow rate of 2 ml/min. Proteins were eluted using a 400 ml linear gradient of 50–1000 mM KCl using MonoQ buffer II (50 mM Tris HCl pH 8, 1M KCl, 1 mM EDTA, 5 % glycerol, 1 mM DTT, 0.1 mM PMSF) at 2 ml/min. Fractions of 4 ml were collected using an automated fraction collector. An aliquot of 500 µl of each fraction was concentrated using Amicon Ultra 0.5 ml devices (10 kDa MWCO, Millipore, Watford, UK) by centrifugation at 15 000 x g, until the fraction volume was 50 µl. The fraction was then buffer exchanged into JPDB buffer (50 mM Tris HCl pH 8, 50 mM KCl, 1 mM EDTA, 10 % glycerol) to reduce the salt concentration and to stabilise the proteins. This process was repeated once more. Fractions were then analysed via an *in vitro* ubiquitylation assay using NTH1 as the substrate (**section 3.2.6.7**).

3.2.9.4. Size exclusion (Gel filtration) chromatography

A 24 ml Superdex 200 10/300GL column (GE Healthcare, Little Chafont, UK) was equilibrated in gel filtration buffer (50 mM Tris pH 8, 150 mM KCl, 1 mM EDTA, 5 % glycerol with 1 mM DTT and 0.1 mM PMSF) at a flow rate of 0.5 ml/min using an AKTA-purifier FPLC in a cold cabinet at 4°C. Fractions with potential candidate E3 ligase activity obtained from the previous MonoQ chromatography were concentrated to 500 µl using Amicon Ultra 15 ml centrifugal concentrators (10 kDa MWCO) in a swinging bucket rotor at 4000 x g at 4°C. Concentrated fractions were loaded onto the equilibrated gel filtration column, collecting 0.5 ml fractions. Fractions were once again tested via an *in vitro* ubiquitylation assay using NTH1 as the substrate (**section 3.2.6.7**). During this separation, gel filtration standards consisting of proteins of known molecular weight were also applied to the column. The position from which they eluted (in particular fractions) enabled us to estimate the molecular weight of other unknown proteins eluted from the cellular extract.

3.2.9.5. Hydroxyapatite chromatography

Using an AKTA-purifier FPLC in a cold cabinet at 4°C, a 1 ml CHT ceramic hydroxyapatite column (Bio-Rad, Hemel Hempstead, UK) was equilibrated in hydroxyapatite buffer I (5 mM K_2HPO_4, 5 mM KH_2PO_4, 5 % glycerol) at a flow rate of 1 ml/min. Fractions from the previous purification step were concentrated using Amicon Ultra 15 ml centrifugal concentrators (10 kDa MWCO) in a swinging bucket rotor at 4000 x g at 4°C until the volume reached approximately 500 µl. This volume was then made up to 1 mL in JPDB buffer (50 mM Tris HCl pH 8, 50 mM KCl, 1 mM EDTA, 10 % glycerol) and concentrated once more at 4000 x g at 4°C. This process was repeated twice more as a way to buffer exchange the fractions. After this, the buffer exchanged fractions were added onto the equilibrated 1 mL CHT ceramic hydroxyapatite column. Proteins were eluted using a 20 ml linear gradient of 5–500 mM KPO_4 using hydroxyapatite buffer II (500 mM K_2HPO_4, 500 mM KH_2PO_4, 5 % glycerol) at 1 ml/min. An automated fraction collector was used to collect 0.5 ml fractions. Fractions were once again tested via *in vitro* ubiquitylation assay using NTH1 as the substrate (**section 3.2.6.7**).

3.2.9.6. Final ion exchange chromatography

Active fractions obtained from previous hydroxyapatite column chromatography were pooled and diluted 10-fold in MonoQ buffer I (50 mM KCl, 50 mM Tris HCl pH 8, 1 mM EDTA, 5 % glycerol, 1 mM DTT and 0.1 mM PMSF). A 1 ml Mono Q 5/50 GL column (GE Healthcare, Little Chalfont, UK) was equilibrated in MonoQ buffer I at a flow rate of 1 ml/min using an AKTA-purifier FPLC in a cold cabinet at 4°C. Pooled fractions were added onto the column and proteins eluted using a linear gradient of 50–1000 mM KCl using MonoQ buffer II (50 mM Tris HCl pH 8, 1 M KCl, 1 mM EDTA, 5 % glycerol, 1 mM DTT, 0.1 mM PMSF) over 20 min. Fractions of 0.5 ml were collected using an automated fraction collector until the UV signal stabilised.

3.2.9.7. *In vitro* ubiquitylation assay

In vitro ubiquitylation of his-tagged, recombinant NTH1 (5.8 pmol) by candidate E3 ligase enzymes was analysed in buffer containing 4 mM ATP, 200 µM $CaCl_2$, 1 mM DTT, 5 mM $MgCl_2$, 100 µM MG-132 and 50 mM Tris-HCl (pH8) in pre-cooled low bind Eppendorf tubes. To this, 625 pmol of wild-type or mutant ubiquitin was added along with 0.7 pmol GST-E1 activating enzyme, 2.5 pmol E2 conjugating enzyme (combination of 10 different E2s, unless otherwise stated) and 0.6 nmol ubiquitin

(Boston Biochemicals, Cambridge, USA) in buffer containing 25 mM Tris–HCl (pH 8.0), 4 mM ATP, 5 mM $MgCl_2$, 200 µM $CaCl_2$ and 1 mM DTT were incubated in LoBind protein tubes (Eppendorf, Stevenage, UK) for 1 h at 30°C with agitation. A source of E3 ligase enzyme was either provided in the form of active HeLa cell fractions obtained from column chromatography or in the form of active, purified recombinant E3 ligase enzyme (TRIM26; 19 fmol and 26 fmol). Reactions were stopped by the addition of SDS-PAGE sample buffer (25 mM Tris–HCl (pH 6.8), 2.5% β-mercaptoethanol, 1% SDS, 10% glycerol, 1 mM EDTA, 0.05 mg/ml bromophenol blue) and heated for 5 min at 95°C prior to SDS-PAGE and Western blotting (**section 3.2.1 and section 3.2.2.2**).

3.2.9.8. E3 ubiquitin ligase identification by tandem mass spectrometry

Active candidate E3 ligase enzymes within fractions obtained from the final ion exchange chromatography stage were identified by tandem mass spectrometry. Strataclean resin (Agilent Technologies, Stockport, UK) was used to extract proteins from purified chromatography fractions and subsequently protein were resuspend in 0.05 % (w/v) Rapigest in 25 mM ammonium bicarbonate. Samples were then heated at 80°C for 10 min, reduced with 3 mM DTT at 60°C for 10 min and alkylated in 9 mM iodoacetamide in a dark room for 30 min. Trypsin (1 µg) in 50 mM acetic acid was added and samples mixed via rotation at 37°C for 12 h. Following digestion, samples were acidified by the addition of trifluoroacetic acid (1 % (v/v) and held at 37°C for 45 min, then centrifuged at 17 200 x g for 30 min. The pellets were discarded and supernatants were diluted to ~50 ng/µl in 0.1 % (v/v) trifluoroacetic acid (TFA)/3 % (v/v) acetonitrile. LC peptide separations were completed using an Ultimate 3000 nano system (Dionex/Thermo Fisher Scientific, Hemel Hempstead, UK). For each analysis, the sample was loaded onto a trap column (Acclaim PepMap 100, 2 cm × 75 µm inner diameter, C_{18}, 3 µm, 100 Å) at 5 µl/min with an aqueous solution containing 0.1 % (v/v) TFA and 2 % (v/v) acetonitrile. Following 3 min, the trap column was set in-line with an analytical column (Easy-Spray PepMap® RSLC 50 cm x 75 µm inner diameter, C_{18}, 2 µm, 100 Å). Peptide elution was completed using a linear gradient of solvent A (HPLC grade water with 0.1 % (v/v) formic acid) and solvent B (HPLC grade acetonitrile 80% (v/v) with 0.1 % (v/v) formic acid). Mass spectrometry was then performed using the Q Exactive instrument operated in data dependent positive (ESI+) mode to routinely switch between full scan MS and MS/MS acquisition. Survey full scan MS spectra (*m/z* 300–2000) were obtained with a resolution of 70 000 (*m/*z 200) following accumulation of ions to 1×10^6 target value based on

predictive automatic gain control (AGC) values from the previous full scan. Dynamic exclusion was set to 20 s. The 10 most intense multiply charged ions ($z \geq 2$) were sequentially isolated and fragmented in the octopole collision cell by higher energy collisional dissociation (HCD) with a fixed injection time of 100 ms and 35 000 resolutions. Typical mass spectrometric conditions were as follows: spray voltage, 1.9 kV, no sheath or auxillary gas flow; heated capillary temperature, 275°C; normalised HCD collision energy 30 %. The MS/MS ion selection threshold was set to 2×10^4 counts. A 2 Da isolation width was set. Raw data files were searched in Mascot against the UniProt human database. A precursor ion tolerance of 10 ppm and a fragment ion tolerance of 0.01 Da were used with carbamidomethyl cysteine set as a fixed modification and oxidation of methionine as a variable modification. The false discovery rate against a decoy database was 1 %.

3.2.9.9. Identification of NTH1 ubiquitylation sites by tandem mass spectrometry

To isolate ubiquitylated NTH1, *in vitro* ubiquitylation reactions recombinant Histidine-NTH1 as the substrate protein and recombinant Histidine-TRIM26 as the active E3 ligase, the reactions were separated via two 10% SDS-PAGE gels in tandem. One of them was further subject to Western blotting analysis with NTH1 specific antibodies. The Western blot was utilised to identify the specific region featuring protein bands which correspond to ubiquitylated NTH1. This was represented by protein bands corresponding to NTH1 which had shifted upwards on the SDS-PAGE gel by 8 kDa or multiples of 8 kDa; this is representative of the addition of 8 kDa ubiquitin moieties to specific lysine residues of NTH1. Identification of the specific region containing ubiquitylated NTH1 bands was applied to the 10% SDS-PAGE gel; where the specific region was estimated from visualisation of the Western blot and bands were excised using a scalpel. The excised gel pieces were covered with a minimum volume of 25 mM ammonium bicarbonate in 1.5 ml LoBind Protein tubes (Eppendorf, Stevenage, UK) and heated at 37°C for 15 min. The gel pieces were washed twice more in this way before 10 mM DTT in 25 mM ammonium bicarbonate was added and samples incubated at 56°C for 1 h. Alkylation was then completed by the addition of 55 mM ammonium bicarbonate followed by 25 mM ammonium bicarbonate/acetonitrile (2:1 v/v). For protease digestion, ArgC (10 ng/ul in 25 mM ammonium bicarbonate containing 1 mM DTT) was added and incubated for 15 min on ice. Following this, samples were covered in a minimum volume of 25 mM ammonium bicarbonate and heated at 37°C overnight. Samples were then centrifuged at 17 200 xg, supernatant

removed and vacuum centrifuged to near dryness. Acetonitrile (3 % v/v) and TFA (0.1 % v/v) was added and samples centrifuged for 15 min before transfer to a total recovery vial for LC-MS analysis.

3.2.10. Mammalian cell culture

All tissue culture work was completed in a class II hood with laminar flow (Esco Global, Barnsley, UK), cleaned with 70 % ethanol thoroughly before and following use. Tissue culture reagents, including trypsin, PBS and complete DMEM media (containing 10 % FBS, 2 mM glutamine and 1 % pen-strep) were warmed in a water bath at 37°C before use. Tissue culture work was performed entirely using aseptic techniques. All plastics used were tissue culture grade. Cells were grown in a humidified cell culture incubator with 5 % CO2 at 37°C.

3.2.10.1. Defrosting cell vials

Vials containing frozen cells were obtained from liquid nitrogen storage and rapidly defrosted for 1 min at 37°C in a water bath. Cells were promptly centrifuged at 2000 x g for 5 min and the supernatant discarded to remove DMSO. The cell pellet was resuspended in 12 ml of DMEM media supplemented with hydroxyethyl piperazineethanesulfonic acid (HEPES) modification, 4500 mg/L 25 mM HEPES and sodium bicarbonate, sterile filtered, plus 10 % fetal bovine serum (FBS, non-USA origin, sterile filtered) 2mM L-glutamine, 100 U penicillin, 0.1 mg streptomycin and 1 % MEM Non-essential amino acid solution. The resuspended cells were transferred to a T75 flask and placed in a humidified cell culture incubator at 5 % CO_2 at 37°C. Once cells reached approximately 70-90 % confluency they were subcultured.

3.2.10.2. Subculturing

Once cells in T75 flasks had reached confluency they were subcultured into fresh T75 flasks to maintain cell growth. The DMEM media was removed via aspiration then cells were washed in 5 ml of PBS. Cells were treated with 2 ml of trypsin-EDTA solution (0.25 %) and incubated for 2 min (or until cells had lifted from the flask surface) in the humidified cell culture incubator at 5 % CO_2 at 37°C. Trypsin was neutralized by the addition of 8 ml of supplemented DMEM media and cells were subcultured 1:20 in a fresh T75 flask with 12 ml supplemented DMEM media and placed in a humidified cell culture incubator at 5 % CO_2 at 37°C.

3.2.10.3. Seeding cells for experimentation

Exponentially growing cells were trypsinised as described above. The number of cells in trypsinised cell suspension was determined by cell counting using a haemocytometer. Generally, for 10 cm dishes 0.5 x 10^6 cells per dish were seeded in 5 ml of supplemented DMEM media, whereas, for a 3.5 cm sized dish 1.5 x 10^5 cells were seeded in 2 ml of supplemented DMEM media.

3.2.10.4. Harvesting cells

Outside the tissue culture flow hood, media was removed by aspiration. Cells were washed in cold Dulbecco's PBS (for 10 cm^2 dishes used 5 ml of PBS, for 3.5 cm dishes used 2 ml of PBS) which was also removed via aspiration. A further volume of PBS was added and cells were carefully removed using a cell scraper (Greiner Bio-One) and added to a pre-cooled 15 ml tube on ice. This process was repeated once more before centrifugation at 2000 x g for 5 min at 4°C. The supernatant was discarded and the pellet resuspended in 1 ml of cold Dulbecco's PBS which was transferred to a pre-cooled Eppendorf on ice. The suspension was spun at 2000 x g for 5 mins at 4°C and the supernatant discarded. Pellets were stored at -80°C for at least 1 h.

3.2.10.5. Preparation of whole cell extracts

Before use, 1 µg/ml of each protease inhibitor; aprotinin, pepstatin, chymostatin and leupeptin, and 1 mM PMSF and 1 mM DTT were added to buffer I (10 mM Tris, pH 7.8, 200 mM KCl) and buffer II (10 mM Tris, pH 7.8, 600 mM KCl, 2 mM EDTA, 40 % glycerol, 0.2 % NP-40). After harvesting cells and freezing the pelleted extracts at -80°C for a least 1 h, cell pellets were resuspended in one PCV (no less than 50 µl) in buffer I and then two PCVs of buffer II were also added, then the extract was mixed thoroughly. The cell suspension was mixed via rotation at 4°C for 1 h, then centrifuged at 72 000 x g for 20 min at 4°C. The supernatant containing protein was collected and protein concentration measured using a Bradford assay (**Section 3.2.1**) and stored at -80°C.

3.2.10.6 Biochemical fractionation

Cellular proteins were fractionated into soluble and chromatin bound fractions according to previous descriptions (179). Initially, cells were resuspended in 2 packed cell volumes (PCV) of Buffer I (20 mM Tri-HCl pH 7.4, 2.5 mM $MgCl_2$, 0.5% Nonidet P-40) containing 1 mM PMSF, 1 mM DTT and 1 µg/ml of protease inhibitors

(leupeptin, pepstatin, chymostatin and aprotinin). Re-suspended cells were incubated on ice for 10 min before centrifugation at 10 000 rpm for 2 min to separate the soluble fraction in the supernatant. The nuclear pellet was re-suspended in two PCVs of buffer II (20 mM $NaPO_4$ pH 8.0, 0.5 M NaCl, 1 mM EDTA, 0.75 % Triton X-100, 10 % glycerol and 2 mM $MgCl_2$) containing 1 mM PMSF, 1 mM DTT and 1 µg/ml of protease inhibitors (leupeptin, pepstatin, chymostatin and aprotinin) for 10 min on ice. The suspension then centrifuged at 10 000 rpm for 2 min. The supernatant was collected as the chromatin bound fraction. Protein concentration was determined by the Bradford assay (**Section 3.2.1**) and extracts were stored at -80°C.

3.2.10.7. RNA interference for knockdowns

Cells were cultured in Dulbecco's modified Eagle's medium (DMEM) supplemented with 10 % fetal bovine serum (FBS), 2 mM L-glutamine, 1× penicillin-streptomycin and 1× non-essential amino acids. All cells were cultured at 37°C in 5 % CO_2. For siRNA induced knockdowns, cells were grown in 10 cm dishes for 24 h until 30-50 % confluent and treated with 10 µl Lipofectamine RNAiMAX transfections reagent (Life Technologies, Paisley, UK) in the presence of 140 nM non-targeting, control siRNA (Qiagen, Manchester, UK) or 140 nM TRIM26 siRNA (consisting of 70 nM of two TRIM26 siRNA; 5'-CCGGAGAAUUCUCAGAUAA-3' and 5'-GAGUCACAGGAACUCAUCU-3') for 72 h at 37°C in a humidified cell incubator.

3.2.10.8. Plasmid transfection for overexpression

Cells were cultured in 10 cm dishes until 80% confluent. They were transfected with plasmids (e.g. 110 fmol pCMV-3Tag3a-TRIM26 or 150 fmol pCMV-3Tag3a-NTH1 or 1 µg of PMT-HA-Ub) using 10 µl Lipofectamine 2000 (Life Technologies, Paisley, UK) for 24 h in serum-containing media at 37°C with 5% CO_2 in a humidified cell incubator.

3.2.10.9. Reverse transcription and real-time PCR

An RNeasy Mini kit (Qiagen, Manchester, UK) was used to extract RNA from cell pellets according to the manufacturer's instructions. Briefly, cells were pelleted following an siRNA induced knockdown and resuspended in 350 µl buffer RLT, mixed with 350 µl 70 % ethanol, then the mixture was transferred to a RNeasy Mini spin column and centrifuged at 8000 x g for 15 sec. All subsequent centrifugation stages were completed at this speed and time unless stated otherwise.

Following this, 700 µl Buffer RW1 was added to the column and centrifuged, then 500 µl buffer RPE was added twice and centrifuged after each addition. The column was dried by centrifugation for 1 min before 30 µl RNase free water was added and centrifuged for 1 min to elute RNA. The RNA concentration was measured via a Nanodrop ND-1000 spectrometer (software version V3.7.1) at 260 nm.

From the extracted RNA, cDNA was generated using the GoScript™ Reverse Transcription System (Promega, Southampton, UK) according to the manufacturer's instructions. Up to 5 µg RNA was incubated with 0.5 µg Oligo$(dT)_{15}$ at 70°C for 5 min then cooled on ice for 5 min. A reverse transcription mix was made consisting of; 4 µl GoScript™ 5x reaction buffer, 1.4 mM $MgCl_2$, 0.5 mM PCR nucleotide mix, 0.5 µl Recombinant RNasin ribonuclease inhibitor and 1 µl GoScript™ reverse transcriptase which was made up to 15 µl final volume with nuclease free water. To this the 5 µl RNA and primer mix was then added and incubated at 25°C for 5 min for annealing, extended by heating at 42°C for 1 h and the reverse transcriptase inactivated by incubation at 70°C for 15 min. Following this, SYBR® Select Master Mix (Thermo Scientific, Runcorn, UK) was used to amplify cDNA using primers (**Table 6**) for quantitative Real Time PCR analysis using the 7500 Real Time PCR system (Applied Biosystems, Warrington, UK) software version v2.3. A cycle threshold value (CT) was provided of the run for the gene(s) of interest and the reference gene actin following their knockdown by siRNA. Further calculations (provided below) determined relative quantities of mRNA (RQ value) so that statistical analysis of knockdown efficiency could be calculated. The RQ value allowed us to determine if successful knockdown of target genes has been achieved.

$$\Delta CT = CT_{gene} - CT_{\text{reference gene}}$$
$$\Delta\Delta CT = \Delta CT_{control} - \Delta CT_{treatment}$$
$$RQ = 2^{\Delta\Delta CT}$$

3.2.10.10. Inhibition of the cellular proteasome

Cells were cultured in serum-containing medium until approximately 80% confluent. Cells were washed and treated with either; 10 µl DMSO control or 10 µl MG-132 (carbobenzoxy-Leu-Leu-leucinal) proteasomal inhibitor diluted in serum-containing media for 8 h at 37°C in a humidified cell chamber with 5% CO_2. Cells were then harvested and whole extracts prepared as described (**Section 3.2.10.5**). A total of 40 µg of protein extract obtained from cells with and without MG-132 treatment was

then analysed via 10% SDS-PAGE and Western blotting (**Sections 3.2.2.2 and 3.2.2.3**) with anti-NTH1 antibodies. Levels of NTH1 protein, represented by a protein expression band at a molecular weight of 34.4 kDa on the Western blot, were quantified using the Odyssey image analysis system (Li-cor Biosciences, Cambridge, UK).

3.2.10.11. Immunoprecipitation of FLAG-tagged NTH1

Anti-FLAG M2 magnetic beads (Sigma-Aldrich, Dorset, UK) were used for immunoprecipitation of FLAG-tagged recombinant NTH1, following a partial overexpression of this protein in cells. Cells were harvested and cell extracts prepared (**Section 3.2.10.5**). The protein concentration of each extract was measured via a Bradford assay. Samples were diluted to a final volume of 100 µl in 150 mM KCl buffer (50 mM Tris pH 8, 150 mM KCl, 1mM EDTA, 5% glycerol) and to equal protein concentrations.

For each immunoprecipitation, 10 µl of Anti-FLAG M2 magnetic beads were aliquoted into a clean Eppendorf and washed three times in no salt buffer, using a magnetic separation rack to draw the beads across and discarding the excess buffer by pipetting. The washed beads were then resuspended in 100 µl of no salt buffer and the total volume was added to each cellular extract. Samples were mixed for 2 h on a rotating platform at 4°C. The magnetic rack was then used to immobilize the beads and the supernatant discarded. Beads were then washed in 100 µl of 150 mM KCl buffer by mixing gently with a pipette tip, before immobilising the beads with the magnetic rack and discarding the supernatant. This process was repeated thrice. Finally, the beads were resuspended in 20 µl of 150 mM KCl buffer, with 10 µl of 3x SDS-PAGE loading dye. Samples were heated at 95°C for 5 min, before 15 µl of the final volume was loaded onto an SDS-PAGE gel, followed by Western blotting with HA-tag antibodies to monitor the amount of immunoprecipitated ubiqutiylated protein.

3.2.10.12. Oxidative stress treatment of cells

Following treatment of cells grown in 10 cm dishes with the appropriate mammalian expression plasmid or siRNA induced knockdown, cells were subject to oxidative stress through hydrogen peroxide treatment. The stock solution of hydrogen peroxide (30 %) was diluted to 150 µM final concentration in serum containing media. Cells were washed in 1x PBS then the 150 µM hydrogen peroxide solution was added. Cells were incubated for 15 mins at 37°C in a humidified cell chamber with 5 % CO_2.

Cells were then washed in 1x PBS and fresh media added. For repair time points, cells were returned to the 5 % CO_2 incubator and harvested at the required intervals (0-8 h). For untreated controls, cells were treated with media only.

3.2.10.13. Clonogenic survival assays

Following treatment of cells grown in 35 mm dishes with siRNA or mammalian expression plasmids, cells were treated with hydrogen peroxide (0-300 nM) for 15 min at 37 °C in a humidified cell incubator. Cells were then washed in 1x PBS, trypsinised and counted using a haemocytometer. A defined number of cells were seeded in 2 ml complete DMEM media at two different cell densities in triplet for each hydrogen peroxide treatment in 6-well plates. Number of HCT116$^{p53+/+}$ cells seeded per well in a 6 well plate. For lipofectamine RNAiMAX only; 0 nM H_2O_2 250 and 500, 50 nM H_2O_2 250 and 500, 100 nM H_2O_2 500 and 1000, 200 nM H_2O_2 1000 and 2000, 300 nM H_2O_2 1000 and 2000. For non-targeting siRNA, TRIM26 siRNA or NTH1 overexpression; 0 nM H_2O_2 250 and 500, 50 nM H_2O_2 500 and 1000, 100 nM H_2O_2 1000 and 2000, 200 nM H_2O_2 1000 and 2000, 300 nM H_2O_2 2000 and 4000. The cell numbers were increased for increasing hydrogen peroxide doses and double the number of cells were used for non-targeting siRNA, TRIM26 siRNA or NTH1 overexpression to compensate for cell plating efficiencies. The plates were incubated in a tissue culture incubator at 37°C, 5 % CO_2 for 10-14 days until colonies were clearly visible (>50 cells/colony). Cells were then fixed and stained by removing media, washing the cells in PBS, and adding 0.5 % crystal violet in 6 % glutaraldehyde (Fisher Scientific UK, Loughborough, UK) for 1 h. The dye was removed, plates were washed in water and left to air dry overnight. Colonies were counted using the GelCount colony analyser (Oxford Optronics, Oxford, UK). Relative colony formation (surviving fraction) was expressed as colonies per treatment level versus colonies that appeared in the untreated control. Statistical analysis was performed using the CFAssay for R package (18).

3.2.10.14. Alkaline single cell gel electrophoresis (comet) assay

Cells grown in 35 mm dishes were trypsinised, diluted to 2x10^5 cells/ml and 250 µl aliquots of the cell suspension, then transferred into the wells of a 24-well plate on ice. The cells were treated with 7.5 µM hydrogen peroxide for 5 min on ice. The reaction was stopped by mixing the cell suspension with 1 ml molten low melting point agarose (at ~35°C), before being transferred to a microscope slide pre-coated with normal melting point agarose. A cover slip was then placed over the cell suspension

mixture and allowed to set on ice. For DNA repair kinetic studies, cells were allowed to undergo DNA repair in-gel for up to 2 h at 37°C in a humidified chamber, prior to lysis in buffer containing 2.5 M NaCl, 100 mM EDTA, 10 mM Tris–HCl pH 10.5, 1% (v/v) DMSO and 1% (v/v) Triton X-100 for at least 1 h at 4°C (112). Following this, slides were transferred to an electrophoresis tank and incubated for 30 min in the dark. Slides were then submerged in cold electrophoresis buffer (300 mM NaOH, 1 mM EDTA, 1% (v/v) DMSO, pH 13) to permit the DNA to unwind. The DNA was electrophoresed at 25 V, 300 mA for 25 min and slides neutralised with three 5 min washes of 0.5 M Tris–HCl (pH 8.0) then allowed to air dry overnight. Slides were rehydrated for 30 min in water (pH 8.0), stained for 30 min with SYBR Gold (Life Technologies, Paisley, UK) diluted 1:20 000 in water (pH 8.0) and allowed to dry prior to imaging. Cells (50 per slide, two slides per time point) were analysed using the Komet 6.0 image analysis software (Andor Technology, Belfast, Northern Ireland) and % tail DNA values averaged from at least three independent experiments.

CHAPTER 4 - RESULTS I

Identification of TRIM26 as the major E3 ubiquitin ligase for NTH1

4.1 Introduction

NTH1 is a key bifunctional glycosylase implicated in the removal of oxidised pyrimidines during the first stages of BER. Removal of base lesions inflicted upon DNA is paramount to maintaining the functionality of each cell. Elimination of DNA base lesions prevents the accumulation of harmful mutations upon cell division, which can result in dysregulated cellular activity leading to cancer development. Crucially, NTH1 is the primary enzyme involved in the repair of Tg, which is a particularly mutagenic base lesion (42, 76, 165). Owing to the importance of NTH1, the repair enzyme is expressed ubiquitously and well conserved across phylogeny.

Due to continued fluctuations in levels of DNA damage, it is imperative that BER repair enzymes are regulated to enable cells to provide effective DNA repair. Indeed, previous work has demonstrated that the levels of a number of BER enzymes are regulated by the PTM, ubiquitylation (46, 125, 126). For instance, levels of the major replicative polymerase implicated in BER, Pol β, have been shown to be regulated by ubiquitylation. The addition of singular ubiquitin moieties by the E3 ligase Mule was shown to act as a prerequisite for the addition of ubiquitin chains by another E3 ubiquitin ligase CHIP that signals for proteosomal degradation (126). Conversely, deubiquitylation of Pol β by USP47 initiates accumulation of levels of the repair protein (121). In this way, it is acknowledged that ubiquitylation can be utilised to efficiently modify cellular levels of BER proteins to suitably respond to fluctuating DNA damage levels.

Ubiquitylation involves the covalent attachment of single or multiple moieties of ubiquitin onto target proteins. The process is mediated by a cascade of three enzymes; an E1 activating enzyme, an E2 conjugating enzyme and finally an E3 ligase enzyme. Generally, attachment of single ubiquitin molecules regulates activity, localisation or protein-protein/protein-DNA interactions, whereas addition of chains of ubiquitin moieties often influences protein stability. In this capacity, ubiquitylation is a highly dynamic process that regulates numerous cellular activities. Due to the influence ubiquitylation has on cellular processes it is particularly important that the process is highly specific towards substrate proteins. To facilitate this, specificity of

the reaction is largely dictated by the existence of over 600 individual E3 ligase enzymes (81)**.**

Despite accumulating evidence of regulation of BER via ubiquitylation, investigations regarding the ubiquitylation dependent regulation of proteins present upstream in the BER process, is lacking in comparison to more well characterised BER proteins (48). For instance, and central to this thesis, proteomic screens have identified that NTH1 is ubiquitylated, but the ubiquitylation enzymes involved have not been elucidated (34)**.** Most recently, colleagues from our laboratory began to address this discrepancy; they purified and identified the major E3 ligases responsible for the ubiquitylation of the DNA glycosylase, NEIL1 (46). Identifying the E3 ligase enzymes specific to NTH1 will serve as an important tool for determining the role that ubiquitylation plays in regulating NTH1 activity, localisation, stability or cellular interactions. Therefore, the primary aim of the work detailed in this chapter was to purify and identify the E3 ligase(s) in human cells that act on NTH1.

4.2. Purification of recombinant NTH1

Recombinant histidine-tagged NTH1 was overexpressed and purified using a bacterial expression plasmid (kindly provided by Dr. Allinson, University of Lancaster). The expression product of the pET28NTH1 plasmid consisted of the coding sequence (P78549-2). The pET28NTH1 expression plasmid was transformed into Rosetta (DE3) pLysS competent cells and colonies grown on selective medium, according to the antibiotic resistance (kanamycin) of the expression plasmid. Resistant colonies were selected and cultured initially in 5 ml of LB media overnight with appropriate selective antibiotics at 37°C in a shaking incubator at 250 rpm. The overnight culture was then used to generate a 40 mL feeder culture in the presence of appropriate antibiotics. Once the OD_{600nm} of the feeder culture reached 0.6, it was diluted to generate a 400 mL expression culture. When the OD_{600nm} of the expression culture reached 0.6, protein expression was induced via the addition of IPTG and cultured for a further 3 h at 30°C. Following this, the bacterial cell culture was harvested and cells resuspended in lysis buffer in the presence of protease inhibitors to enable protein purification. Expressed, recombinant Histidine-tagged NTH1 was purified by affinity chromatography, using a 1 ml HisTrap chromatography column, utilising an AKTA-purifier FPLC with a gradient elution of 5 mM to 500 mM imidazole (**Figure 18**, A). The purity of fractions containing recombinant NTH1 was analysed by 10 % SDS-PAGE (**Figure 18**, B) with Western blotting using antibodies specific to NTH1 detection (**Figure 18**, C).

The molecular weight of His-tagged NTH1 (P78549-2) is 33.6 kDa. From SDS-PAGE separation and Western blot analysis (**Figure 18, B and C**), it was apparent that relatively pure NTH1, represented by the presence of a strong banding pattern at the expected molecular weight, was present in chromatography fractions 17-27. This strong band was confirmed to be NTH1 by Western blotting using antibodies that specifically cross-react with the protein, again in fractions 17-27 (**Figure 18, C**). Consequently, the purest fractions (19-27) were pooled and concentrated using 10 kDa centrifugal filters, as well as being buffer exchanged into JPDB buffer, to generate a concentrated stock of NTH1 for subsequent *in vitro* ubiquitylation assays.

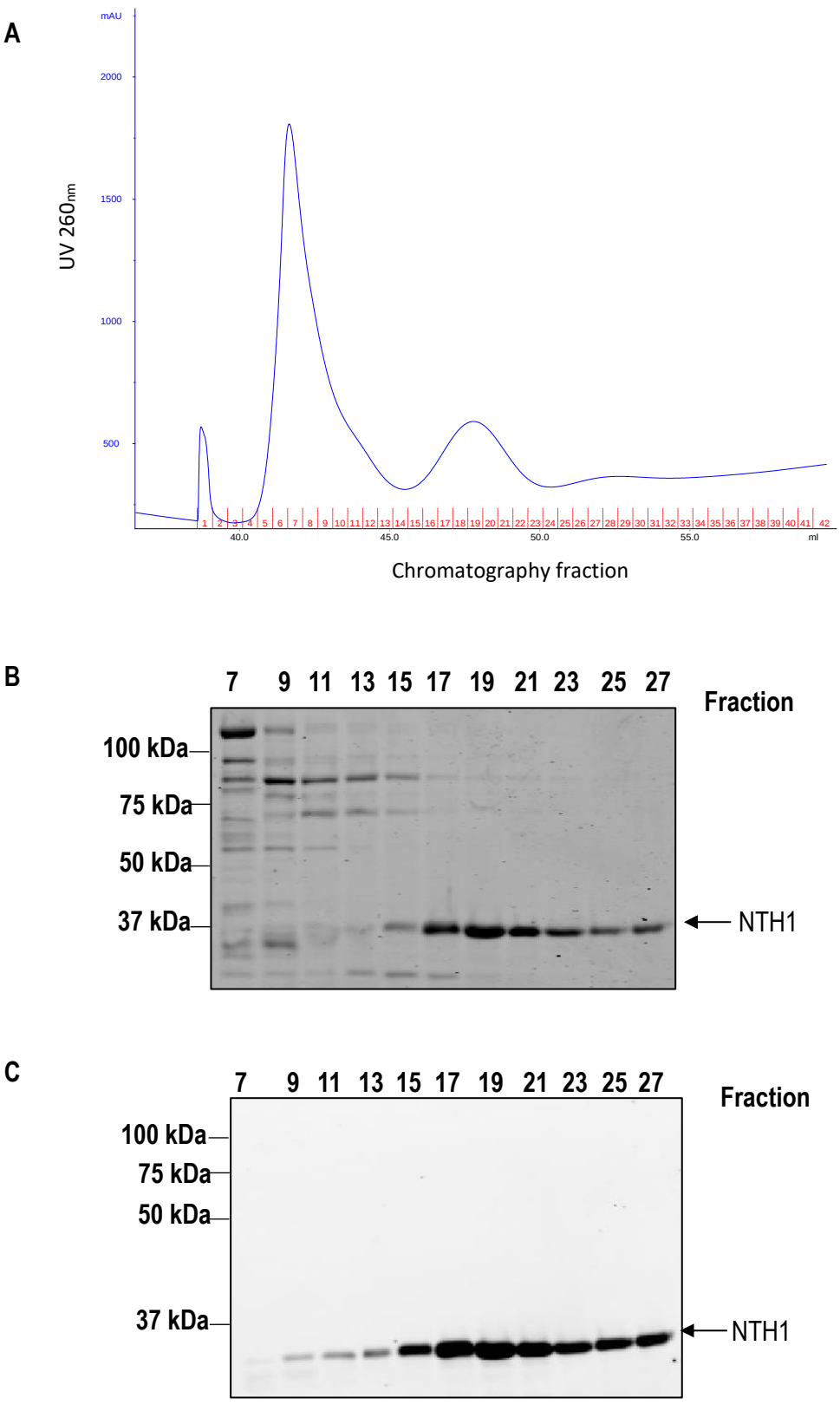

Figure 18. Purification of histidine-tagged recombinant NTH1 via affinity chromatography. A bacterial expression plasmid for histidine-tagged NTH1 (P78549-2) was transformed into Rosetta2 (DE3) pLySs bacterial cells and grown into a 400 ml expression culture before inducing protein expression. Bacterial cell pellets were then harvested before cells were lysed in the presence of protease inhibitors.

Recombinant NTH1 was then purified using a 1 ml HisTrap affinity chromatography column with a linear gradient of 5 mM to 500 mM imidazole. The UV trace is provided, with the fraction number shown below in red (**A**). Chromatography fractions were collected and purity analysed by 10% SDS-PAGE (**B**) and Western blotting using antibodies specific to NTH1 (**C**).

4.3. Purification of the cellular E3 ligase specific to NTH1

Identification of the direct mechanism of ubiquitylation of NTH1, may facilitate further studies determining the cellular effects of ubiquitylation-dependent regulation NTH1. This largely relies on identification of the E3 ligase enzyme(s) that ubiquitylate of NTH1. Since there are believed to be over 600 individual E3 ligase enzymes, this process initially involved purification of candidate E3 ligase enzymes from the cellular milieu. This was achieved by combining a series of column chromatography separation techniques (**Figure 19**), using an AKTA-purifier FPLC, with an *in vitro* ubiquitylation assay incorporating NTH1 as a substrate protein. Following each column chromatography stage within the purification scheme, each fraction obtained was subject to an *in vitro* ubiquitylation assay, containing GST-E1 activating enzyme, nine different E2 conjugating enzymes and ubiquitin, with Histidine-tagged, recombinant and purified NTH1 as a substrate (**Figure 18**). The presence of active E3 ligase(s) specific to NTH1 was provided in the form of the cellular proteins within the chromatography fractions being tested. The ubiquitylation reactions were carried out at 30 °C for 1 h and completed reactions were analysed by SDS-PAGE separation, followed by Western blot analysis using NTH1 antibodies. The presence of active candidate E3 ligase enzymes was determined by fractions which demonstrated bands of NTH1 with an increased shift in molecular weight of approximately 8 kDa, or multiples of 8 kDa. This characteristic banding pattern likely represents the addition of 8 kDa ubiquitin moieties onto specific lysine residues of the substrate protein, NTH1. Using this method, it was understandably assumed that these fractions contain active E3 ligase(s) specific to NTH1. Active fractions were pooled, concentrated and passed over the sequential chromatography column, according to the purification scheme (**Figure 19**) to further purify the candidate E3 ligase(s) to near homogeneity. Following the final purification step, candidate peptides were analysed via mass spectrometry.

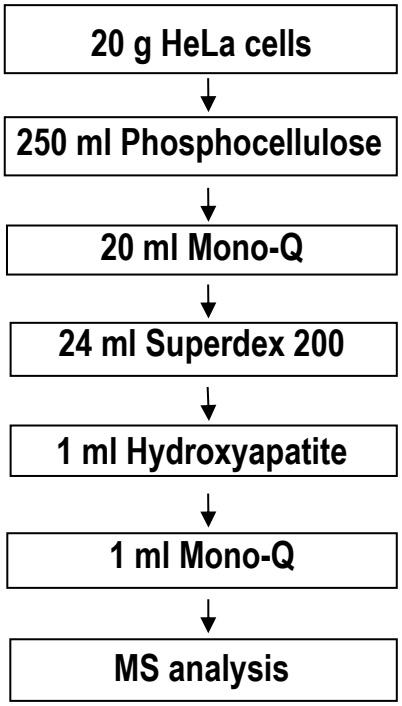

Figure 19. Purification scheme utilised for the isolation of candidate E3 ligase enzymes specific to recombinant NTH1 from HeLa cells. HeLa extract was prepared from a 20 g HeLa pellet then passed over a fully equilibrated Phosphocellulose cation exchange column. Proteins were eluted using a KCl containing buffer and the NTH1 specific ubiquitylation activity of eluted proteins was evaluated by using the chromatography fractions as an E3 ligase source in an i*n vitro* ubiquitylation assay with recombinant NTH1. Completed assays were evaluated by SDS-PAGE and western blot analysis with NTH1 antibodies. Active fractions were purified further sequentially using a 20 ml Mono-Q anion exchange column eluted using a KCl gradient, a 24 ml Superdex 200 gel filtration column, a hydroxyapatite column and a final 1 ml Mono-Q anion exchange column. Fractions demonstrating ubiquitylation activity at each stage and the presence of a candidate E3 ligase enzyme specific to NTH1 were then subject to mass spectrometry (MS) analysis to identify candidate peptides.

4.3.1. Phosphocellulose chromatography

The purification process was initiated by the preparation of a cell extract from a commercially obtained 20 g HeLa cell pellet. The HeLa cell pellet was thoroughly resuspended in the presence of protease inhibitors, dialysed and precipitated proteins removed via centrifugation. The HeLa cell suspension was passed over a pre-equilibrated Phosphocellulose cation exchange column, which preferentially binds positively charged proteins, including those with DNA-binding properties. The column was washed with buffer containing 150 mM KCl, to collect unbound proteins (PC150 fraction), before bound proteins were displaced by a single step-elution using 1000 mM KCl containing buffer (PC1000 fraction). Both fractions (PC150 and PC1000)

were subject to an *in vitro* ubiquitylation assay, using recombinant Histidine-tagged NTH1 as the substrate. The completed reactions were separated by 10% SDS-PAGE followed by Western blotting using NTH1 specific antibodies (**Figure 20**).

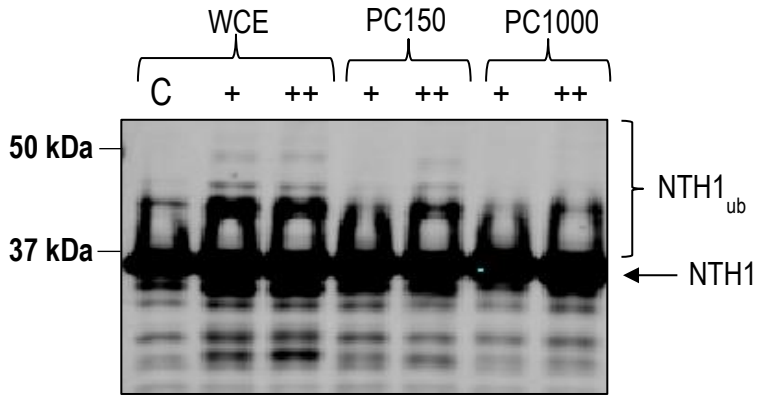

Figure 20. Western blot analysis of the *in vitro* ubiquitylation assay with recombinant NTH1 following cation exchange column chromatography separation of HeLa cell extract. Whole cell extract was prepared from a 20 g commercially available HeLa cell pellet and loaded onto a pre-equilibrated Phosphocellulose cation exchange column. The unbound proteins (PC150) were collected by washing the column in buffer containing 150 mM KCl. Bound proteins were eluted in a singular step-elution with buffer containing 1000 mM KCl (PC1000). Heat denatured (C) HeLa whole cell extract (WCE) or 2.5 μg (+) or 5 μg (++) of WCE was used as the E3 source in an i*n vitro* ubiquitylation assay. Equally 2.5 μg (+) or 5 μg (++) of each fraction (PC150 or PC1000) was subject to the same *in vitro* ubiquitylation reaction containing 0.7 pmol GST-E1 activating enzyme, 2.5 pmol of nine separate E2 conjugating enzymes and 0.6 nmol ubiquitin, with 5.8 pmol of histidine-tagged, recombinant NTH1 as a substrate. Active E3 ligase specific to NTH1 was present in the cell extracts within the chromatography fractions tested. The ubiquitylation assays were carried out at 30°C for 1 h, before completed reactions were separated by 10 % SDS-PAGE and analysed via Western blotting, using NTH1 specific antibodies. Molecular weight markers (kDa), unmodified histidine-tagged NTH1 (NTH1) and ubiquitylated histidine-tagged NTH1 ($NTH1_{ub}$) are indicated. A shift upwards in molecular weight of 8 kDa, or multiples of 8 kDa, is indicative of ubiquitylation.

Heat denatured HeLa whole cell extract was included in this assay as a negative control (**Figure 20**; lane 1). It is anticipated that the heat denaturation of proteins within this extract would have impeded any potential E3 ligase activity. Therefore, it is expected that there would be no observable ubiquitylation of recombinant NTH1 in the presence of heat denatured HeLa extract. Indeed, NTH1 ubiquitylation was not observed in this instance. An upward shift in the protein expression band for NTH1 by approximately 8 kDa is indicative that ubiquitylation of specific lysine residues by an

active E3 ligase may have occurred. Higher molecular weight bands of recombinant NTH1 are observed with the addition of whole cell extract containing active E3 ligase(s) (**Figure 20**; lanes 2 and 3). A comparable shift in molecular weight of NTH1 is observed using increasing amounts of the PC150 chromatography fraction (**Figure 20**; lanes 4 and 5). Weaker ubiquitylation of NTH1 was observed using the maximal amount of PC1000 fraction (**Figure 20**; lane 7), however, this was not as prominent as the ubiquitylation observed in the presence of the PC150 fraction. This suggested that the unbound protein eluting from the Phosphocellulose column contained the major E3 ligase enzyme enabling the ubiquitylation of NTH1. It is for this reason that the PC150 fraction was selected and passed over the subsequent purification columns.

4.3.2. Anion exchange chromatography

The PC150 fraction obtained from cation exchange chromatography was diluted two-fold with no salt containing buffer to reduce the salt concentration and passed over a 20 ml Mono-Q anion exchange column pre-washed with buffer containing 50 mM KCl. Proteins were eluted using a linear gradient from 50 mM to 1 M KCl (**Figure 21, A**) which generated >80 protein fractions. Alternative fractions were subjected to an *in vitro* ubiquitylation assay using recombinant NTH1 as the substrate. The reactions were analysed via 10% SDS-PAGE and Western blotting with NTH1 antibodies (**Figure 21, B, C and D**).

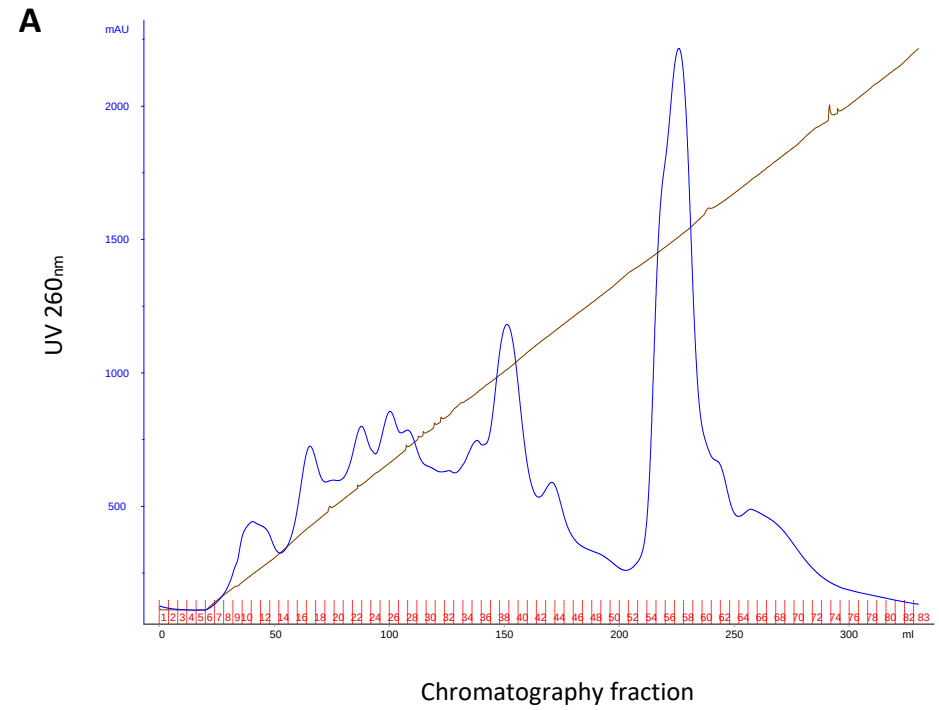
A
mAU
2000
1500
1000
500
UV 260nm
0
50
100
150
200
250
300
ml
Chromatography fraction
B
6 8 10 12 14 16 18 20 22 24 26 28 Fraction
50 kDa
37 kDa
NTH1
KCl
NTH1-E3 1
C
30 32 34 36 38 40 42 44 46 48 50 52 Fraction
75 kDa
50 kDa
37 kDa
NTH1 ub
NTH1
KCl

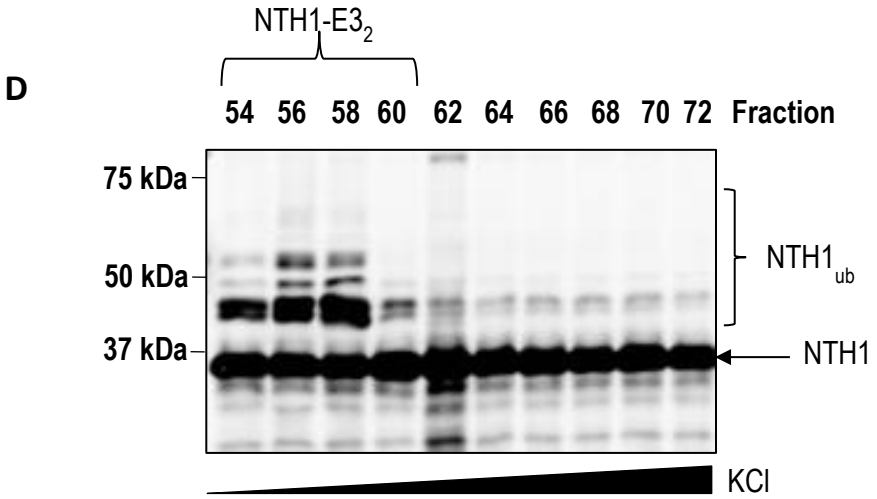

Figure 21. Purification of candidate E3 ligase enzymes specific recombinant NTH1 from HeLa cell extract by anion exchange chromatography. The unbound protein fraction obtained from cation exchange column was diluted two-fold and separated on a 20 ml Mono-Q anion exchange chromatography column using a linear gradient of 50 mM KCl to 1000 mM KCl. The chromatography trace is provided, with the UV at 260 nm represented by the blue line, conductivity represented by the brown line and the chromatography fractions are shown in red (**A**). Alternate fractions were subject to an *in vitro* ubiquitylation assay containing 0.7 pmol GST-E1 activating enzyme, 2.5 pmol of nine individual E2 conjugating enzymes and 0.6 nmol ubiquitin, with 5.8 pmol histidine-tagged recombinant NTH1 as a substrate. The presence of E3 ligase enzymes was provided by the cellular proteins within the chromatography fractions tested. Ubiquitylation assays were carried out at 30 °C for 1 h before completed reactions were separated by 10% SDS-PAGE and analysed via Western blotting, using NTH1 specific antibodies (B, C and D). Molecular weight markers (kDa), unmodified histidine-tagged NTH1 (NTH1) and ubiquitylated histidine-tagged NTH1 (NTH1$_{ub}$) are indicated.

Following Western blot analysis of completed *in vitro* ubiquitylation assays, it was apparent that there were two separate, major NTH1 ubiquitylation activities (**Figure 21, C and D**). An upward shift in the molecular weight bands of NTH1, representing an increase in molecular weight of 8 kDa (or multiples of 8 kDa), was observed largely in fractions 46-50 (**Figure 21;** NTH1-E3$_1$) and a much stronger activity was observed in fractions 54-60 (**Figure 21;** NTH1-E3$_2$). Interestingly, these separate activities could indicate the presence of two different active E3 ligases capable of facilitating the ubiquitylation of recombinant NTH1. Due to the banding patterns of each activity, it was anticipated that NTH1-E3$_1$ represents an E3 ligase which monoubiquitylates NTH1 due to there being one singular shift of molecular weight of NTH1 suggesting the addition of just one ubiquitin moiety. Conversely, it is expected that NTH1-E3$_2$ signifies an E3 ligase which can polyubiquitylate NTH1. This is due to the banding pattern demonstrating the addition of multiple 8 kDa ubiquitin moieties (**Figure 21;**

NTH1-$E3_2$). There were difficulties in purifying the NTH1-$E3_1$ activity further beyond this point, as the activity was very weak and unstable, so the primary focus was to identify the more prominent, and major E3 ligase activity for NTH1 present as NTH1-$E3_2$. As a result, anion exchange fractions representing the NTH1-$E3_2$ activity (**Figure 21, D** fractions 54-60, NTH1-$E3_2$) were combined and further separated using gel filtration (size exclusion) chromatography.

4.3.3. Gel filtration chromatography

Gel filtration separates proteins on the basis of their molecular size and has the additional benefit of being able to indicate the molecular weight of the active E3 ligase within separated fractions. The anion exchange fractions representing the major E3 activity for NTH1 (**Figure 21,** fractions 54-60, NTH1-$E3_2$) were combined and passed over the pre-equilibrated gel filtration (size exclusion) chromatography column. The fractions with a peak in protein quantity were confirmed by analysis of the peaks in UV at 260 nm in the chromatography trace (**Figure 22, A**). Protein containing fractions were subject to the *in vitro* ubiquitylation assay as previous, utilising recombinant NTH1 as the substrate. The completed ubiquitylation assays were separated by 10 % SDS-PAGE followed by analysis via Western blotting using antibodies against NTH1 (**Figure 22, B**).

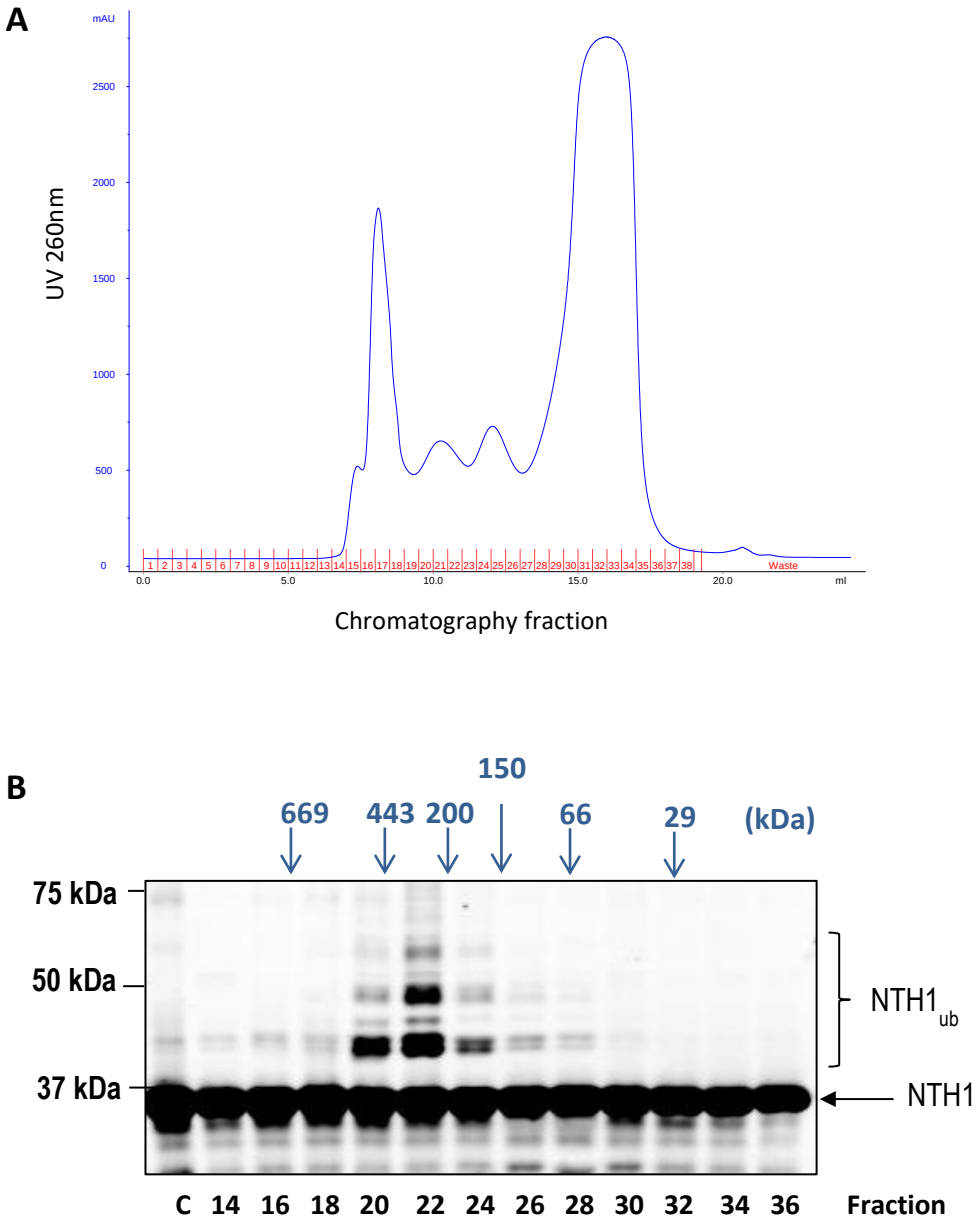

Figure 22. Purification of candidate E3 ligase enzymes specific recombinant NTH1 from HeLa cell extract using size exclusion chromatography. Select fractions from anion exchange chromatography were combined and added to a 24 ml Superdex 200 size exclusion chromatography column. The chromatography trace is provided, with the UV at 260 nm represented by the blue line and the chromatography fractions are shown in red (**A**). Fractions exhibiting a peak in protein were utilised in an *in vitro* ubiquitylation assay containing 0.7 pmol GST-E1 activating enzyme, 2.5 pmol of nine separate E2 conjugating enzymes and 0.6 nmol ubiquitin, with 5.8 pmol recombinant NTH1 as a substrate. The assays were carried out at 30 °C for 1 h before completed reactions were separated by 10% SDS-PAGE and analysed via Western blotting using NTH1 antibodies (**B**). As a control (**B**, lane C), 5 μg heat-denatured whole HeLa cell extract (which is expected to contain no active enzymatic activity) was used in the assay instead of active fraction. Molecular weight markers (kDa), unmodified histidine-tagged NTH1 (NTH1) and ubiquitylated histidine-tagged NTH1

($NTH1_{ub}$) are indicated. In addition, the peak NTH1 ubiquitylation is present in fractions containing proteins approximately 443 kDa–150 kDa in size (as indicated)

.

Following gel filtration chromatography, a peak of ubiquitylation activity specific to recombinant NTH1 was apparent between gel filtration fractions 20-24; demonstrated by a characteristic banding pattern of ~8 kDa shifts of increased molecular weight of NTH1 indicative of polyubiquitylation (**Figure 22, B**). Interestingly, fraction 20 contained proteins with an estimated molecular weight of ~443 kDa, whereas, fraction 24 contained proteins that were approximately 150 kDa in size (**Figure 22, B**). Overall, this suggests that the E3 ligase specific for the *in vitro* polyubiquitylation of recombinant NTH1 could potentially have a molecular weight of between 150 kDa and 443 kDa. Gel filtration fractions 20-24 were combined and passed over a pre-equilibrated ceramic hydroxyapatite chromatography column.

4.3.4 Hydroxyapatite chromatography

Hydroxyapatite is a crystalline form of calcium phosphate which can actually bind both acidic and basic proteins. Fractions 20-24 from the previous gel filtration chromatography separation (**Figure 22, B**) were passed over a pre-equilibrated hydroxyapatite chromatography column. Proteins were eluted from the column via a linear gradient of 5 mM to 500 mM KH_2PO_4 and fractions were collected (**Figure 23, A**). Fractions containing a peak in eluted protein were subject to an *in vitro* ubiquitylation assay using Histidine-tagged, recombinant NTH1 as a substrate. Completed reactions were subject to separation by 10% SDS-PAGE, followed by Western blot analysis using antibodies against NTH1 (**Figure 23, B**).

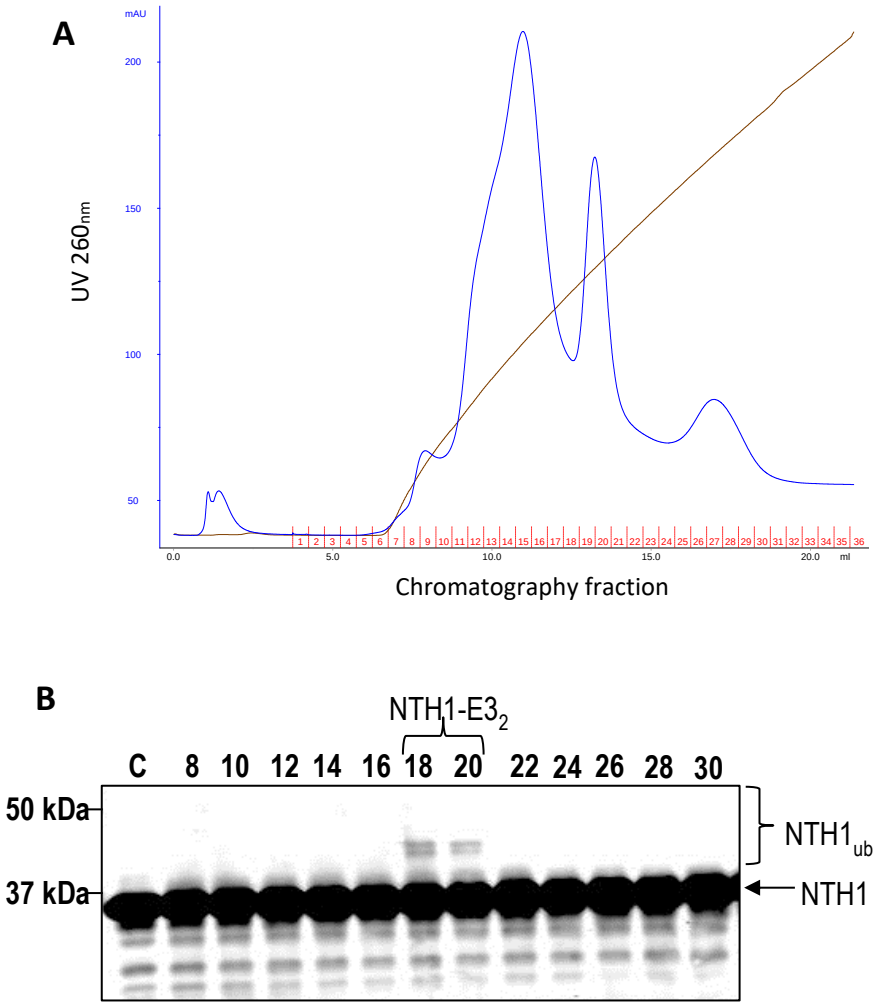

Figure 23. Purification of candidate E3 ligase enzymes specific recombinant NTH1 from HeLa cell extract using hydroxyapatite chromatography. Active fractions from size exclusion chromatography were combined and passed over a 1 ml CHT ceramic hydroxyapatite chromatography column using a linear gradient of 5 mM to 500 mM KPO_4. The chromatography trace is provided, with the UV at 260 nm represented by the blue line, conductivity represented by the brown line and the chromatography fractions are shown in red (**A**). Collected fractions were subject to an *in vitro* ubiquitylation assay with 0.7 pmol GST-E1 activating enzyme, 2.5 pmol of nine E2 conjugating enzymes, 0.6 nmol ubiquitin with 5.8 pmol histidine-tagged recombinant NTH1 as a substrate. Active E3 ligase specific to NTH1 was present in the cell extracts within the chromatography fractions tested. The assay reactions were carried out at 30 °C for 1 h before completed reactions were separated by 10% SDS-PAGE and analysed via Western blotting using NTH1 antibodies (**B**). As a control (**B**, lane C), 5 μg heat-denatured whole HeLa cell extract (which is expected to contain no active enzymatic activity) was used in the assay instead of active fraction. Molecular weight markers (kDa), unmodified histidine-tagged NTH1 (NTH1) and ubiquitylated histidine-tagged NTH1 ($NTH1_{ub}$) are indicated.

Western blot analysis confirmed that hydroxyapatite fractions 18-20 possess E3 ligase activity specific to NTH1, signified by a shift in molecular weight of recombinant

NTH1 upwards on the SDS-PAGE gel (**Figure 23, B**). There is a notable decrease in the strength of ubiquitylation signal following the hydroxyapatite chromatography separation; in particular the amount of polyubiquitylation is substantially reduced (compare **Figure 22, B** and **Figure 23, B**). This could be due to loss of activity of the candidate E3 ligase following interaction with the hydroxyapatite column. Likewise, the activity of the ligase enzyme could have been affected by storage and repeated thawing throughout the purification process. Following hydroxyapatite separation, the active fractions 18-20 (**Figure 23, B**) were combined and passed over a final 1 ml Mono-Q anion exchange chromatography column.

4.3.5. Final anion exchange chromatography

Chromatography fractions containing active E3 ligase activity following hydroxyapatite separation were pooled and passed over a final 1 ml Mono-Q anion exchange chromatography column, which has an improved resolution than the previously used 20 ml Mono-Q column featured in the purification scheme (**Figure 19**). The 1 ml Mono-Q anion exchange chromatography column was pre-equilibrated with 50 mM KCl buffer, before samples were added. Proteins were eluted using a linear gradient of 50 mM to 1000 mM KCl and fractions were collected. The chromatography trace is provided (**Figure 24, A**), with peaks in UV at 260 nm representing protein presence. Fractions featuring a peak in protein were subject to an *in vitro* ubiquitylation assay with Histidine-tagged recombinant NTH1 as a substrate. Completed assays were separated by 10% SDS-PAGE analysed by Western blotting using NTH1 specific antibodies (**Figure 24, B**).

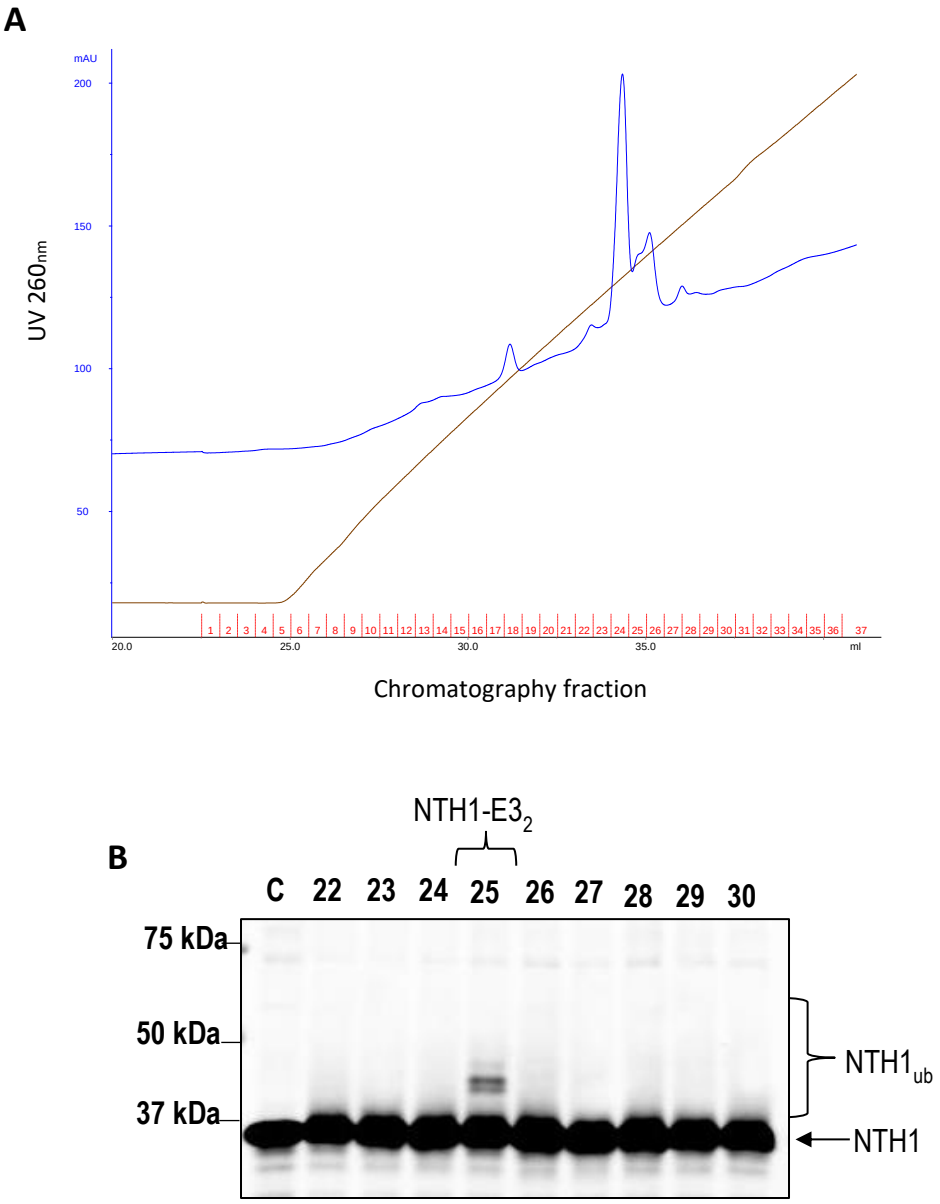

Figure 24. Purification of candidate E3 ligase enzymes specific recombinant NTH1 from HeLa cell extract using final Mono-Q anion exchange chromatography fractions. Active fractions from hydroxyapatite chromatography were combined and passed over a 1 ml Mono-Q anion exchange chromatography column using a linear gradient of 50 mM to 1000 mM KCl. The chromatography trace is provided, with the UV at 260 nm represented by the blue line, conductivity represented by the brown line and the chromatography fractions are shown in red (**A**). Collected fractions featuring peak protein were subject to an *in vitro* ubiquitylation assay with 0.7 pmol GST-E1 activating enzyme, 2.5 pmol of nine separate E2 conjugating enzymes and 0.6 nmol ubiquitin, with 5.8 pmol of recombinant NTH1 as a substrate. Active E3 ligase presence specific to NTH1 was provided in the cell extracts within the chromatography fractions tested. The assay reactions were carried out at 30 °C for 1 h before completed reactions were separated by 10% SDS-PAGE

and analysed via Western blotting, using NTH1 specific antibodies (**B**). As a control (**B**, lane C), 5 μg heat-denatured whole HeLa cell extract (which is expected to contain no active enzymatic activity) was used in the assay instead of active fraction. Molecular weight markers (kDa), unmodified histidine-tagged NTH1 (NTH1) and ubiquitylated histidine-tagged NTH1 ($NTH1_{ub}$) are indicated.

From Western blot analysis of the *in vitro* ubiquitylation assays performed using the final Mono-Q anion exchange chromatography fractions, it was apparent that the presence of a candidate E3 ligase specific to recombinant NTH1, was isolated in just one chromatography fraction (**Figure 24, A**, fraction 25). Once again, there is an observable decrease in the NTH1 ubiquitylation activity within this fraction compared to the initial chromatography separations and the amount of polyubiquitylation is not as obvious. As mentioned previously, the decrease in activity could largely be due to a natural degradation, or loss of activity of the candidate E3 ligase during storage throughout the series of purification steps. Furthermore, the candidate E3 ligase activity may have diminished due to the loss of other proteins, which form complexes with the E3 ligase and support its polyubiquitylation activity. Consequently, the identity of the candidate peptides within the active fraction (**Figure 24, B;** fraction 25) was investigated by mass spectrometry analysis.

4.3.6. Mass spectrometry identification of TRIM26 as an NTH1 specific E3 ligase

Tandem mass spectrometry was employed to identify candidate E3 ligase enzymes present in the peak NTH1 ubiquitylation activity fraction following the final ion exchange chromatography stage (**Figure 24, B;** fraction 25). The mass spectrometry analysis was kindly completed by Professor Robert Beynon and Dr. Deborah Simpson, based at the Institute of Integrative Biology, University of Liverpool. Peptides were formed from the proteins present within the active fraction via trypsinisation and were detected by LC-MS/MS mass spectrometry. To identify candidate proteins, the spectra of proteins obtained from LC-MS/MS were compared using Mascot against the UniProt human database. The list of candidate proteins consisted of 45 proteins in total (**see Appendix**), with only one known to possess any E3 ligase activity from studies within the literature (**Table 7**) which was in the top scoring peptides within the list. Indeed this protein, Tripartite motif-containing protein 26 (TRIM26), has been shown to have E3 ligase activity, mainly implicated in the immune response (168). The protein score for detection of TRIM26 was 62 (**Table 7**) with overall sequence coverage of 19 % (**Figure 25**). This result suggested that

TRIM26 was the major candidate protein that was purified from human cell extracts that is an active E3 ligase for NTH1.

Table 7. A list of peptides detected by LC-MS/MS to identify candidate E3 ligase enzymes specific to recombinant NTH1. Peptides from an ion exchange chromatography fraction, demonstrating ubiquitylation of NTH1, were subject to tandem mass spectrometry. Peptides were resuspended, reduced and trypisinsed to yield peptides for LC separations using an Ultimate 3000 nano system. Mass spectrometry was then performed using the Q Exactive instrument operated in data dependent positive (ESI+) mode to routinely switch between full scan MS and MS/MS acquisition. Survey full scan MS spectra (*m/z* 300–2000) were obtained with a resolution of 70 000 (*m/z* 200) following accumulation of ions to 1×10^6 target value based on predictive automatic gain control values from the previous full scan. Raw data files were searched in Mascot against the UniProt human database. The false discovery rate against a decoy database was 1 %. Within a list of 45 candidate peptides, tripartite motif-containing protein 26 (TRIM26) was the only peptide with known ubiquitylation potential. The peptide score of TRIM26 was 62 with overall coverage of 18 %. The position of TRIM26 within the list of candidate proteins is highlighted in red text.

Number	Score	Description
Q01105	530	Protein SET
P35527	395	Keratin, type I cytoskeletal 9
P35908	257	Keratin, type I cytoskeletal 2
P13645	220	Keratin, type I cytoskeletal 10
P04264	216	Keratin, type II cytoskeletal 1
P04259	109	Keratin, type II cytoskeletal 6B
P02533	107	Keratin, type I cytoskeletal 14
P08579	101	U2 small nuclear ribonucleoprotein B
P39687	95	Acid leucine-rich nuclear phosphoprotein 32
P13647	93	Keratin, type II cytoskeletal 5
P62318	93	Small nuclear ribonucleoprotein Sm D3
P09661	90	U2 small nuclear ribonucleoprotein A
P62318	84	Small nuclear ribonucleoprotein F
P02538	76	Keratin, type II cytoskeletal 6A
P62316	74	Small nuclear ribonucleoprotein Sm D2
O00629	69	Importin subunit alpha-3
P05455	66	Lupus La protein
P14678	66	Small nuclear ribonucleoprotein-associated proteins B and B’
Q12899	**62**	**Tripartite motif-containing protein 26**
Q92688	61	Acid leucine-rich nuclear phosphoprotein 32
P07437	59	Tubulin beta chain

P11142	58	Heat shock cognate 71 kDa protein
P11021	53	78 kDa glucose-related protein

1 MATSAPLRSL EEEVTCSICL DYLRDPVTID CGHVFCRSCT TDVRPISGSR
51 PVCPLCKKPF KKENIRPVWQ LASLVENIER LKVDKGRQPG EVTREQQDAK
101 LCERHREK**LH YYCEDDGK**LL CVMCRESREH RPHTAVLMEK AAQPHREKIL
151 NHLSTLRRDR DK**IQGFQAK**G EADILAALKK LQDQRQYIVA EFEQGHQFLR
201 EREEHLLEQL AKLEQELTEG REKFKSRGVG ELAR**LALVIS ELEGKAQQPA**
251 **AELMQDTRDF LNR**YPRKK**FW VGKPIAR**VVK KKTGEFSDK**L LSLQR**GLREF
301 QGKLLR**DLEY K**TVSVTLDPQ SASGYLQLSE DWK**CVTYTSL YKSAYLHPQQ**
351 **FDCEPGVLGS KGFTWGK**VYW EVEVEREGWS EDEEEGDEEE EGEEEEEEEE
401 AGYGDGYDDW ETDEDEESLG DEEEEEEEEE EEVLESCMVG VARDSVKRKG
451 DLSLRPEDGV WALRLSSSGI WANTSPEAEL FPALRPRRVG IALDYEGGTV
501 TFTNAESQEL IYTFTATFTR RLVPFLWLKW PGTR**LLLRP**

Figure 25. Peptides and peptide fragments of TRIM26 detected by LC-MS/MS. Peptides from an ion exchange chromatography fraction, demonstrating ubiquitylation of NTH1, were subject to tandem mass spectrometry. Peptides were re-suspended, reduced and trypsinised to yield peptides for LC separations using an Ultimate 3000 nano system. Mass spectrometry was then performed using the Q Exactive instrument operated in data dependent positive (ESI+) mode to routinely switch between full scan MS and MS/MS acquisition. Survey full scan MS spectra (*m/z* 300–2000) were obtained with a resolution of 70 000 (*m/*z 200) following accumulation of ions to 1×10^6 target value based on predictive automatic gain control (AGC) values from the previous full scan. Raw data files were searched in Mascot against the UniProt human database. The false discovery rate (FDR) against a decoy database was 1 %. Within a list of 45 candidate peptides, tripartite motif-containing protein 26 (TRIM26) was the only peptide with known ubiquitylation potential. The peptide score of TRIM26 was 141.21 with overall coverage of 19%. Peptide fragments detected within the sequence for TRIM26 are highlighted in red.

4.4. TRIM26 is the active E3 ligase purified from HeLa cell extracts that ubiquitylates NTH1

Despite mass spectrometry analysis identifying TRIM26 as the only peptide with known E3 ligase activity in the final active chromatography fraction, there are still over 600 E3 ligases proposed to exist. With this in mind, it was possible that the active fraction could contain another E3 ligase responsible for NTH1 ubiquitylation, which had been overlooked and not able to be detected by mass spectrometry. Therefore, it became imperative that we confirmed TRIM26 as the active E3 ligase specific to NTH1 using further methods.

4.4.1. TRIM26 protein in purified active fractions aligns with NTH1 ubiquitylation activity

Firstly, to confirm the presence of TRIM26 in the peak active fraction following the final ion exchange chromatography stage, fractions 22-30 (**Figure 24, A and B**) were separated by 10 % SDS-PAGE and analysed via Western blotting. However, on this occasion immunoblotting was completed using antibodies specific to TRIM26 (**Figure 26, B**). The molecular weight of TRIM26 is known to be approximately 62 kDa and indeed the peak presence of TRIM26 protein correlates with the peak NTH1 ubiquitylation activity when the two Western blot membranes are aligned (**Figure 26, A and B;** comparing fraction 25). It is apparent that TRIM26 presence is in fact within multiple fractions (**Figure 26;** B, fractions 23-28), whereas ubiquitylation of NTH1 is largely only visible in fraction 25 (**Figure 26;** A, fraction 25). This discrepancy could be due to a minimum threshold of TRIM26 protein required for activity. This theory is supported by the observation that the peak presence of TRIM26 still corresponds with NTH1 ubiquitylation (**Figure 26, A and B**).

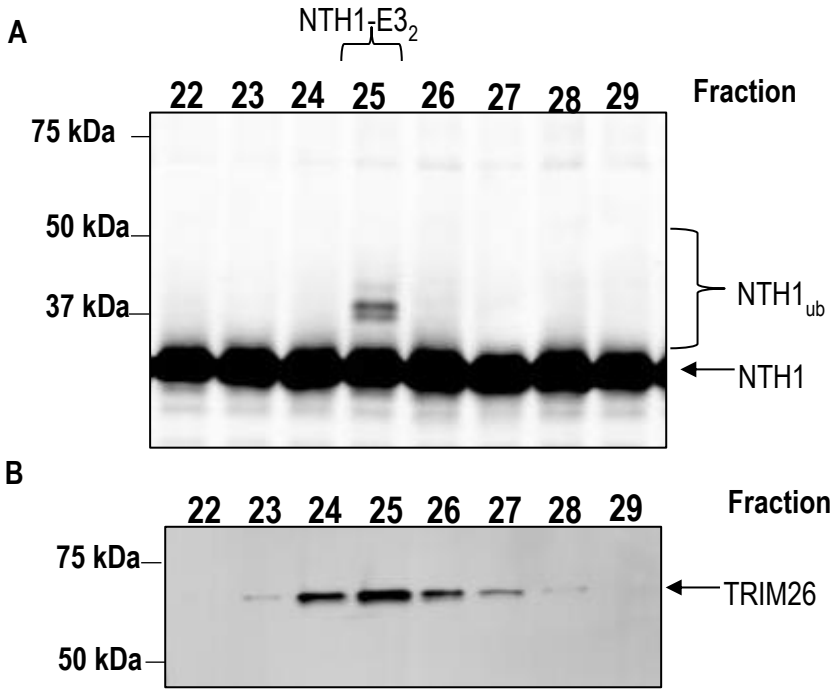

Figure 26. Alignment of the Western blot analysis of *in vitro* ubiquitylation reactions using recombinant NTH1 as a substrate (A) with the presence of TRIM26 (B). Anion exchange chromatography fractions were subject to an *in vitro* ubiquitylation assay containing 0.7 pmol GST-E1 activating enzyme, 2.5 pmol of nine separate E2 conjugating enzymes and 0.6 nmol ubiquitin, with 5.8 pmol of recombinant NTH1 as a substrate. The assay reactions were carried out at 30 °C for 1 h before completed reactions were separated by 10% SDS-PAGE and analysed via Western blotting using NTH1 specific antibodies (**A**). Molecular weight markers (kDa), unmodified histidine-tagged NTH1 (NTH1) and ubiquitylated histidine-tagged NTH1 ($NTH1_{ub}$) are indicated. Ubiquitylation of NTH1, represented by an upward shift in molecular weight of 8 kDa, occurred in fraction 25 (**A**). To verify that tripartate motif containing 26 (TRIM26) is the active E3 ligase within fraction 25, the same anion

exchange fractions were separated by 10 % SDS-PAGE and analysed by Western blotting with TRIM26 specific antibodies (**B**). The peak presence of TRIM26 in fraction 25 aligns with the ubiquitylation of recombinant NTH1 (**A** and **B**).

4.4.2. Cloning and purification of His-tagged, recombinant TRIM26 protein

To further prove that TRIM26 is an active E3 ligase specific to ubiquitylation of NTH1, recombinant TRIM26 protein was aimed to be expressed and purified from bacterial cells. The protein would then be employed in place of active chromatography fractions generated from HeLa cell extract fractionation within *in vitro* ubiquitylation assays with NTH1 as a substrate. It was anticipated that TRIM26 would induce observable NTH1 ubiquitylation *in vitro*. The first step in this process was the recloning of the TRIM26 DNA sequence into a bacterial expression plasmid.

4.4.2.1. LIC cloning of TRIM26

A LIC strategy was employed to clone the *trim26* gene from a mammalian expression plasmid (kindly provided by Prof A. Garcia-Sastre, The Icahn School of Medicine at Mount Sinai, USA), into a bacterial expression plasmid (pET28a). LIC cloning uses the exonuclease activity of T4 DNA polymerase to generate complementary overhangs to aid the stable association between an expression vector fragment and an insert (**Figure 17**). An empty pET28a vector (from Novagen), was amplified using oligonucleotides flanked by LIC sequences (**Table 4**). Separately to this, an insert of histidine-tagged *trim26* within the mammalian expression plasmid, was PCR amplified using oligonucleotides flanked by the same LIC sequences as those used to amplify the expression plasmid (**Table 4**). Following the separate PCR reactions, the size of the DNA products obtained were analysed on agarose gels as an indication that the correct sequences had been amplified (**Figure 27**). The empty pET28 vector is known to be 5369 base pairs (**Figure 16**). Following analysis of five separate PCR amplification reactions on agarose gels with a DNA ladder consisting of DNA fragments of known base pair lengths, it was apparent that products of 5369 base pairs had been obtained in all reactions (**Figure 27, A**; lanes 1-5). These reactions were selected and pooled for subsequent PCR purification.

Separately to this the *trim26* gene insert was PCR amplified. It was apparent that PCR products of the expected size of 1617 base pairs had been obtained in all amplification reactions (**Figure 27, B**; lanes 1-4). Despite PCR products of the approximate size of 1617 base pairs, being visible across all four lanes, reactions 2 and 4 (**Figure 27; B**,

lanes 2 and 4) contained amplification products of this approximate size with the least impurities; demonstrated by the lack of other additional bands following agarose gel analysis. Therefore, these reactions were selected and pooled for subsequent PCR purification.

The pooled PCR reactions were then subjected to incubation with DpnI, which acts to remove methylated, template DNA. Following this, the DNA was further purified using a PCR purification kit. Afterwards, complementary overhangs between the pET28 expression plasmid and the *trim26* insert were formed by using the exonuclease activity of T4 DNA polymerase. To ensure that complementary overhangs are formed by T4 DNA polymerase activity, dCTP was added to the polymerase reaction containing the pET28 vector, whereas, dGTP was added to the reaction containing the *trim26* insert. The addition of one dNTP to each reaction leads to an equilibrium of exonuclease and polymerase activity at the site of the first occurrence of this nucleotide. The complementary overhangs generated using this method were then annealed together by incubating different ratios of insert and vector (1:1 and 1:3).

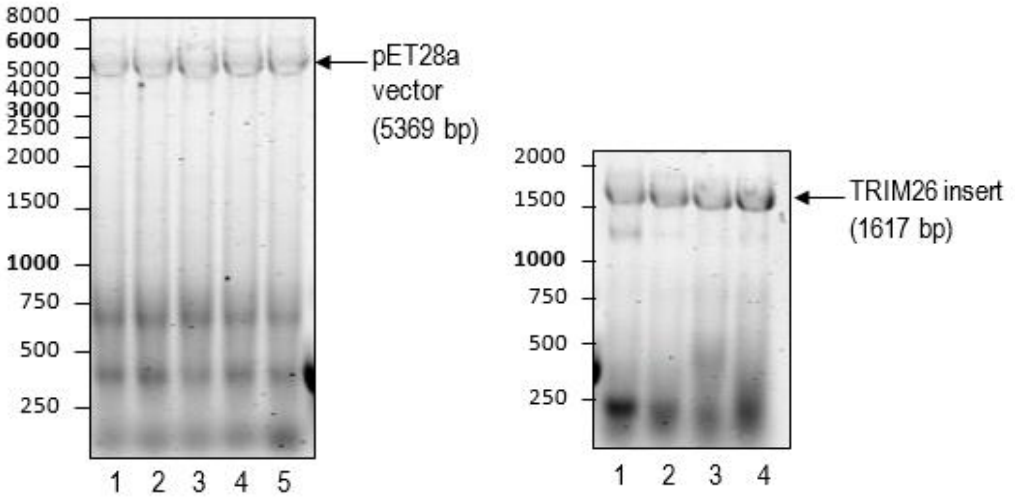

Figure 27. PCR amplification of a pET28a vector (A) and an insert for TRIM26 expression (B) for use in a ligase independent cloning (LIC) strategy. An empty pET28a vector was PCR amplified using relevant oligonucleotides flanked by corresponding LIC sequences. All five reactions (A, lanes 1-5) were completed in the presence of GC buffer only. The size of each reaction product was confirmed using a 1% agarose gel (**A**). As bands corresponding to the correct size (5369 bp) were apparent in all reactions, they were all subject to DpnI treatment and pooled during PCR purification. Similarly, an insert for *trim26* gene was also PCR amplified using relevant oligonucleotides flanked by corresponding LIC sequences and the size of the reaction products analysed on a 1% agarose gel (**B**). Reaction 1 was performed in the presence of HF buffer, with the addition of DMSO in reaction 2 (lanes 1 and 2), whereas, reaction 3 was performed with GC buffer, with the addition of DMSO in reaction 4 (lanes 3 and 4). From this it was apparent that all four reactions (B, lanes

1-4) yielded PCR products displaying DNA bands corresponding to products of the expected size (1617). All four reactions were therefore subject to DpnI treatment before being pooled during PCR purification.

Constructs of pET28TRIM26 were amplified by transformation into library efficient DH5α bacterial cells and grown on selective media. Successful colonies were inoculated into a 5 ml culture of LB media containing 150 µg of selective antibiotic (kanamycin) and grown overnight at 37°C and 250 rpm. Amplified plasmid DNA was then purified from bacterial contaminants using the QIAprep Spin Miniprep Kit. A diagnostic digest using an appropriate restriction enzyme, Van91I, was then performed as a preliminary method to assess the identity of each plasmid. Products of the restriction digest were analysed on a 0.8% agarose gel (**Figure 28**). From this, it was apparent that the correct sized products (6309 and 705 bp) were obtained following digestion of plasmids 1, 2 and 4 (**Figure 28**, lanes 1, 2 and 4). However, the presence of bolder bands of the expected sizes following restriction enzyme digestion of plasmid 4 (**Figure 28**, lane 4) suggests the highest concentration of plasmid. For this reason, plasmid 4 (**Figure 28**, lane 4) was selected and sequenced using the Sanger Sequencing Service (Source Bioscience Sequencing, Nottingham, UK) which further confirmed the correct ligation of the *trim26* gene insert into the respective pET28a expression vector.

A

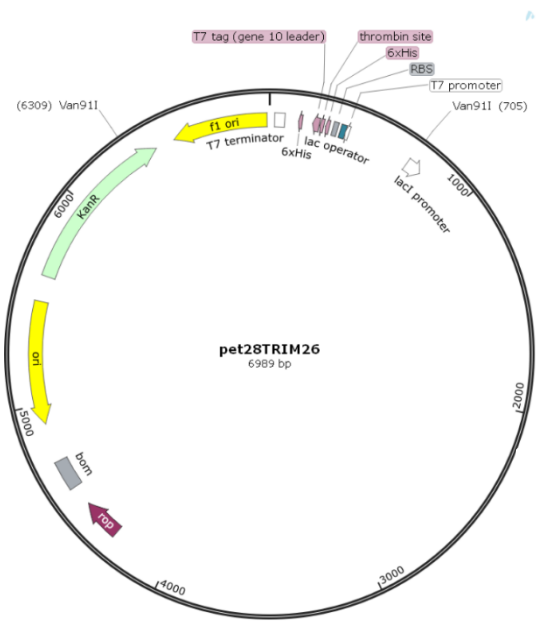

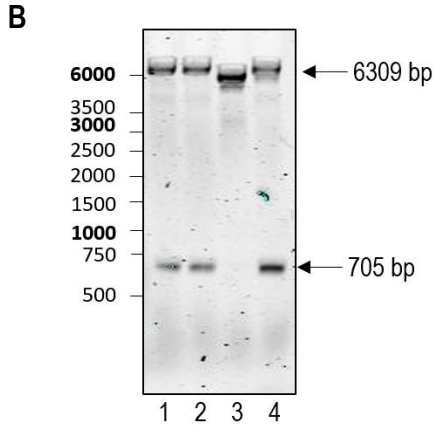

Figure 28. Restriction digest to determine the successful generation of an insert corresponding to TRIM26 ligated into a pET28 expression plasmid via a ligase independent cloning (LIC) strategy. Different ratios of PCR purified pET28a vector and *trim26* gene insert DNA were incubated (1:1, lanes 1 and 2 or 1:3, lanes 3 and 4) for 10 mins at 22°C as part of the LIC cloning strategy. Plasmid constructs were transformed into library efficient DH5α bacterial cells grown on selective agar. A 5 ml overnight culture of successful colonies was generated in the presence of selective antibiotics before plasmid DNA was purified via the QIAprep Spin Miniprep Kit. A restriction digest of plasmid DNA using Van91 was then performed to preliminary assess if the correct construct has been formed. A schematic of the pET28TRIM26 bacterial expression vector formed is depicted, showing the restriction sites of Van91 and the expected sizes of the DNA fragments formed (**A**). Products of the restriction digest were analysed on a 0.8% agarose gel. Lanes 1-4 represent four different plasmids being assessed (**B**). From this it was apparent that the correct digest sizes (6309bp and 705 bp) were produced via digestion of plasmids 1, 2 and 4 (lanes 1, 2 and 4). However, plasmid 4 appeared to have a higher concentration represented by bolder bands on the agarose gel (lane 4). This plasmid was then sequenced via the Sanger Sequencing Service to further confirm the correct sequence.

4.4.2.2. Bacterial expression of TRIM26

A test expression was performed in order to optimise which bacterial cell line provided maximum TRIM26 protein expression. The constructs were transformed into a range of Rosetta cells which were then grown in a 5 ml culture of LB media containing 150 µg of selective antibiotic (kanamycin) and grown overnight at 37°C and 250 rpm. Following this, a 40 ml culture was generated in the presence of selective antibiotic incubated at 37°C and 250 rpm, until the OD_{600nm} was approximately 0.6. An aliquot of the cell suspension was removed before protein expression was induced via IPTG for 3 h at 37°C and 250 rpm. An aliquot of the induced cell suspension was then removed. The aliquots of cell suspension before and after IPTG induction were

resuspended in SDS loading buffer, sonicated and denatured at 95ºC for 5 min before loading onto a 10% SDS-PAGE gel for analysis of cellular proteins (**Figure 28**).

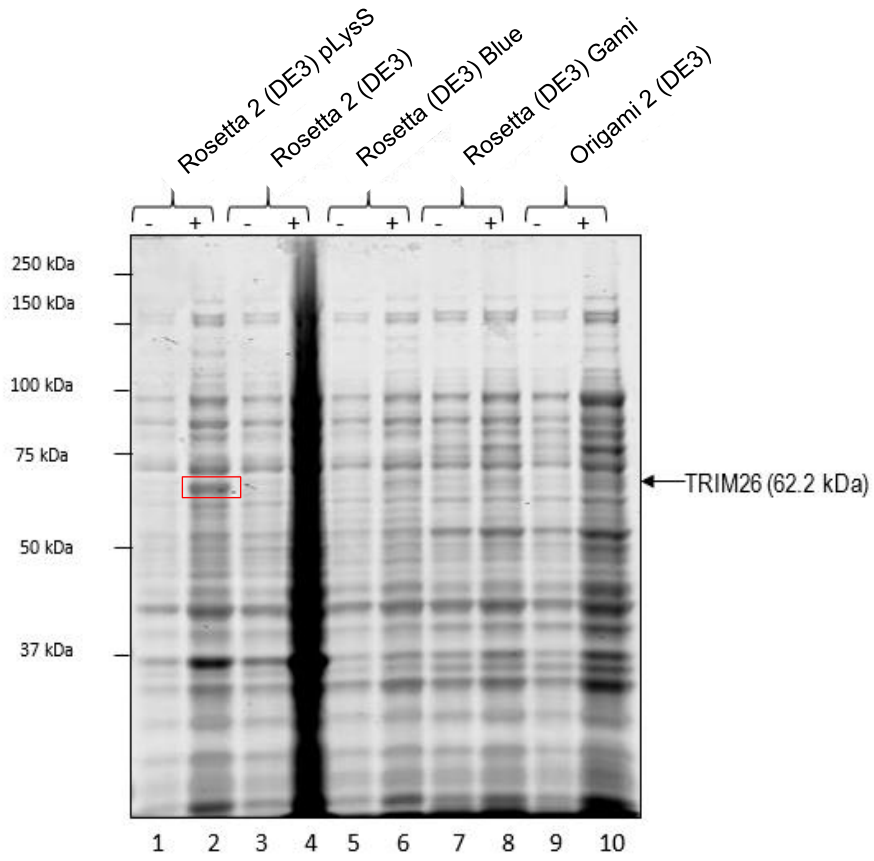

Figure 28. Test expression of a pET28TRIM26 plasmid in a range of Rosetta cell lines to obtain maximum histidine-tagged TRIM26 protein expression. A construct of a pET28a expression vector containing an insert corresponding to histidine-tagged TRIM26 protein expression was generated via a Ligase Independent Cloning (LIC) strategy. The plasmid was transformed into a range of Rosetta cell lines; Rosetta 2(DE3) pLysS cells (lanes 1-2), Rosetta 2 cells (lanes 3-4), Rosetta-blue cells (lanes 5-6) Rosetta-gami cells (lanes 7-8) and Origami 2 (DE3) cells (lanes 9-10). Following transformation, a 5 ml overnight culture with 150 µg selective antibiotics of each transformed cell line was generated, followed by a 40 ml expression culture in the presence of selective antibiotics. The expression culture was grown until the OD_{600nm} reached 0.6. An aliquot of the culture was then removed before induction of protein expression (-) via the addition of 1 mM IPTG for 3 h at 30°C, 225 rpm. After this, an aliquot after IPTG induction was also removed (+). Each aliquot was re-suspended in SDS-loading buffer, sonicated, heated to 95ºC for 5 min before proteins were analysed via SDS-PAGE on a 10 % gel. Samples pre-IPTG (-) and post-IPTG induction (+) were analysed in tandem. The protein expression of TRIM26, represented by a protein band at 62.2 kDa, is most apparent using Rosetta (DE3) pLysS cells (lane 2, +); highlighted using a red box.

From the test expression, it was apparent that only Rosetta2 (DE3) pLysS cells appeared to provide the optimum expression of histidine-tagged TRIM26 protein

(**Figure 28;** lane 2), represented by the boldest band at a molecular weight of approximately 62.2 kDa. Despite this, the protein still appeared not to be significantly overexpressed in large amounts. For this reason and to increase protein quantity for purification, three 400 ml expression cultures of Rosetta2 (DE3) pLysS containing the pET28a-TRIM26 construct were generated. Protein expression of TRIM26 was then induced for 3 h at 30°C and 250 rpm, via the addition of 1 mM IPTG. The three cell cultures were then combined and the bacterial cells were then pelleted, resuspended in lysis buffer with protease inhibitors then cells lysed via incubation with lysozyme followed by sonication. Cellular debris was removed by centrifugation and the supernatant filtered using syringe filters.

In order to purify Histidine-tagged TRIM26 protein, the filtered supernatant was then applied to a pre-equilibrated 1 ml HisTrap column. Proteins were separated via affinity chromatography using a gradient elution of 5 mM to 500 mM imidazole. The chromatography trace is provided (**Figure 29, A**), with peaks in UV at 260 nm representing protein presence. The purity of the chromatography fractions was evaluated by 14% SDS-PAGE in addition to Western blotting with TRIM26 specific antibodies. Histidine-tagged TRIM26 has a molecular weight of approximately 62.2 kDa. Using this as a reference, from the SDS-PAGE analysis there was a suggestion that TRIM26 was present in chromatography fractions 8-24, peaking in approximately fractions 12-14, although not in significant quantities (**Figure 29, B**). The Western blot further confirmed this, although the antibodies appeared to have a greater cross-reactivity with either the degradation products of TRIM26, or with bacterial protein contaminants (**Figure 29, C**). Due to this, the purest TRIM26 containing fractions (fractions 11-16) were selected, pooled and concentrated using 10 kDa centrifugal filters for further purification by ion exchange (MonoQ) chromatography.

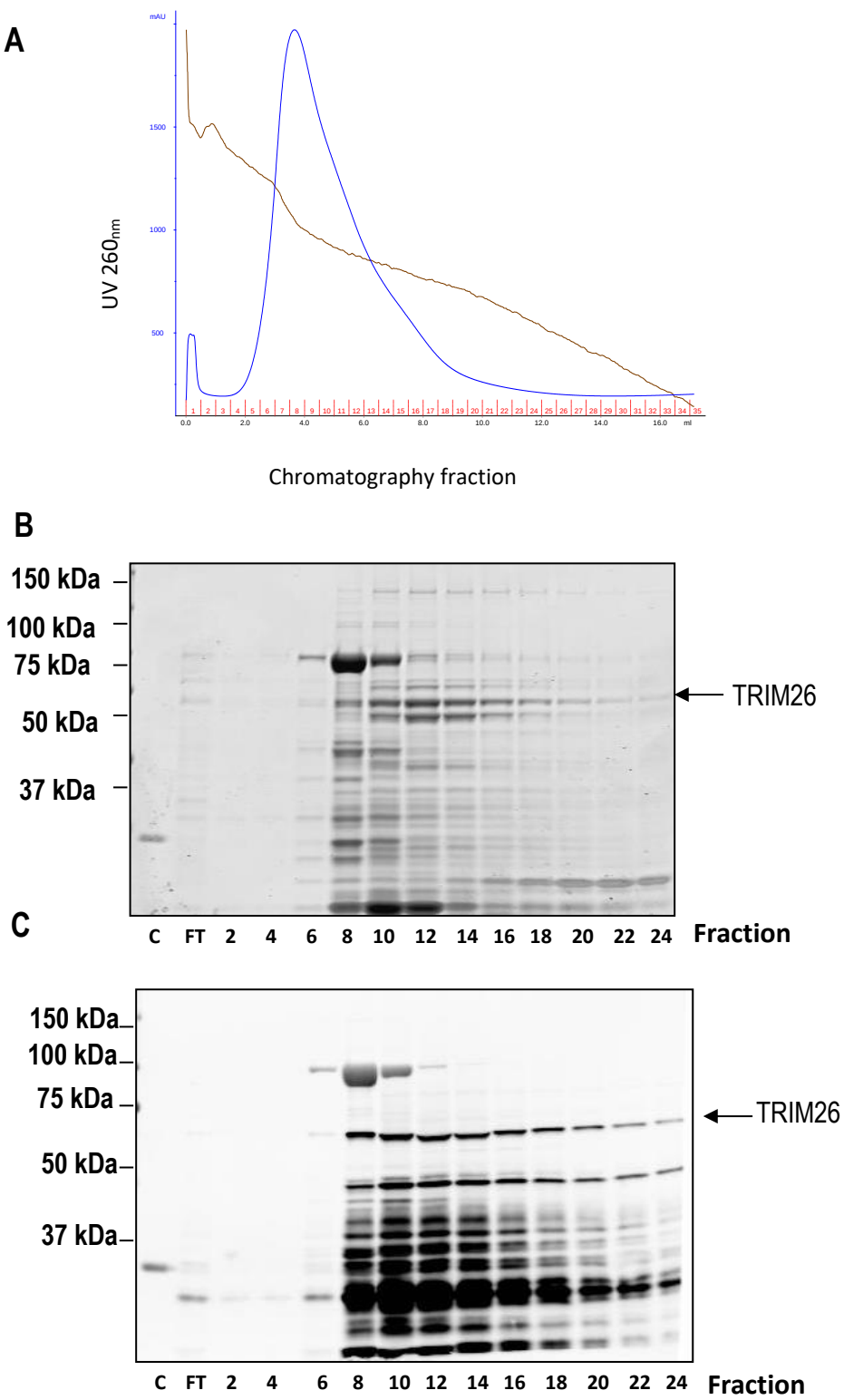

Figure 29. Affinity chromatography purification of recombinant TRIM26 following bacterial expression of the relevant plasmid. Bacterial cells transformed with pET28a-TRIM26 bacterial expression plasmid were cultured into a 400 ml expression culture until the OD_{650nm} reached 0.6. Bacterial expression of recombinant TRIM26 was then induced via of isopropyl β-D-1-thiogalactopyranoside (IPTG) for 3 h at 30°C. Bacterial cells were then pelleted and lysed by sonication in the presence of protease inhibitors. Recombinant TRIM26 was separated from bacterial proteins

via affinity chromatography using a 1 ml HisTrap column and a linear gradient elution of 5 mM to 500 mM imidazole. The chromatography trace is provided, with the UV at 260 nm represented by the blue line, conductivity represented by the brown line and the chromatography fractions are shown in red (**A**). Chromatography fractions were collected and purity analysed by 14% SDS-PAGE (**B**) and Western blotting using antibodies specific to TRIM26 (**C**). Molecular weight markers (kDa) and TRIM26 presence is indicated.

The chromatography trace following separation of TRIM26-containing protein fractions using a 1 ml ion exchange (MonoQ) chromatography column is provided (**Figure 30, A**) with peaks of protein present that were subject to 14 % SDS-PAGE separation in addition to Western blotting with TRIM26 specific antibodies. From this, it was apparent that protein bands corresponding to the molecular weight of TRIM26 (62.2 kDa) were most likely present in fractions 11-14 (**Figure 30, B**). These bands were also visible by Western blotting although as in the previous figure, the antibodies used are of very poor quality and have a higher cross-reactivity with a likely degradation product of TRIM26 at 50 kDa which is significantly less abundant as observed following SDS-PAGE analysis (**Figure 30, C**). Fractions 11-14 were selected, pooled and concentrated using 10 kDa centrifugal filters to generate a concentrated TRIM26 stock for subsequent assays. To improve preservation of the activity of the concentrated stock of the recombinant E3 ubiquitin ligase, it was stabilised by the addition of a 50 % glycerol solution (1:1), aliquoted and stored at -80°C.

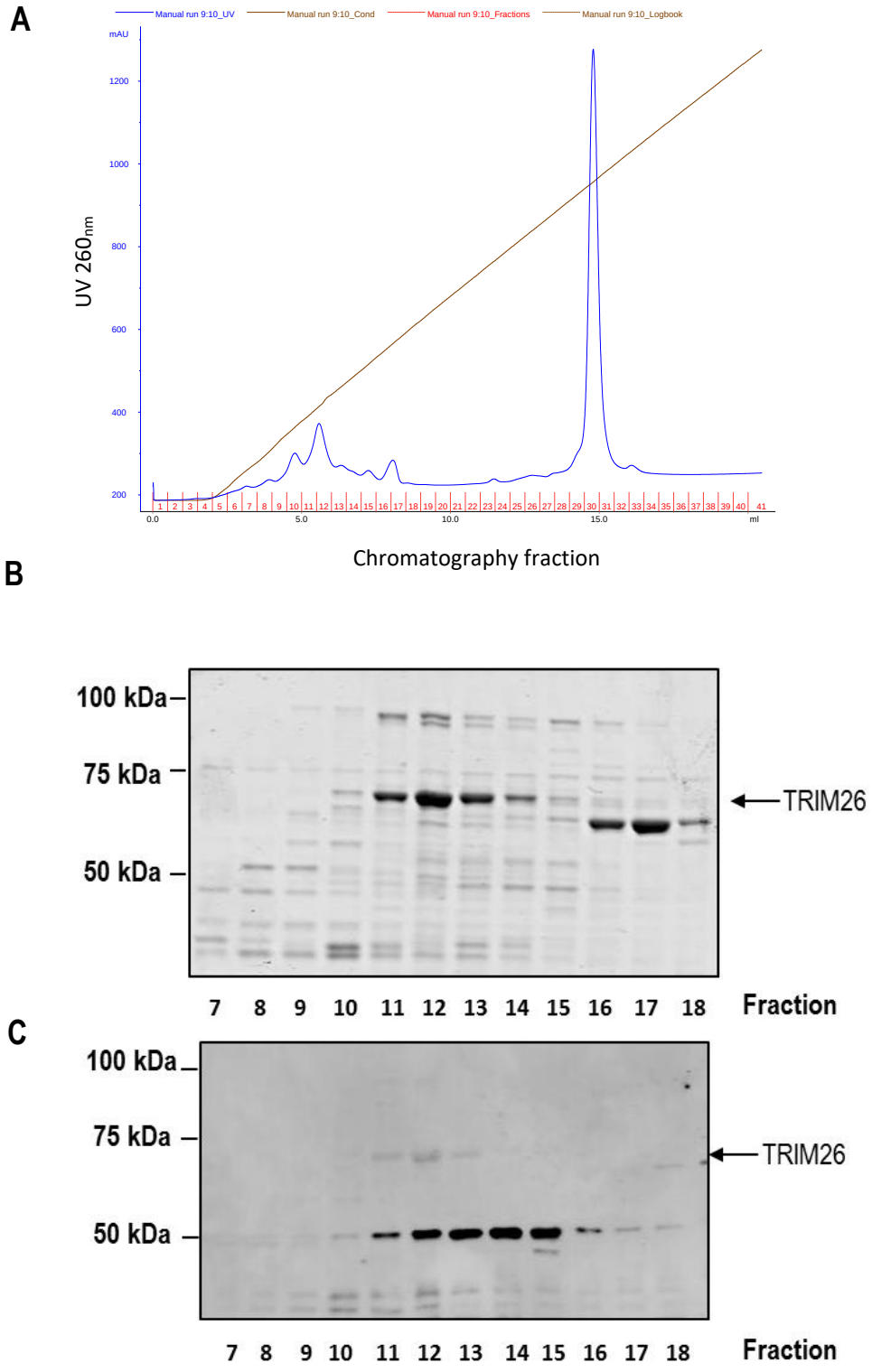

Figure 30. Ion exchange chromatography purification of recombinant TRIM26. Recombinant TRIM26 was expressed using a pET28 bacterial expression plasmid in Rosetta2 (DE3) pLysS cells. The recombinant histidine-tagged TRIM26 protein was separated from bacterial contaminants using affinity chromatography and select fractions pooled and concentrated before being added to a pre-equilibrated 1 ml MonoQ ion exchange chromatography column. The chromatography trace is provided, with the UV at 260 nm represented by the blue line, conductivity represented

by the brown line and the chromatography fractions are shown in red (**A**). Proteins were eluted by a linear gradient of 50 mM to 1000 mM KCl. Fractions were collected and analysed by 14 % SDS-PAGE (**B**) followed by Western blotting with TRIM26 specific antibodies (**C**). Molecular weight markers (kDa) and TRIM26 presence are indicated.

4.4.2.3 Activity of recombinant TRIM26 against NTH1 and E2 dependency

Purification of recombinant TRIM26 enabled further verification that it is indeed the active cellular E3 ligase which acts on NTH1. An increasing amount (19 fmol or 26 fmol) of purified recombinant TRIM26 was used in an *in vitro* ubiquitylation assay containing recombinant NTH1 as the substrate protein, with GST-E1 activating enzyme, nine E2 conjugating enzymes and ubiquitin. The reaction was carried out at 30 °C in a shaking incubator for 1 h at 800 rpm. The completed assay was then separated by 10 % SDS-PAGE and analysed by Western blotting using NTH1 specific antibodies (**Figure 31**).

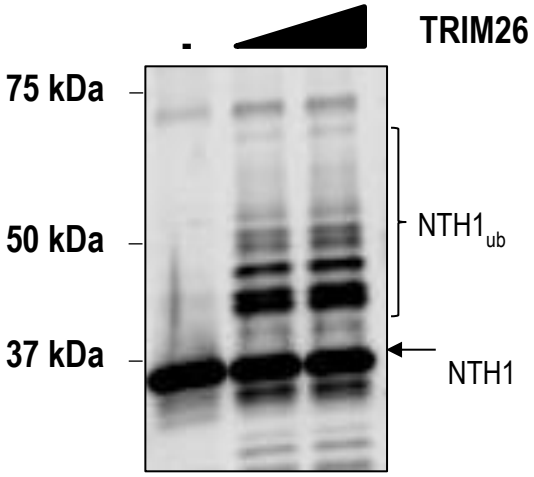

Figure 31. Western blot analysis of an *in vitro* ubiquitylation assay featuring recombinant TRIM26 as the E3 ligase in the presence of NTH1 as the reaction substrate. Ubiquitylation assays were performed by combining 0.7 pmol GST-E1 activating enzyme, 2.5 pmol of nine E2 conjugating enzymes, 0.6 nmol ubiquitin and 5.8 pmol of histidine-tagged, recombinant NTH1. To this, a titration of recombinant TRIM26 (0 fmol, 19 fmol and 26 fmol) was added separately to each ubiquitylation assay. The assay reactions were carried out at 30 °C for 1 h in a shaking incubator at 800 rpm, before completed reactions were separated by 10 % SDS-PAGE and analysed via Western blotting using NTH1 specific antibodies. Ubiquitylation of NTH1 was apparent in reactions containing recombinant TRIM26 only and was not present in the control reaction containing no TRIM26 (-). Molecular weight markers (kDa), unmodified histidine-tagged NTH1 (NTH1) and ubiquitylated histidine-tagged NTH1 ($NTH1_{ub}$) are indicated.

Visualisation of the Western blot analysis shows that in the presence of recombinant TRIM26 there is an observable banding pattern demonstrating a shift in molecular weight of NTH1 (**Figure 30**; lanes 2 and 3). This represents that moieties of ubiquitin (8 kDa in size) are likely to have been added onto specific lysine residues of NTH1 via the active E3 ligase. An upward shift in molecular weight of NTH1 is not observed in the absence of recombinant TRIM26 (**Figure 30**; lane 1). Overall, this observation confirms that TRIM26 is an active *in vitro* E3 ligase enzyme that is targeting ubiquitylation of recombinant NTH1.

A final assessment used to verify that TRIM26 is the active E3 ligase specific to NTH1, was completion of an E2 dependency screen (**Figure 31**). It is acknowledged that E3 ligase enzymes demonstrate dependency on the presence of specific E2 conjugating enzymes to effectively ubiquitylate substrate proteins. Based on this, the E2 dependency of active chromatography fractions purified from HeLa cell extracts from the gel filtration stage (**Figure 22**) of the purification process (**Figure 19**) was compared to the E2 specificity of recombinant TRIM26. For the E2 screen, *in vitro* ubiquitylation assays were performed using recombinant NTH1 as the substrate protein combined with GST-E1 activating enzyme and ubiquitin. To each reaction, an individual E2 conjugating enzyme was added separately (UbcH2, UbcH3, UbcH5a, UbcH5b, UbcH5c UbcH6, UbcH7, UbcH8 or UbcH10). The presence of E3 ligase activity was provided in the form of a volume of active gel filtration chromatography fraction (**Figure 22;** fraction 22) or recombinant TRIM26. The assay reactions were carried out at 30 °C for 1 h at 800 rpm, before separation by 10 % SDS-PAGE and analysis via Western blotting using NTH1 specific antibodies. The Western blots were aligned for ease of comparison (**Figure 32**).

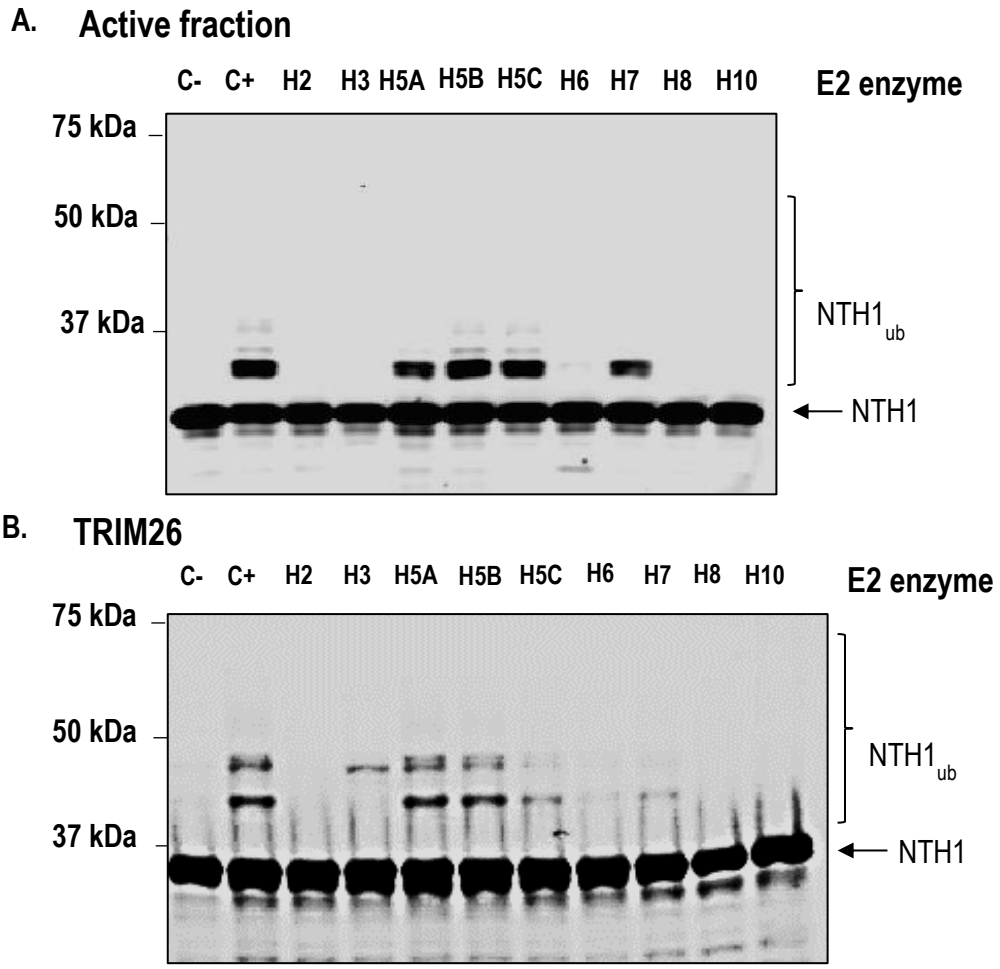

Figure 32. Western blot analysis of *in vitro* ubiquitylation assays examining the E2 specificity of the E3 ligase in an active chromatography fraction compared to recombinant TRIM26. Ubiquitylation assays were performed by combining 0.7 pmol GST-E1 activating enzyme, 0.6 nmol ubiquitin and 5.8 pmol of histidine-tagged recombinant NTH1 as a substrate. To this, 2.5 pmol of each E2 conjugating enzyme (UbcH2, UbcH3, UbcH5a, UbcH5b, UbcH5c UbcH6, UbcH7, UbcH8 or UbcH10) was added separately. E3 ligase activity was provided in the form of 2.5 µl of active gel filtration chromatography fraction (A) or by the addition of 26 fmol of recombinant TRIM26 (B). The ubiquitylation assays were carried out at 30 °C for 1 h at 800 rpm, before completed reactions were separated by 10 % SDS-PAGE and analysed via Western blotting using NTH1 antibodies. Control reactions included the addition of no E2 conjugating enzymes (C-) or the addition of all nine E2 enzymes combined (C+). Molecular weight markers (kDa), unmodified histidine-tagged NTH1 (NTH1) and ubiquitylated histidine-tagged NTH1 ($NTH1_{ub}$) are indicated.

In control reactions in the absence of an E3 ligase there is no evidence of NTH1 ubiquitylation (**Figure 32, A and B**, lane 1). However as expected, ubiquitylation of NTH1 is stimulated by either active purified fraction or TRIM26 in the presence of all nine E2 conjugating enzymes (**Figure 32, A and B**, lane 2). On investigating the E2 dependency of the E3 ligase acting on NTH1 *in vitro*, it is apparent that the active E3

ligase present within the active purified fraction from HeLa cell extracts is dependent on the following E2 conjugating enzymes; UbcH5A, UbcH5B, UbcH5C and UbcH7 (**Figure 32, A**). Ubiquitylation of NTH1, represented by an upwards shift in molecular weight of approximately 8 kDa, is observed within reactions containing only these E2 conjugating enzymes. The degree of ubiquitylation appears equivalent to that observed when all nine E2 conjugating enzymes are present (**Figure 32, A**, lane 2). In addition, ubiquitylation of NTH1 with TRIM26 as the active E3 ligase also demonstrates specificity to the same E2 conjugating enzymes; UbcH5A, UbcH5B, UbcH5C and UbcH7. This is once again represented by an upward shift in molecular weight of recombinant NTH1. The ubiquitylation appears strongest in the presence of UbcH5A, UbcH5B and UbcH5C, and to a lesser extent UbcH7, which appear relatively similar to that observed when all E2 conjugating enzymes are present within the ubiquitylation reaction (**Figure 32, B**, lane 2). Overall, the E3 ligase in the active chromatography fraction and recombinant TRIM26 both appear mostly dependent on the UbcH5 subset of E2 conjugating enzymes. This overlap in E2 specificity further improves our confidence that TRIM26 is indeed the E3 ligase that ubiquitylates NTH1 *in vitro*.

4.5. Results I summary

Ubiquitylation is a major PTM utilised by cells to modulate the stability, activity, localisation or interactions of cellular proteins. Indeed, ubiquitylation-dependent regulation of a number of cellular proteins implicated in DNA repair has already been documented. Ubiquitylation is mediated by a cascade of three enzymes; E1 activating enzymes, E2 conjugating enzymes and E3 ubiquitin ligases. The substrate specificity of the reaction is largely dictated by the E3 ubiquitin ligase enzymes, of which there are more than 600 present in human cells. Previous studies have focused on identifying the ubiquitylation enzymes specific to the regulation of substrate proteins of interest. Colleagues from our laboratory have already successfully endeavoured to elucidate the E3 ligase enzymes specific to particular enzymes implicated in the BER pathway (25, 47).

Using a column chromatography approach, combined with an *in vitro* ubiquitylation assay containing recombinant NTH1, I successfully isolated an NTH1 specific ubiquitylating activity from HeLa cells which appeared to promote largely polyubiquitylation. Surprisingly, mass spectrometry analysis of the final purified active fraction revealed the presence of just one protein with known ubiquitylation capabilities; TRIM26. Indeed, the maximal level of TRIM26 protein by Western blotting

correlated well with the ubiquitylation of NTH1 in the final chromatography fractions. Most significantly, when recombinant TRIM26 purified from bacterial overexpression was employed in the *in vitro* ubiquitylation assay, it induced significant ubiquitylation of recombinant NTH1 which compared well with that observed with active chromatography fractions purified from HeLa cell extracts. Likewise, recombinant TRIM26, in ubiquitylating NTH1 also exhibited overlapping dependency on the same E2 conjugating enzymes (mainly UbcH5a, UbcH5b and UbcH5c), as purified active fractions from HeLa cells. This also correlates with studies screening interactions between TRIM proteins and E2 families which demonstrated that TRIM proteins generally exhibit dependency on UbcH5a, UbcH5b UbcH5c, UbcH6 and UbcH9 (63).

Together, these results advocate that TRIM26 is the active, major cellular E3 ligase associated with ubiquitylation of NTH1. This correlates with a recent finding within our laboratory which also identified TRIM26 as the E3 ligase enzyme acting on another BER glycosylase, NEIL1 (46). In this study, the E3 ligase specific to NEIL1 was purified using the same approach incorporating column chromatography and *in vitro* ubiquitylation assays. Studies in U2OS cells demonstrated that TRIM26 stabilised steady-state NEIL1 levels. Furthermore, stabilisation of NEIL1 following TRIM26 knockdown contributed to cellular resistance to ionising radiation, highlighting the importance of TRIM26 in regulating the cellular DNA damage response (46). Now I demonstrate that TRIM26 may in fact have two cellular targets for ubiquitylation-dependent degradation within the BER pathway, the DNA glycosylases NEIL1 and NTH1. It could be hypothesized that TRIM26 may act as a master regulator of enzymes implicated in BER. In this instance, TRIM26 may regulate these two specific BER proteins due to the redundancy in base damage specificity demonstrated between the two glycosylase enzymes, specifically the repair of oxidised pyrimidines in DNA. Studies have previously shown that NEIL1 may act as a back-up glycosylase for the removal of Tg residues when NTH1 activity is hindered (78, 149). It could be speculated that TRIM26 regulates the transition between NTH1 and NEIL1 activity when one of the enzymes is rendered inactive or not present in adequate amounts. Furthermore, this observation could suggest that BER enzymes regulated by specific E3 ligase enzymes may be grouped according to overlapping substrate specificities, such as the BER glycosylase enzymes. The reality of this assumption will only be realised after more extensive studies regarding the ubiquitylation dependent regulation of all of the DNA glycosylase enzymes involved in DNA base excision, in addition to the enzymes involved in the other major steps of BER.

TRIM26 belongs to a well-conserved subfamily of E3 ligases, termed the TRIM ligases, of which there are more than 70 members. Each TRIM enzyme demonstrates conserved structures comprising of a RING domain, one or two B-box zinc fingers and a coiled coil domain. It is believed that the RING domain confers E3 ligase activity of the TRIM family of enzymes and is able to bind to other small molecular proteins used to post-translationally modulate proteins, including SUMO proteins (115). It has been shown that the coiled coil domain can self-associate to form large protein complexes which occupy discrete subcellular compartments (115). This may account for the fact that purified TRIM26 from the gel filtration chromatography stage of HeLa extract purification was located within fractions of 150-443 kDa; suggesting that the 62 kDa protein had potentially formed multimers or associates with other proteins as part of a larger complex (**Figure 22**). Emerging roles for TRIM dependent regulation of cellular pathways implicated in carcinogenesis including cellular proliferation, DNA repair and apoptosis, have been identified (63). Furthermore, TRIM proteins have an essential role in the regulation of signalling pathways involved in innate immunity and anti-viral response (115, 161). The most abundant RING finger ligase; TRIM28, is often deemed a master regulator of the genome due to its association with multiple complexes instigated in managing gene expression and in particular, TRIM28 mediates the turnover of a number of transcription factors (182). This emphasises the critical role that TRIM dependent regulation plays within the cellular context.

Alike to the roles of other TRIM proteins reported in the literature, TRIM26 has already been shown to play a role in the anti-viral response and tumour suppression (169). Low expression levels of TRIM26 have been correlated with worse prognosis in hepatocellular carcinoma (168, 169, 188). Bioinformatics revealed that TRIM26 could modulate gene sets related to cancer cell metabolism. In addition, silencing of TRIM26 within cells promoted cell proliferation, migration and invasion (169). A separate study showed that TRIM26 acts as a tumour suppressor in non-small-cell lung cancer (188). Overexpression of TRIM26 inhibited cell growth and induced apoptosis potentially related to downregulation of B-cell lymphoma 2 (Bcl-2), although the molecular mechanism underlying this link remains unexplored. It is also unknown if there is a correlation between the E3 ligase activity of TRIM26 and its anti-apoptotic properties (188). Nevertheless, the E3 ligase activity of TRIM26 has been associated with regulation of the antiviral response (168). Viral infection results in the activation of the transcription factor, IRF3, which has a number of downstream effects, including the production of interferons and clearance of the viral contaminant. Regulation of nuclear IRF-3 was shown to be reliant on proteasomal degradation facilitated by K-48 linked

polyubiquitylation instigated by TRIM26 (168). Another example of the TRIM26 regulation of transcription factors is apparent via the TRIM26 induced degradation of the transcription factor IID (TFIID) subunit TAF7, in cultured mouse mammary epithelial cells. However, the regulation of this particular transcription factor is not associated in the regulation of the cellular viral response, but is implicated in the arrest of cellular proliferation (109).

Following my evidence that NTH1 is a target for ubiquitylation by TRIM26, it became important to employ the *in vitro* ubiquitylation assays with other techniques to determine which specific lysine residues of NTH1 are ubiquitylated by the E3 ligase. Identification of the specific lysine residues of NTH1 that are ubiquitylated by TRIM26 would further support that TRIM26 is the active E3 ligase which acts on NTH1. Furthermore, identification of specific post-translational modification sites is an important preliminary step towards understanding the biological role of the covalent modification. Due to the diverse functions of ubiquitylation, experiments utilising ubiquitylation deficient mutants are increasingly important for understanding the molecular impact of ubiquitylation of specific substrates.

CHAPTER 5 - RESULTS II

NTH1 is ubiquitylated by TRIM26 within the N-terminal region

5.1 Introduction

After confirmation that TRIM26 is the major E3 ligase enzyme, purified from human cell extracts, which ubiquitylates NTH1 *in vitro,* the next objective was to identify the lysine residues of NTH1 that are ubiquitylated by the E3 ligase. Not only will this further support that TRIM26 ubiquitylates NTH1 *in vitro,* but it may also enable us to primarily assess the molecular role of ubiquitylation. Preliminary structural studies in the literature, regarding structural features of NTH1, are largely based on similarities to the bacterial homologue. Although, Ikeda *et al* (1998) used a glutathione S-transferase fusion polypeptide of recombinant human full-length NTH1 to directly identify the catalytic residue of the glycosylase (68). Sequence analysis strategies confirmed that Lys-212 was implicated in NTH1 activity. Indeed, replacement of Lys-212 with a Gln residue inactivated NTH1, plus substitution with an Arg residue affected catalytic specificity (68). Despite homology of conserved catalytic residues between human NTH1 and its bacterial counterpart, it has been acknowledged that human NTH1 exhibits an extended N-terminal tail (90). Kinetic studies have demonstrated that the N-terminal residues are not linked to glycolytic activity, but may be implicated in putative signals regulating activity or protein-protein interactions (68). Controlled proteolysis experiments using truncated versions of NTH1 have suggested that the extended N-terminal tail may have an inhibitory effect on NTH1 activity (90). The sequence of three isoforms of human NTH1 have been elucidated; M-8, M+1 and M+8. The canonical sequence of NTH1 is the M-8 isoform and consists of 312 amino acids. The M+1 isoform of NTH1 lacks the first 1-8 N-terminal residues, whereas, the M+8 isoform lacks the first 1-15 N-terminal residues. The M+1 isoform is believed to represent the translationally active form of human NTH1 (**Figure 5.1** and **Figure 5.3;** Full-length NTH1) and is 304 amino acid residues in length. All of the biological isoforms of human NTH1 contain a total of 17 lysine residues, which could be subject to post-translational modification, via ubiquitylation (**Figure 33;** red text).

```
        10         20         30         40         50
MCSPQESGMT ALSARMLTRS RSLGPGAGPR GCREEPGPLR RREAAAEARK
        60         70         80         90        100
SHSPVKRPRK AQRLRVAYEG SDSEKGEGAE PLKVPVWEPQ DWQQQLVNIR
       110        120        130        140        150
AMRNKKDAPV DHLGTEHCYD SSAPPKVRRY QVLLSLMLSS QTKDQVTAGA
       160        170        180        190        200
MQRLRARGLT VDSILQTDDA TLGKLIYPVG FWRSKVKYIK QTSAILQQHY
       210        220        230        240        250
GGDIPASVAE LVALPGVGPK MAHLAMAVAW GTVSGIAVDT HVHRIANRLR
       260        270        280        290        300
WTKKATKSPE ETRAALEEWL PRELWHEING LLVGFGQQTC LPVHPRCHAC
       310
LNQALCPAAQ GL
```

Figure 33. The sequence of the human NTH1 isoform M+1. The sequence of the major human NTH1 isoform (M+1) is depicted. The M+1 isoform of human NTH1 differs from the canonical sequence of full length human NTH1, as it lacks the N-terminal 1-8 residues and begins at residue Met9; which is believed to represent the translational start of biologically active NTH1. Full-length human NTH1 consists of 312 amino acid residues, whereas, the M+1 NTH1 isoform consists of 304 amino acid residues. Both forms of NTH1 possess a total of 17 lysine residues (K), which are highlighted in yellow. (Protein identifier: **P78549-2**).

Interestingly, a single nucleotide polymorphism (D239Y) of NTH1 has been revealed within 6.2 % of the global population (55). Cellular expression of the D239Y variant advocated that individuals with this hereditary polymorphism may be more susceptible to genomic instability and cancer. This was due to the fact that cells expressing the D239Y exhibited increased chromosomal aberrations, increased foci formation, anchorage-independent growth and invasive properties. Similarily, cells expressing the variant were more sensitive to genotoxic agents, with increased DNA double strand break formation observed (55). Due to the presence of this variant within the population, as well as identifying the site of ubiquitylation of NTH1 by TRIM26, I also aimed to investigate if the ubiquitylation dependent regulation of the D239Y variant differed compared to wild type NTH1. It was of interest to establish if this could account for the disrupted cellular phenotype observed in variant expressing cells.

5.2 Analysis of sites of NTH1 ubiquitylation by tandem mass spectrometry

To identify the sites within NTH1 that are subject to ubiquitylation by TRIM26, I firstly employed a tandem mass spectrometry approach to analyse the products of *in vitro* ubiquitylation reactions. Following separation of an *in vitro* ubiquitylation reaction

containing recombinant His-NTH1 and recombinant His-TRIM26, proteins were separated by 10 % SDS-PAGE and stained using Instant Blue (**Figure 34, A**). From the stained gel, the positions of migration of TRIM26 and NTH1 could be identified, although it was difficult to visualise bands corresponding to ubiquitylated NTH1, largely due to interference from contaminants or degradation products of TRIM26. However, using Western blotting analysis, ubiquitylation of NTH1 could clearly be observed only in the presence of both TRIM26 and ubiquitin (**Figure 34, B;** $NTH1_{Ub}$). Therefore, the region corresponding to monoubiquitylated NTH1 was located and excised from the stained gel, proteins were then extracted from the gel pieces and digested with either trypsin or Arg-C, before being analysed via LC-MS.

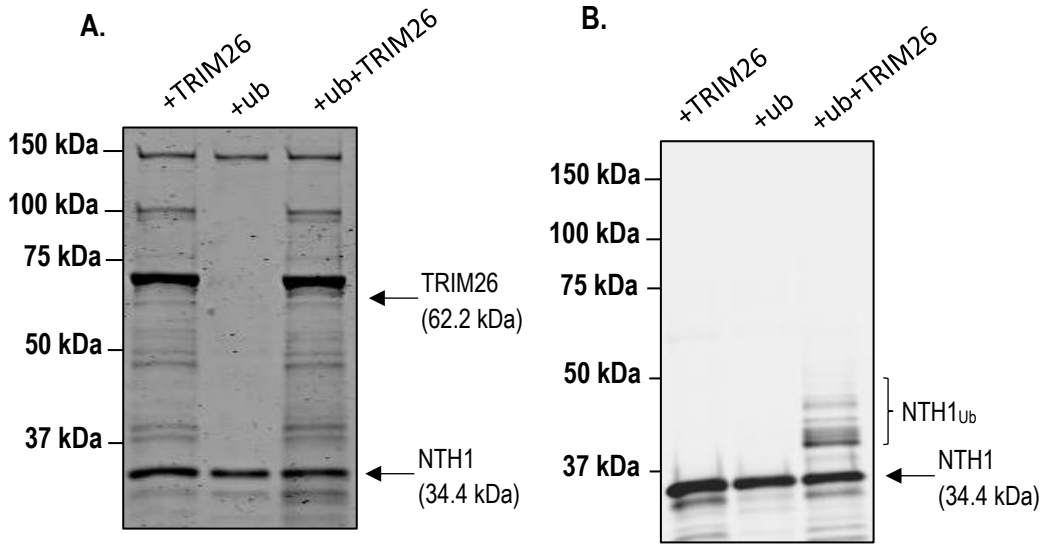

Figure 34. Separation of *in vitro* ubiquitylation assays containing recombinant NTH1 for tandem mass spectrometry analysis of potential sites of TRIM26 dependent ubiquitylation of NTH1. Ubiquitylation assays were performed by combining 0.7 pmol GST-E1 activating enzyme, 5 pmol of UbcH5a and 5.8 pmol of histidine-tagged, recombinant NTH1. To reaction one, 26 fmol of recombinant TRIM26 was also added (+TRIM26 only, lane 1). To the second reaction, 0.6 nmol ubiquitin (+Ub only, lane 2) was added. Finally, both 26 fmol of recombinant TRIM26 and 0.6 nmol ubiquitin was added to the third reaction (+TRIM26 only + Ub, lane 3). The assay reactions were carried out at 30 °C for 1 h in a shaking incubator at 800 rpm. Reactions were terminated by the addition of SDS loading dye and proteins separated by 10 % SDS-PAGE and Instant Blue staining (**A**) and also analysed via Western blotting using NTH1 specific antibodies (**B**). Ubiquitylation of NTH1 was apparent in reactions containing both recombinant ubiquitin, in combination with recombinant TRIM26 (+TRIM26 + Ub, lane 3), but was not present in the control reactions (lane 1 and lane 2). Molecular weight markers (kDa), unmodified histidine-tagged NTH1 (NTH1) and ubiquitylated histidine-tagged NTH1 ($NTH1_{ub}$) are indicated. The position of bands corresponding to ubiquitylated NTH1 were determined by Western blot analysis (**B**) and were excised from the SDS-PAGE gel

(**A**). Proteins were extracted from gel pieces and digested using either trypsin or Arg-C, before analysis via LC-MS.

Unfortunately, we could not obtain adequate peptide coverage to enable adequate analysis of full-length NT1 protein. For example, digestion with trypsin (cleaving after lysine and arginine residues) was 35 %. Similarly, digestion with ArgC (cleaving after arginine residues) yielded 30 % coverage of the entire NTH1 protein; which only included 3 lysine residues.

As tandem mass spectrometry analysis of potential sites of TRIM26 dependent ubiquitylation of NTH1 was unsuccessful, it was decided that an alternative approach, relying on the generation of truncated versions of the DNA glycosylase, would be pursued. For this approach, truncated versions of NTH1 would be created via manipulation of a bacterial expression plasmid encoding the *nth1* gene. Plasmids encoding truncated NTH1 proteins would then be transformed and overexpressed in *E. coli* and purified from bacterial contaminants using column chromatography before being subject to analysis by *in vitro* ubiquitylation assays containing recombinant TRIM26. It was expected that truncated versions of NTH1 lacking the lysine residues that are specifically ubiquitylated by TRIM26 would not exhibit the characteristic banding pattern representative of ubiquitylation following SDS-PAGE and Western blotting analysis.

5.3. Generation of truncated versions of NTH1 by PCR and LIC cloning

To more successfully examine the region of NTH1 containing the lysine residues that are subject to TRIM26 dependent ubiquitylation, truncated versions of NTH1 were generated for assessment via *in vitro* ubiquitylation assays, using recombinant TRIM26. It was anticipated that a truncated version of NTH1 containing the lysine residues that are subject to ubiquitylation would exhibit an observable 8 kDa shift in molecular weight following incubation with TRIM26. A summary of the truncations generated is provided (**Figure 35**). Whereas, truncated versions of NTH1 lacking the necessary ubiquitylated lysine residues, would not demonstrate this characteristic shift in molecular weight.

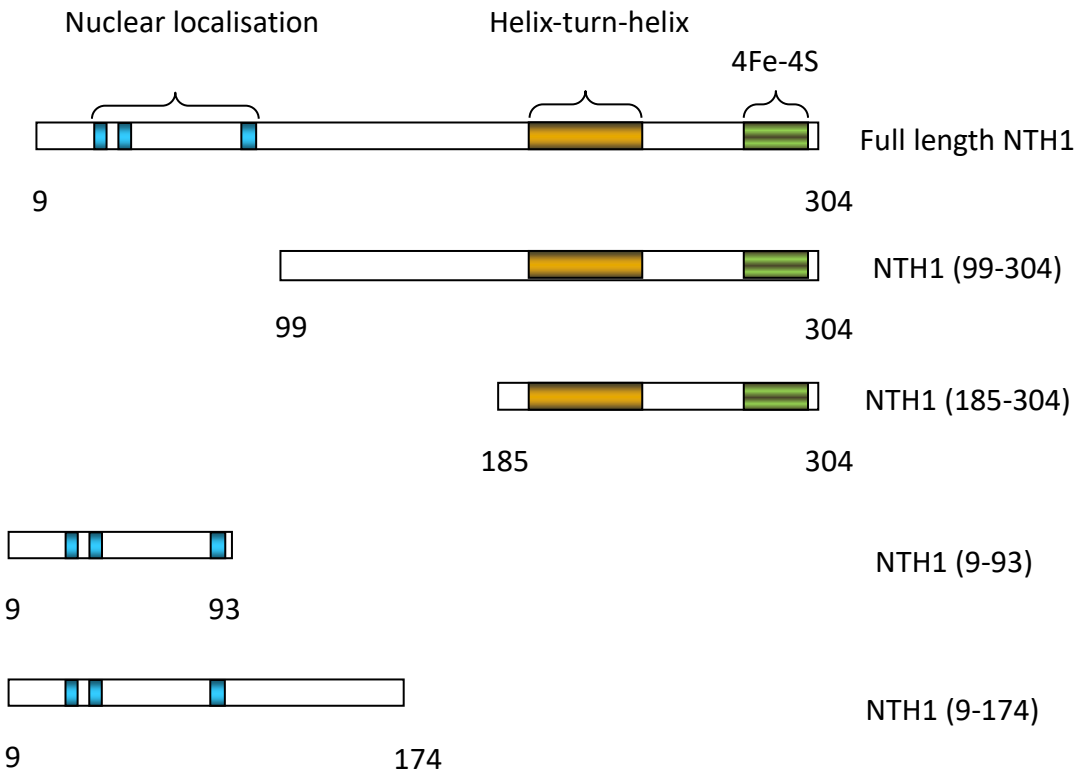

Figure 35. Schematic representation of the structural features of NTH1 and the truncated versions of NTH1 created to assess potential sites of TRIM26 dependent ubiquitylation *in vitro*. The N-terminal region of NTH1 contains nuclear localisation regions (represented in blue). The C-terminal region of NTH1 contains a helix-hairpin-helix domain (in yellow) and an iron-sulphur 4[Fe-4S] cluster loop (in green), which have been linked to DNA binding functionalities. To assess potential sites of TRIM26 dependent ubiquitylation of NTH1, truncated versions of full-length NTH1 were generated using a LIC cloning approach to generate pET28 bacterial expression plasmids which would express NTH1 variants. Overall, two C-terminal truncations were created; NTH1 99-304 and NTH1 185-304 alongside two N-terminal truncated variants; NTH1 9-93 and NTH1 9-174.

Truncated versions of NTH1 were created using a LIC cloning approach, whereby firstly an empty pET28a bacterial expression vector was PCR amplified. The size of an empty pET28 plasmid is 5369 bp (**Figure 16**). Following agarose gel analysis of four PCR amplification reactions, generation of the pET28 construct was generally successful across all reactions **(Figure 36, A**, lanes 1-4), with similar yields of empty pET28 vector obtained in each reaction. Reactions 1-4 were completed in the presence of different reaction buffers: reaction 1 contained HF buffer, reaction 2 contained HF buffer with DMSO, whereas, reaction 3 was completed in the presence of GC buffer, with reaction 4 containing GC buffer with DMSO. As similar yields of

empty pET28 vector obtained in each reaction, all four reactions were selected, pooled and purified from the PCR reactions for subsequent stages. Alongside this, inserts encoding truncations of the *nth1* gene were PCR amplified using specifically designed primers which were used in combination with the pET28NTH1 plasmid (obtained from Dr. Allinson) encoding the full-length gene. Firstly, inserts corresponding to C-terminal truncated versions of NTH1; NTH1 99-305 and NTH1 185-305, were amplified (**Figure 36, B** and **C**). The size of the insert corresponding to NTH1 99-305 is approximately 663 bp. After completing a number of PCR amplification reactions, it was apparent that all four reactions had yielded amplified NTH1 99-305, represented by DNA bands of the appropriate size following agarose gel analysis (**Figure 36, B**, lanes 1-4). To note, the reaction conditions for all of the plasmid inserts match those for the amplification of the vector DNA; reaction 1 contained HF buffer, reaction 2 contained HF buffer with DMSO, whereas, reaction 3 was completed in the presence of GC buffer, with reaction 4 containing GC buffer with DMSO. The levels of NTH1 99-305 insert DNA produced was variable across each reaction, represented by the varying intensity of the agarose gel bands. Due to this, reaction 1 (**Figure 36, B**, lane 1) was selected and purified from the PCR reactions for subsequent stages. The size of the PCR product of NTH1 185-305 is 405 bp and following analysis of four PCR reactions using agarose gel analysis, it was apparent that a similar yield of bands corresponding to the relevant sized products had been obtained across all four lanes (**Figure 36, C**, lanes 1-4). All four reaction products were selected, pooled and purified from the PCR reactions for later LIC cloning stages. Aside to this, inserts corresponding to N-terminal truncated versions of NTH1; NTH1 9-174 and NTH1 9-93, were similarly generated using primers incubated with the pET28aNTH1 plasmid encoding the full-length gene (**Figure 36, D**). The size of the PCR product for NTH1 9-93 was 313 bp. Once again, four amplification reactions were established and similar levels and purify of the DNA product were obtained in all four lanes (**Figure 36, D**, 1-4). Therefore, these were pooled and subject to PCR purification. Likewise, four amplification reactions were set-up to generate NTH1 9-174; the product size of which was expected to be 556 bp. Yet again, all amplification reactions yielded similar PCR product levels, so they were pooled and purified from the PCR reactions (**Figure 36, D**, 5-8).

Following generation of the empty pET28 vector and a number of inserts encoding the NTH1 truncations, a LIC cloning strategy was employed to anneal the two different components together by incubating different ratios of the vector to *nth1* gene insert DNA.

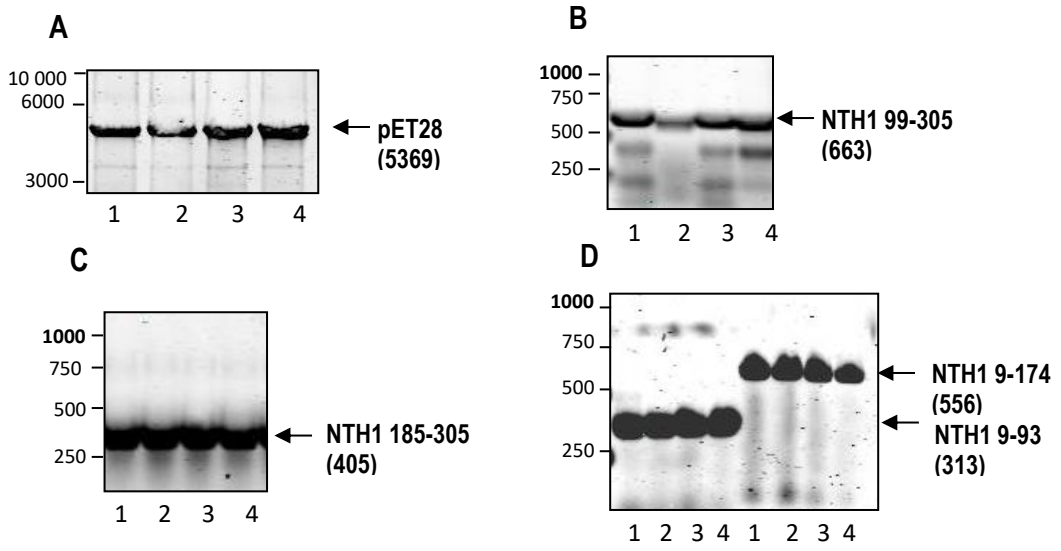

Figure 36. PCR amplification of the products required to generate the bacterial expression plasmids for truncated versions of NTH1. DNA corresponding to an empty pET28a bacterial expression vector was PCR amplified using custom oligonucleotides with LIC overhangs (**A**), alongside inserts corresponding to C-terminal truncations of NTH1; 99-305 (**B**) and 185-305 (**C**) or N-terminal truncations of NTH1; 9-93 and 9-174 (**D**), using custom oligonucleotides with complementary LIC overhangs incubated with a pET28NTH1 bacterial expression plasmid. Lanes 1-4 were completed in the presence of different reaction buffers (1: HF buffer, 2: HF buffer with DMSO, 3: GC buffer, 4: GC buffer with DMSO). The size of the PCR products was analysed using 1 % agarose gels in 1x TAE. The expected sizes of each PCR product in base pairs are featured in brackets.

Individual LIC reactions were transformed into *E. coli* and plasmid DNA purified from overnight bacterial cultures. Initially, the correct sequences of the bacterial expression plasmids generated to create truncated versions of NTH1 were confirmed via a Van9I restriction digest. The sizes of the digestion products were visualised using agarose gel electrophoresis analysis (**Figure 37**). For the pET28NTH1 9-93 plasmid construct digestion products of the expected sizes, 3984 bp, 1242 bp and 430 bp were observed (**Figure 37;** Lane 1). Similarly, products of the expected sizes; 3984 bp, 1485 bp and 430 bp, were confirmed following digestion of the pET28NTH1 9-174 plasmid construct (**Figure 37;** Lane 2). Likewise, digestion products of the expected sizes; 3984 bp, 1260 bp and 430 bp, were apparent following digestion of the pET28NTH1 99-305 bacterial expression plasmid (**Figure 37;** Lane 3). Finally, products of the expected sizes; 3984 bp, 1518 bp and 430 bp, could be seen following Van91I

digestion of the pET28NTH1 185-305 bacterial expression plasmid (**Figure 37;** Lane 4). Observation of restriction digest products of the expected sizes suggested that the composition of the bacterial expression plasmids for each NTH1 truncation were correct. To confirm this, each plasmid was also analysed by gene sequencing provided by the Source Bioscience Sanger Sequencing service (see Appendix).

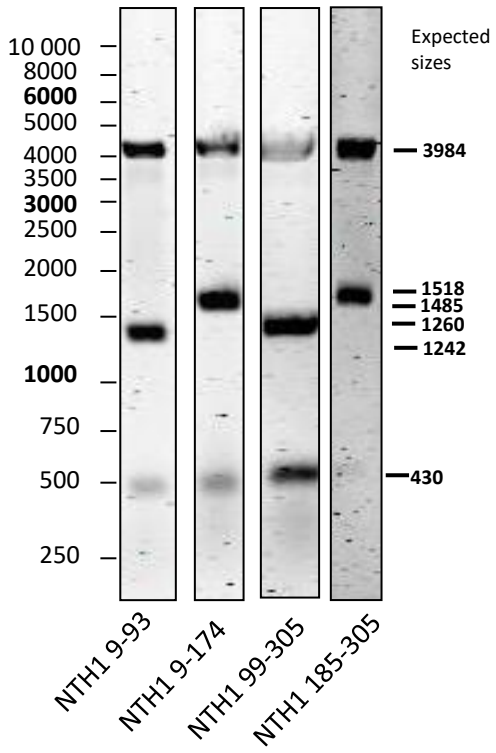

Figure 37. Preliminary analysis of the sequences of PCR constructs for NTH1 truncations using restriction digests. The sequences of plasmids for bacterial expression of truncated versions of NTH1 (9-93, 9-174, 185-305 and 99-305) generated using a LIC technique, were initially assessed via a restriction digest, using Van91. The sizes of the PCR fragments after the restriction digest were analysed using 1 % agarose gels in 1x TAE. Expected sizes of the DNA digests are provided.

Following confirmation of the correct DNA sequences of the bacterial expression plasmids encoding the *nth1* truncated gene inserts, the constructs were transformed into Rosetta 2(DE3) pLysS cells, cultures were grown and NTH1 truncated proteins overexpressed using IPTG induction. The bacterial cells were pelleted by centrifugation, and each NTH1 truncated protein was purified by His-trap affinity chromatography using an AKTA-purifier FPLC.

5.3.1 Affinity chromatography purification of NTH1 9-93

Bacterial cells expressing the N-terminal truncation of NTH1 consisting of residues 9-93, were re-suspended in lysis buffer containing protease inhibitors and lysed via incubation with lysozyme followed by bursts of sonication. The histidine-tagged NTH1 9-93 truncation was then separated from bacterial protein contaminants by affinity chromatography with an AKTA purifier FPLC. The cell lysate was loaded onto a 1 ml HisTrap chromatography column pre-equilibrated in lysis buffer containing PMSF. Bound proteins were collected by a 20 ml gradient elution using elution buffer containing 500 mM imidazole. The chromatography trace is provided, with peaks in UV representing peaks in protein expression (**Figure 38, A**, blue line). Fractions were subject to analysis by SDS-PAGE analysis and Instant blue staining (**Figure 38, B**) and also by Western blotting with anti-histidine antibodies to select fractions containing purified his-tagged NTH1 9-93 (**Figure 38, C**). The approximate molecular weight of the truncated version of NTH1 comprising of residues 9-93 is 13.5 kDa. From SDS-PAGE and staining analysis of the chromatography fractions, it was apparent that protein bands of this molecular weight were present largely in fractions 18-28 (**Figure 38, B** and **C**). In addition, protein bands at this position demonstrated cross-reactivity with anti-histidine antibodies, further advocating that these bands represent truncated NTH1 9-93 (**Figure 38, C**). For this reason, fractions 19-28 were selected containing the purest NTH1 protein, pooled and concentrated using Amicon Ultra 15 ml centrifugal concentrators (10 kDa MWCO) in a swinging bucket rotor at 4000 x g to generate a concentrated stock of NTH1 9-93 protein.

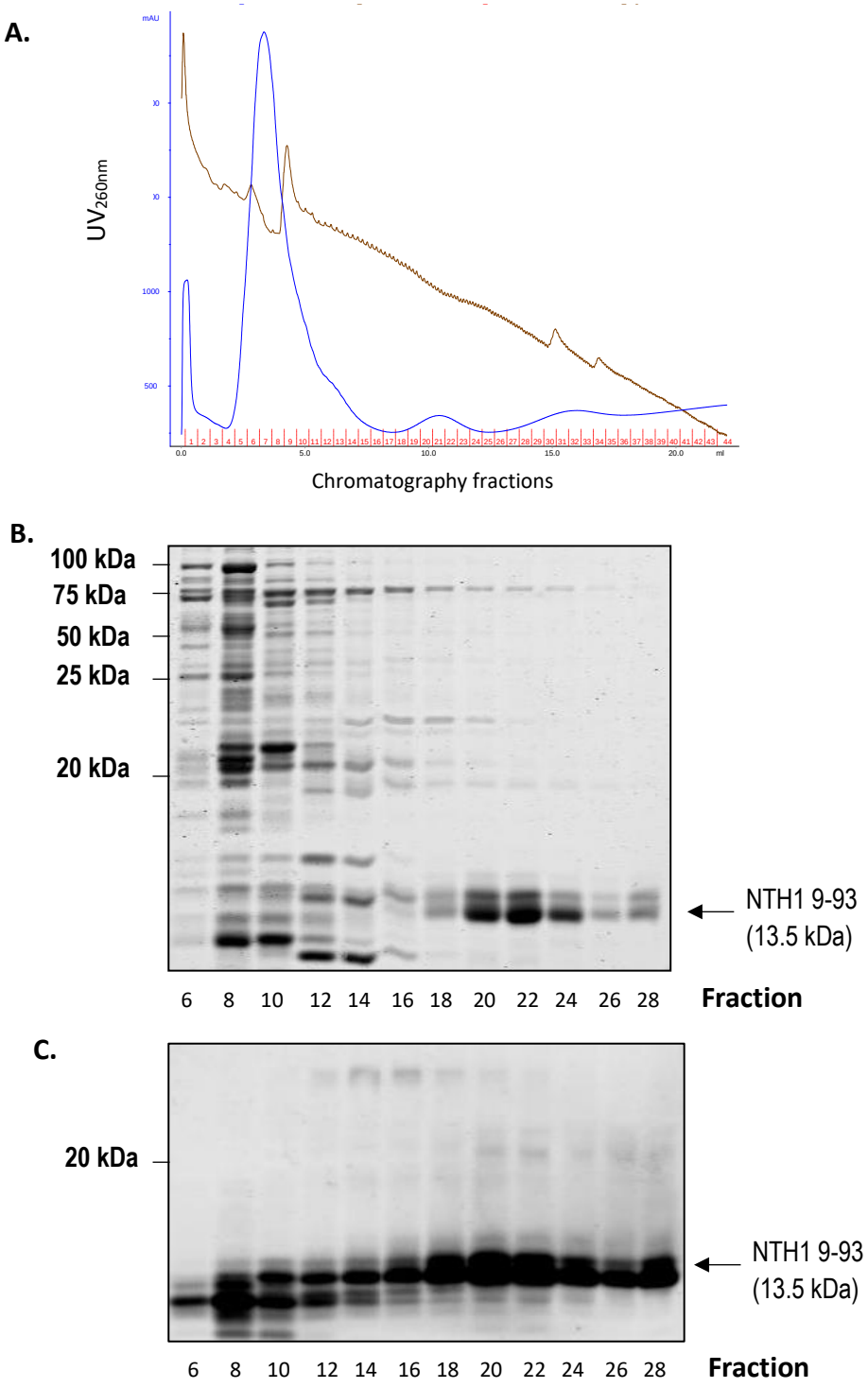

Figure 38. Analysis of affinity chromatography purification of the N-terminal truncation of NTH1 9-93 by SDS-PAGE and Western blotting with anti-histidine antibodies. Bacterial cells transformed with pET28a-NTH1 9-93 bacterial expression plasmid were cultured into a 400 ml expression culture until the OD_{650nm} reached 0.6. Bacterial expression of recombinant NTH1 9-93 was then induced via of isopropyl β-D-1-thiogalactopyranoside (IPTG) for 3 h at 30°C. Bacterial cells were then pelleted and lysed by sonication in the presence of protease inhibitors. Recombinant NTH1 9-93 was separated from bacterial proteins via affinity chromatography using a 1 ml HisTrap column and a linear gradient elution of 5 mM to 500 mM imidazole. The chromatography trace is provided, with the UV at 260 nm represented by the blue

line, conductivity represented by the brown line and the chromatography fractions are shown in red (**A**). Chromatography fractions were collected and purity analysed by 16 % SDS-PAGE (**B**) and Western blotting using antibodies specific to the histidine tag featured on recombinant NTH1 (**C**). Molecular weight markers (kDa) and NTH1 9-93 presence is indicated.

5.3.2 Affinity chromatography purification of NTH1 9-174

Bacterial cells expressing the N-terminal truncation of NTH1 consisting of residues 9-174 were lysed via incubation with lysozyme, followed by bursts of sonication. The histidine-tagged NTH1 9-174 truncation was then separated from bacterial protein contaminants by affinity chromatography with an AKTA purifier FPLC. The cell lysate was loaded onto a 1 ml HisTrap chromatography column pre-equilibrated in lysis buffer containing PMSF. Bound proteins were collected by a 20 ml gradient elution using elution buffer containing 500 mM imidazole. The chromatography trace is provided, with peaks in UV representing peaks in protein expression (**Figure 39, A**). Fractions were subject to analysis by SDS-PAGE and Instant blue staining (**Figure 39, B**) and also by Western blotting with anti-histidine antibodies to select fractions with purified his-tagged NTH1 9-174 (**Figure 39, C**). The approximate molecular weight of the truncated version of NTH1 comprising of residues 9-174 is 22.5 kDa. From SDS-PAGE and staining analysis, it was apparent that protein bands of this molecular weight were present in fractions 16-24 (**Figure 39, B**). However, evidence of a substantial amount of protein degradation was observed; represented by a more intense protein band at ~15 kDa within these fractions. This was further confirmed by analysis of fractions by Western blotting analysis whereby little full length truncated NTH1 9-174 protein was observed (**Figure 39;** C, protein degradation bands). To resolve this protein degradation, bacterial expression of NTH1 9-174 was repeated and the affinity chromatography purification stage was completed in the presence of increased concentrations of each protease inhibitor to the affinity chromatography buffers in an attempt to stabilise the NTH1 truncated protein. The proteins present in each chromatography fraction (**Figure 40, A**) were analysed separately via SDS-PAGE and Instant blue staining (**Figure 40, B**) and by Western blotting with anti-histidine antibodies (**Figure 40, C).** Unfortunately, a similar level of degradation of the NTH1 9-174 truncated protein was observed despite the attempts made to stabilise the expression product and largely a 15 kDa protein product was observable partially by Western blotting analysis (**Figure 40, C**, protein degradation bands). It was decided that analysis of this particular truncation of NTH1 via the *in vitro* ubiquitylation assay would be unlikely to yield conclusive evidence regarding elucidating the site of TRIM26 dependent ubiquitylation. For this reason, this truncation product was omitted

from subsequent analysis via the i*n vitro* ubiquitylation assay. It was anticipated that adequate information regarding the position of ubiquitylation of NTH1 could be obtained through analysis of the other truncations generated in this particular approach (**Figure 35**).

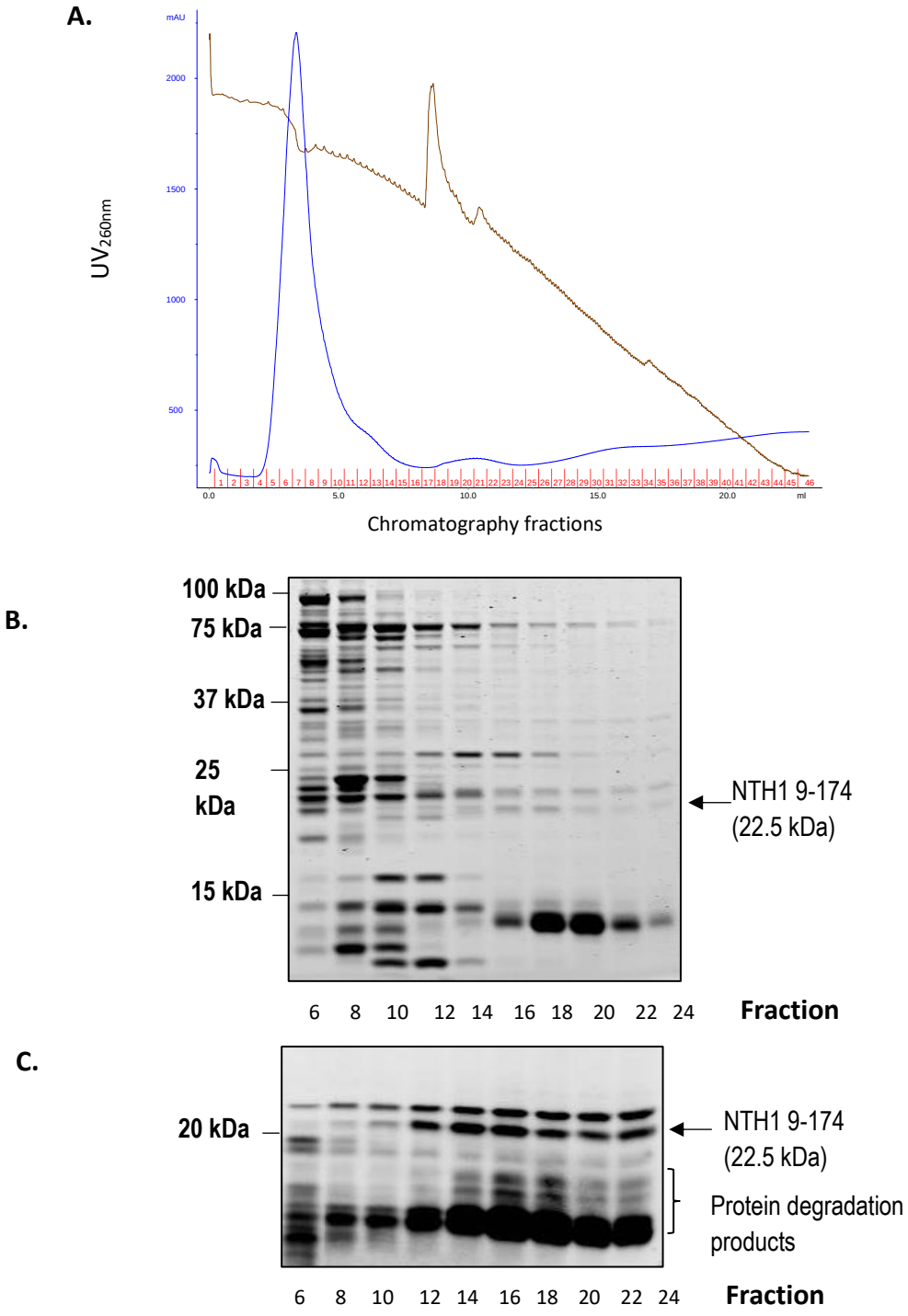

Figure 39. Analysis of affinity chromatography purification of the N-terminal truncation of NTH1 9-174 by SDS-PAGE and Western blotting with anti-histidine antibodies. Bacterial cells transformed with pET28a-NTH1 9-174 bacterial expression plasmid were cultured into a 400 ml expression culture until the OD_{650nm}

reached 0.6. Bacterial expression of recombinant NTH1 9-174 was then induced via of isopropyl β-D-1-thiogalactopyranoside (IPTG) for 3 h at 30°C. Bacterial cells were then pelleted and lysed by sonication in the presence of protease inhibitors. Recombinant NTH1 9-174 was separated from bacterial proteins via affinity chromatography using a 1 ml HisTrap column and a linear gradient elution of 5 mM to 500 mM imidazole. The chromatography trace is provided, with the UV_{260nm} represented by the blue line, conductivity represented by the brown line and the chromatography fractions are shown in red (**A**). Chromatography fractions were collected and purity analysed by 16 % SDS-PAGE (**B**) and Western blotting using antibodies specific to the histidine tag featured on recombinant NTH1 (**C**). Molecular weight markers (kDa) and NTH1 9-174 presence is indicated.

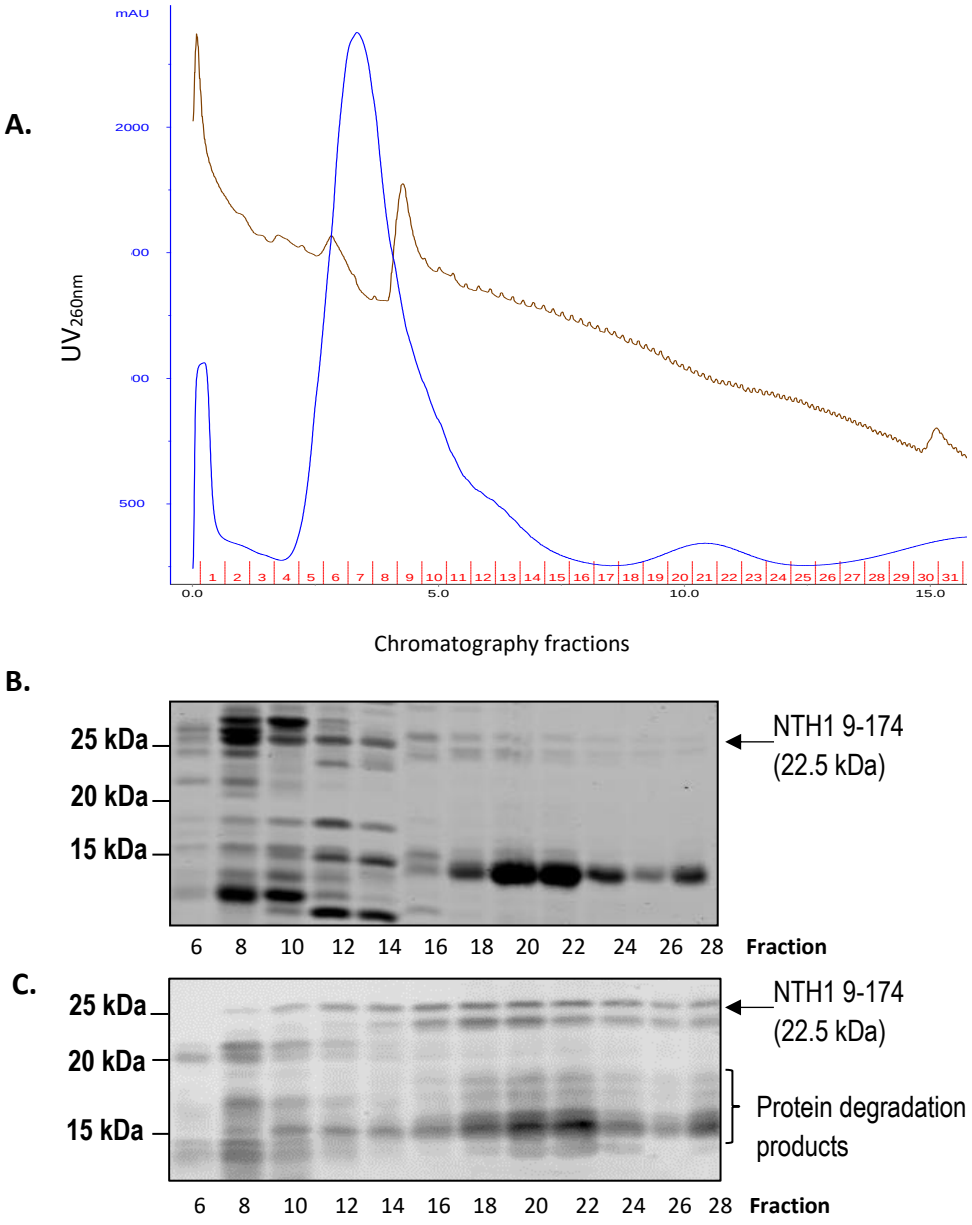

Figure 40. Repeat analysis of affinity chromatography purification of the N-terminal truncation of NTH1 9-174 by SDS-PAGE and Western blotting with anti-

histidine antibodies. Bacterial cells transformed with pET28a-NTH1 9-174 bacterial expression plasmid were cultured into a 400 ml expression culture until the OD_{650nm} reached 0.6. Bacterial expression of recombinant NTH1 9-174 was then induced via of isopropyl β-D-1-thiogalactopyranoside (IPTG) for 3 h at 30°C. Bacterial cells were then pelleted and lysed by sonication in the presence of protease inhibitors. Recombinant NTH1 9-174 was separated from bacterial proteins via affinity chromatography using a 1 ml HisTrap column and a linear gradient elution of 5 mM to 500 mM imidazole. Chromatography fractions were collected and purity analysed by 16 % SDS-PAGE (**A**) and Western blotting using antibodies specific to the histidine tag featured on recombinant NTH1 (**B**). Molecular weight markers (kDa) and NTH1 9-174 presence is indicated.

5.3.3 Affinity chromatography purification of NTH1 99-305

Bacterial cells expressing the C-terminal truncation of NTH1 consisting of residues 99-305 were lysed via incubation with lysozyme, followed by bursts of sonication. The histidine-tagged NTH1 99-305 truncation was then separated from bacterial protein contaminants by affinity chromatography with an AKTA purifier FPLC. The cell lysate was loaded onto a 1 ml HisTrap chromatography column pre-equilibrated in lysis buffer containing PMSF. Bound proteins were collected by a 20 ml gradient elution using elution buffer containing 500 mM imidazole. The chromatography trace is provided, with peaks in UV representing peaks in protein expression (**Figure 41, A**). Fractions were subject to analysis by SDS-PAGE and Instant blue staining (**Figure 41, B**) and also Western blotting with anti-histidine antibodies to select fractions with purified his-tagged NTH1 99-305 (**Figure 41, C**). The approximate molecular weight of the truncated version of NTH1 comprising of residues 99-305 is 25.4 kDa. From SDS-PAGE and staining analysis, it was apparent that protein bands of this molecular weight were present in fractions 8-20, although several other protein bands appeared in this region but also at a lower molecular weight (**Figure 41, B**). In addition, a protein band at ~25 kDa demonstrated cross-reactivity with anti-histidine antibodies; suggesting that this band represents truncated NTH1 99-305 protein (**Figure 41, C**). However, due to consideration of protein purity, fractions 11-20 were selected, pooled and concentrated using Amicon Ultra 15 ml centrifugal concentrators (10 kDa MWCO) in a swinging bucket rotor at 4000 x g to generate a concentrated stock of NTH1 99-305 protein.

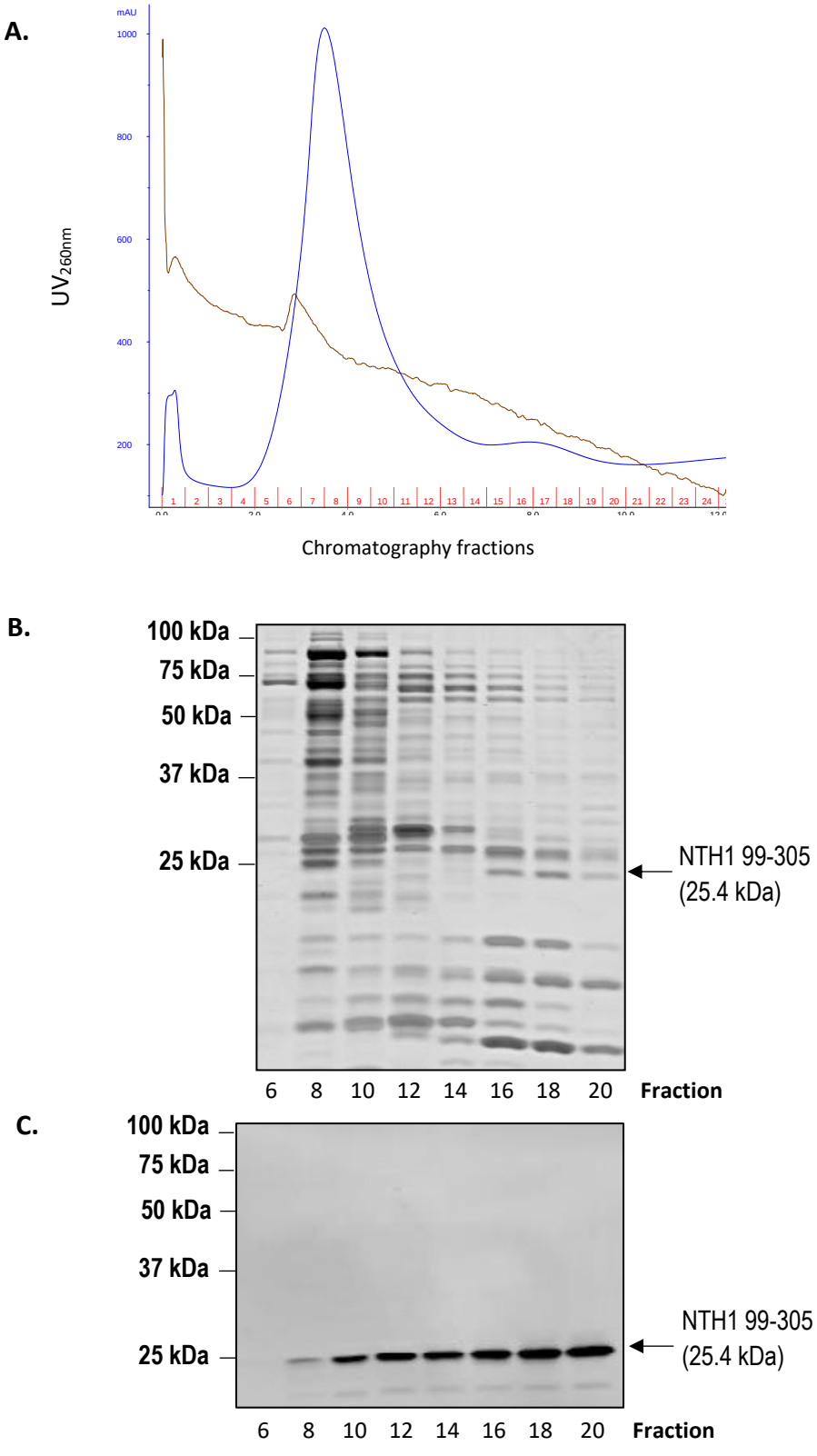

Figure 41. Affinity chromatography purification of the C-terminal truncation of NTH1 99-305 by SDS-PAGE and Western blotting with anti-histidine antibodies. Bacterial cells transformed with pET28a-NTH1 99-305 bacterial expression plasmid were cultured into a 400 ml expression culture until the OD_{650nm} reached 0.6. Bacterial expression of recombinant NTH1 99-305 was then induced via of isopropyl β-D-1-thiogalactopyranoside (IPTG) for 3 h at 30°C. Bacterial cells were then pelleted and

lysed by sonication in the presence of protease inhibitors. Recombinant NTH1 99-305 was separated from bacterial proteins via affinity chromatography using a 1 ml HisTrap column and a linear gradient elution of 5 mM to 500 mM imidazole. The chromatography trace is provided, with the UV260nm represented by the blue line, conductivity represented by the brown line and the chromatography fractions are shown in red (**A**). Chromatography fractions were collected and purity analysed by 16 % SDS-PAGE (**B**) and Western blotting using antibodies specific to the histidine tag featured on recombinant NTH1 (**C**). Molecular weight markers (kDa) and NTH1 99-305 presence is indicated.

Due to concerns related to potential bacterial contaminants impacting the ubiquitylation capacity of the NTH1 99-305 truncation, the recombinant protein was further separated via gel filtration chromatography using a Superdex 75 chromatography 10/300GL column (GE Healthcare, Little Chafont, UK) equilibrated in gel filtration buffer (50 mM Tris pH 8, 150 mM KCl, 1 mM EDTA, 5 % glycerol with 1 mM DTT and 1 mM PMSF) using an AKTA-purifier FPLC at 4°C. The chromatography trace is provided, with peaks in UV representing peaks in protein expression (**Figure 42, A**). Collected fractions were analysed via SDS-PAGE and Instant blue staining (**Figure 42, B**) and by Western blotting analysis with anti-histidine antibodies (**Figure 42, C**). From SDS-PAGE and staining analysis, a protein corresponding to the molecular weight of NTH1 99-305 at 25 kDa appears to be present largely in fractions 21-25 (**Figure 42, B**). Additionally, from Western blotting analysis, it was observed that protein bands of approximately 25.4 kDa were apparent largely in two peaks of fractions 15-19 and 23-29 (**Figure 42, C**). However, SDS-PAGE and staining analysis in combination with Western blotting analysis enabled us to refine the presence of fractions containing the least bacterial contaminants and the maximal levels of the NTH1 99-305 truncation. Due to this, it was decided that fractions 21-25 would be selected, pooled and concentrated using Amicon Ultra 15 ml centrifugal concentrators (10 kDa MWCO) in a swinging bucket rotor at 4000 x g to generate a concentrated stock of NTH1 99-305 protein of refined purity.

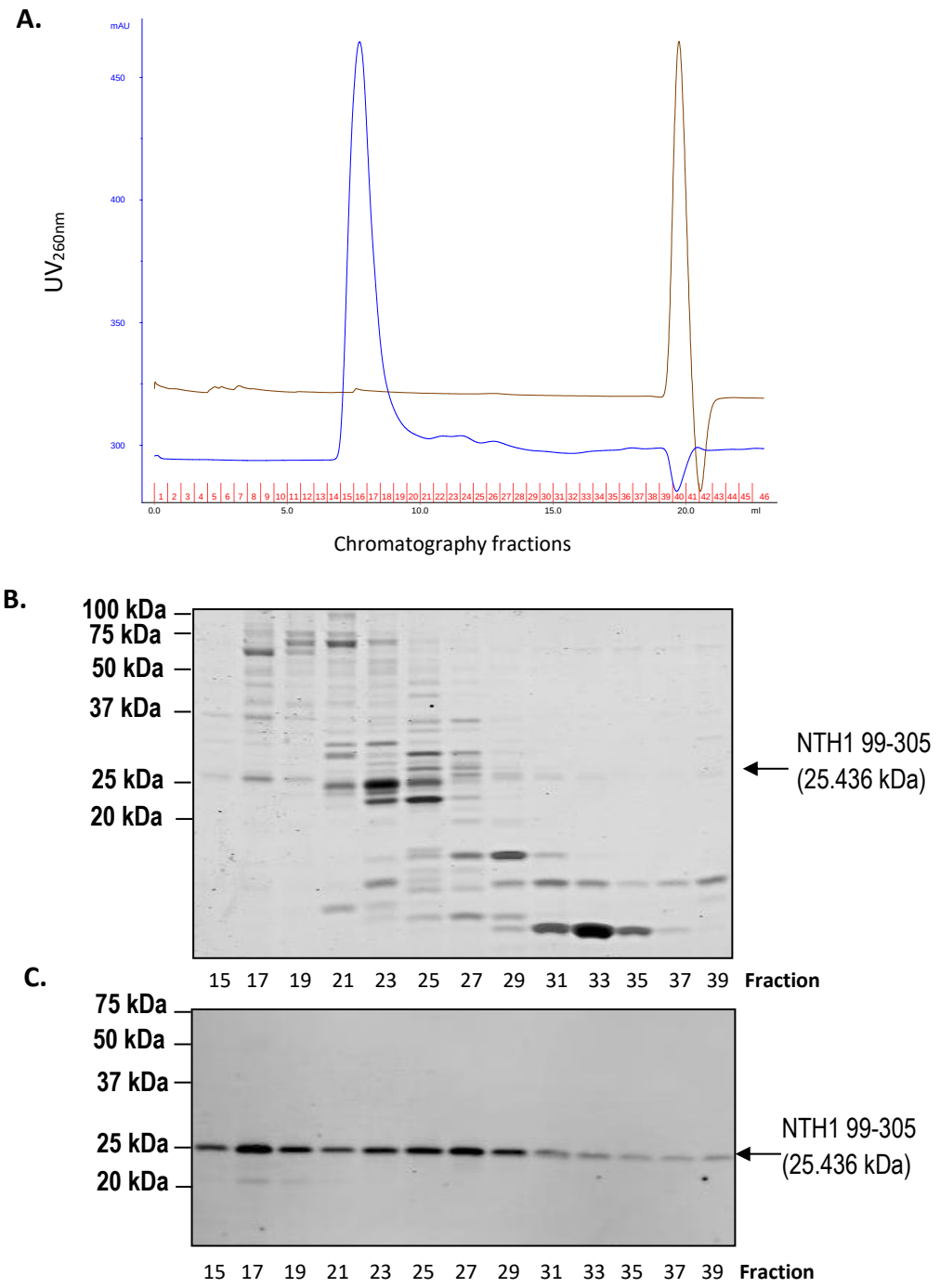

Figure 42. Size exclusion chromatography purification of the C-terminal truncation of NTH1 99-305 by SDS-PAGE and Western blotting with anti-histidine antibodies. Affinity chromatography fractions containing NTH1 99-305 were selected, pooled and concentrated using Amicon Ultra 15 ml centrifugal concentrators (10 kDa MWCO) to approximately 500 µl before being loaded onto a size exclusion Superdex 75 chromatography column, pre-equilibrated with gel filtration buffer (50 mM Tris pH 8, 150 mM KCl, 1 mM EDTA, 5 % glycerol with 1 mM DTT and 1 mM PMSF) using an AKTA-purifier FPLC in a cold cabinet at 4°C, collecting 0.5 ml fractions. The chromatography trace is provided, with the UV260nm represented by the blue line, conductivity represented by the brown line and the chromatography fractions are shown in red (**A**). Fractions were analysed via 16 %

SDS-PAGE (**B**) and Western blotting with anti-histidine antibodies (**C**). Molecular weight markers (kDa) and NTH1 99-305 presence is indicated.

5.3.4 Affinity chromatography purification of NTH1 185-305

Bacterial cells expressing the C-terminal truncation of NTH1 consisting of residues 185-305 were lysed via incubation with lysozyme, followed by bursts of sonication. The histidine-tagged NTH1 185-305 was then separated from bacterial protein contaminants by affinity chromatography with an AKTA purifier FPLC. The cell lysate was loaded onto a 1 ml HisTrap chromatography column pre-equilibrated in lysis buffer containing PMSF. Bound proteins were collected by 20 ml gradient elution using elution buffer containing 500 mM imidazole. The chromatography trace is provided, with peaks in UV representing peaks in protein expression (**Figure 43, A**). Fractions were subject to analysis by SDS-PAGE and Instant Blue staining (**Figure 43, B**) and by Western blotting with anti-histidine antibodies to select fractions with purified his-tagged NTH1 185-305 (**Figure 43, C**). The approximate molecular weight of the truncated version of NTH1 comprising of residues 185-305 is 13.2 kDa. From SDS-PAGE and staining analysis, a protein of molecular weight of ~13 kDa was present in fractions 14-20 although these also contained other higher molecular weight proteins (**Figure 43, B**). However Western blotting analysis revealed the presence of a protein band of this molecular weight present in fractions 10-20 as demonstrated by cross-reactivity with anti-histidine antibodies (**Figure 43; C**); suggesting that this band represents truncated NTH1 185-305. However, due to consideration of protein purity, fractions 16-20 were selected, pooled and concentrated using Amicon Ultra 15 ml centrifugal concentrators (10 kDa MWCO) in a swinging bucket rotor at 4000 x g to generate a concentrated stock of NTH1 185-305 protein.

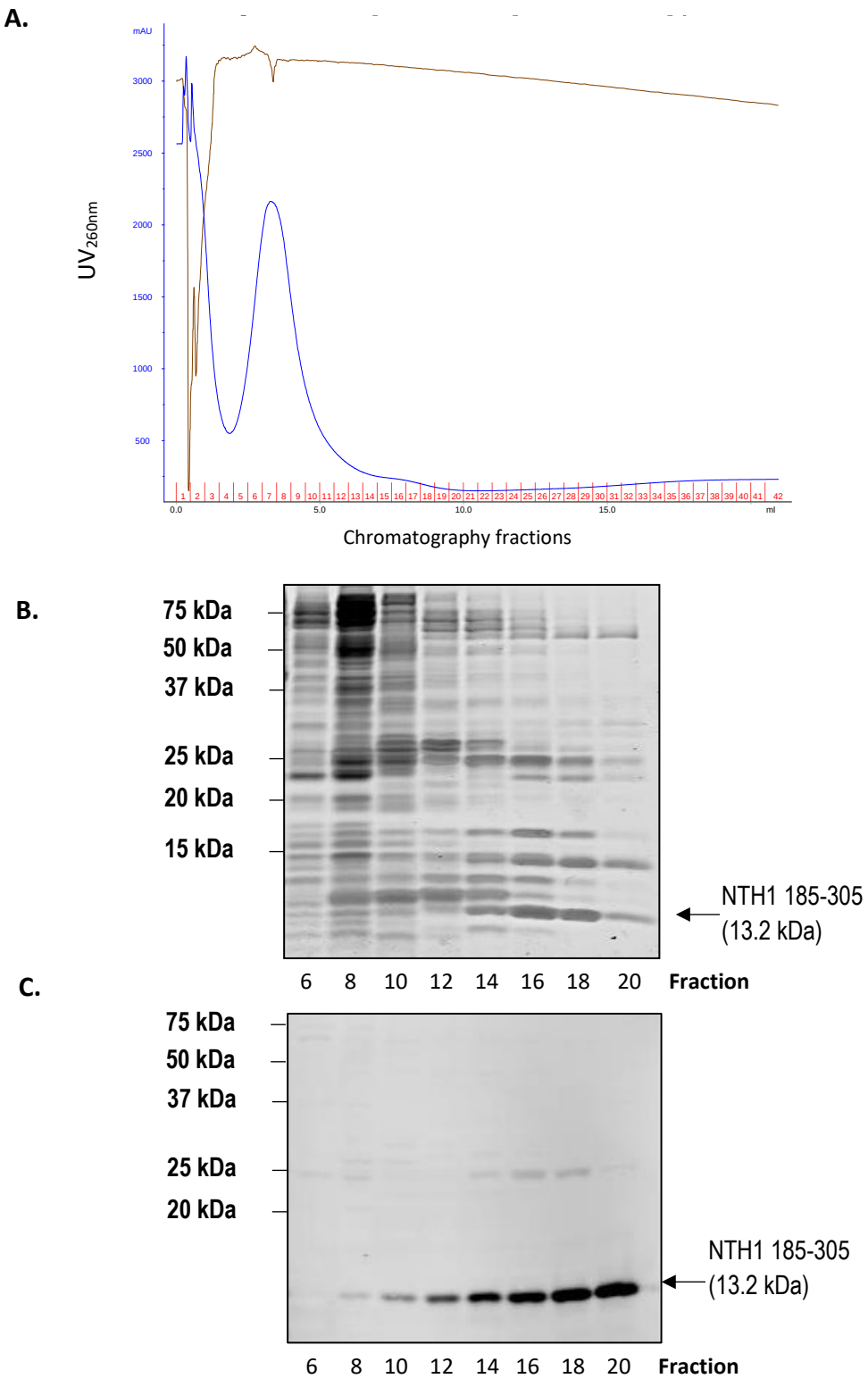

Figure 43. Affinity chromatography purification of the C-terminal truncation of NTH1 185-305 by SDS-PAGE and Western blotting with anti-histidine antibodies. Bacterial cells transformed with pET28a-NTH1 185-305 bacterial expression plasmid were cultured into a 400 ml expression culture until the OD_{650nm} reached 0.6. Bacterial expression of recombinant NTH1 185-305 was then induced via of isopropyl β-D-1-thiogalactopyranoside (IPTG) for 3 h at 30°C. Bacterial cells were then pelleted and lysed by sonication in the presence of protease inhibitors.

Recombinant NTH1 185-305 was separated from bacterial proteins via affinity chromatography using a 1 ml HisTrap column and a linear gradient elution of 5 mM to 500 mM imidazole. The chromatography trace is provided, with the UV_{260nm} represented by the blue line, conductivity represented by the brown line and the chromatography fractions are shown in red (**A**). Chromatography fractions were collected and purity analysed by 16 % SDS-PAGE (**B**) and Western blotting using antibodies specific to NTH1 (**C**). Molecular weight markers (kDa) and NTH1 185-305 presence is indicated.

To further improve the purity of the NTH1 185-305 protein, it was decided to further separate proteins within these fractions based on size exclusion chromatography. For this, concentrated affinity chromatography fractions were loaded onto a Superdex 75 gel filtration chromatography column pre-equilibrated in gel filtration buffer using an AKTA-purifier FPLC at 4°C. The chromatography trace is provided, with peaks in UV representing peaks in protein expression (**Figure 44, A**). Fractions were collected and analysed via SDS-PAGE and Instant Blue (**Figure 44, B**) and by Western blotting with anti-histidine antibodies (**Figure 44, C**). SDS-PAGE staining analysis showed that the gel filtration fractions, 16-20 contained a protein of the expected molecular weight of 13.2 kDa (**Figure 44, B**). Moreover, this protein demonstrated cross-reactivity with NTH1 antibodies; further advocating that this banding pattern corresponds to the presence of histidine tagged, recombinant NTH1 185-305 (**Figure 44, C**). Therefore, gel filtration chromatography fractions 16-20 were selected, pooled and concentrated using Amicon Ultra 15 ml centrifugal concentrators (10 kDa MWCO) in a swinging bucket rotor at 4000 x g to generate a concentrated stock of relatively pure NTH1 185-305 protein.

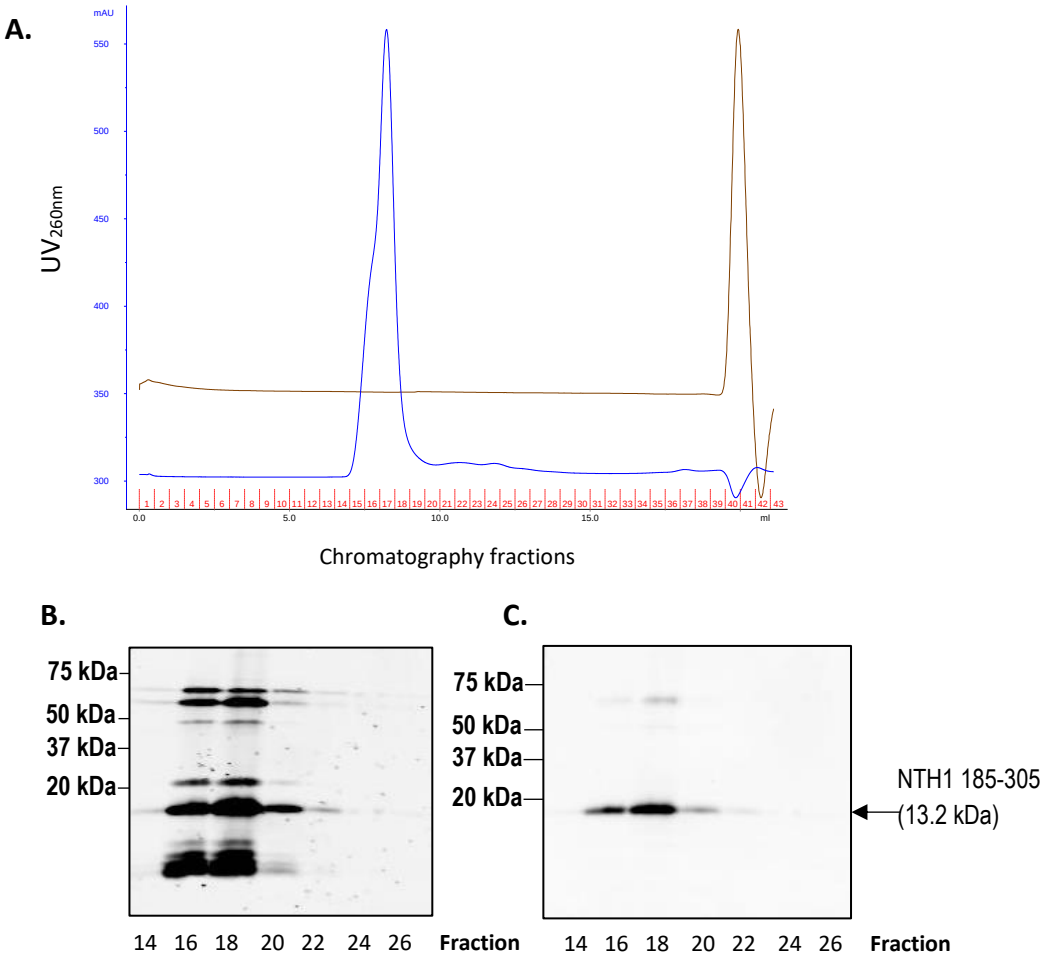

Figure 44. Size exclusion chromatography purification of the C-terminal truncation of NTH1 185-305 by SDS-PAGE and Western blotting with anti-histidine antibodies. Affinity chromatography fractions containing NTH1 185-305 were selected, pooled and concentrated using Amicon Ultra 15 ml centrifugal concentrators (10 kDa MWCO) to approximately 500 µl before being loaded onto a size exclusion Superdex 75 chromatography column, pre-equilibrated with gel filtration buffer (50 mM Tris pH 8, 150 mM KCl, 1 mM EDTA, 5 % glycerol with 1 mM DTT and 1 µM PMSF) using an AKTA-purifier FPLC in a cold cabinet at 4°C, collecting 0.5 ml fractions. The chromatography trace is provided, with the UV260nm represented by the blue line, conductivity represented by the brown line and the chromatography fractions are shown in red (**A**). Fractions were analysed via 16 % SDS-PAGE (**B**) and Western blotting with NTH1 antibodies (**C**). Molecular weight markers (kDa) and NTH1 185-305 presence is indicated.

5.3.5 Analysis of NTH1 truncations via *in vitro* ubiquitylation by TRIM26

After expressing and purifying truncated versions of NTH1, I analysed which truncated proteins contained the lysine residues that are subject to TRIM26 dependent ubiquitylation. To do this, equimolar amounts of each NTH1 truncation was subject to an *in vitro* ubiquitylation assay in the absence (-) of recombinant TRIM26, or with the addition of 19 fmol of recombinant TRIM26 (+) or 26 fmol recombinant TRIM26 (++). Completed reactions were analysed via SDS-PAGE in combination with Western blot analysis using antibodies recognising either the NTH1 specific antibodies (**Figure 45**).

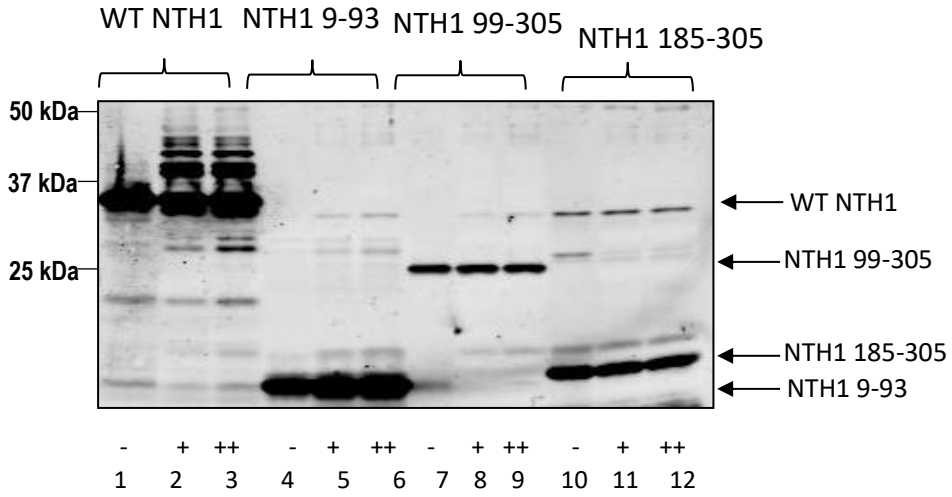

Figure 45. Western blotting analysis of truncated versions of NTH1 following *in vitro* ubiquitylation with recombinant TRIM26. Ubiquitylation assays were performed by combining 0.7 pmol GST-E1 activating enzyme, 5 pmol of UbcH5a conjugating enzymes and 0.6 nmol ubiquitin with either 5.8 pmol of wild type histidine-tagged, recombinant NTH1 (WT) or histidine-tagged, recombinant versions of each NTH1 truncation; NTH1 9-93, NTH1 99-305 or NTH1 185-305. For each version of NTH1 being analysed, a titration of recombinant TRIM26; 0 fmol (-), 19 fmol (+) and 26 fmol (++) was added to distinct ubiquitylation assays. The assay reactions were carried out at 30 °C for 1 h in a shaking incubator at 800 rpm, before completed reactions were separated by 10 % SDS-PAGE and analysed via Western blotting using NTH1 specific antibodies (B). Molecular weight markers (kDa), are indicated.

Despite extensive effort, it was apparent that determination of ubiquitylated sites of NTH1 using truncated versions of the glycosylase was somewhat initially inconclusive. Truncations of NTH1 from the N-terminal end of the protein appeared to significantly impede the level of ubiquitylation observed in the presence of either titrated concentration of TRIM26 (**Figure 45**; lanes 8-9 and 11-12). It was anticipated therefore that the N-terminus of NTH1 containing the lysine residues that are subject

to TRIM26 dependent ubiquitylation would still exhibit the banding pattern associated with ubiquitylation following the *in vitro* assay. However, this was not observed (**Figure 45**; lanes 5-6) despite the observation that the full length NTH1 protein in the presence of TRIM26 was still efficiently ubiquitylated (**Figure 45**; lanes 2-3). There is some suggestion that only in the presence of TRIM26, NTH1 99-305 demonstrates an upward shift of bands at 33 kDa representative of ubiquitylation (**Figure 45**, lanes 8 and 9), however, it could be concluded that these bands may in fact represent other protein contaminants associated with the addition of recombinant TRIM26. This is supported by the presence of protein bands at a similar molecular weight following *in vitro* ubiquitylation of other NTH1 truncations (**Figure 45**, lanes 5 and 6, 11 and 12). The fact that no significant ubiquitylation of the NTH1 9-93 protein was observed would suggest that either this truncation does not contain the lysine residues for TRIM26-dependent ubiquitylation, or that the protein does not contain the domains that promote TRIM26 binding. Overall, it would appear that significantly disrupting the structure of the full-length NTH1 protein via creating truncated versions may in fact significantly inhibit any potential ubiquitylation via TRIM26.

In an attempt to further clarify if any specific domains of NTH1 demonstrated evidence of TRIM26 dependent ubiquitylation, I repeated the *in vitro* ubiquitylation assay once more. In this experiment, I decided to focus on the N-terminal truncated NTH1 products (99-305 and 185-305) in this additional assay (**Figure 46**). Once more, no obvious signs of ubiquitylation of these truncated proteins (**Figure 46**; lanes 5-6 and 8-9) was apparent, in comparison to the full-length protein which demonstrated significant TRIM26-dependent ubiquitylation (**Figure 46**; lanes 2 and 3). The appearance of bands of increased molecular weights, observed only in the presence of TRIM26, could be believed to represent ubiquitylation of the 99-305 and 185-305 truncated proteins (**Figure 5.46;** lanes 5, 6, 8 and 9). However, protein bands of similar molecular weights can also be observed in alternative reactions, even lacking TRIM26 (**Figure 46;** lane 4 and 7). It was concluded that these banding patterns may in fact signify protein impurities associated with the ubiquitylation assay itself and that truncated versions of NTH1, proved to provide little clarification regarding which specific lysine residues are subject to TRIM26-dependent modification. However, given that depletion of even the first 98 amino acids of NTH1 (in 99-305 truncation) appeared to completely supress ubiquitylation of the protein by TRIM26, this at least indicated that ubiquitylation was potentially within the N-terminus of the protein.

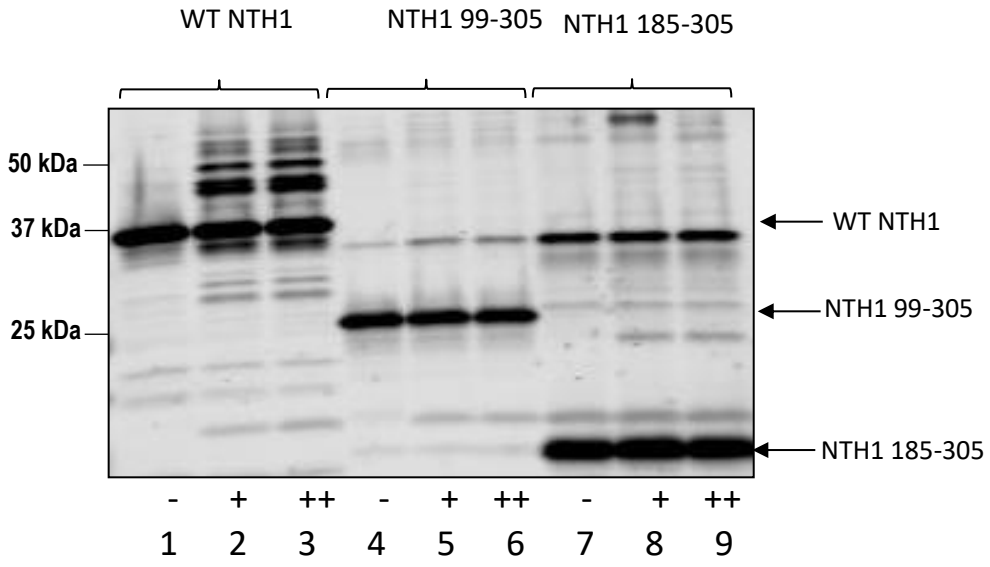

Figure 46. Repeat Western blotting analysis of truncated versions of NTH1 following *in vitro* ubiquitylation with recombinant TRIM26. Ubiquitylation assays were performed by combining 0.7 pmol GST-E1 activating enzyme, 5 pmol of UbcH5a conjugating enzymes and 0.6 nmol ubiquitin with either 5.8 pmol of wild type histidine-tagged, recombinant NTH1 (WT) or histidine-tagged, recombinant versions of each NTH1 truncation; NTH1 99-305 or NTH1 185-305. For each version of NTH1 being analysed, a titration of recombinant TRIM26; 0 fmol (-), 19 fmol (+) and 26 fmol (++) was added to distinct ubiquitylation assays. The assay reactions were carried out at 30 °C for 1 h in a shaking incubator at 800 rpm, before completed reactions were separated by 10 % SDS-PAGE and analysed via Western blotting using NTH1 specific antibodies (B). Molecular weight markers (kDa), are indicated.

5.4 Analysis of ubiquitylation of site specific mutants of NTH1 by TRIM26

Since identification of TRIM26 dependent ubiquitylation of NTH1 remained inconclusive using truncated versions of the glycosylase, it was decided that a site-directed mutagenesis approach should be adopted. Not only would this allow us to identify more specifically certain NTH1 lysine residues that are subject to ubiquitylation, but it also minimised the disruption of the structure of the full-length enzyme which would hopefully minimise the instability of the NTH1 mutants. In addition this approach would limit any reduction in binding of TRIM26 via specific domains, and thus improve the chances of identifying NTH1 ubiquitylation sites. For this strategy, conservative substitution of certain lysine residues to arginine residues was performed. It was anticipated that conservatively substituting lysine residues with an amino acid demonstrating similar biochemical characteristics and charge would cause the least disruption of the overall structure of the glycosylase enzyme and

would enable to discover which substitution caused the greatest reduction in TRIM26-dependent ubiquitylation capacity. Therefore, as part of this strategy I began to mutate each lysine residue sequentially from each terminal end of the NTH1 enzyme, however, due to reports in the literature, it was decided that our main emphasis would initially focus on mutation of the lysine residues situated at the N-terminal end of NTH1. For instance, it is known that human NTH1 possesses an extended N-terminal section compared to its bacterial homologues (90). Kinetic studies have suggested this extended N-terminal region is not associated with the glycolytic activity of the enzyme but could be implicated in regulation (68). In addition, it has been shown that the extended N-terminal region could inhibit NTH1 activity (90). As described in the previous section, deletion of the immediate N-terminus of NTH1 (first 98 amino acids) was sufficient to inhibit ubiquitylation of the remainder of the protein by TRIM26. Cumulatively, these results tentatively advocate that the N-terminal region of human NTH1 could be regulated by signalling modifications, such as ubiquitylation, which may act to control NTH1 activity but also stability.

For this reason, the following point mutations were created (**Table 8**); with site directed mutagenesis of N-terminal residues being the initial primary focus. However additionally, a C-terminal lysine mutant of NTH1 was also created, whereby, two proximal lysine residues (245 and 246, were substituted together) (**Table 8**). The intention was that if no conclusive effects on NTH1 ubiquitylation were observed following site directed mutagenesis of these specific residues, then I would continue substituting each lysine residue simultaneously from each terminal end of NTH1.

Table 8. The custom oligonucleotides which were used to generate NTH1 point mutants to analyse the site of TRIM26 dependent ubiquitylation. For each site directed mutagenesis reaction 0.3 µM of forward oligonucleotide and 0.3 µM reverse oligonucleotides were incubated with 0.02 U/ µl of High Fidelity Phusion Polymerase, 1x Phusion HF buffer, 200 µM dNTPS and 250 pg/µl pET28NTH1 plasmid in a final reaction volume of 50 µl (made up with deionised water). The PCR reactions were performed by one cycle of denaturation at 98°C for 2 min, followed by 18 cycles of; 98°C for 30 s, 55°C for 1 min and 72°C for 5 min, followed by a final extension stage at 72°C for 20 min.

Mutant	Forward oligonucleotide sequence (5'-3')	Reverse oligonucleotide sequence (5'-3')
K42R	CAG-AAG-CGA-GGA-GAA-GCC-ACA-GCC-CC	GGG-GCT-GTG-GCT-TCT-CCT-CGC-TTC-TGC
K48R	ACA-GCC-CCG-TGA-GGC-GTC-CGC-GG	CCG-CGG-ACG-CCT-CAC-GGG-GC
K52R	GCG-TCC-GCG-GAG-AGC-ACA-GAG-ACT-GC	GCA-GTC-TCT-GTG-CTC-TCC-GCG-GAC-GC
K48, 52R	GCC-CCG-TGA-GGC-GTC-CGC-GGA-GAG-CAC-AG	CTG-TGC-TCT-CCG-CGG-ACG-CCT-CAC-GGG-G

K67R	GGG-CTC-GGA-CAG-TGA-GAG-AGG-TGA-GGG	CCC-TCA-CCT-CTC-TCA-CTG-TCC-GAG-CCC
K245, 246R	CTG-AGG-TGG-ACC-AGG-AGG-GCA-ACC-AAG-TCC-C	GAC-TTG-GTT-GCC-CTC-CTG-GTC-CAC-CTC-AGC-C

5.4.1 Generation of site specific mutants of NTH1 by PCR

In order to achieve site specific lysine mutants of NTH1, specific oligonucleotide primers were designed to confer a desired lysine to arginine mutation in the pET28NTH1 plasmid (kindly provided by Dr. Allinson, University of Lancaster). The custom primers were incubated with the target plasmid in the presence of Phusion High-Fidelity DNA polymerase (ThermoFisher Scientific, UK) and amplified by PCR. The custom oligonucleotides used to generate each NTH1 mutation are provided (**Table 8**). The ability of the reaction to generate the correct sized PCR product was assessed on a 1 % agarose gel (**Figure 47**). The expected size of each pET28a expression plasmid containing an insert encoding the mutated *nth1* gene was 6,239 bp. Evaluation of the PCR reactions, verified that plasmids of this approximate size had been generated each containing the required mutations (**Figure 47**).

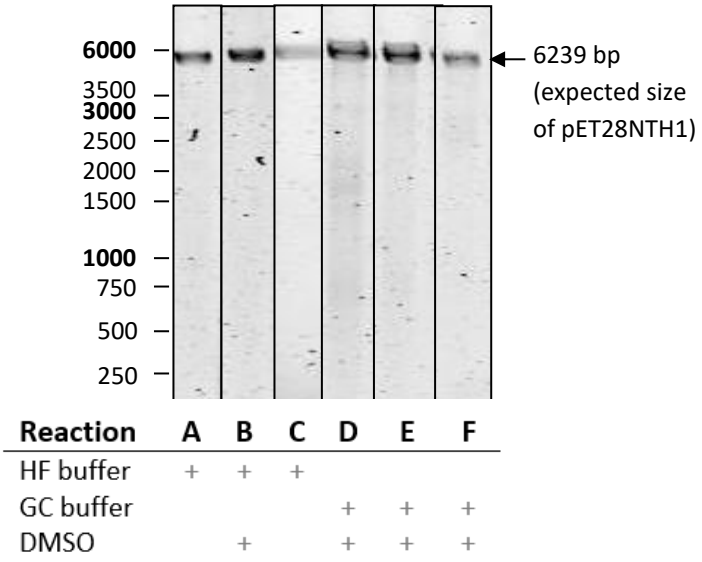

Figure 47. PCR products following site directed mutagenesis of the pET28NTH1 bacterial expression plasmid. Per PCR reaction 250 pg/µl of pET28NTH1 bacterial expression plasmid was incubated with 0.02 U/µl high fidelity Phusion polymerase, 200 µM dNTPs, 0.3 µM custom forward primer, 0.3 µM custom reverse primer and 1 x Phusion HF buffer (h) or GC buffer (g) with/without DMSO ($^{+}$). **A**: pET28NTH1K42R, **B**: pET28NTH1K245,246R, **C**: pET28NTH1K52R, **D**: pET28NTH1K48R, **E**: pET28NTH1K67R, **F**: pET28NTH1K48,52R The size of the PCR products was analysed using 1 % agarose gels in 1x TAE. The expected sizes of each PCR product in base pairs are featured.

Noticeably, this analysis could not confirm whether the *nth1* gene contained the required point mutation. Therefore, plasmids of pET28NTH1 containing the desired lysine to arginine point mutation were subject to treatment with DpnI to remove methylated DNA corresponding to the template DNA containing the wild type *nth1* gene sequence, before being transformed into library efficient bacterial DH5α cells grown on selective agar containing kanamycin. Successfully grown colonies were then grown in overnight cultures and plasmid DNA was isolated via the QIAprep Spin Miniprep Kit (QIAGEN). The success of each site-directed mutagenesis reaction was analysed by DNA sequencing each plasmid using the Sanger Sequencing Service (see Appendix).

5.4.2 Purification of site specific mutants of NTH1

All of the plasmids containing the appropriate point mutations (K42R, K48R, K52R, K48,52R, K67R, K245,246R) were transformed into Rosetta 2(DE3) pLysS cells, cultures were grown and protein expression was induced using IPTG. Cell lysates were generated and each mutant NTH1 protein was purified separately by affinity chromatography using separate 1 ml HisTrap affinity chromatography columns attached to an AKTApurifier chromatography system at 4°C. Proteins were eluted using a 20 ml gradient of 5 mM to 500 mM imidazole.

5.4.2.1 Affinity chromatography purification of K42R

The bacterial expression plasmid encoding pET28NTH1K42R was transformed into Rosetta 2(DE3) pLysS cells which were cultured to 400 ml before recombinant protein expression was induced via IPTG addition. Following this, cells were pelleted and re-suspended in lysis buffer containing protease inhibitors before being lysed via incubation with lysozyme in combination with bursts of sonication. Cell debris was removed by centrifugation and cell lysates were syringe filtered before being applied to a 1 ml HisTrap column attached to an AKTA purifier FPLC. Bound proteins were eluted via a 20 ml gradient elution of 5 mM to 500 mM imidazole, collecting 0.5 ml fractions. The chromatography trace is provided, with peaks in UV representing peaks in protein expression (**Figure 48, A**). The protein content of the chromatography fractions collected was assessed via 10 % SDS-PAGE and Instant Blue staining (**Figure 48, B**) and also by Western blotting analysis using NTH1 specific antibodies (**Figure 48, C**).

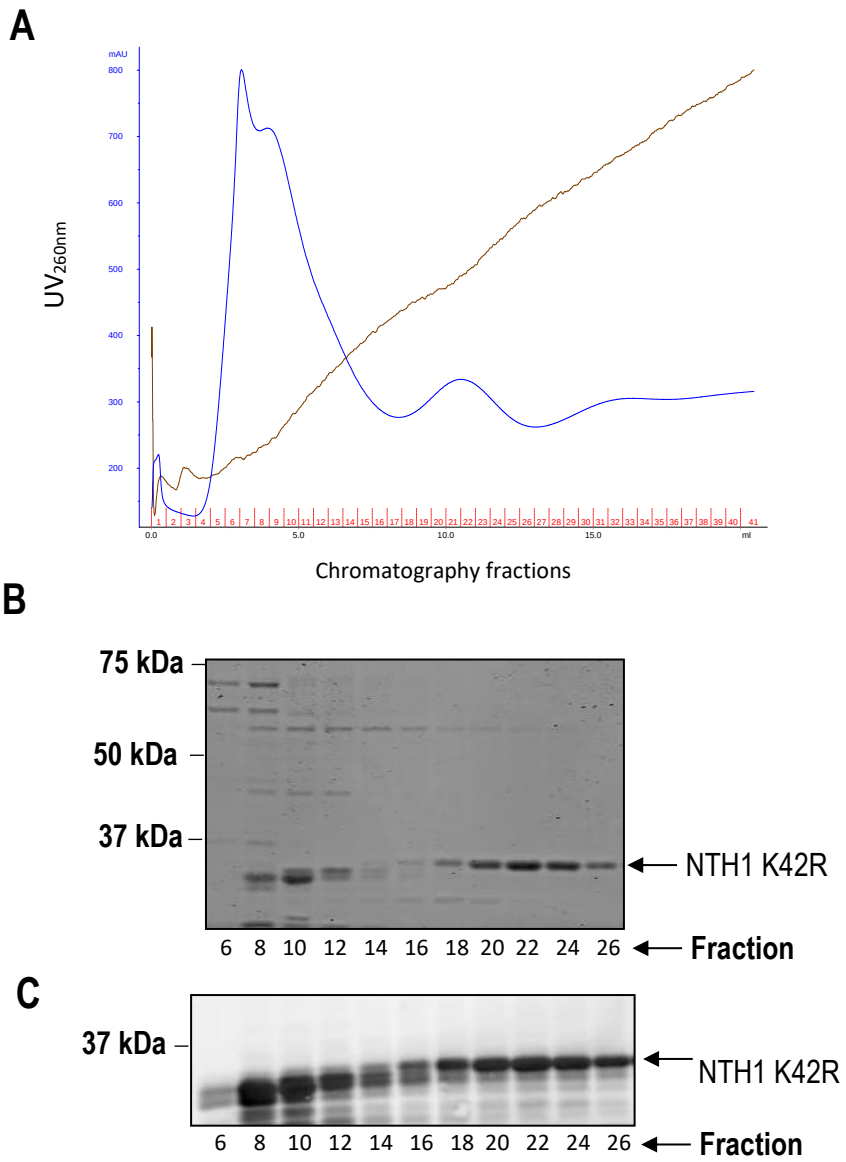

Figure 48. Affinity chromatography of NTH1 point mutation at lysine residue 42 (K42R). Point mutations of NTH1 lysine residues (K) to arginine (R) residues were created via site-directed mutagenesis of a pET28NTH1 plasmid using custom oligonucleotides with Phusion High-fidelity DNA polymerase. Plasmid constructs were transformed into Rosetta 2(DE3) pLysS cells and protein expression induced via 1 mM IPTG in a 400 ml culture for 3 h at 37°C, 250 rpm. The bacterial suspension was pelleted by centrifugation and supernatant removed. The Rosetta 2(DE3) pLysS cells were re-suspended in lysis buffer with protease inhibitors before the cells were lysed open via incubation with lysozyme followed by sonication. Cells were pelleted by centrifugation and the supernatant filtered through syringe filters. Filtered supernatant was applied to a pre-equilibrated 1 ml His-trap affinity chromatography column. Proteins were eluted via a gradient of 5 mM to 500 mM imidazole. The chromatography trace is provided, with the UV260nm represented by the blue line, conductivity represented by the brown line and the chromatography fractions are shown in red (**A**). The contents of select chromatography fractions were analysed via 10 % SDS-PAGE (**B**) and Western blotting with NTH1 specific antibodies (**C**). Molecular weight markers (kDa) are indicated as well as fraction numbers and the presence of the NTH1 mutation.

Following SDS-PAGE protein analysis of the chromatography fractions, it was apparent that fractions 18-26 contained protein bands of the expected molecular weight of NTH1 (**Figure 48, A and B**; 34.4 kDa), and that these proteins also demonstrated cross-reactivity to the anti-NTH1 antibodies utilised (**Figure 48, C**). For this reason, these fractions were believed to contain NTH1 K42R and consequently fractions 20-26 containing relatively pure protein were selected, pooled and concentrated using Amicon Ultra 15 ml centrifugal concentrators (10 kDa MWCO) in a swinging bucket rotor at 4000 x g until the volume reached approximately 500 µl. This volume was then made up to 1 mL in JPDB buffer (50 mM Tris HCl pH 8, 50 mM KCl, 1 mM EDTA, 10 % glycerol) and concentrated once more at 4000 x g. This process was repeated twice more to buffer exchange the fractions.

5.6.3.2 Affinity chromatography purification of K52R

The bacterial expression plasmid encoding pET28NTH1K52R was transformed into Rosetta 2(DE3) pLysS cells and a 400 ml culture was grown and recombinant protein expression was induced via the addition of IPTG. Cells were pelleted, re-suspended in lysis buffer containing protease inhibitors, before being lysed using lysozyme and sonication. Bacterial cell debris was removed by centrifugation and the cell lysate was syringe filtered before being applied to a 1 ml HisTrap column attached to an AKTA purifier FPLC. Bound proteins were eluted via 20 ml gradient elution of 5 mM to 500 mM imidazole, collecting 0.5 ml fractions. The chromatography trace is provided, with peaks in UV representing peaks in protein expression (**Figure 49, A**). Collected chromatography fractions were assessed via 10 % SDS-PAGE and Instant Blue staining (**Figure 49, B**) and also by Western blotting analysis using NTH1 specific antibodies (**Figure 49, C**).

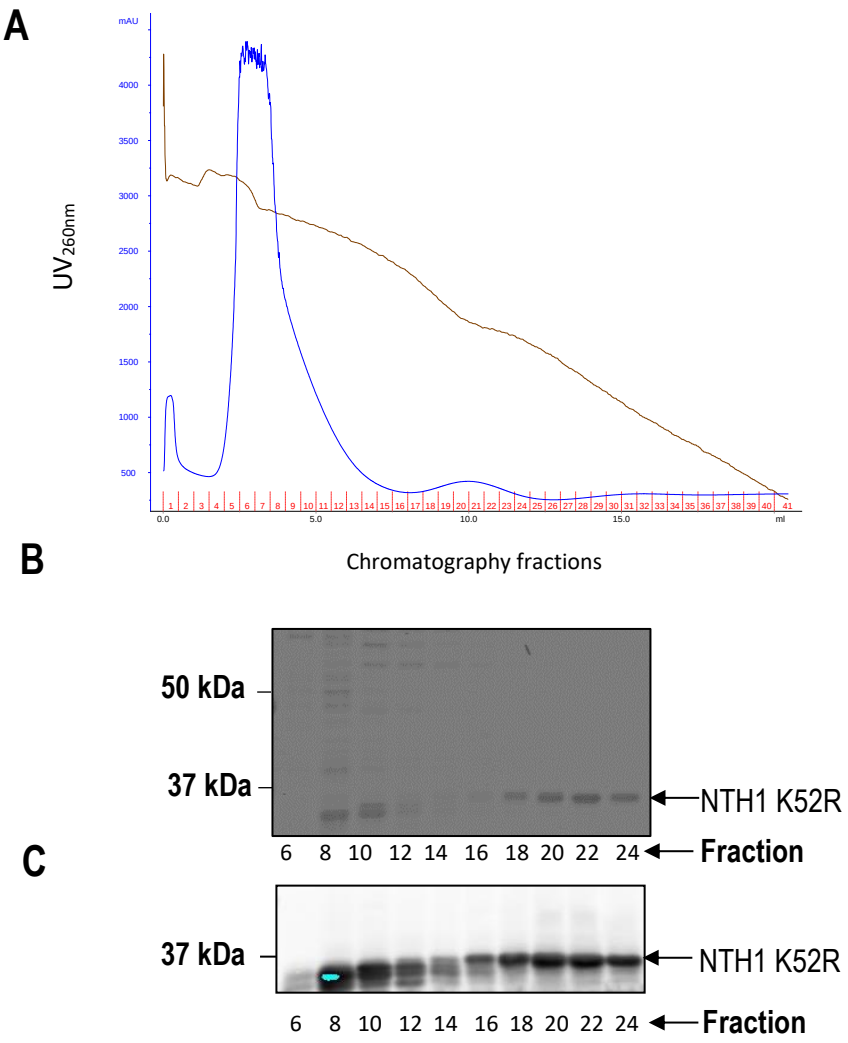

Figure 49. Affinity chromatography of NTH1 point mutation at lysine residue 52 (K52R). Point mutations of NTH1 lysine residues (K) to arginine (R) residues were created via site-directed mutagenesis of a pET28NTH1 plasmid using custom oligonucleotides with Phusion High-fidelity DNA polymerase. Plasmid constructs were transformed into Rosetta 2(DE3) pLysS cells and protein expression induced via 1 mM IPTG in a 400 ml culture for 3 h at 37°C, 250 rpm. The bacterial suspension was pelleted by centrifugation and supernatant removed. The Rosetta 2(DE3) pLysS cells were re-suspended in lysis buffer with protease inhibitors before the cells were lysed open via incubation with lysozyme followed by sonication. Cells were pelleted by centrifugation and the supernatant filtered through syringe filters. Filtered supernatant was applied to a pre-equilibrated 1 ml His-trap affinity chromatography column. Proteins were eluted via a gradient of 5 mM to 500 mM imidazole. The chromatography trace is provided, with the UV260nm represented by the blue line, conductivity represented by the brown line and the chromatography fractions are shown in red (**A**). The contents of select chromatography fractions were analysed via 10 % SDS-PAGE (**B**) and Western blotting with NTH1 specific antibodies (**C**). Molecular weight markers (kDa) are indicated as well as fraction numbers and the presence of the NTH1 mutation.

Following SDS-PAGE protein analysis of the chromatography fractions, it was apparent that fractions 18-24 contained protein bands of the expected molecular weight for NTH1 K52R, which cross-reacted with anti-NTH1 antibodies (**Figure 49, A and B**; 34.4 kDa). These fractions were selected, pooled and concentrated using Amicon Ultra 15 ml centrifugal concentrators (10 kDa MWCO) until the final volume reached approximately 500 µl. This volume was then made up to 1 mL in JPDB buffer (50 mM Tris HCl pH 8, 50 mM KCl, 1 mM EDTA, 10 % glycerol) and concentrated once more at 4000 x g. This process was repeated twice more to buffer exchange the fractions.

5.4.2.3 Affinity chromatography purification of K48R

The bacterial expression plasmid encoding pET28NTH1K48R was transformed into Rosetta 2(DE3) pLysS cells, a culture of 400 ml was grown and protein expression induced by IPTG. Cells were pelleted, re-suspended in lysis buffer containing protease inhibitors and lysed. Bacterial cell contaminants were removed by centrifugation, a cell lysate prepared and applied to a 1 ml HisTrap column attached to an AKTA purifier FPLC. Bound proteins were eluted via 20 ml gradient elution of 5 mM to 500 mM imidazole, collecting 0.5 ml fractions. The chromatography trace is provided, with peaks in UV representing peaks in protein expression (**Figure 50, A**). Collected fractions were assessed via 10 % SDS-PAGE and Instant Blue staining (**Figure 50, B**) and also by Western blotting analysis using NTH1 specific antibodies (**Figure 50, C**).

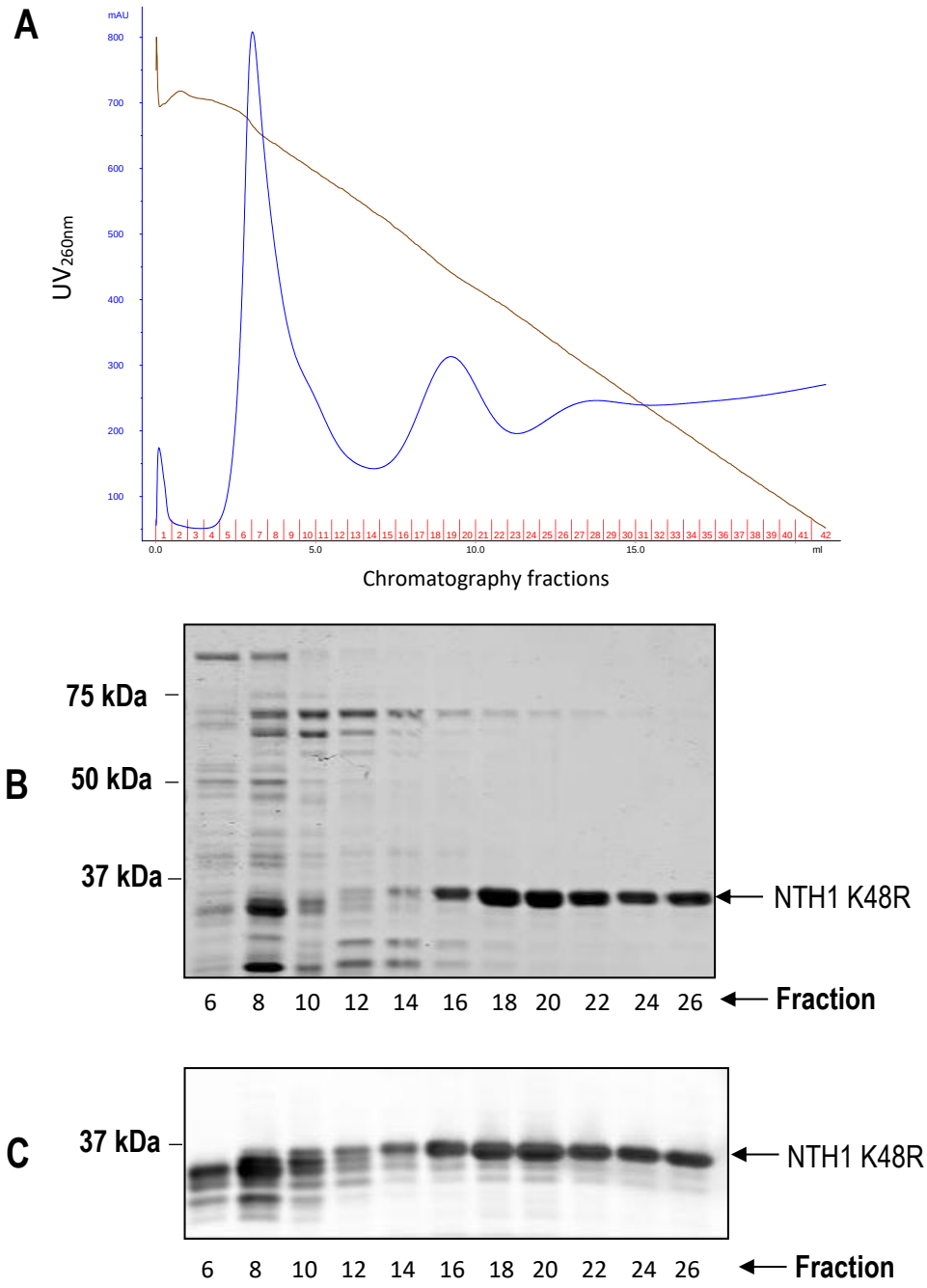

Figure 50. Affinity chromatography of NTH1 point mutation at lysine residue 48 (K48R). Point mutations of NTH1 lysine residues (K) to arginine (R) residues were created via site-directed mutagenesis of a pET28NTH1 plasmid using custom oligonucleotides with Phusion High-fidelity DNA polymerase. Plasmid constructs were transformed into Rosetta 2(DE3) pLysS cells and protein expression induced via 1 mM IPTG in a 400 ml culture for 3 h at 37°C, 250 rpm. The bacterial suspension was pelleted by centrifugation and supernatant removed. The Rosetta 2(DE3) pLysS cells were re-suspended in lysis buffer with protease inhibitors before the cells were lysed open via incubation with lysozyme followed by sonication. Cells were pelleted by centrifugation and the supernatant filtered through syringe filters. Filtered supernatant was applied to a pre-equilibrated 1 ml His-trap affinity chromatography column. Proteins were eluted via a gradient of 5 mM to 500 mM imidazole. The chromatography trace is provided, with the UV260nm represented by the blue line, conductivity represented by the brown line and the chromatography fractions are

shown in red (**A**). The contents of select chromatography fractions were analysed via 10 % SDS-PAGE (**B**) and Western blotting with NTH1 specific antibodies (**C**). Molecular weight markers (kDa) are indicated, as well as fraction numbers and the presence of the NTH1 mutation.

Following SDS-PAGE protein analysis of the chromatography fractions, it was apparent that fractions 16-26 contained protein bands corresponding to NTH1 K48R and this was further confirmed by Western blotting analysis using NTH1-specific antibodies (**Figure 50; A and B**; 34.4 kDa). These fractions were selected, pooled and concentrated using Amicon Ultra 15 ml centrifugal concentrators (10 kDa MWCO) until 500 µl in volume. This volume was then made up to 1 mL in JPDB buffer (50 mM Tris HCl pH 8, 50 mM KCl, 1 mM EDTA, 10 % glycerol) and concentrated once more at 4000 x g. This process was repeated twice more to buffer exchange the fractions.

5.4.2.4 Affinity chromatography purification of K67R

The bacterial expression plasmid encoding pET28NTH1K67R transformed into Rosetta 2(DE3) pLysS cells, a 400 ml cell culture was grown and IPTG used to induce protein expression. Cells were pelleted, re-suspended in lysis buffer containing protease inhibitors and lysed. Bacterial cell contaminants were removed by centrifugation, the cell lysate was filtered and applied to a 1 ml HisTrap column attached to an AKTA purifier FPLC. Bound proteins were eluted via 20 ml gradient elution of 5 mM to 500 mM imidazole, collecting 0.5 ml fractions. The chromatography trace is provided, with peaks in UV representing peaks in protein expression (**Figure 51, A**). Collected fractions were assessed via 10 % SDS-PAGE and Instant Blue staining (**Figure 51, B**) and also by Western blotting analysis using NTH1 specific antibodies (**Figure 51, C**).

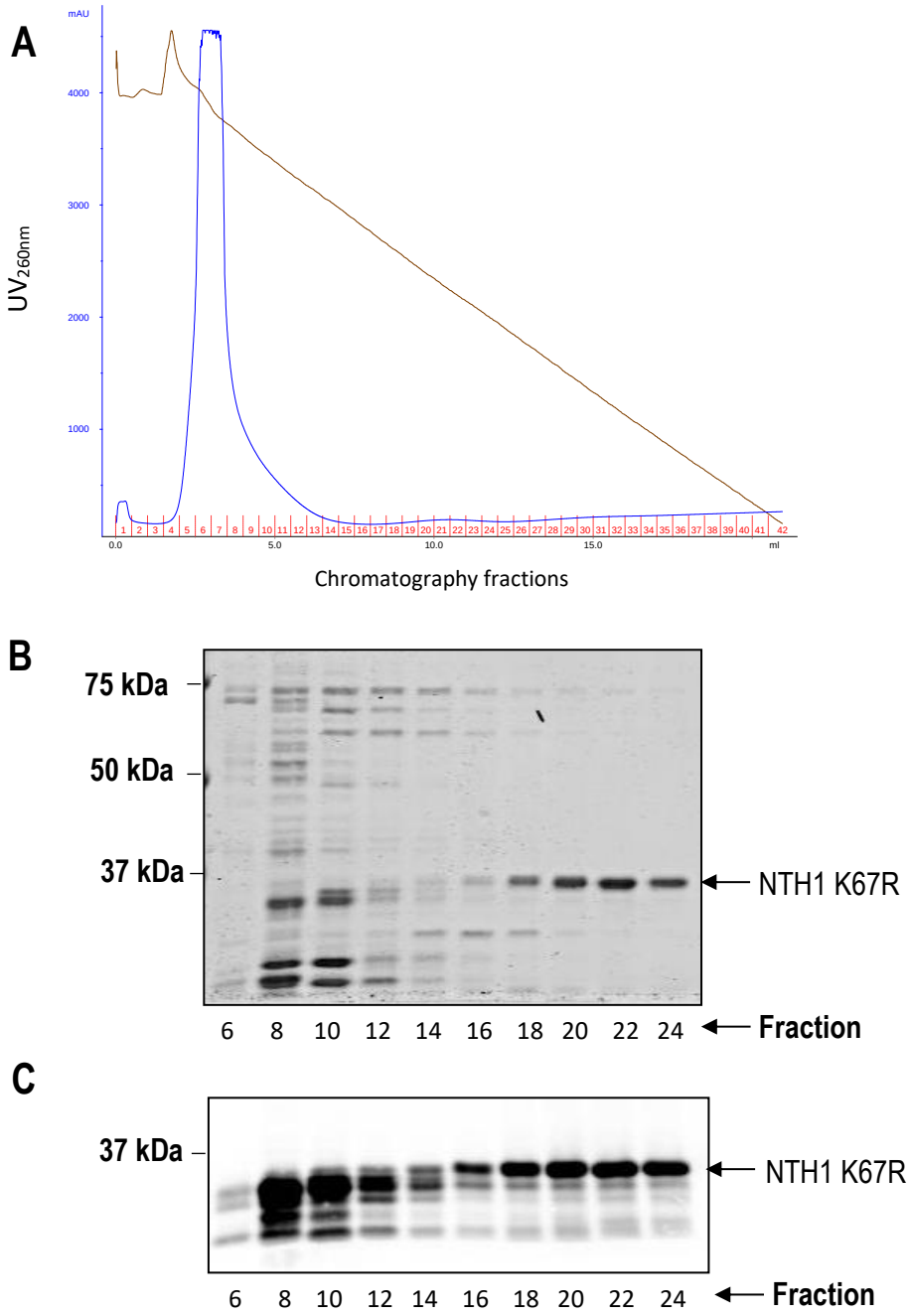

Figure 51. Affinity chromatography of NTH1 point mutation at lysine residue 67 (K67R). Point mutations of NTH1 lysine residues (K) to arginine (R) residues were created via site-directed mutagenesis of a pET28NTH1 plasmid using custom oligonucleotides with Phusion High-fidelity DNA polymerase. Plasmid constructs were transformed into Rosetta 2(DE3) pLysS cells and protein expression induced via 1 mM IPTG in a 400 ml culture for 3 h at 37°C, 250 rpm. The bacterial suspension was pelleted by centrifugation and supernatant removed. The Rosetta 2(DE3) pLysS cells were re-suspended in lysis buffer with protease inhibitors before the cells were lysed open via incubation with lysozyme followed by sonication. Cells were pelleted by centrifugation and the supernatant filtered through syringe filters. Filtered supernatant was applied to a pre-equilibrated 1 ml His-trap affinity chromatography column. Proteins were eluted via a gradient of 5 mM to 500 mM imidazole. The chromatography trace is provided, with the UV_{260nm} represented by the blue line, conductivity represented by the brown line and the chromatography fractions are

shown in red (**A**). The contents of select chromatography fractions were analysed via 10 % SDS-PAGE (**B**) and Western blotting with NTH1 specific antibodies (**C**). Molecular weight markers (kDa) are indicated as well as fraction numbers and the presence of the NTH1 mutation.

Following SDS-PAGE protein analysis of the chromatography fractions, it was apparent that fractions 18-24 largely contained protein bands corresponding to NTH1 K67R (**Figure 5.19A**; 34.4 kDa). This was supported by Western blotting analysis which similarly demonstrated that fractions 18-24 contained protein that cross-reacted with NTH1-specific antibodies. These fractions were selected, pooled and concentrated using Amicon Ultra 15 ml centrifugal concentrators (10 kDa MWCO) until 500 µl in volume. This volume was then made up to 1 mL in JPDB buffer (50 mM Tris HCl pH 8, 50 mM KCl, 1 mM EDTA, 10 % glycerol) and concentrated once more at 4000 x g. This process was repeated twice more to buffer exchange the fractions.

5.4.2.5 Affinity chromatography purification of K48,52R

The bacterial expression plasmid encoding pET28NTH1K48,52R was transformed into Rosetta 2(DE3) pLysS cells, a 400 ml culture was grown and IPTG added to induce protein expression. Cells were pelleted by centrifugation, re-suspended in lysis buffer containing protease inhibitors and lysed. Bacterial cell contaminants were removed by centrifugation, a cell lysate was prepared and applied to a 1 ml HisTrap column attached to an AKTA purifier FPLC. Bound proteins were eluted via 20 ml gradient elution of 5 mM to 500 mM imidazole, collecting 0.5 ml fractions. The chromatography trace is provided, with peaks in UV representing peaks in protein expression (**Figure 52, A**). Collected fractions were assessed via 10 % SDS-PAGE and Instant Blue staining (**Figure 52, B**) and also by Western blotting analysis using NTH1 specific antibodies (**Figure 52, C**).

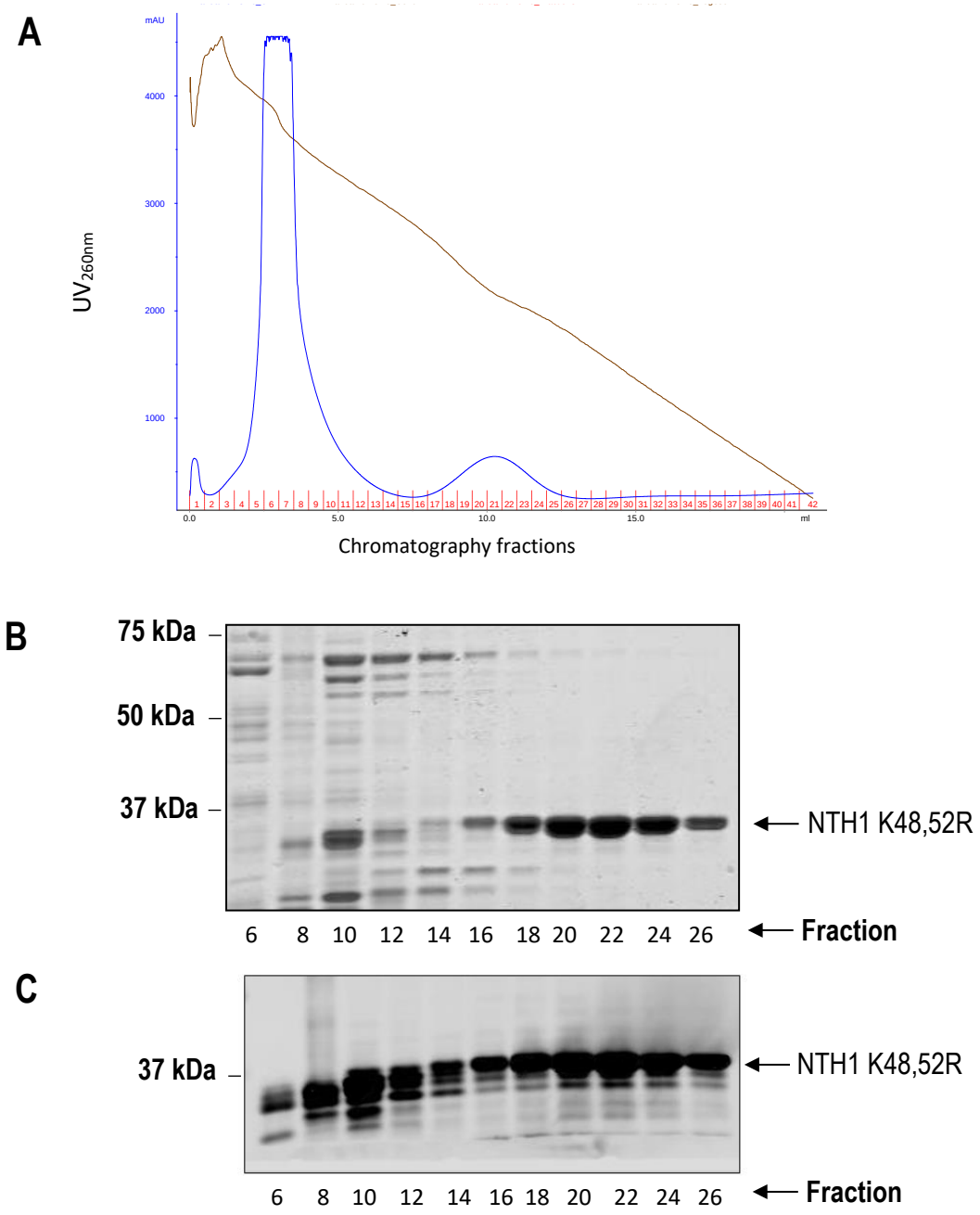

Figure 52. Affinity chromatography of NTH1 point mutation at lysine residues 48 and 52 (K48, 52R). Point mutations of NTH1 lysine residues (K) to arginine (R) residues were created via site-directed mutagenesis of a pET28NTH1 plasmid using custom oligonucleotides with Phusion High-fidelity DNA polymerase. Plasmid constructs were transformed into Rosetta 2(DE3) pLysS cells and protein expression induced via 1 mM IPTG in a 400 ml culture for 3 h at 37°C, 250 rpm. The bacterial suspension was pelleted by centrifugation and supernatant removed. The Rosetta 2(DE3) pLysS cells were re-suspended in lysis buffer with protease inhibitors before the cells were lysed open via incubation with lysozyme followed by sonication. Cells were pelleted by centrifugation and the supernatant filtered through syringe filters. Filtered supernatant was applied to a pre-equilibrated 1 ml His-trap affinity chromatography column. Proteins were eluted via a gradient of 5 mM to 500 mM imidazole. The chromatography trace is provided, with the UV260nm represented by the blue line, conductivity represented by the brown line and the chromatography fractions are shown in red (**A**). The contents of select chromatography fractions were

analysed via 10 % SDS-PAGE (**B**) and Western blotting with NTH1 specific antibodies (**C**). Molecular weight markers (kDa) are indicated as well as fraction numbers and the presence of the NTH1 mutation.

Following SDS-PAGE protein analysis of the chromatography fractions, it was apparent that fractions 18-26 contained protein bands corresponding to NTH1 K48, 52R and which was confirmed utilising Western blotting containing NTH1-specific antibodies (**Figure 52, A and B**; 34.4 kDa). These fractions were selected, pooled and concentrated using Amicon Ultra 15 ml centrifugal concentrators (10 kDa MWCO) until 500 µl in volume. This volume was then made up to 1 mL in JPDB buffer (50 mM Tris HCl pH 8, 50 mM KCl, 1 mM EDTA, 10 % glycerol) and concentrated once more at 4000 x g. This process was repeated twice more to buffer exchange the fractions.

5.4.2.6 Affinity chromatography purification of K245,246R

The bacterial expression plasmid encoding pET28NTH1K245,246R was transformed into Rosetta 2(DE3) pLysS cells, a 400 ml culture was grown and protein expression induced with IPTG. Cells were pelleted by centrifugation, re-suspended in lysis buffer containing protease inhibitors and lysed. Bacterial cell contaminants were removed by centrifugation, a cell lysate was prepared and applied to a 1 ml HisTrap column attached to an AKTA purifier FPLC. Bound proteins were eluted via 20 ml gradient elution of 5 mM to 500 mM imidazole, collecting 0.5 ml fractions. The chromatography trace is provided, with peaks in UV representing peaks in protein expression (**Figure 53, A**). Collected fractions were assessed via 10 % SDS-PAGE and Instant Blue staining (**Figure 53, B**) and by Western blotting analysis using NTH1 specific antibodies (**Figure 53, C**).

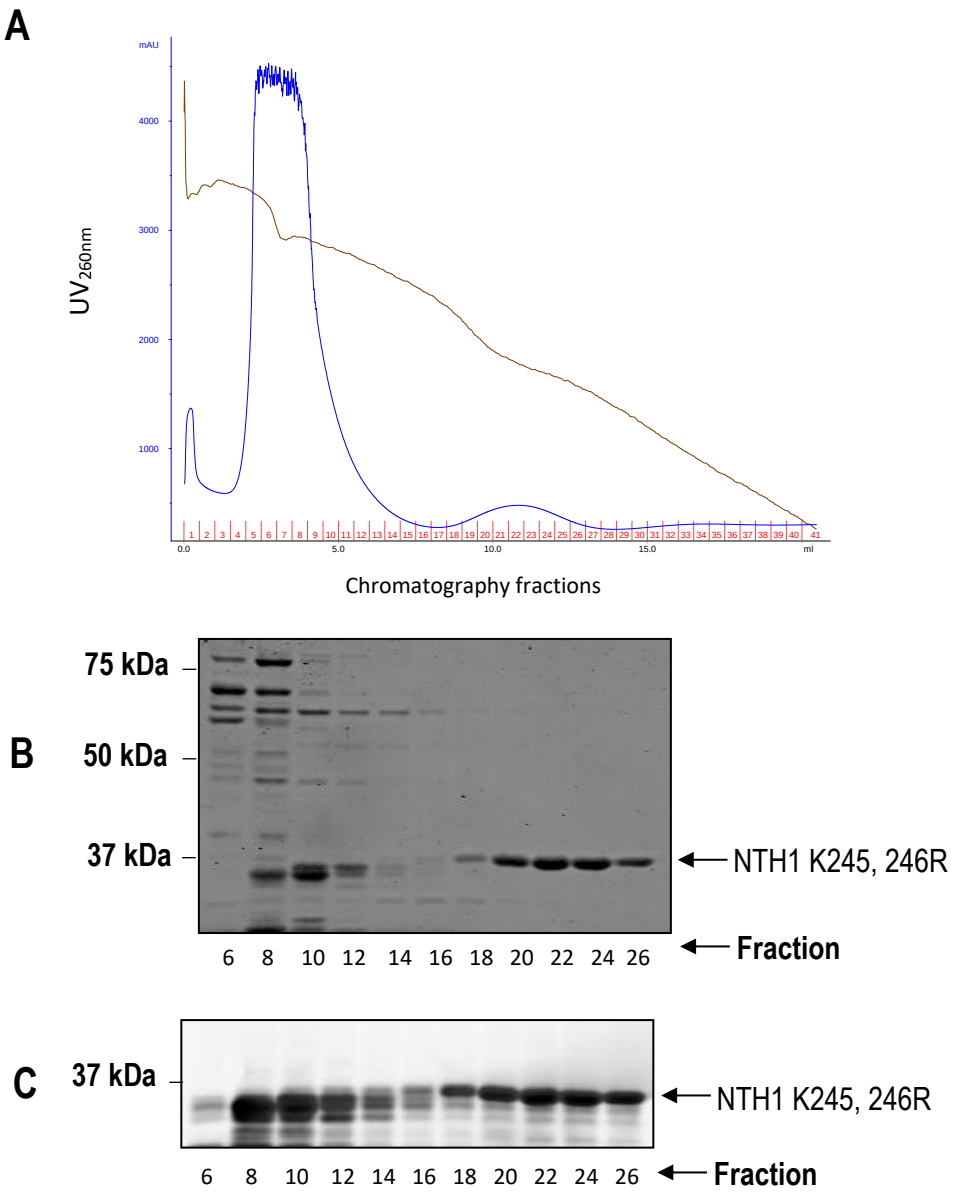

Figure 53. Affinity chromatography of NTH1 point mutation at lysine residues 245 and 246 (K245, 246R). Point mutations of NTH1 lysine residues (K) to arginine (R) residues were created via site-directed mutagenesis of a pET28NTH1 plasmid using custom oligonucleotides with Phusion High-fidelity DNA polymerase. Plasmid constructs were transformed into Rosetta 2(DE3) pLysS cells and protein expression induced via 1 mM IPTG in a 400 ml culture for 3 h at 37°C, 250 rpm. The bacterial suspension was pelleted by centrifugation and supernatant removed. The Rosetta 2(DE3) pLysS cells were re-suspended in lysis buffer with protease inhibitors before the cells were lysed open via incubation with lysozyme followed by sonication. Cells were pelleted by centrifugation and the supernatant filtered through syringe filters. Filtered supernatant was applied to a pre-equilibrated 1 ml His-trap affinity chromatography column. Proteins were eluted via a gradient of 5 mM to 500 mM imidazole. The chromatography trace is provided, with the UV260nm represented by the blue line, conductivity represented by the brown line and the chromatography fractions are shown in red (**A**). The contents of select chromatography fractions were analysed via 10 % SDS-PAGE (**B**) and Western blotting with NTH1 specific antibodies (**C**). Molecular weight markers (kDa) are indicated as well as fraction numbers and the presence of the NTH1 mutation.

Following SDS-PAGE protein analysis of the chromatography fractions, it was apparent that fractions 18-26 largely contained protein bands corresponding to NTH1 K245,246R and these bands also cross-reacted with NTH1-specific antibodies by Western blotting (**Figure 53, A and B**; 34.4 kDa). These fractions were selected, pooled and concentrated using Amicon Ultra 15 ml centrifugal concentrators (10 kDa MWCO) until 500 µl in volume. This volume was then made up to 1 mL in JPDB buffer (50 mM Tris HCl pH 8, 50 mM KCl, 1 mM EDTA, 10 % glycerol) and concentrated once more at 4000 x g. This process was repeated twice more to buffer exchange the fractions.

5.4.2.7 Affinity chromatography purification of K42,48,52,67R

The bacterial expression plasmid encoding pET28NTH1K42,48,52,67R was transformed into Rosetta 2(DE3) pLysS cells, a 400 ml culture was grown and protein expression induced with IPTG. Cells were pelleted by centrifugation, re-suspended in lysis buffer containing protease inhibitors and lysed. Bacterial cell contaminants were removed by centrifugation, a cell lysate was prepared and applied to a 1 ml HisTrap column attached to an AKTA purifier FPLC. Bound proteins were eluted via 20 ml gradient elution of 5 mM to 500 mM imidazole, collecting 0.5 ml fractions. The chromatography trace is provided, with peaks in UV representing peaks in protein expression (**Figure 54, A**). Collected fractions were assessed via 10 % SDS-PAGE and Instant Blue staining (**Figure 54, B**) and by Western blotting analysis using NTH1 specific antibodies (**Figure 54, C**).

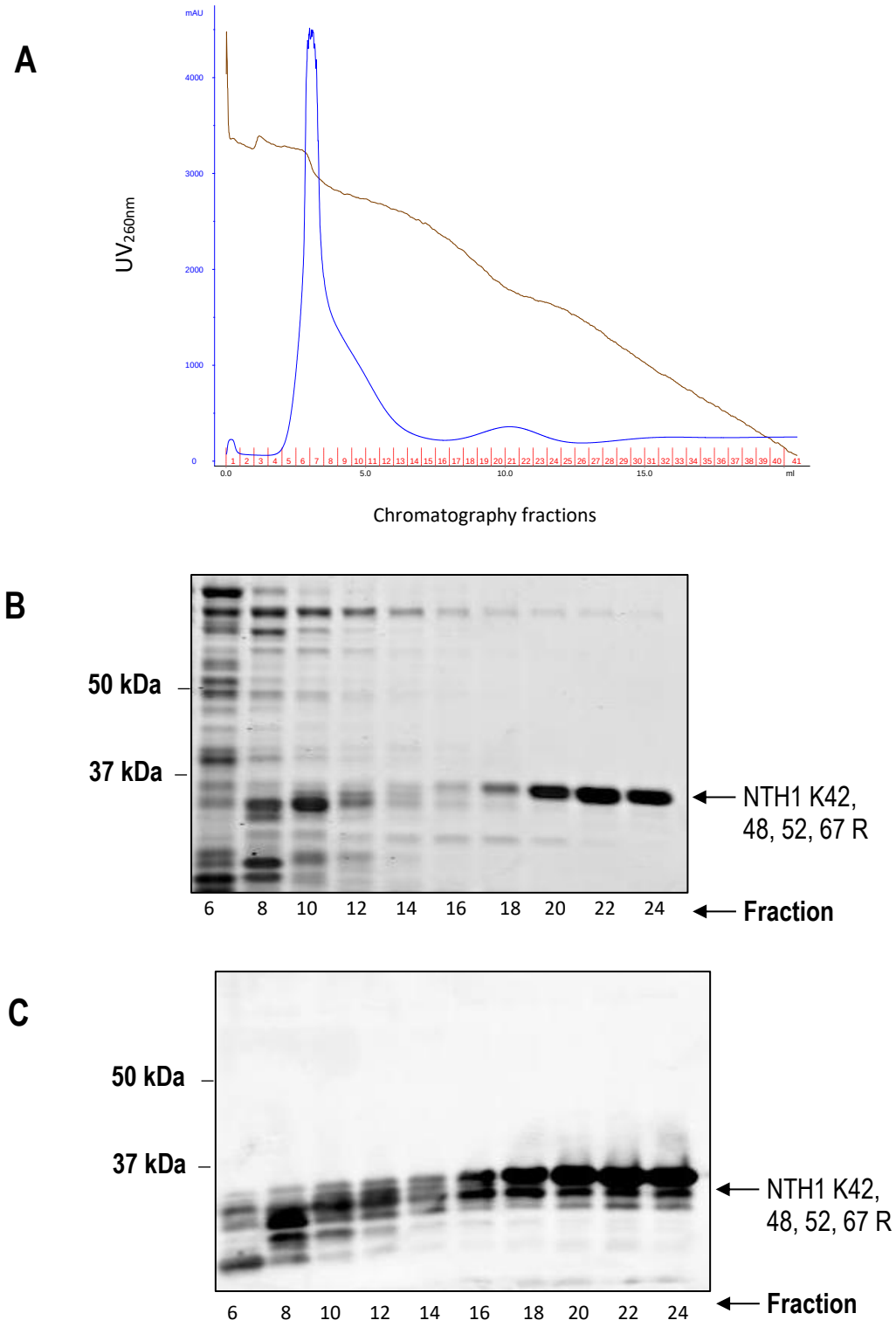

Figure 54. Affinity chromatography of NTH1 point mutation at lysine residues 42, 48, 52, 67 (K42, 48, 52, 67 R). Point mutations of NTH1 lysine residues (K) to arginine (R) residues were created via site-directed mutagenesis of a pET28NTH1 plasmid using custom oligonucleotides with Phusion High-fidelity DNA polymerase. Plasmid constructs were transformed into Rosetta 2(DE3) pLysS cells and protein expression induced via 1 mM IPTG in a 400 ml culture for 3 h at 37°C, 250 rpm. The bacterial suspension was pelleted by centrifugation and supernatant removed. The Rosetta 2(DE3) pLysS cells were re-suspended in lysis buffer with protease inhibitors before the cells were lysed open via incubation with lysozyme followed by sonication.

Cells were pelleted by centrifugation and the supernatant filtered through syringe filters. Filtered supernatant was applied to a pre-equilibrated 1 ml His-trap affinity chromatography column. Proteins were eluted via a gradient of 5 mM to 500 mM imidazole. The chromatography trace is provided, with the UV260nm represented by the blue line, conductivity represented by the brown line and the chromatography fractions are shown in red (**A**). The contents of select chromatography fractions were analysed via SDS-PAGE (**B**) and Western blotting with NTH1 specific antibodies (**C**). Molecular weight markers (kDa) are indicated as well as fraction numbers and the presence of the NTH1 mutation.

5.4.2.8 Activity of TRIM26 on site specific mutants of NTH1

Purified wild-type full-length NTH1 and site-specific mutants of NTH1 (K42R, K48R, K52R and K67R containing single mutations; K48,52R, K245,246R containing double mutations) were subsequently subject to the *in vitro* ubiquitylation assay, with increasing concentrations of recombinant TRIM26. Completed reactions were separated by SDS-PAGE and analysed by Western blotting using NTH1 specific antibodies (**Figures 55, 56 and 57**). It was expected that replacement of the lysine residues of NTH1 that are subject to TRIM26 dependent ubiquitylation, would significantly impede the upward shift in molecular weight of NTH1 observed via Western blotting analysis, thus representing reduced ubiquitylation capacity.

It was apparent that TRIM26 dependent ubiquitylation was impeded when lysine residues located within the N-terminal region were substituted for arginine residues (**Figure 45**). Mutation of single lysine residues at positions 42 or 52 caused the most obvious reduction in the levels of ubiquitylated NTH1 (**Figure 55, A**). When quantified, the K42R and K52R mutations induced nearly a 50 % decrease in $NTH1_{Ub}$ ratio when normalised to WT NTH1 (**Figure 55, B**). This is in contrast to mutation of two lysine residues, 245 and 246 located at the C-terminal end of NTH1. Substitution of these two lysine residues induced only an approximate 30 % reduction in the level of $NTH1_{ub}$ compared to WT NTH1. (**Figure 55**).

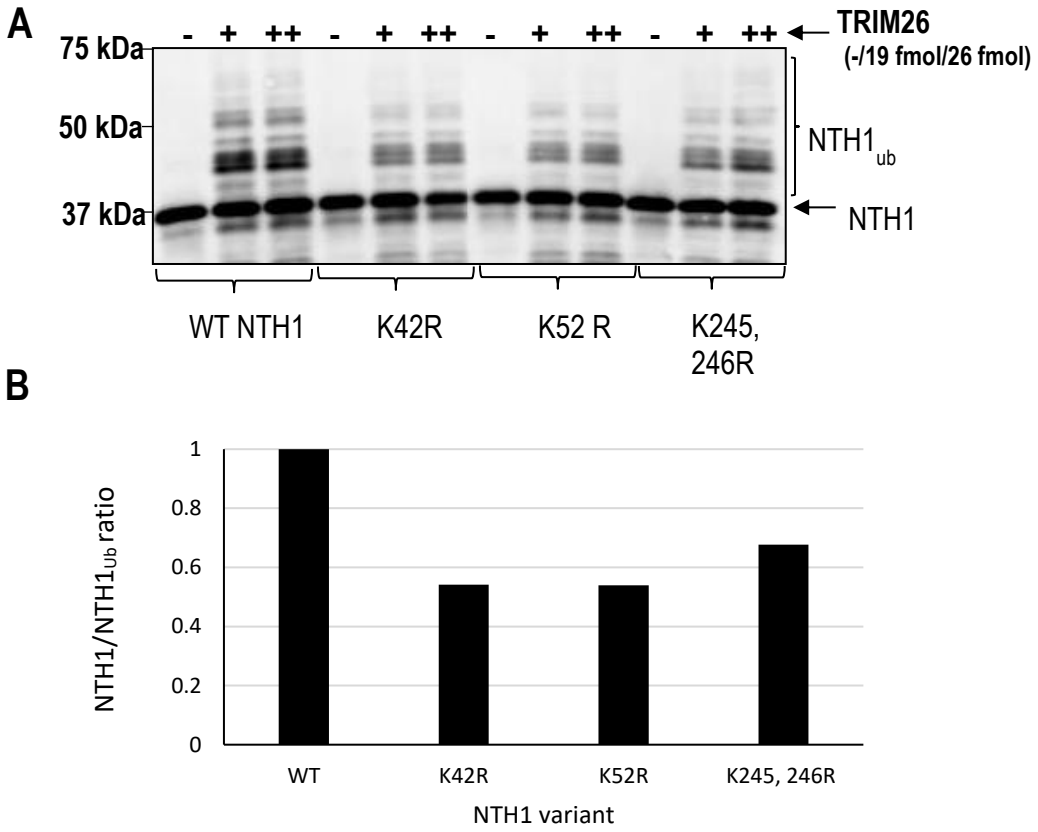

Figure 55. Western blotting analysis of *in vitro* ubiquitylation assays using recombinant TRIM26 with a range of NTH1 lysine mutants. Ubiquitylation assays were performed by combining 0.7 pmol GST-E1 activating enzyme, 5 pmol of UbcH5a conjugating enzymes, 0.6 nmol ubiquitin and 5.8 pmol of histidine-tagged, recombinant NTH1 lysine mutants; K42R, K52R, or K245 246R. To this, a titration of recombinant TRIM26; 0 fmol (-), 19 fmol (+) and 26 fmol (++) was added separately to each ubiquitylation assay. The assay reactions were carried out at 30 °C for 1 h in a shaking incubator at 800 rpm, before completed reactions were separated by 10 % SDS-PAGE and analysed via Western blotting using NTH1 specific antibodies. Molecular weight markers (kDa), unmodified histidine-tagged NTH1 (NTH1) and ubiquitylated histidine-tagged NTH1 ($NTH1_{ub}$) are indicated. Bands representing an upward shift in molecular weight of NTH1, with the addition of 26 fmol of TRIM26, were quantified using the Image Studio Lite Licor software. The ratio of NTH1 and $NTH1_{ub}$ was calculated and normalised against WT NTH1/$NTH1_{ub}$ ratio, which was set to 1 (**B**).

Following this observation, I continued to generate and analyse the effects alternative N-terminal lysine mutants had on the ubiquitylation on NTH1. Interestingly, substitution of two lysine residues at positions 48 and 52 resulted in very little difference in NTH1 ubiquitylation compared to the wild type protein (**Figure 56, A**), causing an approximate 10 % reduction in $NTH1_{ub}$ in the presence of 26 fmol of TRIM26 when compared to WT NTH1 (**Figure 56, B**). The K48R substitution alone

resulted in a slightly more substantial reduction in $NTH1_{ub}$ (**Figure 56, A**) of approximately 30 % in the presence of 26 fmol of TRIM26 (**Figure 56, B**).

However, the most obvious reduction of $NTH1_{ub}$ was observed when the lysine residue at position 67 was mutated (**Figure 56, A**). Substitution of this residue caused over a 70 % reduction in ubiquitylation bands in the presence of 26 fmol TRIM26 (**Figure 56, B**). Although, it is worth noting that the efficiency of the quantified reaction (**Figure 56, A**, lane 12) may not be completely effective as the level of ubiquitylation in the presence of the lower quantity of TRIM26 seems slightly increased, whereas it would be expected that the higher amount of the E3 ligase would induce the higher level of ubiquitylation of NTH1 even when impeded by a specific lysine substitution. Despite this, it is still apparent that across both reactions containing TRIM26, the K67R substitution causes the most substantial reduction in $NTH1_{ub}$ (**Figure 56, A**). Cumulatively these data suggest that the lysine residues within the N-terminus of NTH1 are critical for ubiquitylation, although specifically that K67 may be the major residue which is ubiquitylated by TRIM26. To explore this concept further, it was decided that a quadruple mutant with multiple N-terminal lysine residues replaced with arginine residues; K42,48,52,67R, would be created (**Figure 54**). This was then subject to an *in vitro* ubiquitylation assay alongside the wild type and the K67R NTH1 single lysine mutant with recombinant TRIM26 (**Figure 57, A**).

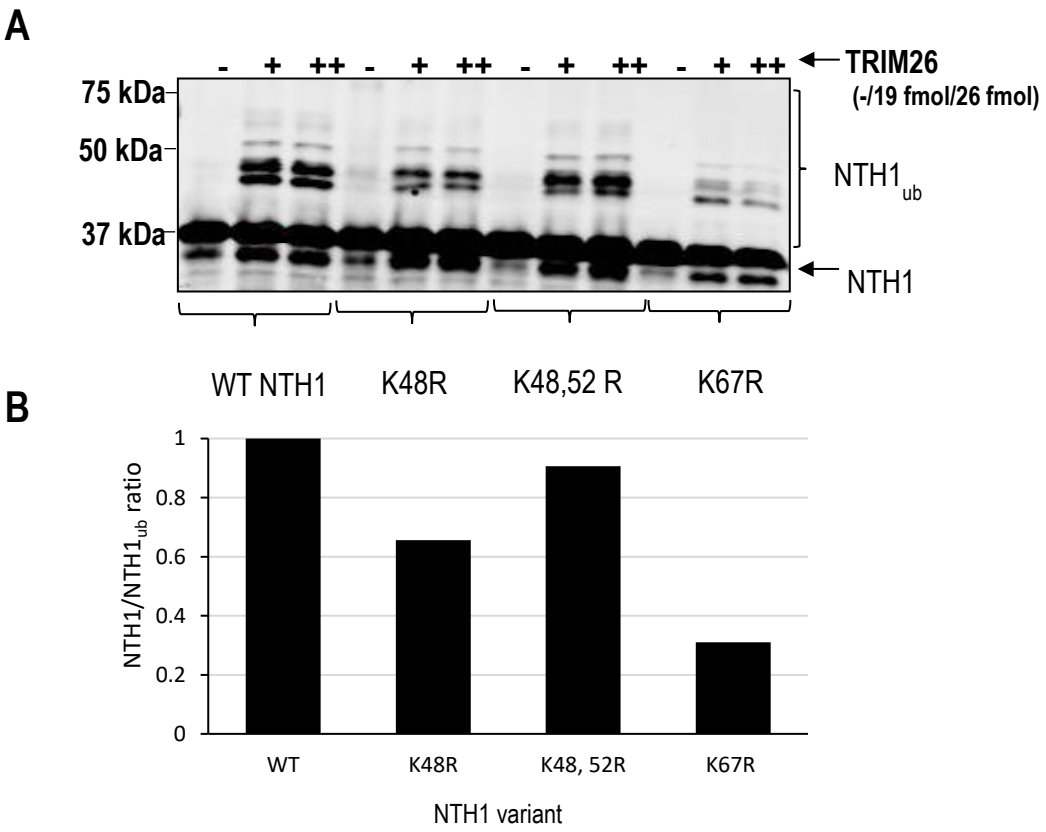

Figure 56. Western blotting analysis of *in vitro* ubiquitylation assays using recombinant TRIM26 with a range of NTH1 lysine mutants. Ubiquitylation assays were performed by combining 0.7 pmol GST-E1 activating enzyme, 5 pmol of UbcH5a conjugating enzymes, 0.6 nmol ubiquitin and 5.8 pmol of histidine-tagged, recombinant NTH1 lysine mutants; K48R, K67R or K48 52R. To this, a titration of recombinant TRIM26; 0 fmol (-), 19 fmol (+) and 26 fmol (++) was added separately to each ubiquitylation assay. The assay reactions were carried out at 30 °C for 1 h in a shaking incubator at 800 rpm, before completed reactions were separated by 10 % SDS-PAGE and analysed via Western blotting using NTH1 specific antibodies (**A**). Molecular weight markers (kDa), unmodified histidine-tagged NTH1 (NTH1) and ubiquitylated histidine-tagged NTH1 ($NTH1_{ub}$) are indicated. Bands representing an upward shift in molecular weight of NTH1, with the addition of 26 fmol of TRIM26, were quantified using the Image Studio Lite Licor software. The ratio of NTH1 and $NTH1_{ub}$ was calculated and normalised against WT NTH1/$NTH1_{ub}$ ratio, which was set to 1 (**B**).

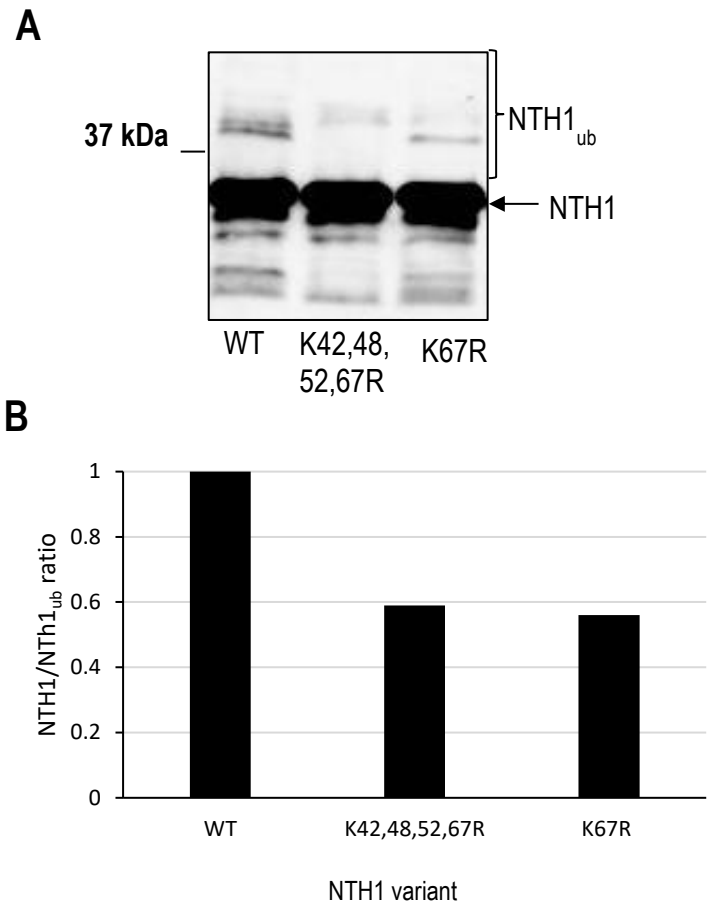

Figure 57. Western blotting analysis of *in vitro* ubiquitylation assays using recombinant TRIM26 with a range of NTH1 lysine mutants. Ubiquitylation assays were performed by combining 0.7 pmol GST-E1 activating enzyme, 5 pmol of UbcH5a conjugating enzymes, 0.6 nmol ubiquitin and 5.8 pmol of histidine-tagged, recombinant NTH1 lysine mutants; K67R and a quadruple mutant consisting of K42,48,52,67R. To this, 19 fmol of recombinant TRIM26 was added separately to each ubiquitylation assay. The assay reactions were carried out at 30 °C for 1 h in a shaking incubator at 800 rpm, before completed reactions were separated by 10 % SDS-PAGE and analysed via Western blotting using NTH1 specific antibodies (**A**). Molecular weight markers (kDa), unmodified histidine-tagged NTH1 (NTH1) and ubiquitylated histidine-tagged NTH1 ($NTH1_{ub}$) are indicated. Bands representing an upward shift in molecular weight of NTH1, with the addition of 26 fmol of TRIM26, were quantified using the Image Studio Lite Licor software. The ratio of NTH1 and $NTH1_{ub}$ was calculated and normalised against WT NTH1/$NTH1_{ub}$ ratio, which was set to 1 (**B**).

Following further investigation regarding the site of NTH1 ubiquitylation, it is apparent that both the K67R NTH1 and quadruple mutant (K42,48,52,67R) also containing this particularly lysine substitution have significantly reduced levels of TRIM26 dependent ubiquitylation (**Figure 57, A**) of around 50 %. However, it is worth noting that the efficiency of the *in vitro* ubiquitylation assays for this particular set of reactions was not completely efficient, as even with the addition of WT NTH1 and TRIM26 the level of $NTH1_{ub}$ bands was not as intense as previously observed throughout the project. Reasons for this could be due to a loss of activity of the E3 ligase enzyme, following multiple freeze-thaw cycles during each use. This theory is likely since these ubiquitylation reactions were completed near to the final stages of the project. Despite the inefficient ubiquitylation reactions, a reduction in NTH1 ubiquitylation was consistently observed with the mutation of just K67R alone; which is consistent with the previous result and further advocates that this residue is the major site specifically ubiquitylated by TRIM26. This suggests that ubiquitylation of NTH1 has been significantly hindered by the loss of this specific lysine residue present within the N-terminus of the protein. Cumulatively this provides evidence that lysine 67 is the major ubiquitylation site by TRIM26, with lysines 42, 48 and 52 acting as more minor sites that are modified by TRIM26.

5.4.2.9 Activity of TRIM26 versus D239Y NTH1

In addition to investigating the impact of disrupting the major site of NTH1 ubiquitylation in cells, I also employed a site-directed mutagenesis approach to examine the D239Y variant of NTH1 described in the literature (55). This variant is reportedly present in 6.2 % of the global population and is associated with increased genome instability. Using custom primers in a PCR reaction with high fidelity Phusion DNA polymerase, the expression vector for the D239Y variant was generated from a pET28NTH1 plasmid and subsequently transformed into DH5α cells (**Figure 58**).

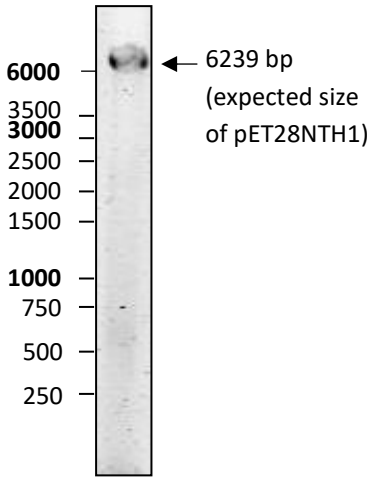

Figure 58. PCR product following site directed mutagenesis of the pET28NTH1 bacterial expression plasmid to generate the D239Y variant. Per PCR reaction 250 pg/µl of pET28NTH1 bacterial expression plasmid was incubated with 0.02 U/µl high fidelity Phusion polymerase, 200 µM dNTPs, 0.3 µM custom forward primer, 0.3 µM custom reverse primer and 1 x Phusion GC buffer (g) with/without DMSO ($^{+}$) to generate pET28NTH1D239Y. The size of the PCR product was analysed using a 1 % agarose gel in 1x TAE. The expected size of the PCR product in base pairs is featured.

Overnight bacterial cultures were grown and plasmid DNA was extracted and sequenced using the Sanger Sequencing Service (Source Bioscience Sequencing, Nottingham, UK) (see Appendix). Confirmed plasmids encoding the D239Y point mutation were transformed into Rosetta 2(DE3) pLysS cells, a 400 ml culture was grown and protein expression induced using IPTG. Following preparation of a lysate from the bacterial cell pellet generated by centrifugation, the NTH1 D239Y protein was purified by His-trap affinity chromatography using a 20 ml gradient elution of imidazole from 5 to 500 mM (**Figure 58, A**). Chromatography fractions were analysed via 10 % SDS-PAGE and Instant Blue staining (**Figure 58, B**) and also by Western blotting (**Figure 58, C**). From this, it was apparent that a protein band of the expected 34.4 kDa molecular weight which also cross-reacted with NTH1-specific antibodies was located in fractions 16-26 (**Figure 58, B and C**). For the purposes of reducing the presence of other protein contaminants, fractions 18-26 were selected, pooled and concentrated using Amicon Ultra 15 ml centrifugal concentrators (10 kDa MWCO) until 500 µl in volume. This volume was then made up to 1 mL in JPDB buffer (50 mM Tris HCl pH 8, 50 mM KCl, 1 mM EDTA, 10 % glycerol) and concentrated once more at 4000 x g. This process was repeated twice more to buffer exchange the fractions.

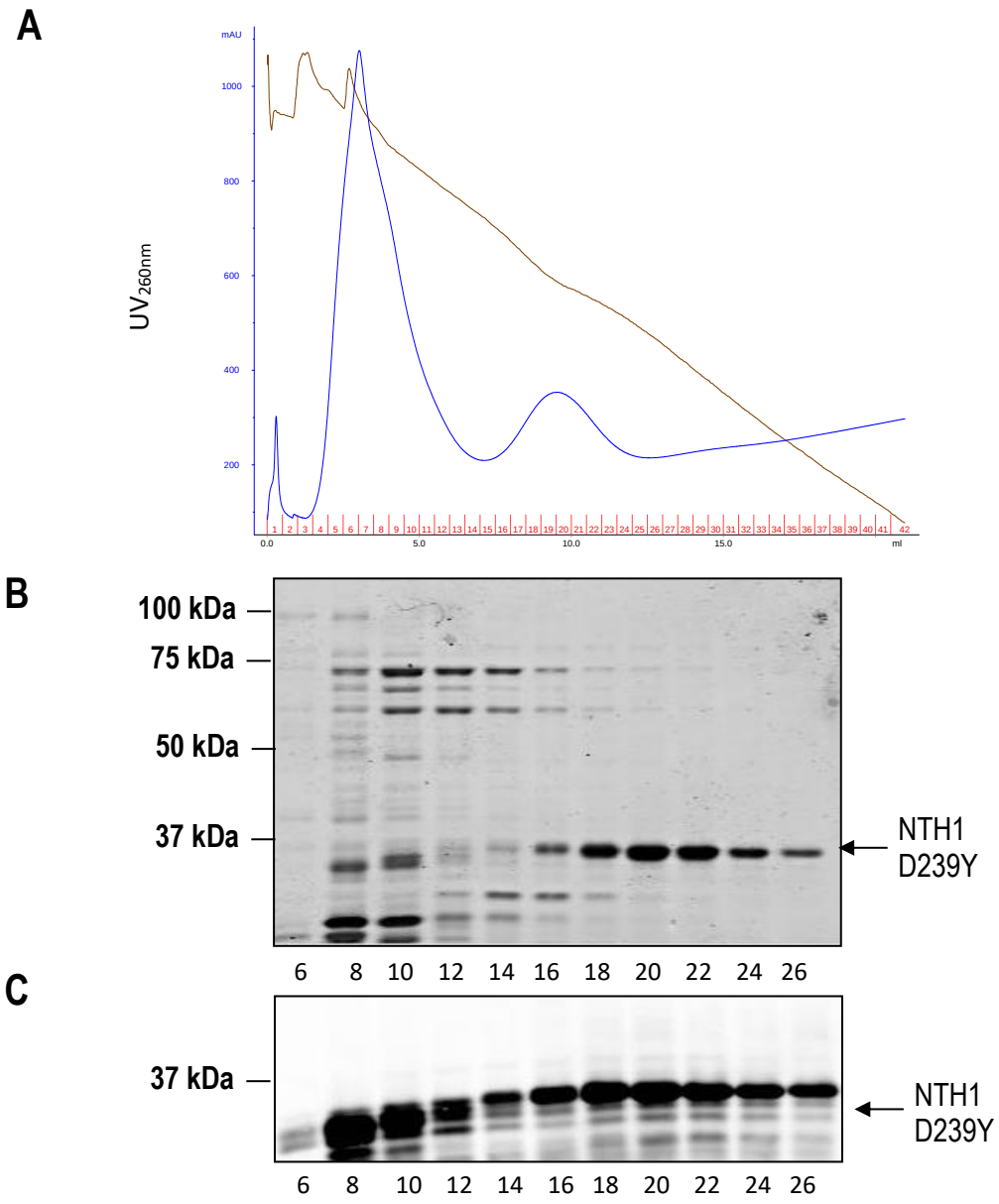

Figure 59. Analysis of HisTrap chromatography of the NTH1 point mutation, D239Y. The mutant version of NTH1 D239Y was created via site-directed mutagenesis of a pET28NTH1 plasmid using custom oligonucleotides with Phusion High-fidelity DNA polymerase. Plasmid constructs were transformed into Rosetta 2(DE3) pLysS cells and protein expression induced via 1 mM IPTG in a 400 ml culture for 3 h at 37°C, 250 rpm. The bacterial suspension was pelleted by centrifugation and supernatant removed. The Rosetta 2(DE3) pLysS cells were resuspended in lysis buffer with protease inhibitors before the cells were lysed open via incubation with lysozyme followed by sonication. Cells were pelleted by centrifugation and the supernatant filtered through syringe filters. Filtered supernatant was applied to a pre-equilibrated 1 ml His-trap affinity chromatography column. Proteins were eluted via a gradient of 5 mM to 500 mM imidazole. The contents of each fraction were analysed via 10 % SDS-PAGE (B) and Western blotting with NTH1 specific antibodies (C). Protein bands corresponding to D239Y NTH1 protein expression were most apparent in fractions 18-26. These fractions were pooled and concentrated.

The concentrated stock of NTH1 D239Y was then subject to an *in vitro* ubiquitylation assay, alongside wild-type NTH1, in the presence of titrated amounts of TRIM26. Completed reactions were analysed by 10 % SDS-PAGE and Western blotting with NTH1 specific antibodies (**Figure 60**).

Interestingly, it was discovered that ubiquitylation of NTH1 by TRIM26 appeared significantly impeded by the D239Y substitution (**Figure 60, A;** lanes 5 and 6). The upward shift in molecular weight of NTH1, associated with the addition of ubiquitin moieties, is almost completely supressed by the presence of the D239Y substitution, since ubiquitylation is reduced by more than 80 % (**Figure 60, B**). This is especially obvious when directly comparing reactions containing wild-type NTH1 (**Figure 60, A;** lanes 2 and 3) to reactions containing the D239Y variant (**Figure 60, A;** lanes 5 and 6). This result suggests that the aspartate residue in position 239 could potentially affect the ubiquitylation dependent regulation of NTH1 via TRIM26. It is likely that substitution of the aspartic acid residue at this position impacts the tertiary structure of NTH1, thus influencing its ability to interact with TRIM26. In the wider context, the inability of NTH1 to be regulated appropriately due to a change in tertiary structure, instigated by the D239Y substitution, could potentially contribute to the genomic instability and cellular transformation exhibited by cells expressing the D239Y variant (55).

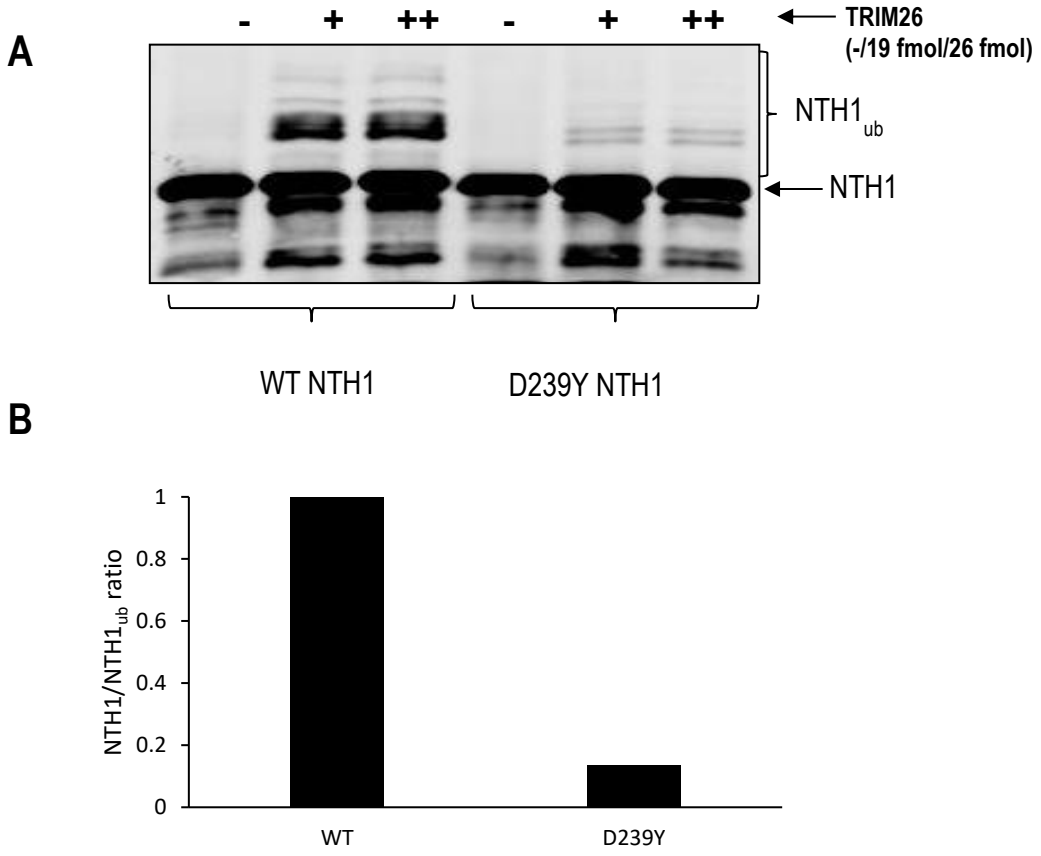

Figure 60. Western blotting analysis of *in vitro* ubiquitylation assays using recombinant TRIM26 with a NTH1 D239Y mutant. Ubiquitylation assays were performed by combining 0.7 pmol GST-E1 activating enzyme, 5 pmol of UbcH5a conjugating enzymes, 0.6 nmol ubiquitin and 5.8 pmol of histidine-tagged, recombinant NTH1 (WT) or a mutant version of NTH1 (D239Y NTH1). To this, 0 fmol (-), 19 fmol (+), or 26 fmol (++) of recombinant TRIM26 was added separately to each ubiquitylation assay. The assay reactions were carried out at 30 °C for 1 h in a shaking incubator at 800 rpm, before completed reactions were separated by 10 % SDS-PAGE and analysed via Western blotting using NTH1 specific antibodies (**A**). Molecular weight markers (kDa), unmodified histidine-tagged NTH1 (NTH1) and ubiquitylated histidine-tagged NTH1 ($NTH1_{ub}$) are indicated. Bands representing an upward shift in molecular weight of NTH1, with the addition of 26 fmol of TRIM26, were quantified using the Image Studio Lite Licor software. The ratio of NTH1 and NTH1ub was calculated and normalised against WT NTH1/NTH1ub ratio, which was set to 1 (**B**).

5.5. Results Summary

NTH1 contains a total of 17 lysine residues, which are potential targets for TRIM26 dependent ubiquitylation (**Figure 33**). To elucidate which sites within NTH1 are subject to ubiquitylation, I first adopted a mass spectrometry approach to analyse the products of *in vitro* ubiquitylation reactions. However, despite digestions with either trypsin or ArgC, full coverage of the peptides within NTH1 was not obtained and so could not fully determine any specific lysine residues as sites of ubiquitylation. Therefore, I created truncation mutants of NTH1 and assessed which section of the protein was subject to TRIM26 dependent ubiquitylation. Results from this appeared somewhat inconclusive, although it was observed that deletion of the first 98 amino acids of NTH1 caused a suppression of ubiquitylation by TRIM26, suggesting that this region contains the major sites of ubiquitylation (**Figure 45**). However, I was unable to show that a truncation containing the immediate N-terminus (9-99) of NTH1 was a substrate for ubiquitylation by TRIM26. Arguably, this could be because the protein is not of sufficient size, therefore, does not structurally resemble the full-length protein which may prevent TRIM26 protein binding.

Following this, it was decided that a site directed mutagenesis approach of each separate lysine residue would be more informative. Reports in the literature suggest that the extended N-terminal region of human NTH1 could be subject to post-translational modifications, including ubiquitylation (68, 90). Furthermore, and as mentioned above, deletion of the first 98 amino acids of NTH1 inhibited the ubiquitylation of the truncated NTH1 99-305 protein (**Figure 45**). Therefore, my primary focus regarding site-directed mutagenesis was mainly targeted towards the N-terminal lysine residues within this region (positions 42, 48, 52 and 67). I also generated a C-terminal point mutation (positions 245 and 246) for comparison. It was anticipated that if disruption of ubiquitylation was not observed following mutation of these individual specific lysine residues, then I would continue to mutate each lysine residue sequentially from each terminal end of the glycosylase; with a specific focus on the N-terminus. Overall, I discovered that conservative subsitution of lysine 42, 48 or 52 to arginine, or a double mutant at lysines 48 and 52, had a minor impact on the degree of ubiquitylation of NTH1 via TRIM26 (**Figure 55**). However, mutation of lysine 67 to arginine caused a noteable reduction in NTH1 ubiquitylation, suggesting that this is the main target for TRIM26 dependent regulation *in vitro* (**Figure 56**). Deletion of all four lysine residues (42, 48, 52 and 67) on the N-terminus of NTH1 appeared to completely supress ubiquitylation of the protein by TRIM26 *in vitro* (**Figure 57**), reinforcing the truncation analysis data that the lysine residues present in this region

are the major targets for TRIM26-dependent ubiquitylation. However, I conclude that lysine 67 in NTH1 is the major critical target for TRIM26, with lysines 42, 48 and 52 acting as minor ubiquitylation sites.

In addtion to this, I also investigated the ubiquitylation dependent regulation of the D239Y NTH1 variant which has been shown to be present in 6.2 % of the global population and to be inactive as a DNA glycosylase (55). This protein has also been suggested to cause genomic instability and be associated with cancer development. I demonstrated that the D239Y variant is not an efficient target for ubiquitylation by TRIM26 *in vitro* (**Figure 58**), suggesting that this mutant may not be sufficiently regulated by the UPP in cells. Therefore as well as the D239Y variant being inactive as a DNA glycosylase, I also predict that this protein may accumuate in cells as a result of the lack of recognition of the protein by TRIM26-dependent ubiquitylation and subsequent proteasomal degradation.

CHAPTER 6 - RESULTS III

The cellular regulation of NTH1 by ubiquitylation

6.1 Introduction

The BER pathway is one of the major DNA repair pathways employed by cells to manage minor DNA insults, including individual base lesions. NTH1 is one of the major DNA glycosylases which excises oxidised pyrimidines (including 5-hydroxycytosine, 5-hydroxyuracil and Tg), during the initial stages of BER. Attributable to this critical cellular role, reduced expression of NTH1 protein has been observed in gastric, liver and prostate cancer, suggesting that accumulation of DNA damage, repaired by NTH1 could be a contributor to the promotion of these cancers. Together, this highlights the importance of preserving cellular NTH1 protein levels in maintaining genome stability and preventing the development of cancer.

A number of BER proteins have already been shown to be regulated by the PTM, ubiquitylation. The specific enzymes involved in the enzymatic cascade, facilitating ubiquitin attachment to each BER enzyme, particularly the E3 ubiquitin ligases, have started to be elucidated (25, 48). From this, it is apparent that the effects of ubiquitylation vary considerable depending on the substrate protein. For instance, polyubiquitylation of APE1 has been shown to be regulated via the E3 ligase, UBR3 that controls the steady state levels of the protein (102). This is also apparent for PNKP; a Cul4A-DDB1-Roc1 complex is the major E3 ligase shown to ubiquitylate and regulate PNKP (124). This process was demonstrated to be dependent on the adaptor protein, STRAP (124). Furthermore, CHIP was identified as the major E3 ligase which polyubiquitylates Pol β for proteasomal degradation (125). Another E3 ligase, Mule monoubiquitylates Pol β at multiple sites, causing its retention in the cytoplasm (126). It is important to consider the dynamic ways in which multiple E3 ligase enzymes may inflict different biological effects on substrate BER proteins, via manipulation of the diverse UPP code.

Gathering detailed knowledge regarding the regulation of BER proteins may improve our understanding of the cellular response to DNA damage, which could ultimately aid the development of novel drug targets for the prevention or treatment of human diseases. In the treatment of cancer, particularly those associated with elevated NTH1 levels, therapeutic strategies could be developed to specifically reduce the levels of the glycosylase. This approach could be combined with current strategies (such as

radiotherapy and chemotherapy) to improve patient sensitivity to treatment options, which target the cancer by influencing DNA damage. Consequently, these options could improve patient response rates and decrease mortality.

For this reason, it is important to explore the effects of ubiquitylation dependent regulation of NTH1 in the cellular context. In previous chapters, I have identified TRIM26, as the major E3 ligase involved in the enzymatic cascade facilitating ubiquitin attachment to NTH1 *in vitro*. I have also identified that the N-terminal region of NTH1 (particularly lysine 67) is subject to regulation via polyubiquitylation by TRIM26, suggesting that the protein may be targeted for proteasomal degradation. The following chapter aims to explore the mechanisms of TRIM26 dependent regulation of NTH1 in cells, with a specific focus on examining the role of TRIM26 in regulating NTH1 protein stability. Furthermore, the importance of this mechanism in the cellular response to DNA damage will be examined.

6.2 NTH1 is regulated by the UPP in cells

Initially, to assess if NTH1 is a target for ubiquitylation-dependent proteasomal degradation in cells, levels of NTH1 in whole cell extract were assessed before and after exposure to MG-132. MG-132 is a potent inhibitor of the cellular proteasome that acts as a peptide aldehyde which blocks the proteolytic capacity of the β subunit in the 26S proteasome complex. It is anticipated that levels of proteins regulated by ubiquitylation-dependent degradation through the UPP will accumulate following MG-132 exposure.

For the purpose of this study (and subsequent cellular studies), HCT116$^{p53+/+}$ were used. Not only are these cells well characterised in culture, but it was also hoped that since a homozygous loss-of-function germline mutation in the NTH1 gene predisposes to a new subtype of BER-associated adenomatous polyposis and colorectal cancer (175), understanding the mechanism of regulation of NTH1 in HCT116$^{p53+/+}$ cells could be clinically relevant in the eventual treatment of this disease.

HCT116$^{p53+/+}$ cells were cultured in 10 cm dishes until approximately 80 % confluency was achieved. Cells were then treated with 10 μM of MG-132 (or DMSO only as a control), in serum-containing media and incubated at 37°C for 8 h, to allow protein levels to accumulate as a consequence of proteasomal inhibition. Following this, the media was removed and cells harvested in cold PBS. Whole cell extract was then prepared and NTH1 levels assessed by separation of proteins by 10 % SDS-PAGE followed by Western blotting using NTH1 specific antibodies (**Figure 61, A**). Western

blots were further probed with tubulin specific antibodies to act as a loading control to enable quantification of changes of NTH1 irrespective of loading discrepancies. Three biological replicates of the experiment were performed and the average values compared (**Figure 61, B**).

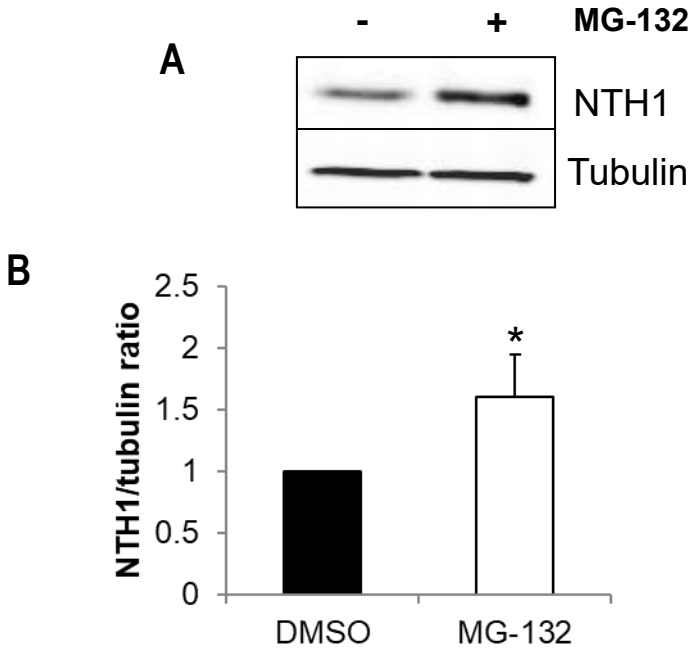

Figure 61. Accumulation of NTH1 levels normalised to tubulin in human colon carcinoma (HCT116$^{p53+/+}$) cells following treatment with the proteasomal inhibitor MG-132 for 8 h. HCT116$^{p53+/+}$ cells were cultured in serum-containing medium until approximately 80 % confluent. Cells were then treated with either 10 µM DMSO control (-) or 10 µM MG-132 proteasomal inhibitor (+) for 8 h in serum-containing media. Cells were harvested and extracts prepared using the Tanaka method. Cell extract proteins were separated by 10 % SDS-PAGE and NTH1 levels analysed by Western blotting using NTH1 specific antibodies. Tubulin specific antibodies were also used to probe the same Western blot analysis to act as a loading control (A). Levels of NTH1 expression were quantified relative to tubulin expression using an Odyssey imaging system. Three biological replicates were completed (B). *p<0.05 as analysed by a two-sample t-test.

Treatment of cells with the potent proteasome inhibitor MG-132, resulted in the accumulation of the protein levels of NTH1 (**Figure 61, B**). In the presence of MG-132, average NTH1 protein levels increased by approximately 1.6-fold. This difference was statistically significant using a two-sample *t*-test ($p<0.05$), suggesting that NTH1 levels are regulated by ubiquitylation dependent degradation in cells. This finding correlates with proteomic screens which have identified that NTH1 is subject to ubiquitylation, but the enzymes involved have yet to be elucidated (34). This finding therefore further suggests that the stability of NTH1 is ubiquitylation dependent, so

the next logical stage was to confirm the role of TRIM26 in this process and establish if ubiquitylation dependent regulation of NTH1 is TRIM26 dependent in cells.

6.3 TRIM26 regulates NTH1 dependent ubiquitylation in cells

After discovering that NTH1 is ubiquitylated and degraded by the proteasome, the next obvious experimental step was to assess if NTH1 is ubiquitylated in cells, specifically by TRIM26. To achieve this, I analysed the effect of combined overexpression of HA-tagged TRIM26 (kindly provided by Prof A. Garcia-Sastre, The Icahn School of Medicine at Mount Sinai, USA) and Flag-tagged NTH1 in the presence of HA-tagged ubiquitin (HA-Ub) in HCT116$^{p53+/+}$ cells. In order to complete this experimentation, the flag-tagged mammalian expression plasmid encoding the *nth1* gene was cloned from the pET28aNTH1 plasmid. The mammalian expression plasmid for NTH1, pCMV-3Tag-NTH1 was generated using a LIC cloning strategy (**Section 5.4.2.9, Figure 58**).

Initially, a test expression of both of these plasmids was conducted in HCT116$^{p53+/+}$ cells to assess the optimal concentration of plasmid needed to attain suitable overexpression of both proteins of interest (**Figure 62**). Expression of either protein of interest was confirmed via comparison to a Lipofectamine 2000 control, containing transfection reagent alone. Following transfection, cells were incubated at 37°C in a humidified cell culture incubator for 24 h. Cells were then harvested in cold PBS, pelleted by centrifugation and proteins extracted. Cell extracts were analysed by 10 % SDS-PAGE and Western blotting. From this preliminary test, it was understood that transfection of 110 fmol of pCMV-3Tag3a-HA-tagged-TRIM26 yielded sufficient overexpression of the E3 ligase (**Figure 62**, **A**). Furthermore, transfection of 150 fmol of pCMV-3Tag-FLAG-tagged-NTH1 induced good expression of NTH1 (**Figure 62**, **B**).

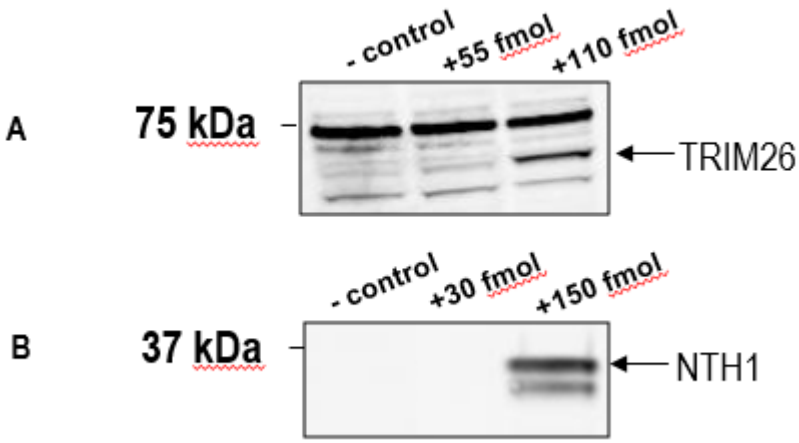

Figure 62. Protein expression levels of TRIM26 (A) and NTH1 (B) following the transfection of titrated amounts of corresponding mammalian expression plasmids. HCT116$^{p53+/+}$ cells were cultured in 10 cm dishes in serum-containing media until 80% confluent. For test expression of the of pCMV-3Tag3a-TRIM26 mammalian expression vector (**A**) cells were transfected with 10 µl Lipofectamine 2000 (- control), or either 55 fmol or 110 fmol of pCMV-3Tag3a-TRIM26 mammalian expression vector. For test expression of the pCMV-3Tag3a-NTH1 mammalian expression plasmid (**B**) cells were transfected with 10 µl Lipofectamine 2000 (- control), or either 30 fmol or 150 fmol of pCMV-3Tag3a-TRIM26 mammalian expression vector. Transfected cellular cultures were incubated for 24 h at 37°C in a humidified cell incubator. Cells were then harvested in cold PBS, pelleted and cellular protein extracted via the Tanaka method. Protein expression was analysed by 10 % SDS-PAGE and Western blotting using antibodies specific to TRIM26 (**A**) or FLAG-TAG (**B**). From this, it was evident that 110 fmol of pCMV-3Tag3a-TRIM26 and 150 fmol of pCMV-3Tag3a-NTH1 are required for overexpression of each protein.

Previous studies within the laboratory dictated an appropriate concentration of mammalian vector PMT123 HA-Ub (270 fmol) to use in HCT116$^{p53+/+}$ cells (46). These concentrations of plasmids were then utilised to examine levels of ubiquitylated NTH1 in cells using immunoprecipitation.

A plasmid expressing HA-tagged ubiquitin alone, or in combination with Flag-tagged NTH1 and HA-tagged TRIM26, was transfected into HCT116$^{p53+/+}$ cells, and after 24 h, cells were treated with MG-132 to allow accumulation of ubiquitylated proteins. Cells were then harvested in cold PBS, pelleted by centrifugation and proteins extracted and used for immunoprecipitation of NTH1. Using a Flag pulldown of NTH1 in the absence of TRIM26, I show evidence of moderate levels of NTH1 polyubiquitylation as indicated by a smear of protein cross-reacting with the HA antibodies above 50 kDa (Flag-NTH1$_{ub}$), which is absent in cells expressing HA-

tagged ubiquitin only as a control (**Figure 63, A**, compare lanes 1 and 2). This demonstrates specific ubiquitylation of NTH1 by an E3 ligase present within the HCT116$^{p53+/+}$ cells. Cellular ubiquitylation of Flag-tagged NTH1 was further enhanced by co-expression with HA-tagged TRIM26 (**Figure 63, A,** compare lanes 2 and 3), demonstrating clear evidence that NTH1 is a target for ubiquitylation specifically by TRIM26 in cultured cells.

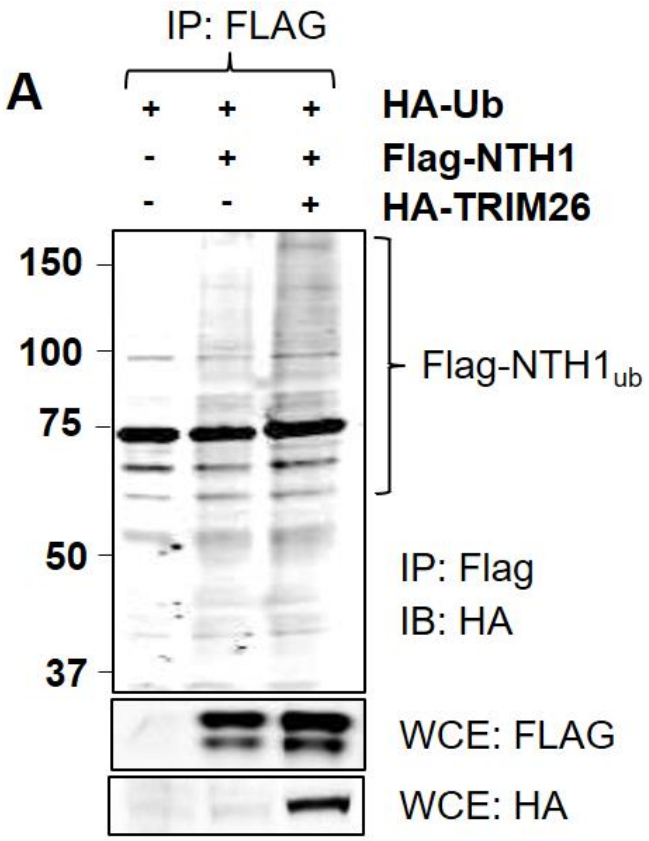

Figure 63. Examination of the ubiquitylation of NTH1 in cells by TRIM26. HCT116$^{+/+}$ cells were cultured in serum-containing media until approximately 80 % confluent. Cells were then treated with 270 fmol of PMT-HA-Ub only, or 270 fmol of PMT-HA-Ub plus 150 fmol pCMV-3Tag3a-NTH1 and 110 fmol of pCMV-3Tag3a-TRIM26 or 270 fmol of PMT-HA-Ub with 110 fmol of pCMV-3Tag3a-TRIM26. Cells were cultured 24 h in serum-containing media at 37°C in a humidified cell incubator then treated with 10 µM of MG-132 for 6 h. Cell extracts were prepared using the Tanaka method. For immunoprecipitation 10 µl of Anti-FLAG M2 magnetic beads with equal concentrations of cellular protein extract from each treatment were mixed for 2 h on a rotor at 4°C. Magnetic beads were washed in buffer containing 150 mM KCl to eliminate unbound proteins before levels of ubiquitylated NTH1 bound to the Anti-FLAG M2 magnetic beads were analysed by Western blotting.

6.4 Effect of lysine 67 on the stability of NTH1

Since discovering that NTH1 is a target for TRIM26 ubiquitylation in cultured cells, it was considered interesting to establish if disruption of the major site of TRIM26 dependent ubiquitylation of NTH1, lysine 67 (previously identified by *in vitro* studies), affected NTH1 stability in cells. This would be achieved by overexpressing wild type NTH1 and the K67R NTH1 variant in cells and examining their stability. To investigate this, mammalian expression plasmids for both proteins were generated. The mammalian expression plasmid for NTH1, pCMV-3Tag-NTH1, was generated using a LIC cloning strategy whereby the *nth1* gene was cloned from the pET28aNTH1 bacterial expression plasmid. Once generated, this was then subject to site directed mutagenesis using the appropriate primers to yield the pCMV-3Tag-NTH1-K67R expression plasmid.

The empty pCMV-3Tag vector and the insert for wild type NTH1 variant were amplified separately (**Figure 64**). The size of the PCR products obtained were analysed on a 1 % agarose gel; a PCR product related to the approximate size of the pCMV-3Tag vector of 4214 bp was obtained (**Figure 64, A**), plus a PCR product related to the approximate size of the NTH1 insert of 1824 bp was also obtained (**Figure 64, B**).

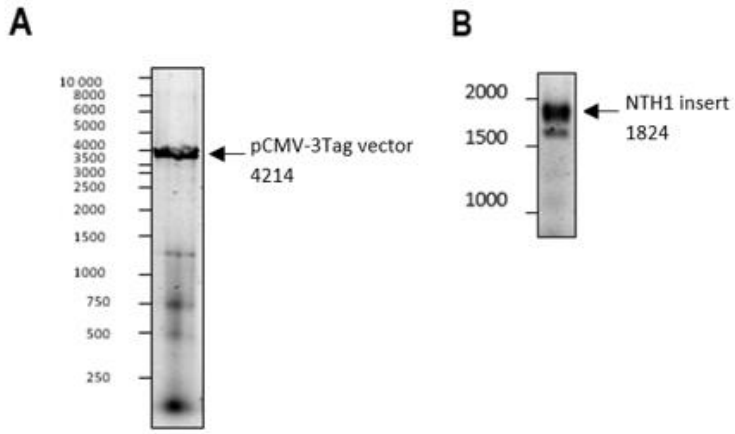

Figure 64. PCR amplification of a pCMV-3TAG vector (A) and an insert for NTH1 mammalian expression (B) for use in a ligase independent cloning (LIC) strategy. An empty pCMV-3TAG vector was PCR amplified using relevant oligonucleotides flanked by corresponding LIC sequences. The reaction was completed in the presence of GC buffer only. The size of each reaction product was confirmed using a 1 % agarose gel (**A**). As bands corresponding to the correct size (4214 bp), this was subject to DpnI treatment and pooled during PCR purification. Similarly, an insert for NTH1 expression was also PCR amplified using relevant oligonucleotides flanked by corresponding LIC sequences and the size of the reaction products analysed on a 1 % agarose gel (**B**). The NTH1 insert reaction was performed in the presence of GC buffer. From this it was apparent that the reaction yielded PCR

products displaying DNA bands corresponding to products of the expected size (1824 bp). The reaction was therefore subject to DpnI treatment before being pooled during PCR purification.

Following this, the PCR products were subject to incubation with DpnI, to remove methylated, template DNAand the plasmid DNA was purified using a PCR purification kit. Afterwards, complementary overhangs were formed using the exonuclease activity of T4 DNA polymerase with only one dNTP in each respective reaction mix. The complementary overhangs were then annealed together by incubating insert and vector at a ratio of 1:1. Constructs were amplified by transformation into library efficient DH5α bacterial cells and grown on selective media. Successful colonies were inoculated into a 5 ml culture of LB media containing selective antibiotic. Amplified plasmid DNA was then purified from bacterial contaminants using the QIAprep Spin Miniprep Kit. A diagnostic digest using an appropriate restriction enzyme, ArvII, was then performed as a preliminary method to assess the identity of each plasmid. Products of the restriction digest were analysed on a 1 % agarose gel (**Figure 65**). From this, it was apparent that the correct sized products (2654, 1487, 1015 bp) were obtained following digestion of the generated plasmid (**Figure 65**, lane 2). To confirm this, the plasmid was also sequenced using the Sanger Sequencing Service (Source Bioscience Sequencing, Nottingham, UK) which further proved that the pCMV-3Tag-NTH1 vector had been created.

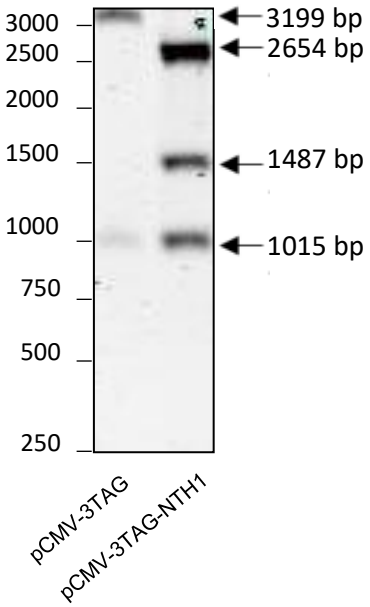

Figure 65. Restriction digest to determine the successful generation of an insert corresponding to NTH1 ligated into a pCMV-3TAG expression plasmid via a ligase independent cloning (LIC) strategy. An empty pCMV-3TAG vector was PCR

amplified using relevant oligonucleotides flanked by corresponding LIC sequences. Separately, an insert for NTH1 expression was also PCR amplified using relevant oligonucleotides flanked by corresponding LIC sequences. The size of both PCR products was confirmed on a 1% agarose gel before being subject to DpnI treatment and PCR purification. A ratio of vector and insert were then incubated (1:1) for 10 min at 22°C. Plasmid constructs were transformed into library efficient DH5α bacterial cells grown on selective agar. A 5 ml overnight culture of successful colonies was generated in the presence of selective antibiotics before plasmid DNA was purified via the QIAprep Spin Miniprep Kit (QIAGEN). A restriction digest of plasmid DNA using ArvII was then performed to preliminary assess if the correct construct has been formed. Products of the restriction digest were analysed on a 0.8 % agarose gel. The lanes (I and II) represent two different plasmids being assessed. Lane I is the control empty pCMV-3TAG vector, from this it was apparent that the correct digest sizes (3199 bp and 1015 bp) were produced via digestion of the plasmid. Lane II is pCMV-3TAG-NTH1 vector. From this it was apparent that the correct digest sizes (2654, 1487, 1015 bp) were produced via digestion of the plasmids. Note that the presence of bands above these expected sizes were believed to represent supercoiled DNA. This plasmid was then sequenced via the Sanger Sequencing Service to further confirm the correct sequence.

Following the successful generation of the pCMV-3Tag-NTH1 vector, the mammalian expression plasmid for the K67R mutant was generated from this using a site-directed mutagenesis approach (**Figure 66**). The size of the PCR product was analysed using a 1 % agarose gel, however, this could not prove that the base substitution had been incorporated. Therefore, the plasmid was subject to sequencing using the Sanger Sequencing Service (Source Bioscience Sequencing, Nottingham, UK) to confirm this (see supplementary for sequencing data).

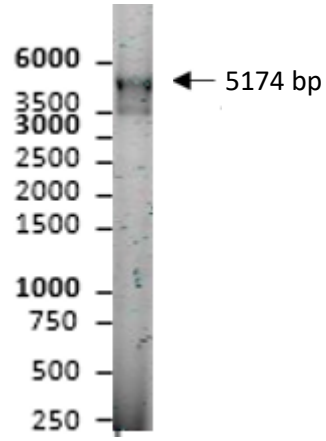

Figure 66. PCR product following site directed mutagenesis of the pCMV-3Tag-NTH1 vector bacterial expression plasmid to generate the NTH1 K67R variant. Per PCR reaction 250 pg/µl of pCMV-3Tag-NTH1 bacterial expression plasmid was incubated with 0.02 U/µl high fidelity Phusion polymerase, 200 µM dNTPs, 0.3 µM custom forward primer, 0.3 µM custom reverse primer and 1 x Phusion GC buffer with DMSO to generate pCMV-3Tag-NTH1-K67R plasmid. The size of the PCR product

was analysed using a 1 % agarose gel in 1x TAE. The expected size of the PCR product in base pairs (5174 bp) is highlighted.

Following this, equal amounts of wild type pCMV-3Tag-NTH1 and pCMV-3Tag-K67R-NTH1 mammalian expression plasmids were transfected into HCT116$^{p53+/+}$ cells with Lipofectamine 2000 transfection reagent. Following transfection, cells were incubated at 37°C in a humidified cell culture incubator for 24 h. Cells were then harvested in cold PBS, pelleted by centrifugation and proteins extracted. Cell extracts were analysed by 10 % SDS-PAGE and Western blotting using NTH1 specific antibodies. Western blots were also probed with tubulin specific antibodies, which acted as a loading control (**Figure 67, A**). Protein stability was quantified relative to the tubulin loading control following the transfection of 25 fmol of both NTH1 variants. Three biological replicates were performed to ensure reproducibility (**Figure 67, B**).

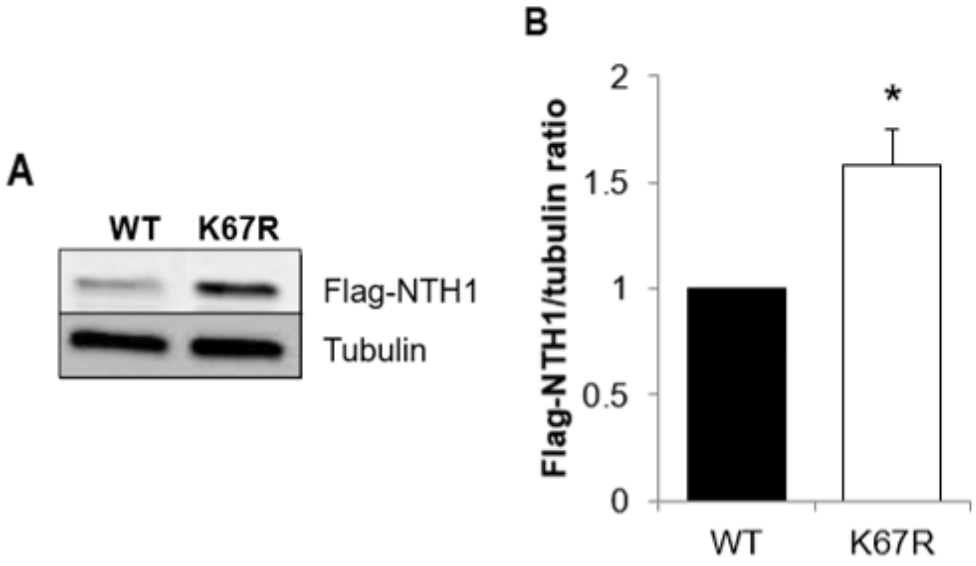

Figure 67. Protein expression levels of wild type NTH1 (WT NTH1) and lysine 67 NTH1 variant (K67R NTH1) following the transfection of titrated amounts of corresponding mammalian expression plasmids. HCT116+/+ cells were cultured in 10 cm dishes in serum-containing media until 80 % confluent. Cells were transfected with 25 fmol of pCMV-3Tag3a-NTH1 or 25 fmol of pCMV-3Tag3a-K67R-NTH1 using Lipofectamine 2000 transfection reagent. Transfected cellular cultures were incubated for 24 h at 37°C in a humidified cell incubator. Cells were then harvested in cold PBS, pelleted and cellular protein extracted via the Tanaka method. Protein expression was analysed by 10 % SDS-PAGE and Western blotting using antibodies specific to NTH1 and tubulin loading control (**A**). Included is the mean NTH1/tubulin ratio across three biological replicates, with standard errors normalised

to the untreated control which was set to 1.0. *p<0.0005 as analysed by a one sample t-test (**B**).

Remarkably, results demonstrated that the substitution of lysine 67 to arginine of NTH1 caused a statistically significant increase in the stability of the glycosylase (by approximately 1.6 fold) when compared to the wild type protein (**Figure 67, B**). Overall, this provides further evidence that lysine 67 is a major site of NTH1 ubiquitylation in the cellular context. This data suggests that the stability of newly synthesised NTH1 protein may be dependent on lysine 67, which is a target site for TRIM26 dependent ubiquitylation and is associated with regulating protein stability.

6.5 Quantification of siRNA dependent TRIM26 knockdown

To further study the cellular impact of NTH1 ubiquitylation by TRIM26, I aimed to examine the effects of siRNA-mediated depletion of TRIM26 in cultured HCT116$^{p53+/+}$ cells. Firstly, to demonstrate that siRNA sequences targeting TRIM26 are effective in reducing *trim26* gene expression, quantitative PCR (qPCR) was performed using RNA extracted from cells. HCT116$^{p53+/+}$ cells were cultured in serum-containing media in 10 cm dishes until 30-50 % confluent. Then they were transfected with Lipofectamine RNAiMAX only as a control, or 70 nM TRIM26 siRNA sequence 1 (5'-CCGGAGAAUUCUCAGAUAA-3'), or 70 nm TRIM26 siRNA sequence 2 (5'-GAGUCACAGGAACUCAUCU-3'), or 70 nm of both TRIM26 siRNA sequences combined for 72 h at 37°C in a humidified CO_2 incubator. Cells were harvested in cold PBS, pelleted by centrifugation and RNA extracted. RNA was converted to cDNA by reverse transcription using oligo(dT) and then subject to qPCR analysis. Overall, qPCR analysis confirmed that both TRIM26 siRNA sequences were able to reduce *trim26* expression, with sequence 1 being ~50 % efficient and sequence 2 being ~70 % efficient. However, a superior knockdown (~80%) was achieved when a combination of both TRIM26 siRNA sequences were used (**Figure 68**). Due to this, knockdown of TRIM26 in subsequent studies in HCT116$^{p53+/+}$ cells was achieved via a combination of 70 nM of each siRNA sequence.

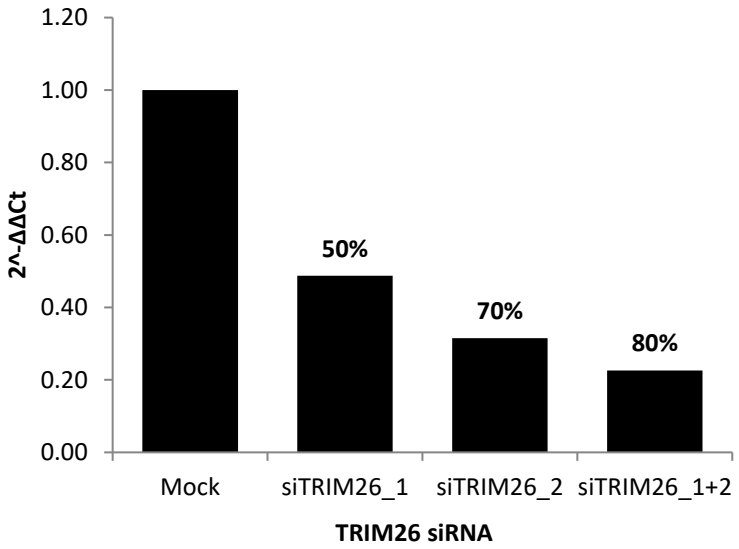

Figure 68. Efficiency of TRIM26 knockdown using siTRIM26_1 or siTRIM26_2 or both combined over 72 h. Cells were grown in 10 cm dishes until 30-50 % confluent and treated with 10 µl Lipofectamine RNAiMAX transfection reagent (Mock), or 70 nM TRIM26 siRNA_1 (5'-CCGGAGAAUUCUCAGAUAA-3'), or 70 nM TRIM26 siRNA_2 (5'-GAGUCACAGGAACUCAUCU-3'), or both TRIM26 siRNA sequences combined for 72 h. Following this, cDNA was created from harvested cell pellets and subject to qPCR analysis which confirms that a superior knockdown (~80 %) is achieved when both siRNA sequences are present. The percentage knockdown for each siRNA was quantitated by RT-PCR and the gene levels of mRNA (RQ value) calculated from the CT value for the RT-PCR run. Bar chart shows the mock (lipofectamine only) normalised to 1 and the relative gene levels after siRNA knockdown. A non-template control (just primers, no cDNA) was also run for each primer to check for any contamination which could alter results.

6.6 TRIM26 does not regulate cellular steady state levels of NTH1

To investigate if TRIM26 directly influences the steady state levels of NTH1in cells, particularly since TRIM26 promotes polyubiquitylation of NTH1 in cells, levels of NTH1 in whole cell extracts from HCT116$^{p53+/+}$ cells following TRIM26 depletion were investigated. Further to this, the suitability of two non-targeting (NT) controls from two different sources (Qiagen and Eurogentec) were assessed in comparison to Lipofectamine RNAiMAX only treated cells, as the transfection reagent only. It was anticipated that the NT control siRNA sequences should not influence NTH1 protein levels.

HCT116$^{p53+/+}$ cells were cultured in 35 mm dishes until 30-50 % confluent before being transfected with either Lipofectamine RNAiMAX only, TRIM26 siRNA (combining two separate TRIM26 siRNAs as in **Figure 68**), Qiagen NT control siRNA, or Eurogentec NT control siRNA and incubated for 72 h at 37°C in a humidified CO_2 incubator.

Following this, cells were harvested in cold PBS, pelleted by centrifugation and proteins extracted. Cell extracts were separated by 10 % SDS-PAGE and analysed by Western blotting using antibodies specific to NTH1 (**Figure 69, A**). In addition to this, tubulin antibodies were utilised as a loading control to quantify NTH1 protein levels taking into account loading discrepancies. Levels of NTH1 protein expression were normalised to the level in the Lipofectamine RNAiMAX only treated cells, which was given a value of 1 (**Figure 69, B**). Three independent replicates of each treatment were completed and average NTH1 protein expression was compared (**Figure 69, B**).

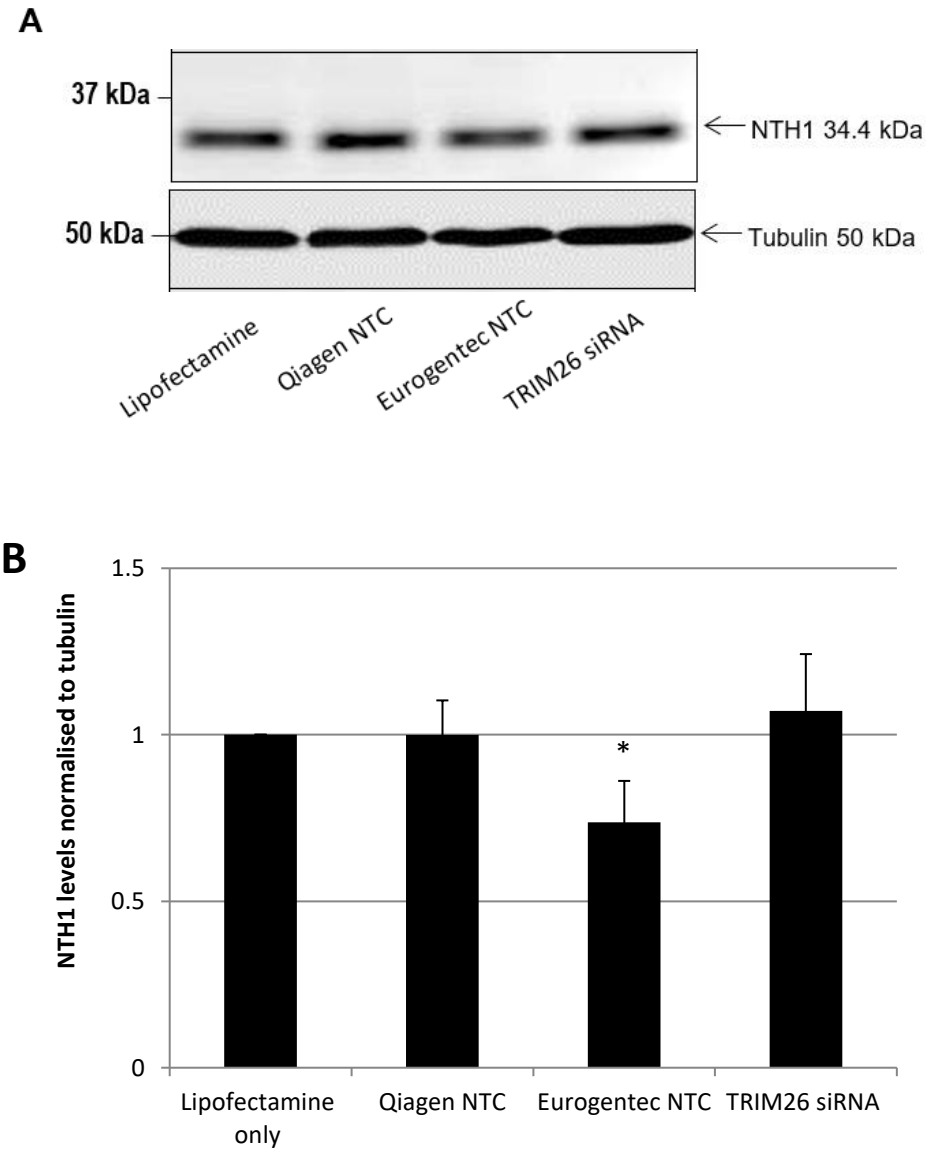

Figure 69. Cellular steady state NTH1 protein levels in HCT116$^{p53+/+}$ whole cell extract, following treatment with; Lipofectamine RNAiMAX only, 140 nM non-targeting (NT) controls (QIAGEN or Eurogentec), or 140 nM TRIM26 siRNA for

72 h. HCT116$^{p53+/+}$ cells were grown in 35 mm dishes for 24 h until 30-50 % confluent and then treated with 2.5 µl Lipofectamine RNAiMAX transfection reagent only, or in the presence of 140 nM Qiagen non-targeting (NT) control siRNA, or 140 nM Eurogentec NT control siRNA or 140 nM TRIM26 siRNA for 72 h. Whole cell extracts were prepared via the Tanaka method and analysed by 10 % SDS-PAGE followed by Western blotting. The presence of NTH1 was observed via immunoblotting using NTH1 antibodies, with tubulin antibodies acting as a loading control (**A**). Levels of NTH1 were quantified relative to tubulin antibodies from at least three independent experiments. The mean NTH1/tubulin ratio was normalised to the Lipofectamine RNAiMAX only control, which was set to 1 (**B**). Statistical significance via independent *t*-tests compared Lipofectamine RNAiMAX only to each treatment (*p <0.05).

Transfection of cells with NT control siRNA derived from Qiagen appeared to cause no dramatic change in NTH1 expression relative to Lipofectamine RNAiMAX only treated cells (**Figure 69, A** and **B**). However, transfection with NT control siRNA obtained from Eurogentec NT siRNA appeared to result in a significant reduction in NTH1 protein levels (p=0.041) (**Figure 69, A** and **B**). This suggests that this specific NT control siRNA may in fact be causing non-specific effects within the cell and will not be a suitable siRNA control in subsequent studies. Following TRIM26 siRNA, quantification of NTH1 protein expression levels in whole cell extracts suggests that a depletion of TRIM26 protein expression does not significantly stabilise NTH1 steady state levels relative to tubulin across three independent replicates, compared to Lipofectamine RNAiMAX only treated cells or the Qiagen NT control siRNA (**Figure 69, A** and **B**). This was surprising given the strong biochemical data acquired *in vitro* demonstrating that TRIM26 can catalyse polyubiquitylation of NTH1. However, these data indicated that TRIM26 does not play a significant role in controlling cellular protein levels of NTH1 in unstressed HCT116$^{p53+/+}$ cells.

6.7 NTH1 localisation is unaffected by TRIM26 depletion

The literature has described that NTH1 is largely localised to the nucleus, with some levels of cytoplasmic NTH1 identified in the mitochondria (69, 95). To clarify this, I investigated the localisation of NTH1 in HCT116$^{p53+/+}$ cells (**Figure 70**). I also aimed to explore if TRIM26 influences the cellular distribution of NTH1 via ubiquitylation by investigating the effects of siRNA induced knockdown of TRIM26 on the localisation of NTH1 protein.

HCT116$^{p53+/+}$ cells were grown in 10 cm dishes and transfected with either Lipofectamine RNAiMAX alone, Qiagen NT control siRNA, or TRIM26 siRNA and

incubated in a humidified CO_2 incubator at 37°C for 72 h. Cells were then harvested in cold PBS, pelleted by centrifugation before being resuspended and incubated in two sequential cell fractionation buffers to generate a soluble cytoplasmic protein fraction, and a chromatin bound protein fraction with a centrifugation step used to generate the two fractions. The protein concentration of each fraction was evaluated by a Bradford assay to enable the separation of equal concentrations of each sample by 10 % SDS-PAGE followed by Western blotting with NTH1 specific antibodies (**Figure 70, A**). In addition, Western blots were immunoblotted with Lamin specific antibodies to act as a loading control for the chromatin bound fraction. Levels of NTH1 protein expression relative to Lamin (at 69 kDa) were then quantified. This was repeated across three independent biological replicates. The average NTH1 protein levels were normalised to NTH1 expression in Lipofectamine RNAiMAX only levels, which was given a value of 1 (**Figure 70, B**).

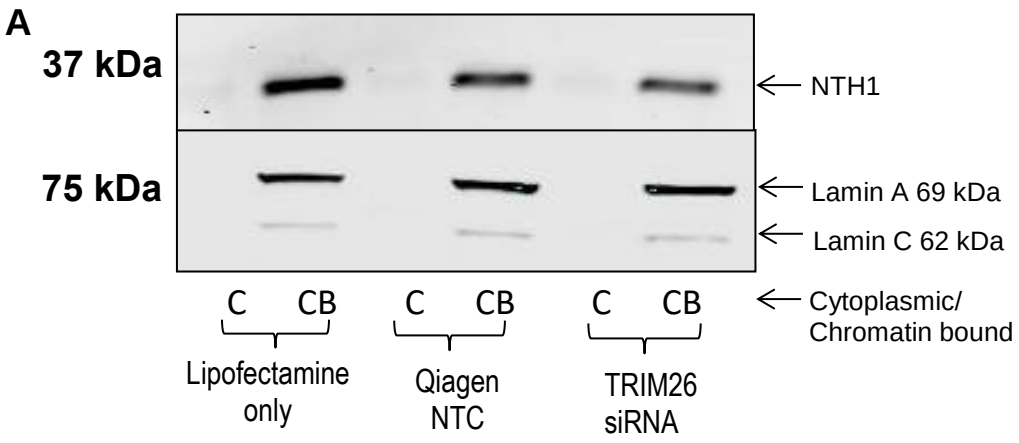

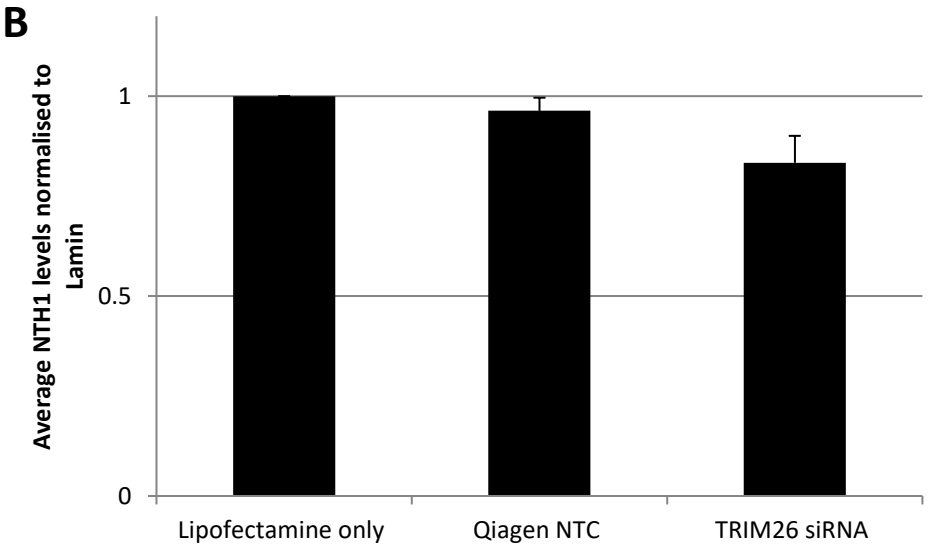

Figure 70. Nuclear expression levels of NTH1 protein in HCT116$^{p53+/+}$ cells following treatment with Lipofectamine RNAiMAX only, 140 nM Qiagen non-targeting (NT) control or 140 nM TRIM26 siRNA. HCT116$^{p53+/+}$ cells were grown in 10 cm dishes until 30-50 % confluent and then treated with 10 µl Lipofectamine RNAiMAX transfection reagent only or with 140 nM Qiagen non-targeting (NT) control or 140 nM TRIM26 siRNA for 72 h. Cells were harvested and fractionated extracts prepared via incubation with fractionation buffer I/II in the presence of protease inhibitors to obtain a soluble cytoplasmic protein fraction and an insoluble nuclear protein fraction. The concentration of each extract was measured via Bradford assay and equal amounts of loaded onto a 10 % SDS-PAGE gel. Levels of NTH1 were analysed by SDS-PAGE followed by Western blotting with NTH1 specific antibodies in addition to Lamin specific antibodies as a loading control (**A**). Three independent repeats were completed and the mean NTH1/lamin ratio normalised to the Lipofectamine RNAiMAX only control, which was set to 1 (**B**). Statistical significance via independent t-tests compared Lipofectamine RNAiMAX only to each treatment (*p <0.05) but no significance was detected.

As predicted, analysis of fractionated extracts demonstrated that NTH1 is almost entirely localised within the chromatin bound protein fraction (**Figure 70, A**, compare lanes 1 and 2). A very slight decrease in NTH1 levels was caused by treatment with Qiagen NT control siRNA although this was within experimental error and was not statistically significant demonstrating that this control siRNA had no dramatic impact on NTH1 protein cellular localisation (**Figure 70, A**, compare lanes 2 and 4). As observed with studies of NTH1 levels in whole cell extracts (**Figure 69**), a knockdown of TRIM26 mediated by siRNA does not result in a significant stabilisation of NTH1 levels, but this experiment now demonstrates that the levels of NTH1 on chromatin are also unaltered (**Figure 70, A**, compare lanes 2 and 6). In fact, a reduction of TRIM26 expression caused a partial decrease in NTH1 protein levels. Furthermore, there was also no redistribution of NTH1 into the soluble fraction as a consequence of TRIM26 siRNA suggesting that an absence of TRIM26, and therefore of NTH1 ubiquitylation, does not appear to impact on cellular localisation and on association of NTH1 with chromatin.

Following this, I aimed to investigate in more detail if NTH1 was further compartmentalised within the nucleus itself and the potential dependence of this on the presence of TRIM26. For this, I amended the original fractionation protocol to generate a soluble nuclear protein fraction in addition to the chromatin bound protein fraction, by the incorporation of an additional step utilising a separate buffer. The localisation of NTH1 was evaluated by protein separation via 10 % SDS PAGE followed by Western blotting with NTH1 specific antibodies. Once again, Lamin antibodies were employed as a loading control for the chromatin bound fraction.

Levels of NTH1 were quantified and normalised against Lamin expression (**Figure 71**).

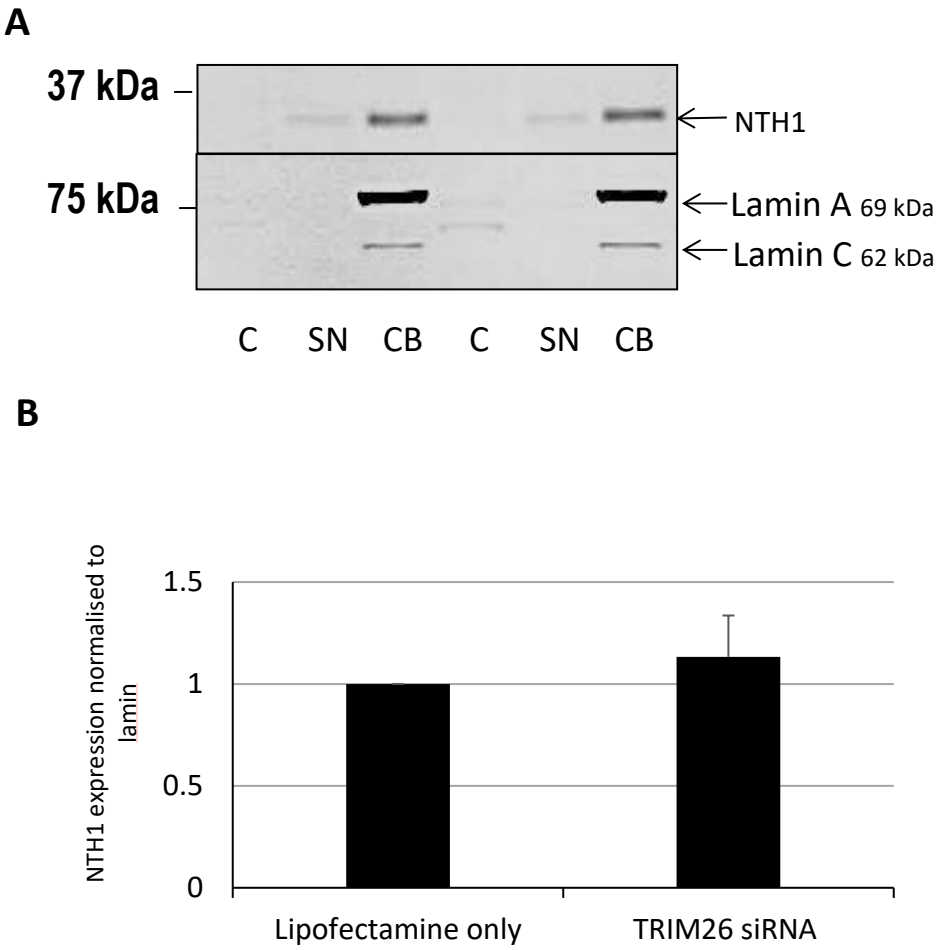

Figure 71. Cytoplasmic (C), soluble nuclear (SN) or chromatin bound (CB) localisation of NTH1 protein in HCT116 cells following treatment with Lipofectamine RNAiMAX only, or 140 nM TRIM26 siRNA. HCT116$^{p53+/+}$ cells were grown in 10 cm dishes until 30-50 % confluent and then treated with 10 µl Lipofectamine RNAiMAX transfection reagent or 140 nm TRIM26 siRNA for 72 h. Cells were harvested then fractionated extracts were prepared via incubation with fractionation buffer I/II in the presence of protease inhibitors combined with a series of centrifugation steps to yield a cytoplasmic protein fraction (C), a soluble nuclear protein fraction (SN) and a chromatin bound protein extract fraction (CB). The concentration of each extract was measured via Bradford assay and equal amounts loaded onto a 10 % SDS-PAGE gel. Levels of NTH1 were analysed by Western blotting with NTH1 specific antibodies and antibodies specific to Lamin were used as a loading control (**A**). NTH1 levels were quantified relative to Lamin (at 69 kDa) across three independent repeats. The mean NTH1/lamin ratio was normalised to the Lipofectamine RNAiMAX only control, which was set to 1 (**B**). Statistical significance via independent t-tests compared Lipofectamine RNAiMAX only to TRIM26 siRNA (*p <0.05), but no significance was detected.

From this modified fractionation protocol of cellular extracts, it was concluded that NTH1 was still consistently largely found within the chromatin bound protein extract, although a trace amount of protein was visible in the soluble nuclear fraction (**Figure 71, A**, lanes 2 and 5). Alike to the other cellular extract studies described previously, the siRNA dependent knockdown of the E3 ligase, TRIM26, did not substantially stabilise NTH1 levels (**Figure 71**). In fact a TRIM26 siRNA induced knockdown resulted in a mild (~10 %) increase in NTH1 protein expression, relative to the Lamin loading control (**Figure 71, B**). Statistical analysis reported that changes in NTH1 expression levels (normalised to Lamin) in the chromatin bound fraction was not significantly different between the two treatment groups ($p=0.58$). Furthermore, an absence of TRIM26 did not impact significantly on the localisation of NTH1 in the chromatin bound fraction and particularly there was no relocalisation of NTH1 into the soluble nuclear fraction (**Figure 71, A**). This suggests that ubiquitylation dependent regulation of the steady state levels of NTH1 may not be directly TRIM26 dependent, or that the turnover rate of the protein in these cells is low under normal conditions. Additionally, this would also suggest that NTH1 is extremely stable when bound to chromatin and is not targeted directly for ubiquitylation by TRIM26.

6.8 DNA damage induction of NTH1

The above results suggest that TRIM26 does not play a substantial role in regulating the cellular steady state levels of NTH1, therefore I hypothesised that NTH1 protein levels are altered under conditions of oxidative stress and particularly following DNA damage. Therefore, I investigated whether TRIM26 regulates DNA damage responsive levels of the DNA glycosylase. For the purpose of inducing DNA damage via oxidative stress, it was decided that hydrogen peroxide exposure would be most appropriate. Hydrogen peroxide was deemed more superior, compared to inducing DNA damage via other methods such as ionising radiation, in more readily causing oxidative DNA damage which would be more applicable to repair by NTH1 (184). Therefore, the first step was to examine whether NTH1 protein is induced following DNA damage induced by hydrogen peroxide. Secondly, to examine if TRIM26 is implicated in regulation of NTH1 in response to hydrogen peroxide exposure, the effects of TRIM26 depletion via a siRNA mediated knockdown was assessed.

$HCT116^{p53+/+}$ cells were cultured in 10 cm dishes until 30-50 % confluent before being transfected with either Qiagen non-targeting (NT) control siRNA, or TRIM26 siRNA in a 37°C humidified CO_2 incubator for 72 h. Following this, DNA damage was induced via exposure to hydrogen peroxide (150 µM) at 37°C in a humidified CO_2 incubator

for 15 min. Untreated cells were subject to treatment with supplemented media only for 15 min as a control. After 15 min, the media only or hydrogen peroxide solutions were aspirated and replaced with fresh, serum-containing media and cells were returned to the 37°C humidified CO_2 incubator and allowed to repair for specified time intervals (0-8 h). At the designated times, cells were harvested in cold PBS, pelleted by centrifugation and extracts prepared. Protein concentrations were assessed using a Bradford assay before equal amounts of each sample were separated by 10 % SDS-PAGE followed by analysis by Western blotting (**Figure 72**). Antibodies specific to NTH1 were used to evaluate NTH1 protein expression over time, with tubulin specific antibodies employed as a loading control. Levels of NTH1 expression were quantified relative to levels of tubulin which was then normalised to levels of NTH1 protein expression observed in untreated cell cultures, which was set to 1 (**Figure 73**).

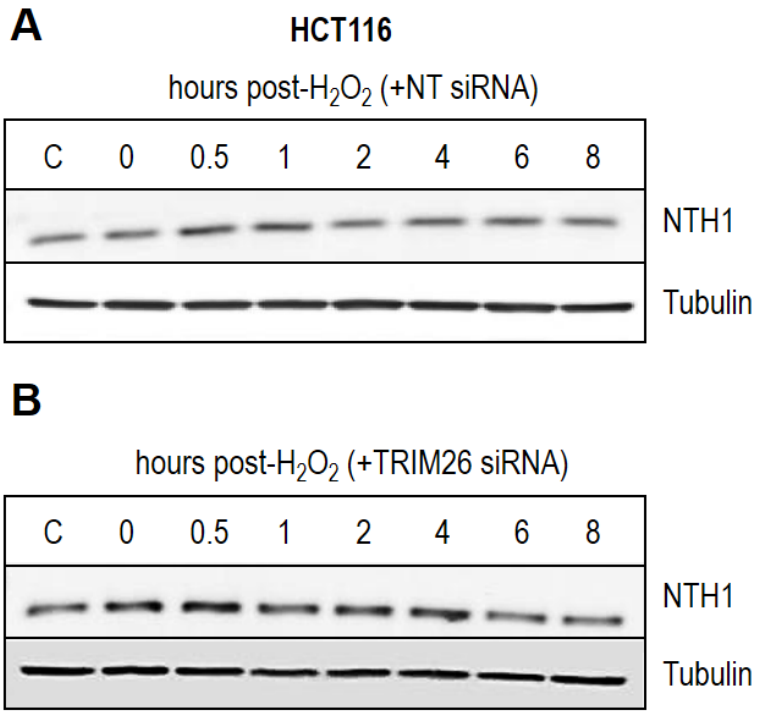

Figure 72. Western blotting analysis of fluctuations in NTH1 protein expression relative to tubulin over time following exposure to hydrogen peroxide following treatment with non-targeting siRNA or TRIM26 siRNA. HCT116$^{p53+/+}$ cells were cultured in 10 cm dishes until 30-50 % confluent before being transfected with (**A**) 140 nM Qiagen non-targeting (NT) control siRNA, or (**B**) 140 nM TRIM26 siRNA in a 37°C humidified cell culture incubator for 72 h. Afterwards, cells were exposed to 150 µM of hydrogen peroxide at 37°C in a humidified cell culture incubator for 15 min. The media was then removed before cells were washed in PBS and immersed in fresh serum-containing media. They were then returned to a 37°C humidified cell culture

incubator and allowed to repair for specified time intervals (0, 0.5, 1, 2, 4, 6, 8 h). At designated times cells were harvested and cell extracts were prepared via the Tanaka method. Protein concentrations were assessed via Bradford assays and equal amounts of extract were analysed by Western blotting. Antibodies specific to NTH1 were used to quantify NTH1 protein expression over time relative to tubulin expression visualised using tubulin specific antibodies.

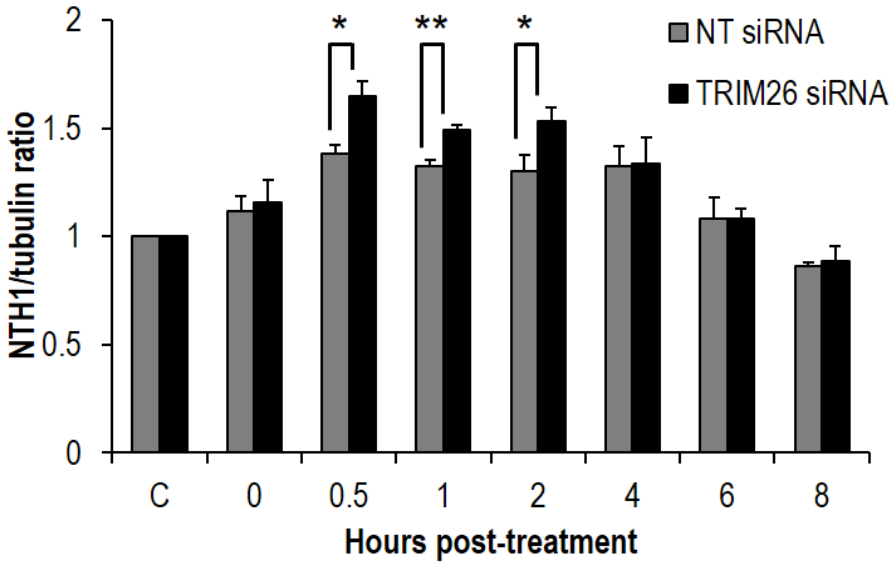

Figure 73. Quantification of immunoblotting analysis of fluctuations in NTH1 protein expression relative to tubulin over time following exposure to hydrogen peroxide following treatment with non-targeting (NT) siRNA or TRIM26 siRNA. HCT116$^{p53+/+}$ cells were cultured in 10 cm dishes until 30-50 % confluent before being transfected with 140 nM Qiagen non-targeting (NT) control siRNA, or 140 nM TRIM26 siRNA in a 37°C humidified cell culture incubator for 72 h. Afterwards, cells were exposed to 150 µM of hydrogen peroxide at 37°C in a humidified cell culture incubator for 15 mins. The media was then removed before cells were washed in PBS and immersed in fresh serum-containing media. Cells were then returned to a 37°C humidified cell culture incubator and allowed to repair for specified time intervals (0, 0.5, 1, 2, 4, 6, 8 h). At designated times, cells were harvested and cell extracts were prepared via the Tanaka method. Protein concentrations were assessed via Bradford assays and equal amounts of extract were analysed by Western blotting. Antibodies specific to NTH1 were used to quantify NTH1 protein expression over time relative to tubulin expression visualised using tubulin specific antibodies. Levels of NTH1 protein relative to tubulin were quantified from at least three independent experiments. Shown is the mean NTH1/tubulin ratio with standard errors normalised to the untreated control which was set to 1.0. *$p<0.05$, **$p<0.02$ as analysed by a one sample t-test of ratios at the respective time points comparing NT control siRNA and TRIM26 siRNA treated cells.

From the time dependent DNA damage response assay, it is apparent that NTH1 protein expression levels in the presence of a NT control siRNA increase by ~1.3-fold from 0.5 h post-treatment, and continue to remain at this level for up to 4 h before returning to the levels seen in the untreated controls after 6-8 h post-treatment with hydrogen peroxide (**Figure 72A** and **Figure 73**). Following the depletion of TRIM26 RNA (using siRNA) there is a modest, but statistically significant increase in NTH1

protein levels above those seen with the NT siRNA control particularly at 0.5-2 h post-treatment (**Figure 72B** and **Figure 73**). It is important to acknowledge that we were only able to deplete ~75 % of TRIM26 RNA (using siRNA), and that cells still contained ~25 % of TRIM26 RNA, which may be supressing the level of induction of NTH1 observed following treatment with hydrogen peroxide. It is worth noting that we attempted to study TRIM26 protein levels in cells, following siRNA medicated depletion, but our observations were limited by the specificity of the TRIM26 antibodies available.

Despite this, the results from this assay advocates that induction of NTH1 in response to cellular DNA damage may be regulated in a TRIM26 dependent manner. It appears that the E3 ligase may play a role in carefully controlling the induction of NTH1 protein levels in response to DNA damage induced by oxidative stress. Due to the bifunctionality of NTH1, uncontrolled over amplification of the glycosylase may result in the excess formation of abasic sites or DNA single strand breaks which would be counteractive to DNA restoration and maintaining genome stability. It is however notable that the protein levels of NTH1 do eventually return to untreated control levels even in the absence of TRIM26, suggesting an alternative mechanism by which NTH1 protein levels are degraded. However, it is possible that the residual RNA levels (~25 %) of TRIM26 may be responsible for this effect. Nevertheless, this supports an important role for TRIM26 in controlling NTH1 protein following DNA damage.

6.9 Cell survival in response to NTH1 regulation

Following the demonstration that regulation of NTH1 protein induction via TRIM26 occurs in response to hydrogen peroxide-induced DNA damage (**Figure 73**) I next aimed to explore whether this influenced the ability of cells to survive post-treatment. Predictably, a further elevation in the protein levels of NTH1 in the absence of TRIM26 (**Figure 73**) should increase resistance of cells to oxidative stress. To assess this, I utilised the clonogenic assay to examine the ability of a single cell to form a defined colony following treatment with hydrogen peroxide (53), and the dependence of this on TRIM26 protein.

Initially, the appropriate concentration of hydrogen peroxide to use was evaluated via a titration assay. HCT116$^{p53+/+}$ cells were cultured in 10 cm dishes until between 30-50 % confluent, before being treated with either Lipofectamine RNAiMAX only or TRIM26 siRNA for 72 h. Following this, cells were treated with increasing concentrations of hydrogen peroxide (0-300 µM) for 15 min at 37 °C. Then cells were

trypsinised and a defined number seeded into 6 well plates before being incubated for up to 2 weeks at 37 °C in a humidified CO_2 incubator. Cells were fixed with glutaraldehyde and stained with crystal violet. Cell survival was determined by counting the fraction of cells which retained the ability to produce colonies, normalised to the untreated control which was set to 1.0. From this single preliminary experiment, it was established that a dose of 0-400 µM hydrogen peroxide was sufficient to produce a suitable survival curve using HCT116$^{p53+/+}$ cells (**Figure 74**). However, it was noticeable even from this preliminary experiment, that cells lacking TRIM26 through siRNA depletion appeared to be more resistant to the cell killing effects of hydrogen peroxide.

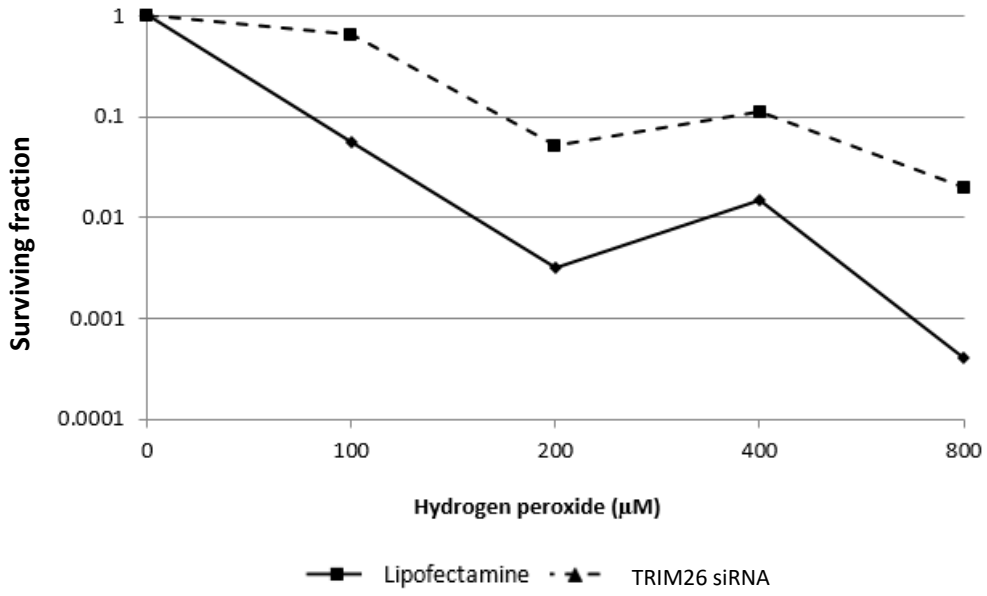

Figure 74. HCT116$^{p53+/+}$ clonogenic cell survival in response to increasing concentrations of hydrogen peroxide with or without TRIM26 depletion. HCT116$^{p53+/+}$ cells were cultured in 10 cm dishes until 30-50 % confluent before being transfected with 10 µl of Lipofectamine RNAiMAX only (Mock, solid line) or 140 nM of TRIM26 siRNA (dashed line) for 72 h. Following this, cells were treated with hydrogen peroxide (0 - 800 µM) for 15 min at 37 °C in a humidified cell incubator. Subsequently, cells were washed in PBS, trypsinised, counted and a defined number seeded into a 6-well plate before being incubated at 37 °C in a humidified cell incubator for up to 2 weeks. Colonies were then fixed and stained with 6 % glutaraldehyde, 0.5 % crystal violet for 30 min. Plates were washed, left to air dry overnight and colonies counted using the GelCount colony analyser (Oxford Optronics, Oxford, UK). Relative colony formation (surviving fraction) was expressed as colonies per treatment level versus colonies that appeared in the untreated control.

In order to avoid potential off target effects induced by NT control siRNA sequences, I then compared the clonogenic cell survival curves following treatment with two

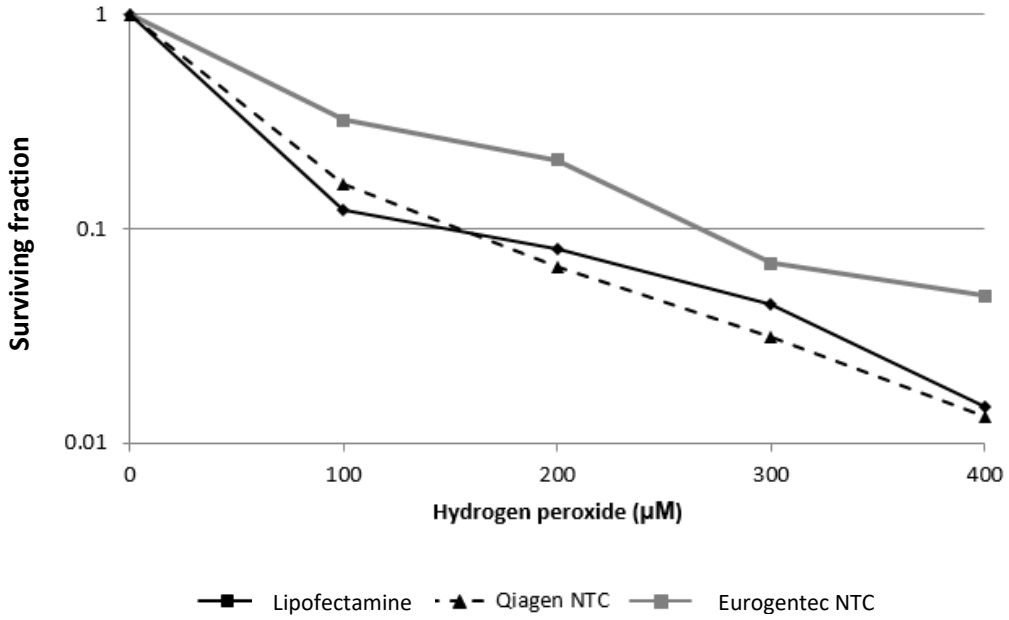

different NT control siRNA sequences obtained from two different sources, to a Lipofectamine RNAiMAX only control (**Figure 74**). Once again, HCT116$^{p53+/+}$ cells were cultured in 10 cm dishes until 30-50 % confluent before being transfected with either Lipofectamine RNAiMAX only, Qiagen NT siRNA, or Eurogentec NT siRNA for 72 h. Following this, cells were treated with increasing concentrations of hydrogen peroxide (0-800 µM) for 15 min. Then a defined number of cells were seeded into 6 well plates in triplicate and incubated for up to 2 weeks at 37 °C in a humidified CO_2 incubator (**Figure 75**).

Figure 75. HCT116 clonogenic cell survival in response to increasing concentrations of hydrogen peroxide with Lipofectamine only, Eurogentec NT siRNA or Qiagen NT siRNA. HCT116 cells were cultured in 10 cm dishes until 30-50 % confluent before being transfected with 10 µl of Lipofectamine RNAiMAX only (Mock, solid line), or 140 nM Eurogentec NTC siRNA (grey line), or 140 nM Qiagen NTC siRNA (dashed line) for 72 h. Following this, cells were treated with hydrogen peroxide (0 – 400 µM) for 15 min at 37 °C in a humidified cell incubator. Subsequently, cells were washed in PBS, trypsinised, counted and a defined number seeded into a 6-well plate before being incubated at 37 °C in a humidified cell incubator for up to 2 weeks. Colonies were then fixed and stained with 6 % glutaraldehyde, 0.5 % crystal violet for 30 min. Plates were washed, left to air dry overnight and colonies counted using the GelCount colony analyser (Oxford Optronics, Oxford, UK). Relative colony formation (surviving fraction) was expressed as colonies per treatment level versus colonies that appeared in the untreated control.

From this second preliminary study, it was apparent that the survival curve induced by the NT control siRNA sequences obtained from Qiagen was most similar to the cell

survival observed by treatment with Lipofectamine RNAiMAX only (**Figure 75**)**.** In contrast, the Eurogentec NT control siRNA caused significantly increased cellular resistance to increasing hydrogen peroxide concentration. Based on this, and on the previous Western blotting data where the Qiagen NT control siRNA had no significant impact on NTH1 protein levels (**Figure 69**), this was deemed as the most suitable control siRNA to utilise in subsequent clonogenic survival assays.

After these preliminary experiments, the influence of TRIM26 depletion on survival of cells in response to hydrogen peroxide was thoroughly examined, in comparison to the Qiagen NT control siRNA, utilising three independent experiments. As expected, with exposure to increasing concentrations of hydrogen peroxide, HCT116$^{p53+/+}$ cell survival decreased across all treatments in a dose dependent manner (**Figure 76**). However following depletion of TRIM26 via siRNA, I found that this caused a statistically significant resistance ($p<0.0001$) to hydrogen peroxide-induced cell killing in comparison to the NT control siRNA treated cells. This is represented by an upward shift of the survival curve compared to the NT control siRNA treated cells. This observable resistance is predictably due to an increased DNA damage response due to induction of NTH1 protein levels that are further stabilised in the absence of TRIM26 protein expression (**Figure 73**). This change in surviving fraction is particularly impressive, especially considering that only a knockdown efficiency of approximately 80 % was achieved using a combination of two siRNA sequences. Nevertheless, this demonstrates that the levels of TRIM26 are important in regulating the cellular response to DNA damage induced by oxidative stress. To additionally support that increased resistance of cells to hydrogen peroxide in the absence of TRIM26 is caused by NTH1 protein accumulation, I overexpressed NTH1 using a mammalian expression plasmid (**Figure 63**) in HCT116$^{p53+/+}$ cells to mimic the conditions of TRIM26 depletion.

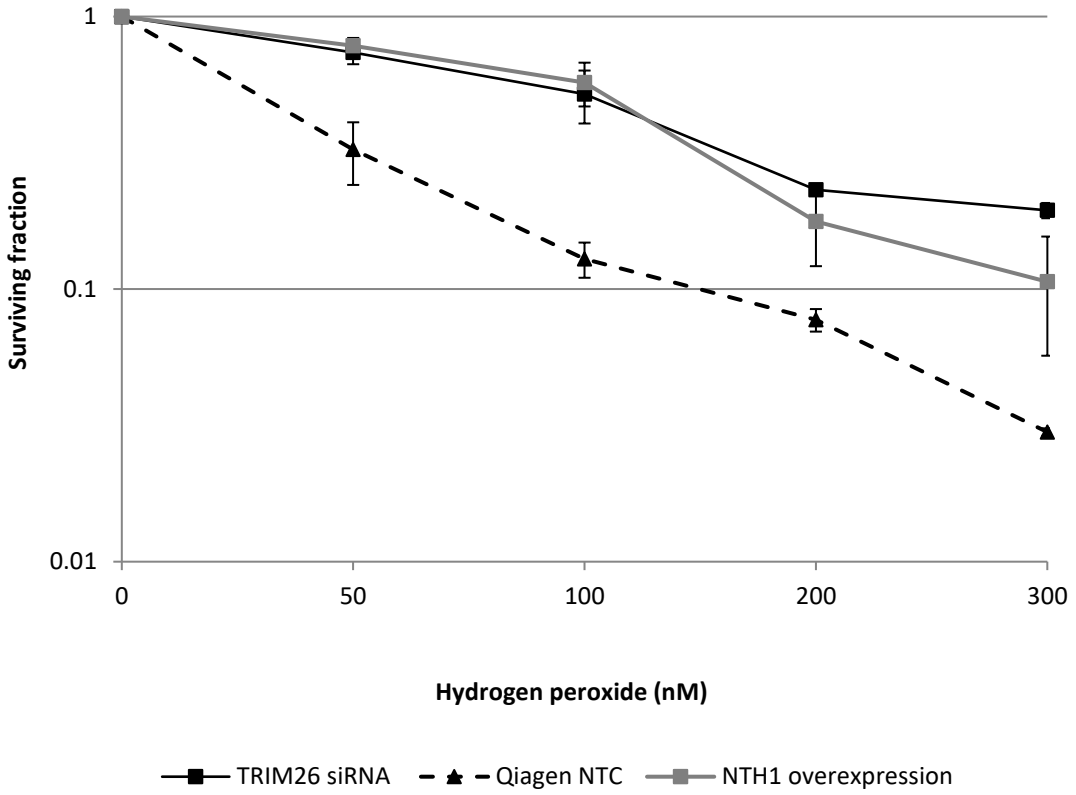

Figure 76. HCT116 clonogenic cell survival in response to increasing concentrations of hydrogen peroxide with 140 nM TRIM26 siRNA, or 140 nM Qiagen NT siRNA, or partial NTH1 overexpression. HCT116 cells were cultured in 10 cm dishes until 30-50 % confluent before being transfected with 10 ul of Lipofectamine RNAiMAX only (blue line), or 140 nM Qiagen NTC siRNA (dashed line), or 140 nM TRIM26 siRNA (black line) for 72 h, or a partial overexpression of 60 ng pCMVNTH1 mammalian plasmid (grey line) for 24 h. Following this, cells were treated with hydrogen peroxide (0 - 300 µM) for 15 min at 37 °C in a humidified cell incubator. Subsequently, cells were washed in PBS, trypsinised, counted and a defined number seeded into a 6-well plate before being incubated at 37 °C in a humidified cell incubator for up to 2 weeks. Colonies were then fixed and stained with 6 % glutaraldehyde, 0.5 % crystal violet for 30 min. Plates were washed, left to air dry overnight and colonies counted using the GelCount colony analyser (Oxford Optronics, Oxford, UK). Relative colony formation (surviving fraction) was expressed as colonies per treatment level versus colonies that appeared in the untreated control. Statistical analysis was performed using the CFAssay for R package (18).

Exogenous NTH1 expression appeared able to recapitulate cellular resistance to hydrogen peroxide. This was statistically significant ($p<0.0001$) when compared to the NT siRNA control treated cells (**Figure 76**), and the level of resistance was similar to that achieved following treatment of cells with TRIM26 siRNA. This is consistent with the observation that depletion of TRIM26 induces increased cell survival directly by causing an elevation in NTH1 protein levels following conditions of cellular oxidative DNA damage.

6.10 DNA damage repair kinetics and dependence on TRIM26

Since I effectively demonstrated that depletion of TRIM26 protein expression levels modulates cellular sensitivity to hydrogen peroxide by regulating NTH1 protein induction, I next aimed to examine the impact on cellular DNA damage repair kinetics. Since I had shown that cellular survival is increased following TRIM26 siRNA, which can be mimicked by NTH1 overexpression, then predictably this is due to increased capacity for oxidative DNA damage repair due to increased NTH1 protein levels. Originally developed in 1984, the single cell gel electrophoresis (comet) assay is a widely used technique used to visualise and quantify DNA damage within individual cells (114). More specifically, I aimed to utilise the alkaline comet assay to analyse the repair of hydrogen peroxide induced DNA strand breaks and alkali-labile sites, which are generated directly or as intermediates of DNA base damage repair (145). The goal was then to establish if TRIM26 had any effect on DNA damage repair kinetics when protein expression levels of the E3 ligase were depleted using siRNA, and the contribution of NTH1 protein specifically to this effect.

HCT116$^{p53+/+}$ cells were therefore seeded into 35 mm dishes and cultured until at least 80 % confluency was achieved. After this, exponentially growing cells in each culture were trypsinised and cells in suspension were transferred into a 24-well plate. DNA damage was induced by treating cells in suspension with hydrogen peroxide. Previous work within our group had determined treating cells in suspension with a genotoxin before embedding them within agarose is superior in terms of analysing DNA damage repair kinetics compared to treating cultured cells as a monolayer with a genotoxic insult (112). Following hydrogen peroxide treatment of cells in suspension in media for 5 min, cells were diluted in molten low melting point agarose and immediately added onto a glass microscope slide pre-coated in normal melting point agarose. The cell/agarose suspension was covered with a glass coverslip and transferred to a metal tray on ice to encourage the agarose to set. At this point the slides containing cells were placed in a humidified chamber for certain time points (10-120 min) to promote cellular DNA damage repair. After this, the cover slip was removed and cells lysed in cold lysis buffer before subsequent DNA unwinding, electrophoresis and staining of the DNA.

Initially, for the purpose of identifying a suitable hydrogen peroxide concentration to induce an appropriate level of DNA damage of cells in suspension, a titration assay was performed which tested a range of concentrations (0 – 40 µM). From previous experience within our laboratory, the ideal level of detectable DNA damage that

migrates during electrophoresis to form the comet tail (% tail DNA) should be ~40 %, which is also at a point where the cells are able to repair the DNA damage efficiently without going into apoptosis (112).

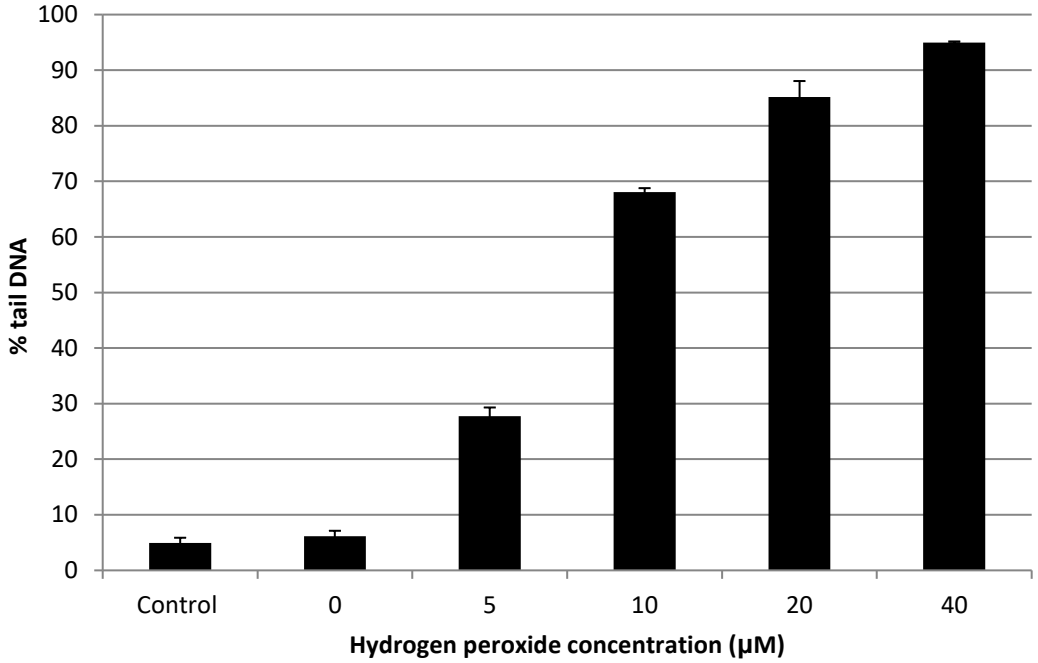

Figure 77. DNA damage repair kinetics as measured by the single cell gel electrophoresis (comet) assay following a titration of increasing concentrations of hydrogen peroxide. HCT116$^{p53+/+}$ cells were cultured in 35 mm dishes until 80 % confluent at 37 °C in a humidified cell incubator. After this, cells were trypsinised, counted and a defined number transferred into a 24-well plate in suspension in media. DNA damage was induced by treating cells with 0-40 µM of hydrogen peroxide for 5 min on ice. Cells are the mixed with molten low melting point agarose (at ~35 °C) before being transferred to a microscope slide pre-coated with normal melting point agarose. A cover slip is then placed over the cell/agarose mixture then the agarose is set by placing on a metal tray on ice for ~ 2 min. The cover slip was then removed and repair halted by placing slides in cold lysis buffer for at least 1 h. The slides were then placed in electrophoresis buffer and DNA allowed to unwind for 30 min before subsequent electrophoresis followed by staining stages. DNA damage was then analysed using Komet 5.5 (Andor Technology, Belfast, UK) measuring 50 cells per slide and >2 slides per time interval. Three independent replicates of the alkaline comet assay were performed to ensure reproducibility and the % tail DNA values are shown.

From the titration assay using increasing concentrations of hydrogen peroxide treatment (**Figure 77**), it was apparent that an optimum level of ~40 % of DNA damage (% tail DNA) was induced using between 5-10 µM of hydrogen peroxide incubated at 5 min at 37 °C in a humidified CO_2 incubator. Below 5 µM of hydrogen peroxide, it is

likely that the level of DNA damage is not sufficient to allow detailed kinetics of DNA damage repair and may affect our observations regarding the impact of TRIM26 depletion. Similarly, beyond 10 µM the level of quantified DNA damage is between 70-90 %. At this level, it is likely that cells will not be able to repair the excessive DNA damage and will probably undergo apoptosis. Therefore, this preliminary study dictated that for subsequent repair studies, a hydrogen peroxide concentration of 7.5 µM would be most appropriate.

For the purpose of investigating the impact of TRIM26 depletion on DNA damage repair kinetics via the alkaline comet assay, HCT116$^{p53+/+}$ cells were cultured in 35 mm dishes until 50 % confluent. Cells were transfected with either Qiagen NT control siRNA or 140 nM TRIM26 siRNA and incubated at 37 °C in a humidified CO_2 incubator for 72 h. Additionally to study the impact of partial overexpression of NTH1, and thus mimicking the effects of TRIM26 depletion, HCT116$^{p53+/+}$ cells were cultured in 35 mm dishes until approximately 80 % confluent before being transfected with pCMV-NTH1 mammalian expression plasmid for 24 h at 37 °C in a humidified CO_2 incubator. After this, all of the treated cells were trypsinised, counted and diluted to 1x10^5 cells/ml and transferred into a 24-well plate in suspension in media. DNA damage was induced by treating cells in suspension with 7.5 µM of hydrogen peroxide for 5 min on ice. Cells were mixed with molten low melting point agarose (at ~35 °C) before being transferred to a microscope slide pre-coated with normal melting point agarose. A cover slip was then placed over the cell/agarose mixture, then the agarose was set by placing on a metal tray on ice for ~ 2 min. For DNA damage repair kinetic studies, the slides were transferred to a humidified chamber pre-warmed at 37 °C and allowed to undergo DNA damage repair for the allocated time intervals (0-120 min). The cover slip was then removed and repair halted by placing slides in cold lysis buffer containing high salt and detergent for at least 1 h. The slides were then placed in electrophoresis buffer and DNA allowed to unwind for 30 min before subsequent electrophoresis. The DNA was stained using SYBR Gold and the levels of DNA single strand breaks and alkali-labile sites was then analysed using Komet 5.5 software (Andor Technology, Belfast, UK) measuring 50 cells per slide and >2 slides per time interval. Overall, three independent replicates of the alkaline comet assay were performed to ensure reproducibility (**Figure 78**). The % tail DNA measured at each time interval was normalised to the % tail DNA measured at the 0 min time interval which is set to 100 %, to allow an assessment of the kinetics of DNA damage repair.

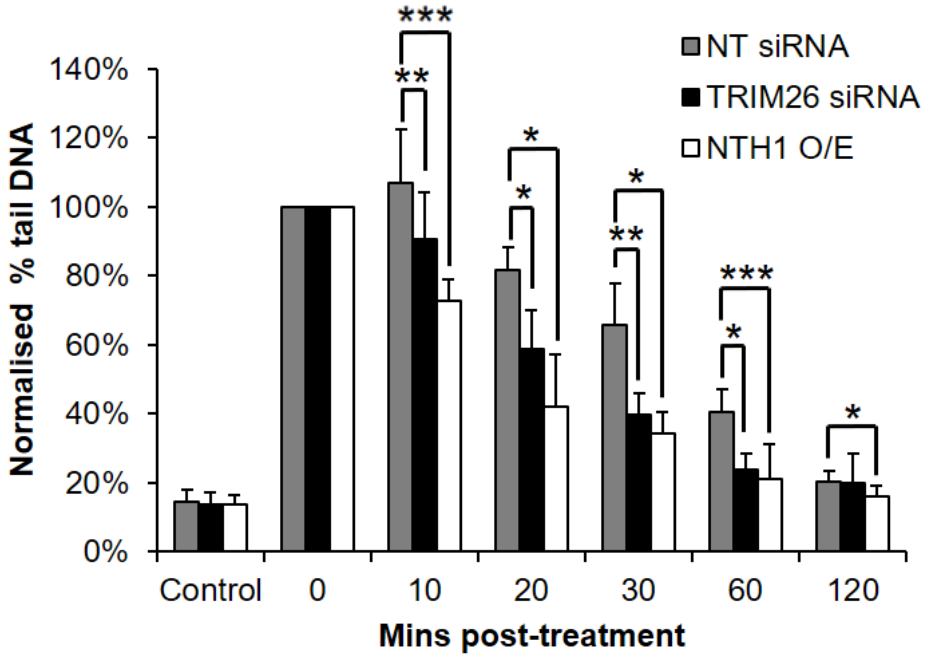

Figure 78. The implication of depleted TRIM26 or partially overexpressed NTH1 protein expression levels on DNA damage repair kinetics as measured by the single cell gel electrophoresis (comet) assay. HCT116$^{p53+/+}$ cells were cultured in 35 mm dishes until 30-50 % confluent before being transfected with either 140 nM Qiagen NT control siRNA or 140 nM TRIM26 siRNA and incubated at 37 °C in a humidified cell incubator for 72 h. Alternatively, for the partial overexpression of NTH1, HCT116$^{p53+/+}$ cells were cultured in 35 mm dishes until 80 % confluent before being transfected with 60 ng of pCMVNTH1 mammalian expression plasmid and incubated at 37 °C in a humidified cell incubator for 24 h. After this, cells were trypsinised, counted and a defined number transferred into a 24-well plate in suspension in media. DNA damage was induced by treating cells with 7.5 µM of hydrogen peroxide for 5 min on ice. Cells were mixed with molten low melting point agarose (at ~35 °C) before being transferred to a microscope slide pre-coated with normal melting point agarose. A cover slip was then placed over the cell/agarose mixture, then the agarose was set by placing on a metal tray on ice for ~ 2 min. For DNA damage repair kinetic studies, the slides were transferred to a humidified chamber pre-warmed at 37 °C and allowed to undergo DNA repair for the allocated time intervals. The cover slip was then removed and repair halted by placing slides in cold lysis buffer for at least 1 h. The slides were then placed in electrophoresis buffer and DNA allowed to unwind for 30 min before subsequent electrophoresis followed by staining stages. DNA damage was then analysed using Komet 5.5 (Andor Technology, Belfast, UK) measuring 50 cells per slide and >2 slides per time interval. Three independent replicates of the alkaline comet assay were performed to ensure reproducibility. The % tail DNA damage measured was normalised to the % tail DNA at the 0 min interval which was set to 100 %. A *t*-test was performed at each time interval comparing Qiagen NTC treated cells with either TRIM26 siRNA treated cells or following a partial overexpression of NTH1 *$p < 0.05$, **$p < 0.02$, ***$p < 0.01$.

Performing the alkaline comet assay with a range of repair times following hydrogen peroxide induced DNA damage, enabled me to investigate differences in repair

kinetics between each treatment. As expected over time, the % tail DNA measured decreased and across all treatments gradually from 0-120 min, and particularly at 120 min the % tail DNA is generally equivalent to that of untreated cells, showing that most of the genomic damage had been repaired and DNA integrity restored. In NT control siRNA treated cells, after 10 min the % tail DNA increases slightly beyond the normalised level at 0 min. This most likely represents the formation of single strand breaks following incision of the DNA backbone after the removal of damaged, oxidised DNA bases (**Figure 78**). However, between 20-60 min following treatment with hydrogen peroxide, the % tail DNA decreases significantly which is consistent with the kinetics of repair of DNA single strand breaks and base damage through the BER pathway.

In comparison to Qiagen NT control siRNA treated cells, it is noticeable that improved DNA damage repair kinetics are observed with an siRNA induced depletion of TRIM26 protein expression levels represented by the average % tail DNA measured being consistently decreased compared to the average % tail DNA of NT control siRNA cells across each of the time intervals (**Figure 78**). This difference is statistically significant at 10-60 min post-treatment (*p < 0.05, **p<0.02) and reflects the increased capacity of TRIM26 depleted cells to perform repair of DNA damage induced by hydrogen peroxide. Furthermore, a partial overexpression of NTH1 also induces faster DNA damage repair kinetics, mimicking the effects of TRIM26 depletion (**Figure 78**). In fact the difference in % tail DNA is statistically significant in NTH1 overexpressing cells compared to Qiagen NT control siRNA treated cells at 10-120 min post-treatment (*p<0.05, **p<0.02, ***p<0.01), demonstrating increased DNA repair capacity of NTH1 overexpressing cells. Therefore I have clearly demonstrated that a partial overexpression of NTH1 mimics the effects of depletion of TRIM26 protein expression levels by improving DNA damage repair kinetics in response to hydrogen peroxide tretament of HCT116$^{p53+/+}$ cells. An overexpression of NTH1 results in an increased presence of the BER glycosylase, meaning that oxidised DNA base lesions induced by hydrogen peroxide exposure may be more readily excised and repaired. Likewise, a depletion of TRIM26 levels may induce faster DNA repair kinetics by directly influencing damage responsive NTH1 protein levels, alike to those observed during the time course assay (**Figure 73**).

6.11 Results III summary

Overall, the main aim of this chapter was to examine the ubiquitylation dependent regulation of NTH1 in a cellular context. In previous Chapters, I identified TRIM26 as

the major E3 ligase involved in the enzymatic cascade which facilitates ubiquitin attachment to recombinant NTH1 during *in vitro* ubiquitylation assays. I also clarified that the N-terminal region of NTH1 is subject to regulation via polyubiquitylation, specifically lysine 67, suggesting that this is the target within the NTH1 protein that is ubiquitylated by TRIM26 for proteasomal degradation. The main purpose of the wirk detailed in this final chapter was to explore the mechanisms of TRIM26 dependent regulation of NTH1 within cells, with a focus on examining the role of TRIM26 in regulating NTH1 protein stability, plus the importance of this mechanism in the cellular response to DNA damage.

In summary, studies in HCT116$^{p53+/+}$ cells confirmed that NTH1 is undoubtedly subject to ubiquitylation dependent regulation in cells. In particular, the accumulation of NTH1 following inhibition of the proteasome by MG-132 suggests that ubiquitylation may influence stabilisation of the protein levels of NTH1. Immunoprecipitation studies following overexpression of TRIM26 in HCT116$^{p53+/+}$ cells provided evidence that this is an E3 ligase enzyme implicated in the ubiquitylation-dependent regulation of NTH1 within cells. Indeed, an increased smearing pattern representative of increased polyubiquitylation was observed following overexpression of TRIM26, suggesting that the protein is eventually targeted for degradation by the proteasome. Data using site-directed of the mammalian expression plasmid for NTH1, suggests that the stability of newly synthesised NTH1 protein may be dependent on lysine 67, which is a target site for TRIM26 dependent ubiquitylation and is associated with regulating protein stability.

By supressing TRIM26 protein expression levels using an siRNA induced knockdown, surprisingly it became increasingly apparent that TRIM26 dependent ubiquitylation was not implicated in the regulation of the steady state protein levels of NTH1. In fact, this was observed in whole cell extract and fractionated cellular extracts which confirmed that NTH1 is largely localised to the nucleus, and mostly chromatin bound. Although, TRIM26 has no impact on either the accumulation of NTH1 on chromatin in unstressed cells, or on the localisation of NTH1 into the cytoplasmic or soluble nuclear compartments of the cell. I demonstrate that TRIM26 in fact regulates DNA damage responsive levels of NTH1 protein. This was supported by analysis of whole cell extract protein expression from HCT116$^{p53+/+}$ cells following different repair times after hydrogen peroxide exposure. Indeed, I firstly demonstrate that NTH1 protein is induced in response to oxidative stress following hydrogen peroxide treatment of cells at time points where BER is most active (0.5-2 h), and that depletion of TRIM26 instigated an enhanced elevation of NTH1 levels in response to the genotoxic

treatment. Heightened stabilisation of NTH1 protein expression in response to TRIM26 suppression may facilitate the ability of cells to survive excessive DNA damage insult, which was demonstrated using the clonogenic survival assay. Increased cellular resistance to hydrogen peroxide following TRIM26 siRNA was observed. Recapitulation of increased cellular survival following TRIM26 depletion was achieved via a partial overexpression of NTH1, resulting in a similar survival curve, as that observed with TRIM26 siRNA mediated knockdown. This supported the hypothesis that the ubiquitylation dependent regulation of NTH1, via TRIM26, may impact on the cellular ability to withstand oxidative stress and genotoxic insults. Related to this, TRIM26 depletion also resulted in faster DNA damage repair kinetics; measured via the alkaline comet assay. Similar repair rates were also observed with partial NTH1 overexpression. Therefore, the alkaline comet assay further advocates that TRIM26 carefully regulates NTH1 protein levels in response to oxidative DNA damage. This interaction influences rates of DNA damage repair and overall survival.

Overall, I have gained additional evidence relating to *in vitro* studies demonstrating that TRIM26 can target NTH1 for polyubiquitylation, and now further provide evidence that this mechanism is important in a cellular context, particular under conditions of oxidative stress. Whilst the literature specifically relating to this is quite sparse, some of the data compare well to reports in the literature. For instance, other groups have documented that NTH1 is predominantly localised to the nucleus (69, 95). Likewise, I also identified that NTH1 is mainly nuclear although predominantly associated with chromatin. This observation is also in agreement with reports in the literature that have recognised that NTH1 may play an important role in the repair of DNA base lesions which are occluded within histone octamers (130). With regards to the ubiquitylation dependent regulation of NTH1, my studies following treatment of cells with a potent proteasomal inhibitor (MG-132) advocate that the glycosylase is subject to ubiquitylation in cells. This observation is supported by a proteomic screen which identified that NTH1 is ubiquitylated, although the enzymes involved in the ubiquitylation process were not elucidated (34)**.** However I now provide evidence that TRIM26 is the major E3 ligase in cells that catalyses ubiquitylation, and subsequent proteasomal degradation, of NTH1. Furthermore I have clearly demonstrated that ubiquitylation-dependent regulation of NTH1 by TRIM26 is a crucial mechanism for controlling the cellular NTH1 protein levels in response to oxidative stress, and therefore is a vital process for maintaining genome stability.

Chapter 7 - Discussion

7.1 Overview

NTH1 is an important biological enzyme implicated in the repair of oxidised pyrimidine DNA nucleobases; such as 5-hydroxyuracil or 5-hydrocytosine, during the BER pathway. Crucially, NTH1 is involved in the excision and repair of the highly mutagenic DNA base lesion, Tg (42, 76, 165). Although *nth1* knockout mouse models display no overt phenotype, due to redundancy between the BER glycosylases (149), *nth1* depleted cells exhibit hypersensitivity to DNA damaging agents (184) and reduced repair capacity of oxidative DNA base lesions (51, 123). Furthermore, double knockout models of *nth1* and *neil1* demonstrate increased tumour incidence (26). More specifically, altered NTH1 expression has been implicated in a number of human cancers; including colorectal cancer (175), prostate cancer (156) and gastric cancer (58). In addition, expression of a single nucleotide polymorphism of NTH1, present in 6.2 % of the global population, results in the accumulation of chromosomal aberrations and cellular transformation (55). Collectively, these observations highlight the importance of NTH1 in the preservation of genomic stability and suggest an anti-tumorigenic role of the glycosylase. Despite this importance, the molecular mechanisms underlying the regulation of cellular NTH1 remain understudied.

Notably, a number of studies have demonstrated that enzymes involved in the BER pathway are regulated by PTMs (25, 48), including ubiquitylation. Indeed, APE1 (102), Pol β (125) and PNKP (124), have all been shown to be regulated by ubiquitylation. Ubiquitylation is a process during which single or multiple ubiquitin moieties are added onto specific lysine residues of substrate proteins, via a cascade of ubiquitylation enzymes. The final stage of ubiquitylation is dependent on the action of E3 ubiquitin ligase enzymes. It is estimated that there are over 600 E3 ligase enzymes, which define the specificity of the ubiquitin attachment to specific substrate proteins. The ubiquitylation dependent regulation of some BER enzymes has already been confirmed, plus the specific E3 ligase enzymes involved have been identified. For instance, the E3 ligase enzymes implicated in the regulation of APE1, Pol β and PNKP have been characterised as UBR3, CHIP and Mule, and Cul-4A-DDB1-STRAP, respectively (102, 124-126). In fact, recent studies within our laboratory, discovered that TRIM26 is the major E3 ligase responsible for the ubiquitylation dependent regulation of the BER glycosylase, NEIL1 (46). Previous studies within the literature have focused on enzymes involved further downstream in the BER pathway (25, 48), particularly, in the DNA polymerase and DNA ligase steps of BER. However, the most recent study in our laboratory (46), highlights that more emphasis should focus on

understanding the regulation of enzymes involved in the initial stages of the BER pathway. In fact, proteomic screens have suggested that numerous DNA glycosylase enzymes are subject to ubiquitylation; including NTH1, MDB4, TDG and NEIL2 (34), but the UPP enzymes involved and the biological impact of this regulation is not fully understood. Furthermore, the limitations of proteome wide studies could even mean that the ubiquitylation dependent regulation of certain proteins remains undetected (34).

Despite the potential limitations of proteomic screens, it was still reasonable to hypothesise that NTH1 was subject to ubiquitylation dependent regulation, catalysed by specific E3 ligase enzymes. Therefore, the overarching aim of this project was to understand the molecular mechanisms employed by human cells to regulate the steady-state and DNA damage induced levels of NTH1 via ubiquitylation, with specific emphasis on discovering the E3 ligase enzymes involved.

7.2 Identification of TRIM26 as the major E3 ligase for NTH1

A well refined, unbiased protein purification technique, previously utilised in our laboratory was employed to identify candidate E3 ligase enzymes. Fractionated human cell extracts are generated using a series of column chromatography columns, then examined for E3 ligase activity via *in vitro* ubiquitylation assays containing the substrate NTH1 protein (46, 125, 126). Using this technique, the major E3 ligase in human cell extracts that catalysed the *in vitro* ubiquitylation of NTH1 was confined to one chromatography fraction. Mass spectrometry analysis identified that TRIM26 was the only candidate E3 ligase present in this ubiquitylated fraction. I further strengthened this finding by repeating *in vitro* NTH1 ubiquitylation assays using recombinant TRIM26, expressed and purified from bacterial cells. Together, these findings identify TRIM26 as the major E3 in human cell extracts that catalyses the ubiquitylation of NTH1.

During isolation and identification of TRIM26 as the major E3 ligase involved in the ubiquitylation of NTH1 *in vitro*, a separate ubiquitylation activity was observed, suggesting the presence of another minor E3 ligase with NTH1 specificity. Unfortunately, the enzyme related to this activity proved unstable and difficult to isolate due to consistent protein degradation. Therefore, potential ongoing investigations within our laboratory to attempt to isolate and identify this additional E3 ligase enzyme may prove interesting. It is probable that NTH1 could be subject to ubiquitylation dependent regulation by multiple E3 ligase enzymes; alike to the regulation of Pol β by CHIP (125) and Mule (126). Due to observations related to

NTH1 increasing in molecular weight by multiples of 8 kDa ,representing the addition of multiple ubiquitin moieties, I proposed that TRIM26 stimulates polyubiquitylation. In contrast, the E3 ligase activity, which I was unable to purify induced largely monoubiquitylation of NTH1 *in vitro*. It is worth noting that the intensity of the protein banding pattern decreased at the latter stages of the purification scheme, presumably due to loss of enzymatic activity induced by multiple incidences of freeze-thaw cycles. However, it could be that the purification scheme led to dissociation of TRIM26 from additional protein binding partners or factors that promote NTH1 polyubiquitylation. The fact that TRIM26 was purified from gel filtration fractions with an estimated molecular weight of between 200-443 kDa further advocates that the protein is multimeric or stably bound to other (unidentified) proteins that may influence its activity. Remarkably, our group has recently demonstrated that another DNA glycosylase, NEIL1, is also subject to ubiquitylation via TRIM26, in addition to another E3 ligase; termed Mule (46). This study utilised the same well-characterised purification technique relying on a series of chromatography columns, in combination with *in vitro* ubiquitylation assays, to purify TRIM26 as one of the major E3 ubiquitin ligases from human cells, responsible for ubiquitylation of NEIL1.

The tripartite motif (TRIM) superfamily of proteins are defined by the presence of conserved domains; including a RING domain, one or two B-box domains and an associated coiled-coil domain in the N-terminal region (63). The RING domain is implicated in the conjugation of proteins with ubiquitin related modifiers; including ubiquitin, SUMO and other ubiquitin-like molecules (63, 115). The RING domain facilitates the biological flexibility of TRIM proteins and may enable involvement in numerous biological pathways. Investigations related to elucidating the role of members of the TRIM superfamily are in preliminary stages. However, TRIM proteins have been shown to be involved in a broad range of processes related to genetic disorders, neurological disorders and cellular transformation (115). For example, recent exome sequencing analysis, revealed an intronic single nucleotide polymorphism in the TRIM26 gene associated with schizophrenia patients (1). Many TRIM proteins have been associated with carcinogenesis, with individual TRIM proteins either being underexpressed or overexpressed and exerting their cancerous effects in individual ways. Certainly, some TRIM proteins are implicated in carcinogenesis through regulation of the abundance or activity of the important tumour suppressor protein, p53. Indeed, TRIM21, TRIM25, TRIM28 and TRIM29 all reduce p53 activity via different mechanisms. As an example, TRIM25 indirectly reduces p53 activity by downregulating a histone acetyltransferase (p300), which

acetylates p53. Acetylation of p53 is required for transcriptional activation of numerous p53 target genes (50). Conversely, there are other TRIM proteins which enhance p53 activity; including, TRIM8, TRIM13 and TRIM19 (50). Another important cellular component that is controlled by TRIM proteins and associated with carcinogenesis is the transcription factor, nuclear factor kappa B (NF-κB). The NF-κB protein also regulates cellular proliferation, apoptosis, immunological process and inflammation (50). Despite studies identifying the diverse cellular roles of TRIM proteins being relatively preliminary, it is becoming increasingly apparent that TRIM proteins play an important function in the regulation of innate immunity. In fact, the most extensive studies regarding the functioning of TRIM proteins has been conducted in relation to human immunodeficiency virus (HIV) infection (115). These investigations have revealed several TRIM family members that interfere with the life cycle of the HIV infection pathway. For instance, TRIM11, TRIM32 and to a lesser extent TRIM22 have been suggested to repress viral gene expression. Likewise, TRIM22 and TRIM15 are believed to inhibit HIV assembly. Although, the precise mechanisms of these interference steps have yet to be resolved, these observations should be approached with caution as it has also been shown that other TRIM proteins can facilitate HIV infection (115). These studies may also have limited relation to regular context, as they are often completed using specific cell lineages, thus TRIM related interference may differ depending on the cell lineage, differentiation status or presence of PTMs. In addition to this, more convincing studies have shown that TRIM proteins are involved in regulation of innate immunity via the action of interferons (IFN) (63). Critically, stimulation of human monocytes and macrophages by IFNγ resulted in the increased expression of up to 26 TRIM genes (out of 44 studied) (115). TRIM8 is one of the proteins that is induced by IFNγ in many cells and it was identified that TRIM8 was implicated in the downregulation of the suppressor of cytokine signalling 1 (SOCS1), which is known to interfere with a well-known inflammatory pathway (JAK/STAT) to downregulate IFN-activated gene expression. Although the precise mechanism through which TRIM8 achieves this has yet to be completely realised, co-expression of TRIM8 with SOCS1 promoted SOCS1 degradation suggesting that TRIM8 could be destabilising SOCS1 potentially by a ubiquitylation dependent mechanism.

TRIM26 has been shown to negatively regulate IFNβ production and an antiviral response by promoting the ubiquitylation dependent degradation of the transcription factor, IRF3 (167). When bound to IRF3, TRIM26 promoted the K48-linked polyubiquitylation dependent degradation and subsequent termination of the

transcription factor (167). Likewise, it is acknowledged that TBK1 is an essential kinase engaged downstream of multiple receptors that mediates IRF3 phosphorylation and activation. A separate study demonstrated that upon viral infection, TRIM26 underwent autoubiquitylation to promote association with NEMO. This association bridged TBK1 to NEMO, enabling the activation of TBK1 (133). These observations highlight the cross-talk between the UPP and regulation of other pathways implicated in innate immunity and survival. Most recently, a separate study identified the involvement of TRIM26 dependent ubiquitylation in the regulation of cellular proliferation in response to transforming growth factor β (TGF-β) stimulation. Following treatment of cells with TGF-β, there was increased expression of TRIM26, which stimulated the polyubiquitylation of the protein TAF7, thereby targeting it for proteasomal degradation (109). The protein TAF7 is an important subunit of the general transcription factor IID (TFIID) complex, which plays a passive role in mediating the regulation of the expression of a number of gene promoters by RNA polymerase II. Degradation of the TAF7 subunit was needed to mediate proliferative arrest. This study demonstrated the key involvement of TRIM26 in this process and in the regulation of gene expression or the cell cycle (109). In addition to this, it has been proposed that TRIM26 regulates cellular apoptosis in non-small-cell lung cancer, via observations of reduced TRIM26 expression in patient samples. Further studies identified that overexpression of TRIM26 inhibited cell growth, plus induced cellular apoptosis, through downregulation of B-cell lymphoma 2 (BCL-2) (188). This was uncovered by simultaneous overexpression of BCL-2, which partially reversed TRIM26-mediated apoptosis in non-small-cell lung cancer cells (188). However, further work is required to elucidate the precise molecular mechanism and role of ubiquitylation in BCL-2 dependent regulation of apoptosis.

Collectively, reports in the literature suggest an increasingly versatile role of TRIM proteins within the cellular context. This would not be completely surprising given the diversity of the superfamily of TRIM proteins; owing to variable arrangement of protein domains, splicing variants, differences in cellular localisation and varying interactivity of protein domains. Currently, our understanding of the mechanisms used by TRIM proteins to restrict viral infection and regulate a number of cellular pathways is limited. This is partly due to our ineffective ability to recognise the functional consequences of every domain that initiates ubiquitylation or addition of ubiquitin-like modifiers plus the nature of every E2 enzyme and their specific protein targets. Furthermore, we do not fully comprehend the modes of modification which result in the inhibition or promotion of substrate protein activities. It is anticipated that structural investigations

will have an increasingly prominent role in elucidating protein interactions between TRIM proteins and their respective cellular targets, as well as the PTMs which may additionally influence these reactions. Progression in this subject may assist the development of novel approaches aimed at preventing infectious diseases, autoimmune conditions, inflammatory disorders and even some cancerous phenotypes.

7.3 TRIM26 ubiquitylates NTH1 within the N-terminus

Studies in the literature have reported the existence of three isoforms of NTH1. However, identification of the NTH1 isoform that is expressed in mammalian cells lacks clarity (94). Despite this oversight, it is acknowledged that all three forms of NTH1 possess a total of 17 lysine residues, which are all potential sites of ubiquitin attachment. With this in mind, it was important to define which specific lysine was subject to ubiquitylation by TRIM26. To identify these ubiquitylation sites within NTH1, I adopted a similar strategy to our previous study (45). During this, a mass spectrometry based approach was used to analyse *in vitro* ubiquitylated NTH1 by TRIM26. Therefore, ubiquitylated NTH1 was separated and isolated by SDS-PAGE analysis, then the protein within specific gel slices was extracted and digested with trypsin prior to analysis. Unfortunately, when using this approach, detection of specific peptides containing the characteristic glycine-glycine motif generated as a consequence of digestion of ubiquitin was elusive. Using ArgC as an alternative digestive enzyme, was also unable to detect any peptides within NTH1 subject to ubiquitylation. Therefore, alternative approaches were undertaken.

From a previous study in our lab, the generation of truncated version of NEIL1, demonstrated that a C-terminal deletion of NEIL1 lacking the final 55 amino acids was unable to be substantially ubiquitylated *in vitro* by TRIM26. Sequentially mutating lysine residues at the C-terminal end of the protein identified 7 lysine residues requiring mutation to fully suppress NEIL1 ubiquitylation. It was confirmed that both Mule and TRIM26 ubiquitylated the same lysine residues (45). With this in mind, I used a similar site directed mutagenesis technique. Despite truncated versions of NTH1 proving susceptible to degradation, preliminary results suggesting that the site of NTH1 ubiquitylation may be N-terminal were gained. This was due to the observation that deletion of the first 98 amino acids of NTH1 supressed TRIM26-dependent ubiquitylation *in vitro*. It is worth noting that the truncated versions of NTH1 may have been particularly susceptible to degradation because the N-terminal region of the protein may be required for stabilisation. Despite studies suggesting that the

extended N-terminal end of mammalian NTH1 may hinder its activity (88), it may have an additional, unidentified role in managing protein stability.

Having attempted a mass spectrometry and a truncated protein approach, I began to generate site specific mutants of NTH1 in a sequential manner, with a focus on the N-terminal end of the protein which would then be used in combination with the *in vitro* ubiquitylation assay with TRIM26. It was anticipated that maintaining a similar size and charged amino acid would cause minimal disruption to the overall structure of NTH1. This approach concluded that TRIM26 ubiquitylation of NTH1 occurs predominantly on lysine 67. Substitution of this residue to arginine significantly impeded *in vitro* ubiquitylation of recombinant NTH1. The substitution of other lysine residues such as K42, K48 and K52, also decreased the level of ubiquitylation of NTH1; although less strikingly than the K67R substitution. Mutation of all four of these lysine residues appeared to completely supress TRIM26-dependent ubiquitylation of NTH1. The effect of the K67R variant on the cellular stability of NTH1 was examined via plasmid overexpression, which concluded that the K67R variant of NTH1 protein was significantly more stable than the wild type glycosylase, providing evidence that the stability of NTH1 is dependent on lysine 67 and further advocates that this is the target site for TRIM26 ubiquitylation. Overall, these investigations suggest that K67 is the major site of ubiquitylation of recombinant NTH1 by TRIM26 *in vitro*, and that other lysine residues within this N-terminal region of the protein act as weaker ubiquitylation sites. This observation that K67 with the N-terminus of NTH1 is a target for ubiquitylation, is in addition to reports in the literature which describe that the extended N-terminal region of mammalian NTH1 may have an inhibitory role on the overall activity of the mammalian homologue of the glycosylase (88). With this in consideration, it is rational to propose that the N-terminal section of NTH1 may be subject to regulation via several PTMs, including ubiquitylation, (as described in this thesis), which act to impede enzymatic activity. Regulation of the activity of BER glycosylases is crucial to cellular survival because unregulated action of these enzymes could lead to increased DNA base excision. This is particularly important when considering bifunctional BER glycosylases, which also incise the DNA backbone. Therefore, unregulated removal of damaged DNA bases and/or the incision of AP sites could compromise the stability of the genome by producing excessive DNA single strand breaks. If these are not repaired by the availability of downstream BER proteins, this could jeopardise genome integrity and increase the likeliness of mutagenesis associated with human disease progression.

Interestingly, the site directed mutagenesis approach I adopted to investigate the site of NTH1 ubiquitylation, presented the opportunity to examine the effects of a naturally occurring point mutation. Reports in the literature have documented the presence of D238Y point mutation in 6.2 % of the global population (54). The mutation is characterised by the substitution of an aspartate residue to tyrosine, within the suspected active site of NTH1. The D239Y NTH1 variant exhibited limited glycosylase activity and was unable to excise Tg from oligonucleotide substrates, even though both D239Y and WT NTH1 bind with similar affinities to DNA containing Tg. Interestingly, addition of D239Y to WT NTH1 results in decreased overall glycosylase activity, suggesting that D239Y and WT compete for binding to damaged bases and that there is a dominant negative effect of D239Y (54). Expression of the D239Y NTH1 variant in human cells resulted in cellular transformation with transfected cells forming significantly greater numbers of colonies and a lack of focus formation. The observation of cellular transformation correlates to the suggestion that individuals who express the mutant NTH1 are likely to have increased risk of cancer. In line with this, cells expressing the D239Y variant exhibited significantly increased genomic instability via increased levels of chromatid breaks and fusions compared to cells expressing with WT NTH1. Related to this, D239Y expressing cells also accumulated DSBs perhaps as a consequence of replication fork collapse upon collision with an unexcised Tg or other replication-blocking lesions (54). Furthermore, expression of D239Y also induced increased sensitivity to DNA damaging agents. I therefore opted to generate recombinant D239Y variant of NTH1 and investigate its impact on TRIM26 dependent ubiquitylation. Surprisingly, analysis showed that the D239Y NTH1 variant was not efficiently ubiquitylated in comparison to the WT protein, which would suggest that the variant is not regulated by ubiquitylation. Of course, this demands further work to distinguish the full effect of the D239Y substitution on NTH1 activity and capacity to be regulated by ubiquitylation in cells. Whilst this was not the major focus of my thesis, this could be an avenue for future research. It would be interesting to evaluate if the D239Y variant exhibits altered protein stability in the cellular context and whether this is specific to ubiquitylation dependent regulation by TRIM26.

7.4 TRIM26 does not regulate steady state levels of NTH1

Given that I had clearly demonstrated that NTH1 is a target for ubiquitylation by TRIM26 *in vitro*, I next aimed to explore the mechanisms of ubiquitylation dependent management of NTH1 in the cellular context, with a particular focus on the role of TRIM26 in modifying NTH1 protein stability. For this purpose, I opted to use a human colon carcinoma cell (HCT116$^{p53+/+}$) line. Not only are these cells well characterised

in culture, but it was also hoped that since a homozygous loss-of-function germline mutation in the NTH1 gene predisposes to a new subtype of BER-associated adenomatous polyposis and colorectal cancer (175), understanding the mechanism of regulation of NTH1 in HCT116$^{p53+/+}$ cells could prove to be clinically relevant in the eventual treatment of this disease. Initially, I discovered elevated levels of cellular NTH1 following inhibition of the proteasome by MG-132 which confirmed that NTH1 levels are regulated in cells by ubiquitylation dependent degradation. This observation is supported by a proteomic screen which has identified that NTH1 is ubiquitylated, although the enzymes involved in the ubiquitylation process were not elucidated (34)**.** Following on from this, I examined the specific role TRIM26 plays on the in cells ubiquitylation dependent regulation of the steady state levels of NTH1. Our previous publication focusing on the ubiquitylation dependent regulation of another DNA glycosylase, NEIL1, demonstrated that TRIM26 (and another E3 ubiquitin ligase Mule) were important in the control of the cellular state levels of NEIL1 (46). This is in contrast to observations within this study, which have shown that TRIM26 is not implicated in modulating the cellular steady state levels of NTH1. Despite observing substantial polyubiquitylation of NTH1 by TRIM26 *in vitro*, depletion of cellular TRIM26 via siRNA in HCT116$^{p53+/+}$ cells had no significant impact on the steady state levels of the glycosylase, suggesting that unlike observations with NEIL1, TRIM26 is not responsible for the regulation of NTH1 in unstressed cells.

Aside to investigating steady state levels, I also examined if TRIM26 may regulate the intracellular localisation of NTH1 using siRNA dependent depletion of TRIM26 in combination with fractionation of protein extracts from HCT116$^{p53+/+}$ cells. Comparable to the literature, I showed that cellular NTH1 was detected in nuclear fractions prepared from HCT116$^{p53+/+}$ cells. Further investigation suggested that NTH1 is in fact tightly associated with chromatin, although a small proportion of NTH1 was still visible in the soluble nuclear fraction. Reports in the literature also showed that isoforms of NTH1 are all localised to the nucleus (69), with minor levels of cytoplasmic NTH1 believed to be predominantly localised in the mitochondria (68). Some reports have recognised that NTH1 is able to repair sterically occluded sites within histone octamers which form the basis of chromatin (130) and further reports have suggested that glycosylases such as NTH1 remain bound to DNA in order to scan for damaged base lesions (166). My observation of the localisation of NTH1 in chromatin bound cellular extract fractions would support the evidence that NTH1 is indeed tightly associated with chromatin and potentially constantly scanning along the DNA, however this requires more extensive investigation, especially to explore the

mechanistic details of this potential association. I further discovered that an siRNA mediated depletion of TRIM26 results in little changes in the levels of NTH1 associated with chromatin, and also no alteration in the cellular distribution of the glycosylase between chromatin bound and cytoplasmic fractions. A similar observation was found with NT control siRNA sequences which lacked a genomic target suggesting that TRIM26 siRNA does in fact have no dramatic effect on the cellular proteins levels of NTH1 or on cellular localisation.

7.5 TRIM26 controls the cellular response of NTH1 to oxidative stress

A recent study from our lab investigating NEIL1 as the glycosylase of interest, suggested that the induction of NEIL1 in response to elevated genotoxicity caused by ionizing radiation, was primarily Mule dependent and did not rely on TRIM26 protein (46). Since I did not observe any changes in the steady state levels or cellular localisation of NTH1 that were dependent on TRIM26, I proposed that TRIM26 may in fact control the regulation of NTH1 protein levels in response to DNA damage. This would be the opposite role for TRIM26 which was observed with NEIL1 regulation. To explore this concept, oxidative stress was induced by hydrogen peroxide that generates oxidative DNA base damage that requires repairing by NTH1, and subsequently the levels of NTH1 at particular time intervals post-treatment were analysed, with or without an siRNA mediated knockdown of TRIM26. This experiment demonstrated that the levels of NTH1 protein expression in the presence of a NT control siRNA sequence increased by ~1.3-fold following 0.5 h exposure to hydrogen peroxide. Protein levels of NTH1 remained elevated for up to 4 h post-treatment before then returning to the levels similar to those observed in the untreated controls after 6-8 h treatment. To our knowledge, this is the first reported evidence that NTH1 protein is induced under conditions of oxidative stress. Subsequent depletion of TRIM26 expression resulted in a significant (~1.7-fold) increase in the protein levels of NTH1, which is beyond the elevated levels observed with NT control siRNA treatment alone, particularly at 0.5-2 h post-treatment. Whilst this is a modest increase in NTH1, this was statistically significant although it is worth noting that the siRNA mediated depletion of TRIM26 was not totally effective, with an estimated cellular expression of 20 % of residual TRIM26 protein remaining. This residual TRIM26 expression may account for the modest increase in NTH1 protein post-treatment, but also the observation that NTH1 protein levels eventually reduce in TRIM26 depleted cells after initial exposure to the genotoxic agent and are similar to those observed in the NT control siRNA cells after 6-8 h post-treatment. Therefore, it is plausible that the residual expression of TRIM26, which was not fully supressed following siRNA

treatment, was able to eventually degrade NTH1. Alternatively, this observation could even be due to the presence of an additional E3 ligase enzyme that appears to be more active several hours following hydrogen peroxide treatment. This is credible given that we are already aware of a secondary E3 ligase activity specific to NTH1 which I was not able to purify due to the stability or activity of the enzyme being unstable. This activity (NTH1-$E3_1$) appeared to mainly facilitate the monoubiquitylation of NTH1 *in vitro* but which may have a more pronounced role in the cellular context. Furthermore, to fully appreciate the effects of TRIM26 in the cellular context, it may be beneficial to repeat assessment of NTH1 protein levels following oxidative stress using a knockout of TRIM26 induced by CRISPR-Cas9 gene editing. This may prove more effective in eliminating the residual 20 % of TRIM26 protein expression which could not be supressed by the effects of transfecting two siRNA sequences. The CRISPR-Cas9 gene editing system is currently being implemented in our laboratory, so the impact of TRIM26 depletion on NTH1 protein levels in response to oxidative DNA damage may be a line of further investigation. Furthermore, purification and identification of the additional E3 ligase enzyme which has already demonstrated specificity towards NTH1 (NTH1-$E3_1$) will be essential and is forming the basis for upcoming investigations.

7.6 TRIM26 dependent ubiquitylation of NTH1 influences DNA repair kinetics and cell survival

To further my investigations into the cellular role of TRIM26 following oxidative stress, the clonogenic assay was utilised to measure cellular survival following treatment with hydrogen peroxide. This is the gold standard assay for examining the impact of genotoxins and DNA damaging agents on cell survival. I revealed that cells exhibited increased survival capacity following exposure to DNA damage upon siRNA induced depletion of TRIM26, in comparison to NT control siRNA treated cells. Importantly, this observation could be recapitulated with a partial overexpression of NTH1 via a mammalian expression plasmid. This result promotes the logic that cells exhibit an increased ability to endure oxidative stress, and thus repair oxidative DNA damage, through modulation of NTH1 which can be manipulated by altering TRIM26 levels. Some observations in the literature support this speculation, with one study also demonstrating that overexpression of NTH1 causes resistance to hydrogen peroxide (184). Therefore, increased cellular levels of NTH1 are able to increase the ability of cells to repair oxidative DNA damage, leading to resistance to oxidative stress. However interestingly, another study by the same group later advocates that overexpression of NTH1 in TK6 cells has the opposite effect following exposure to IR;

with overexpression of NTH1 resulting in an exacerbation of DNA double strand break formation, leading to an elevated sensitivity to the cytotoxic and mutagenic effects of ionizing radiation (185). Researchers suggested that the increased sensitivity was observed due to the attempted repair of radiation damage, presumably at clustered damage sites, by NTH1 which can lead to the formation of potentially lethal and mutagenic double strand breaks in human cells. However, it is difficult to fully agree with this hypothesis given the contradictory observations related to the effects of NTH1 overexpression depending on the source of genotoxicity used to induce cellular DNA damage. This highlights the necessity for further work investigating the regulation of cellular glycosylases in response to different genotoxic agents, which may reveal an increasingly dynamic role of the DNA glycosylase depending on the dominate type of DNA damage inflicted on the genome. Despite conflicting reports, both studies highlight the necessity for tight regulation of NTH1 levels to maintain genomic stability.

Further to this, I utilised the alkaline single gel electrophoresis (comet) assay to examine cellular DNA damage repair kinetics following exposure to the genotoxic agent, hydrogen peroxide. This assay reveals the presence of DNA single strand breaks and alkali-labile sites generated directly, or as intermediates through BER. I demonstrated that cells with reduced levels of TRIM26 demonstrated improved ability to repair DNA damage induced by hydrogen peroxide. Similar to clonogenic survival results, increased kinetics of DNA repair in TRIM26 knockdown cells could be achieved by partially overexpressing NTH1. Yet again, this is alike to conflicting documentation in the literature which showed an association between overexpression of NTH1 and increased ability to repair DNA damage (185). Cumulatively, my observations support the concept that repair of oxidative DNA damage by NTH1 following exposure to elevated levels of genotoxicity is TRIM26 dependent. This data further supports our previous findings, which highlights the importance of TRIM26 in co-ordinating the appropriate cellular response to DNA damage via regulation of an alternative BER glycosylase, NEIL1 (46). Reports in the literature further support the fact that DNA glycosylases need to be tightly regulated to minimise genomic instability.

Overall, an increasingly dynamic role of TRIM26 is now becoming apparent, whereby the E3 ligase is implicated in the regulation of multiple BER glycosylases (at least two identified so far) with different effects in relation to the DNA damage response. Despite this increased knowledge, the cellular mechanism which dictates the outcome of ubiquitylation of either glycosylase under the regulation of TRIM26 remains to be

fully understood. As previously discussed, alteration of DNA damage responsive levels of NTH1 appears to be TRIM26 dependent, whereas management of NEIL1 levels in response to elevated DNA damage was shown to be dependent on another E3 ligase, Mule. The different regulatory effects of TRIM26 on NTH1 and NEIl1 may be due to the different cellular roles of each glycosylase. In particular, NTH1 plays a role in global repair of oxidised pyrimidines, whereas NEIL1 removes these from single stranded DNA associated with transcription or replication. Furthermore, it is worth noting that additional studies regarding different types of DNA damaging agents are required. For example, our most recent study focused on NEIL1 induced DNA damage via IR (46), whereas, this study utilises hydrogen peroxide as a source of genotoxicity. Consequently additional studies are necessary using different sources of genotoxic agents to build a more comprehensive understanding of the impact of regulation of BER components by TRIM26 in response to different types of genomic damage.

It is also worth considering that the differing roles of TRIM26 ubiquitylation of the two glycosylases, NTH1 or NEIL1, may be reliant on additional regulation by alternative post-translation modifications, which may promote or hinder the addition of ubiquitin moieties. However, previous reports have not documented modification of either NTH1 or NEIL1 via other post-translational modifications including, phosphorylation, methylation, acetylation or SUMOylation (25). This area may require further scientific investigation to discover potential association between different PTMs during the regulation of these DNA repair enzymes by ubiquitylation. PTMs of NTH1 could be identified following immunoprecipitation of the protein from cells and subsequent mass spectrometry analysis. However, this analytical approach is not without limitations; with the level of detection depending on the mass shift the PTM causes, the abundance of the modified peptide, the ability of the PTM to withstand rigorous mass spectrometry analysis and finally the impact the PTM has on the ionization efficiency of the peptide. For instance, studies involving phosphorylation are generally restricted by the abundance of the phosphorylated protein available and the sensitivity of detection varies depending on the peptide sequence. Of course, there are techniques to enrich the detection of target proteins and so a mass spectrometry approach may still be a valid tactic to investigate PTMs of NTH1 in the future.

Of course, it is entirely plausible that TRIM26 itself is also be subject to PTM dependent regulation which may regulate it activity towards NTH1 and NEIL1. This mechanism will obviously require further investigation however it will enable us to gain a comprehensive understanding of the molecular and cellular mechanisms employed

to regulate key proteins implicated in the BER pathway, particularly in response to genotoxic stress. Identification and understanding PTMs is crucial for gaining a complete comprehension of cellular biology and potentially lead to the delineation of dysregulated molecular defaults which could underlie the pathogenesis of human diseases, including cancer. Furthermore, a full understanding of the PTMs employed to regulate DNA damage response proteins could facilitate the discovery of novel drug targets which could eventually aid in the treatment of diseases.

7.7 Future work

Future work should focus specifically on furthering our understanding of the interaction and association between NTH1 and TRIM26. One area of investigation is to examine NTH1 activity using oligonucleotide substrates containing oxidative DNA base lesions (eg. Tg) and measuring the rate at which these are processed. This could be used to examine the effects of TRIM26-dependent ubiquitylation of NTH1, on the relative DNA glycosylase activity of the enzyme, which has yet to be fully realised in our current studies. Alike to other protocols in the literature, this technique could be extrapolated to further study the effects of NTH1 activity using a model of chromatin by generating histone octamers with oxidative DNA base lesions, such as 5-hydroxuracil and Tg, in different orientations within the nucleosome structure. For instance, the DNA base lesions could remain easily accessible and facing outwards of the nucleosome structure, or could be occluded by facing towards the nucleosome. It has previously been shown that NTH1 is able to process easily accessible DNA base lesions at a rate which is 10-fold quicker than processing of DNA base lesions which are occluded within the histone octamer and are harder to access (130). It would be interesting to utilise this method to examine the role of TRIM26 in regulating the ability of NTH1 to process chromatin associated DNA base lesions. My expectation is that the addition of ubiquitin (8 kDa protein) to NTH1 by TRIM26 should prevent the DNA glycosylase binding to oxidative DNA damage within free or nucleosomal DNA, and potentially reduce its association with chromatin.

In addition to this, an examination of the fluctuations of NTH1 expression throughout different stages of the cell cycle would be of interest. This concept has already been considered using synchronised cell studies, which described increased transcription of NTH1 throughout the early and mid S-phase pf the cell cycle (95). However, it would be interesting to mediate a knockdown of TRIM26 via siRNA or CRISPR-Cas9 gene editing, to inspect if ubiquitylation is involved in the cell cycle dependent regulation of NTH1, in addition to its role in the cellular DNA damage response.

More importantly, it will also be imperative to assess if the ubiquitylation dependent regulation of NTH1 via TRIM26 occurs in alternative cell lines, other than HCT116$^{p53+/+}$ colorectal cancer cell lines used in this study. It is worth considering that since altered NTH1 levels are linked to colorectal cancer due to the presence of a germline mutation (175), TRIM26-dependent regulation of NTH1 could be restricted to this cell line only. In previous studies, we have utilised U2OS osteosarcoma cell line to investigate NEIL1 regulation and so this could be an initial cell line employed in these further investigations (46). Related to this point, it will also be interesting to establish if TRIM26-dependent regulation of NTH1 is present in normal cells or whether it is limited to cancer cell lines only. This would be particularly interesting from the aspect of developing therapeutic strategies aimed at targeting cancer cell lines whilst sparing normal cells. For instance, if the TRIM26 dependent regulation of NTH1 was strictly observed in cancer cell lines, this could provide an avenue to specifically target this mechanism to affect cancer cells. For example, manipulating the ubiquitylation regulation of NTH1, to cause reduced levels of the glycosylase would reduce the ability of cancer cells to react to DNA damage induced by therapeutic agents which rely on inducing genomic damage, such as radiotherapy. Reduced glycosylase levels specifically within cancer cells, would therefore decrease their ability to withstand genomic damage and result in increased cancer cell death.

In addition, investigating if the DNA damage dependent induction of NTH1 occurs in response to other types of genotoxic stress could prove interesting. Whilst I have demonstrated that induction of NTH1 by TRIM26 occurs in response to oxidative stress induced by hydrogen peroxide, exposure of cells to genotoxic damage via ionising radiation could be used to analyse NTH1 levels in cellular extracts over time. This, in combination with clonogenic survival assays and comet assays could be utilised to assess cellular survival and the effects of DNA damage repair kinetics, respectively. It would be interesting to observe if the alterations in NTH1 levels or cellular response, in terms of frequency but also kinetically, are comparable to those seen following exposure to hydrogen peroxide. The results of this experimentation could in fact demonstrate some differences due to the variation in DNA damage inflicted by each genotoxic source. Hydrogen peroxide treatment is largely associated with the generation of DNA base lesions and single strand breaks, whereas, the energy deposition inflicted by tracks of ionising radiation can result in clustered sites of complex DNA lesions located within a few nanometres of each other, including DSBs (92). Complex DNA damage sites are well known to represent a challenge to the DNA repair machinery resulting in their persistence in cells and DNA post-

irradiation The complexity of the DNA damage associated with IR means that NTH1 may play a key role in their repair through long-patch BER, in collaboration with other types of DNA damage repair pathways, including, NHEJ or HR (71, 96).

Moreover, all of this experimentation could be extended to elucidate the role of the minor E3 ligase activity which I was unable to purify in this particular thesis, largely consistent with issues related to degradation or decreased stability of the candidate E3 ligase enzyme. From our preliminary studies during the initial purification of NTH1 specific E3 ligase enzymes, it would appear that the minor E3 ligase enzyme activity (NTH1-$E3_1$) is mainly associated with monoubiquitylation of NTH1. This was observed by the induction of one, singular shift of approximately 8 kDa in molecular weight of substrate NTH1, following *in vitro* ubiquitylation with active chromatography fractions containing the minor candidate E3 ligase. Ideally, purification and identification of this additional E3 ligase enzyme will be the primary focus of any future investigations. The forthcoming experimentation would also aim to clarify the molecular mechanism and cellular implications of the ubiquitylation dependent regulation of NTH1 via this particular E3 ligase activity. This will be particularly interesting due to preliminary assays suggesting that this activity is associated with monoubiquitylation. For this reason, it could be anticipated that the minor E3 ligase, at least *in vitro*, may induce a different effect on NTH1 in cells, compared to TRIM26. It is reasonable to hypothesise that this alternative ligase activity could regulate NTH1 in a different way. For instance, it may influence the activity, DNA binding or cellular localisation of human NTH1. However, the influence monoubiquitylation may have on NTH1 is difficult to predict due to the multiple roles the attachment of single moieties of ubiquitin can play. For instance, monoubiquitylation of PCNA at stalled replication forks promotes the interactivity of the modified protein (14), whereas monoubiquitylation of SMAD4 inhibits it interactivity with a signalling partner implicated in the TGFβ signalling pathway (44). On the other hand, monoubiquitylation influences the cellular localisation of Pol β and also acts as a prerequisite for polyubiquitylation dependent proteasomal degradation (126). Due to the diverse roles of monoubiquitylation, it is clear that in order to appreciate the effects of monoubiquitylation of NTH1, identification of the E3 ligase responsible is required to facilitate further exploration into the biological consequences of this mechanism.

7.8 Concluding remarks

The work described in this thesis has clearly identified TRIM26 as the major E3 ligase in the ubiquitylation dependent regulation of the BER glycosylase, NTH1. Excitingly,

the outcomes of this work have now been peer-reviewed and accepted for publication in the Molecular and Cellular Biology scientific journal (see appendix). The regulatory mechanism identified is clearly important in regulating the cellular levels of NTH1 in response to oxidative stress. Collectively, this observation in combination with our previously identified role for TRIM26 in modulating the steady state protein levels of another BER glycosylase, NEIL1, highlights an emerging role for TRIM26 in controlling the cellular response to oxidative DNA damage and suggests the E3 ligase may act as a vital regulatory enzyme involved in the BER pathway. Of course, further work is necessary to fully appreciate the role of other PTMs, such as phosphorylation, which may act on both NTH1 and TRIM26 and are therefore important in the regulation of the proteins and of the BER pathway that is responsible for the cellular response to oxidative DNA damage. Furthermore, identification of any additional E3 ligase activities that regulate NTH1, evidence of the existence of at least one such enzyme has been presented in this study, and the impact of these in terms of regulation of the DNA glycosylase particularly in relation to TRIM26, require thorough investigation.

The outcomes of this study are particularly important as investigations regarding regulation of the BER pathway have largely focused on enzymes further downstream in the process. Furthermore, reports in the literature have not yet reported any PTMs which are known to specifically regulate NTH1. Understanding the molecular mechanisms underlying the regulation of NTH1 and of BER are important to extend our comprehensive understanding of the cellular DNA damage response and potentially assist with defining molecular defaults implicated in the pathogenesis of specific cancers or other human diseases. The strategies utilised here could be extrapolated to identify the molecular mechanisms, particularly ubiquitylation dependent regulation, of other proteins involved in other DNA damage response pathways. An increased awareness of the molecular mechanisms underlying the DNA damage response could improve the identification of novel drug targets, facilitate the development of novel therapies or improve sensitivity to current treatment regimes. Overall, enhancing our scientific knowledge of the DNA damage response will be useful for us to fully comprehend the mechanisms underlying human pathologies.

Chapter 8 - References

1. Genome-wide association study identifies five new schizophrenia loci. Nat Genet. 2011 Sep 18;43(10):969-76.
2. Al-Tassan N, Chmiel NH, Maynard J, Fleming N, Livingston AL, Williams GT, et al. Inherited variants of MYH associated with somatic G:C[rarr]T:A mutations in colorectal tumors. Nat Genet. [10.1038/ng828]. 2002 02//print;30(2):227-32.
3. Allinson SL, Dianova, II, Dianov GL. Poly(ADP-ribose) polymerase in base excision repair: always engaged, but not essential for DNA damage processing. Acta Biochim Pol. 2003;50(1):169-79.
4. Ames BN. Endogenous DNA damage as related to cancer and aging. Mutation Research/Fundamental and Molecular Mechanisms of Mutagenesis. 1989 9//;214(1):41-6.
5. Ardley HC, Robinson PA. E3 ubiquitin ligases. Essays Biochem. 2005;41:15-30.
6. Aslanidis C, de Jong PJ. Ligation-independent cloning of PCR products (LIC-PCR). Nucleic Acids Res. 1990 Oct 25;18(20):6069-74.
7. Aspinwall R, Rothwell DG, Roldan-Arjona T, Anselmino C, Ward CJ, Cheadle JP, et al. Cloning and characterization of a functional human homolog of Escherichia coli endonuclease III. Proceedings of the National Academy of Sciences of the United States of America. 1997 08/17/received

10/30/accepted;94(1):109-14.
8. Atamna H, Cheung I, Ames BN. A method for detecting abasic sites in living cells: Age-dependent changes in base excision repair. Proceedings of the National Academy of Sciences of the United States of America. 2000 11/29/accepted;97(2):686-91.
9. Azzam EI, Little JB. The radiation-induced bystander effect: evidence and significance. Hum Exp Toxicol. 2004 Feb;23(2):61-5.
10. Banerjee A, Yang W, Karplus M, Verdine GL. Structure of a repair enzyme interrogating undamaged DNA elucidates recognition of damaged DNA. Nature. [10.1038/nature03458]. 2005 03/31/print;434(7033):612-8.
11. Beard BC, Wilson SH, Smerdon MJ. Suppressed catalytic activity of base excision repair enzymes on rotationally positioned uracil in nucleosomes. Proc Natl Acad Sci U S A. 2003 Jun 24;100(13):7465-70.
12. Bennett RA, Wilson DM, 3rd, Wong D, Demple B. Interaction of human apurinic endonuclease and DNA polymerase beta in the base excision repair pathway. Proc Natl Acad Sci U S A. 1997 Jul 08;94(14):7166-9.
13. Bessho T. Nucleotide excision repair 3' endonuclease XPG stimulates the activity of base excision repairenzyme thymine glycol DNA glycosylase. Nucleic Acids Res. 1999 Feb 15;27(4):979-83.
14. Bienko M, Green CM, Crosetto N, Rudolf F, Zapart G, Coull B, et al. Ubiquitin-binding domains in Y-family polymerases regulate translesion synthesis. Science. 2005 Dec 16;310(5755):1821-4.
15. Boal AK, Genereux JC, Sontz PA, Gralnick JA, Newman DK, Barton JK. Redox signaling between DNA repair proteins for efficient lesion detection. Proceedings of the National Academy of Sciences. 2009;106(36):15237-42.
16. Boon EM, Livingston AL, Chmiel NH, David SS, Barton JK. DNA-mediated charge transport for DNA repair. Proceedings of the National Academy of Sciences. 2003;100(22):12543-7.
17. Bose SN, Davies RJ, Sethi SK, McCloskey JA. Formation of an adenine-thymine photoadduct in the deoxydinucleoside monophosphate d(TpA) and in DNA. Science. 1983 May 13;220(4598):723-5.
18. Braselmann H, Michna A, Hess J, Unger K. CFAssay: statistical analysis of the colony formation assay. Radiat Oncol. 2015;10:223.
19. Brem R, Hall J. XRCC1 is required for DNA single-strand break repair in human cells. Nucleic Acids Res. 2005;33(8):2512-20.
20. Bremm A, Komander D. Emerging roles for Lys11-linked polyubiquitin in cellular regulation. Trends Biochem Sci. 2011 Jul;36(7):355-63.
21. Bruner SD, Norman DP, Verdine GL. Structural basis for recognition and repair of the endogenous mutagen 8-oxoguanine in DNA. Nature. 2000 Feb 24;403(6772):859-66.
22. Budhidarmo R, Nakatani Y, Day CL. RINGs hold the key to ubiquitin transfer. Trends in Biochemical Sciences. 2012 2//;37(2):58-65.
23. Cabelof DC. Haploinsufficiency in mouse models of DNA repair deficiency: modifiers of penetrance. Cell Mol Life Sci. 2012 Mar;69(5):727-40.
24. Caldecott KW. Single-strand break repair and genetic disease. Nat Rev Genet. 2008 Aug;9(8):619-31.
25. Carter RJ, Parsons JL. Base Excision Repair, a Pathway Regulated by Posttranslational Modifications. Mol Cell Biol2016. p. 1426-37.
26. Chan MK, Ocampo-Hafalla MT, Vartanian V, Jaruga P, Kirkali G, Koenig KL, et al. Targeted deletion of the genes encoding NTH1 and NEIL1 DNA N-glycosylases reveals the existence of novel carcinogenic oxidative damage to DNA. DNA Repair (Amst). [Research Support, N.I.H., Extramural]. 2009 Jul 4;8(7):786-94.

27. Chen D, Kon N, Li M, Zhang W, Qin J, Gu W. ARF-BP1/Mule is a critical mediator of the ARF tumor suppressor. Cell. 2005 Jul 1;121(7):1071-83.
28. Cheng KC, Cahill DS, Kasai H, Nishimura S, Loeb LA. 8-Hydroxyguanine, an abundant form of oxidative DNA damage, causes G----T and A----C substitutions. J Biol Chem. 1992 Jan 05;267(1):166-72.
29. Chevillard S, Radicella JP, Levalois C, Lebeau J, Poupon MF, Oudard S, et al. Mutations in OGG1, a gene involved in the repair of oxidative DNA damage, are found in human lung and kidney tumours. Oncogene. 1998;16(23):3083-6.
30. Chou K-M, Cheng Y-C. An exonucleolytic activity of human apurinic/apyrimidinic endonuclease on 3|[prime]| mispaired DNA. Nature. 2002 2002-02-07;415(6872):655-9.
31. Christmann M, Tomicic MT, Roos WP, Kaina B. Mechanisms of human DNA repair: an update. Toxicology. 2003 2003/11/15/;193(1):3-34.
32. Cooke MS, Evans MD, Dizdaroglu M, Lunec J. Oxidative DNA damage: mechanisms, mutation, and disease. The FASEB Journal. 2003;17(10):1195-214.
33. Cortazar D, Kunz C, Selfridge J, Lettieri T, Saito Y, MacDougall E, et al. Embryonic lethal phenotype reveals a function of TDG in maintaining epigenetic stability. Nature. 2011 Feb 17;470(7334):419-23.
34. Danielsen JMR, Sylvestersen KB, Bekker-Jensen S, Szklarczyk D, Poulsen JW, Horn H, et al. Mass Spectrometric Analysis of Lysine Ubiquitylation Reveals Promiscuity at Site Level*. Mol Cell Proteomics2011.
35. Davis AJ, Chen DJ. DNA double strand break repair via non-homologous end-joining. Transl Cancer Res. 2013 Jun;2(3):130-43.
36. Deng L, Wang C, Spencer E, Yang L, Braun A, You J, et al. Activation of the IκB Kinase Complex by TRAF6 Requires a Dimeric Ubiquitin-Conjugating Enzyme Complex and a Unique Polyubiquitin Chain. Cell. 2000 10/13/;103(2):351-61.
37. Diakowska D, Lewandowski A, Kopec W, Diakowski W, Chrzanowska T. Oxidative DNA damage and total antioxidant status in serum of patients with esophageal squamous cell carcinoma. Hepatogastroenterology. 2007 Sep;54(78):1701-4.
38. Dianov G, Price A, Lindahl T. Generation of single-nucleotide repair patches following excision of uracil residues from DNA. Mol Cell Biol. 1992 Apr;12(4):1605-12.
39. Dianov GL, Parsons JL. Co-ordination of DNA single strand break repair. DNA Repair (Amst). 2007 Apr 1;6(4):454-60.
40. Dianova, II, Sleeth KM, Allinson SL, Parsons JL, Breslin C, Caldecott KW, et al. XRCC1–DNA polymerase β interaction is required for efficient base excision repair. Nucleic Acids Res2004. p. 2550-5.
41. Diderich K, Alanazi M, Hoeijmakers J. Premature aging and cancer in nucleotide excision repair-disorders. DNA Repair (Amst). 2011 Jul 15;10(7):772-80.
42. Dizdaroglu M, Karahalil B, Sentürker S, Buckley TJ, Roldán-Arjona T. Excision of Products of Oxidative DNA Base Damage by Human NTH1 Protein. Biochemistry. 1999 1999/01/01;38(1):243-6.
43. Dorn J, Ferrari E, Imhof R, Ziegler N, Hübscher U. Regulation of Human MutYH DNA Glycosylase by the E3 Ubiquitin Ligase Mule. The Journal of Biological Chemistry. 2014 01/17

11/20/received

01/16/revised;289(10):7049-58.
44. Dupont S, Mamidi A, Cordenonsi M, Montagner M, Zacchigna L, Adorno M, et al. FAM/USP9x, a deubiquitinating enzyme essential for TGFbeta signaling, controls Smad4 monoubiquitination. Cell. 2009 Jan 09;136(1):123-35.
45. Dzhekova-Stojkova S, Bogdanska J, Stojkova Z. Peroxisome proliferators: their biological and toxicological effects. Clin Chem Lab Med. 2001 Jun;39(6):468-74.
46. Edmonds MJ, Carter RJ, Nickson CM, Williams SC, Parsons JL. Ubiquitylation-dependent regulation of NEIL1 by Mule and TRIM26 is required for the cellular DNA damage response. Nucleic Acids Research. 2017 10/18

10/11/accepted

10/06/revised

05/20/received;45(2):726-38.
47. Edmonds MJ, Parsons JL. Regulation of base excision repair proteins by ubiquitylation. Exp Cell Res. 2014 Nov 15;329(1):132-8.
48. Edmonds MJ, Parsons JL. Regulation of base excision repair proteins by ubiquitylation. Exp Cell Res. [Review]. 2014 Nov 15;329(1):132-8.
49. Eide L, Luna L, Gustad EC, Henderson PT, Essigmann JM, Demple B, et al. Human Endonuclease III Acts Preferentially on DNA Damage Opposite Guanine Residues in DNA. Biochemistry. 2001 2001/06/01;40(22):6653-9.
50. Elabd S, Cato ACB, Blattner C. Tripartite Motif Proteins-A Protein Family Strongly Linked to Cancer. Ann Pharmacol Pharm 2017; 2 (10).1057.

51. Elder RH, Dianov GL. Repair of Dihydrouracil Supported by Base Excision Repair in mNTH1 Knock-out Cell Extracts. J Biol Chem. 2002 Dec 27;277(52):50487-90.
52. Fantini D, Moritz E, Auvré F, Amouroux R, Campalans A, Epe B, et al. Rapid inactivation and proteasome-mediated degradation of OGG1 contribute to the synergistic effect of hyperthermia on genotoxic treatments. DNA Repair. 2013 3/1/;12(3):227-37.
53. Franken NA, Rodermond HM, Stap J, Haveman J, van Bree C. Clonogenic assay of cells in vitro. Nat Protoc. 2006;1(5):2315-9.
54. Friedman JI, Majumdar A, Stivers JT. Nontarget DNA binding shapes the dynamic landscape for enzymatic recognition of DNA damage. Nucleic Acids Research. 2009;37(11):3493-500.
55. Galick HA, Kathe S, Liu M, Robey-Bond S, Kidane D, Wallace SS, et al. Germ-line variant of human NTH1 DNA glycosylase induces genomic instability and cellular transformation. Proc Natl Acad Sci U S A. 2013 Aug 27;110(35):14314-9.
56. Gallagher PE, Duker NJ. Formation of purine photoproducts in a defined human DNA sequence. Photochem Photobiol. 1989 May;49(5):599-605.
57. Gerlach B, Cordier SM, Schmukle AC, Emmerich CH, Rieser E, Haas TL, et al. Linear ubiquitination prevents inflammation and regulates immune signalling. Nature. [10.1038/nature09816]. 2011 03/31/print;471(7340):591-6.
58. Goto M, Shinmura K, Igarashi H, Kobayashi M, Konno H, Yamada H, et al. Altered expression of the human base excision repair gene NTH1 in gastric cancer. Carcinogenesis. 2009 Aug;30(8):1345-52.
59. Grivennikov SI, Greten FR, Karin M. Immunity, Inflammation, and Cancer. Cell. 2010;140(6):883-99.
60. Haas TL, Emmerich CH, Gerlach B, Schmukle AC, Cordier SM, Rieser E, et al. Recruitment of the linear ubiquitin chain assembly complex stabilizes the TNF-R1 signaling complex and is required for TNF-mediated gene induction. Mol Cell. 2009 2009//;36.
61. Hadian K, Griesbach RA, Dornauer S, Wanger TM, Nagel D, Metlitzky M, et al. NEMO interaction with linear and K63 ubiquitin chains contributes to NF-κB activation. Journal of Biological Chemistry. 2011.
62. Hardeland U, Steinacher R, Jiricny J, Schar P. Modification of the human thymine-DNA glycosylase by ubiquitin-like proteins facilitates enzymatic turnover. Embo J. 2002 Mar 15;21(6):1456-64.
63. Hatakeyama S. TRIM proteins and cancer. Nat Rev Cancer. [Research Support, Non-U.S. Gov't]. 2011 Nov;11(11):792-804.
64. Hegde ML, Hazra TK, Mitra S. Functions of disordered regions in mammalian early base excision repair proteins. Cell Mol Life Sci. 2010 Nov;67(21):3573-87.
65. Hei TK, Zhou H, Ivanov VN, Hong M, Lieberman HB, Brenner DJ, et al. Mechanism of radiation-induced bystander effects: a unifying model. J Pharm Pharmacol. 2008 Aug;60(8):943-50.
66. Hoogstraten D, Nigg AL, Heath H, Mullenders LH, van Driel R, Hoeijmakers JH, et al. Rapid switching of TFIIH between RNA polymerase I and II transcription and DNA repair in vivo. Mol Cell. 2002 Nov;10(5):1163-74.
67. Idriss HT, Al-Assar O, Wilson SH. DNA polymerase β. The International Journal of Biochemistry & Cell Biology. 2002 4//;34(4):321-4.
68. Ikeda S, Biswas T, Roy R, Izumi T, Boldogh I, Kurosky A, et al. Purification and Characterization of Human NTH1, a Homolog ofEscherichia coli Endonuclease III: DIRECT IDENTIFICATION OF LYS-212 AS THE ACTIVE NUCLEOPHILIC RESIDUE. Journal of Biological Chemistry. 1998;273(34):21585-93.
69. Ikeda S, Kohmoto T, Tabata R, Seki Y. Differential intracellular localization of the human and mouse endonuclease III homologs and analysis of the sorting signals. DNA Repair. 2002 10/1/;1(10):847-54.
70. Jackson SP. Sensing and repairing DNA double-strand breaks. Carcinogenesis. 2002;23(5):687-96.
71. Jackson SP. Sensing and repairing DNA double-strand breaks. Carcinogenesis. 2017;23(5):687-96.
72. Jacobs AL, Schär P. DNA glycosylases: in DNA repair and beyond. Chromosoma. 2012 11/0310/11/accepted;121(1):1-20.

73. Jin J, Li X, Gygi SP, Harper JW. Dual E1 activation systems for ubiquitin differentially regulate E2 enzyme charging. Nature. [10.1038/nature05902]. 2007 06/28/print;447(7148):1135-8.
74. Joo H-Y, Zhai L, Yang C, Nie S, Erdjument-Bromage H, Tempst P, et al. Regulation of cell cycle progression and gene expression by H2A deubiquitination. Nature. [10.1038/nature06256]. 2007 10/25/print;449(7165):1068-72.
75. Kaiser SE, Riley BE, Shaler TA, Trevino RS, Becker CH, Schulman H, et al. Protein standard absolute quantification (PSAQ) method for the measurement of cellular ubiquitin pools. Nat Meth. [10.1038/nmeth.1649]. 2011 08//print;8(8):691-6.
76. Kao JY, Goljer I, Phan TA, Bolton PH. Characterization of the effects of a thymine glycol residue on the structure, dynamics, and stability of duplex DNA by NMR. The Journal of biological chemistry. 1993 Aug 25;268(24):17787-93.
77. Karran P, Lindahl T. Hypoxanthine in deoxyribonucleic acid: generation by heat-induced hydrolysis of adenine residues and release in free form by a deoxyribonucleic acid glycosylase from calf thymus. Biochemistry. 1980 Dec 23;19(26):6005-11.

78. Katafuchi A, Nakano T, Masaoka A, Terato H, Iwai S, Hanaoka F, et al. Differential specificity of human and Escherichia coli endonuclease III and VIII homologues for oxidative base lesions. J Biol Chem. 2004 Apr 2;279(14):14464-71.
79. Kim HT, Kim KP, Lledias F, Kisselev AF, Scaglione KM, Skowyra D, et al. Certain Pairs of Ubiquitin-conjugating Enzymes (E2s) and Ubiquitin-Protein Ligases (E3s) Synthesize Nondegradable Forked Ubiquitin Chains Containing All Possible Isopeptide Linkages. Journal of Biological Chemistry. 2007;282(24):17375-86.
80. Klungland A, Höss M, Gunz D, Constantinou A, Clarkson SG, Doetsch PW, et al. Base Excision Repair of Oxidative DNA Damage Activated by XPG Protein. Molecular Cell. 1999 1999/01/01/;3(1):33-42.
81. Komander D, Rape M. The ubiquitin code. Annu Rev Biochem. 2012;81:203-29.
82. Kucherlapati M, Yang K, Kuraguchi M, Zhao J, Lia M, Heyer J, et al. Haploinsufficiency of Flap endonuclease (Fen1) leads to rapid tumor progression. Proc Natl Acad Sci U S A. 2002 Jul 23;99(15):9924-9.
83. Kulak NA, Pichler G, Paron I, Nagaraj N, Mann M. Minimal, encapsulated proteomic-sample processing applied to copy-number estimation in eukaryotic cells. Nature Methods. [Article]. 2014;11(3):319-24.
84. Laat WLd, Jaspers NGJ, Hoeijmakers JHJ. Molecular mechanism of nucleotide excision repair. 1999 1999-04-01.
85. Lindahl T. An N-Glycosidase from Escherichia coli That Releases Free Uracil from DNA Containing Deaminated Cytosine Residues. Proceedings of the National Academy of Sciences. 1974;71(9):3649-53.
86. Lindahl T. DNA repair enzymes. Annu Rev Biochem. 1982;51:61-87.
87. Lindahl T. Instability and decay of the primary structure of DNA. Nature. [10.1038/362709a0]. 1993 04/22/print;362(6422):709-15.
88. Lindahl T, Nyberg B. Rate of depurination of native deoxyribonucleic acid. Biochemistry. 1972 1972/09/01;11(19):3610-8.
89. Liu D, Prasad R, Wilson SH, DeRose EF, Mullen GP. Three-dimensional solution structure of the N-terminal domain of DNA polymerase beta and mapping of the ssDNA interaction interface. Biochemistry. 1996 May 21;35(20):6188-200.
90. Liu X, Roy R. Truncation of Amino-terminal Tail Stimulates Activity of Human Endonuclease III (hNTH1). Journal of Molecular Biology. 2002 8/9/;321(2):265-76.
91. Lomax ME, Cunniffe S, O'Neill P. 8-OxoG retards the activity of the ligase III/XRCC1 complex during the repair of a single-strand break, when present within a clustered DNA damage site. DNA Repair (Amst). 2004 Mar 4;3(3):289-99.
92. Lomax ME, Folkes LK, O'Neill P. Biological consequences of radiation-induced DNA damage: relevance to radiotherapy. Clin Oncol (R Coll Radiol). 2013 Oct;25(10):578-85.
93. Lu AL, Li X, Gu Y, Wright PM, Chang D-Y. Repair of oxidative DNA damage. Cell Biochemistry and Biophysics. 2001 2001//;35(2):141-70.
94. Ludwig DL, MacInnes MA, Takiguchi Y, Purtymun PE, Henrie M, Flannery M, et al. A murine AP-endonuclease gene-targeted deficiency with post-implantation embryonic progression and ionizing radiation sensitivity. Mutat Res. 1998 Oct 21;409(1):17-29.
95. Luna L, Bjoras M, Hoff E, Rognes T, Seeberg E. Cell-cycle regulation, intracellular sorting and induced overexpression of the human NTH1 DNA glycosylase involved in removal of formamidopyrimidine residues from DNA. Mutat Res. 2000 Jul 25;460(2):95-104.
96. Mao Z, Bozzella M, Seluanov A, Gorbunova V. Comparison of nonhomologous end joining and homologous recombination in human cells. DNA Repair (Amst). 2008 Oct 1;7(10):1765-71.
97. Marenstein DR, Chan MK, Altamirano A, Basu AK, Boorstein RJ, Cunningham RP, et al. Substrate Specificity of Human Endonuclease III (hNTH1): EFFECT OF HUMAN APE1 ON hNTH1 ACTIVITY. Journal of Biological Chemistry. 2003;278(11):9005-12.
98. Marenstein DR, Ocampo MTA, Chan MK, Altamirano A, Basu AK, Boorstein RJ, et al. Stimulation of Human Endonuclease III by Y Box-binding Protein 1 (DNA-binding Protein B): INTERACTION BETWEEN A BASE EXCISION REPAIR ENZYME AND A TRANSCRIPTION FACTOR. Journal of Biological Chemistry. 2001;276(24):21242-9.
99. Matsumoto Y, Kim K. Excision of deoxyribose phosphate residues by DNA polymerase beta during DNA repair. Science. 1995 Aug 04;269(5224):699-702.
100. Matsumura Y, Ananthaswamy HN. Toxic effects of ultraviolet radiation on the skin. Toxicology and Applied Pharmacology. 2004 3/15/;195(3):298-308.
101. McWilliam H, Li W, Uludag M, Squizzato S, Park YM, Buso N, et al. Analysis Tool Web Services from the EMBL-EBI. Nucleic Acids Res. 2013 Jul;41(Web Server issue):W597-600.
102. Meisenberg C, Tait PS, Dianova II, Wright K, Edelmann MJ, Ternette N, et al. Ubiquitin ligase UBR3 regulates cellular levels of the essential DNA repair protein APE1 and is required for genome stability. Nucleic Acids Research. 2011;40(2):701-11.
103. Meyer H-J, Rape M. Enhanced Protein Degradation by Branched Ubiquitin Chains. Cell. 2014 5/8/;157(4):910-21.
104. Miyabe I, Zhang QM, Kino K, Sugiyama H, Takao M, Yasui A, et al. Identification of 5-formyluracil DNA glycosylase activity of human hNTH1 protein. Nucleic Acids Research. 2002;30(15):3443-8.

105. Miyake H, Hara I, Kamidono S, Eto H. Oxidative DNA damage in patients with prostate cancer and its response to treatment. J Urol. 2004 Apr;171(4):1533-6.
106. Mol C, David H, John T. Abasic site recognition by two apurinic/apyrimidinic endonuclease families in DNA base excision repair: the 3' ends justify the means. 2000 30 August 2000;460(Issues 3–4):211–29.
107. Monia BP, Ecker DJ, Jonnalagadda S, Marsh J, Gotlib L, Butt TR, et al. Gene synthesis, expression, and processing of human ubiquitin carboxyl extension proteins. Journal of Biological Chemistry. [Article]. 1989;264(7):4093-103.
108. Morales JC, Li L, Fattah FJ, Dong Y, Bey EA, Patel M, et al. Review of Poly (ADP-ribose) Polymerase (PARP) Mechanisms of Action and Rationale for Targeting in Cancer and Other Diseases. Crit Rev Eukaryot Gene Expr. 2014;24(1):15-28.
109. Nakagawa T, Hosogane M, Nakagawa M, Morohoshi A, Funayama R, Nakayama K. Transforming Growth Factor beta-Induced Proliferative Arrest Mediated by TRIM26-Dependent TAF7 Degradation and Its Antagonism by MYC. Mol Cell Biol. 2018 Mar 1;38(5).
110. Nakamura J, Swenberg JA. Endogenous apurinic/apyrimidinic sites in genomic DNA of mammalian tissues. Cancer Res. 1999;59(11):2522-6.
111. Newbold RF, Warren W, Medcalf ASC, Amos J. Mutagenicity of carcinogenic methylating agents is associated with a specific DNA modification. Nature. [10.1038/283596a0]. 1980 02/07/print;283(5747):596-9.
112. Nickson CM, Parsons JL. Monitoring regulation of DNA repair activities of cultured cells in-gel using the comet assay. Front Genet. 2014;5.
113. Nikjoo H, O'Neill P, Goodhead DT, Terrissol M. Computational modelling of low-energy electron-induced DNA damage by early physical and chemical events. Int J Radiat Biol. 1997 May;71(5):467-83.
114. Ostling O, Johanson KJ. Microelectrophoretic study of radiation-induced DNA damages in individual mammalian cells. Biochem Biophys Res Commun. 1984 Aug 30;123(1):291-8.
115. Ozato K, Shin D-M, Chang T-H, Morse HC. TRIM family proteins and their emerging roles in innate immunity. Nature reviews Immunology. 2008;8(11):849-60.
116. Ozkan E, Yu H, Deisenhofer J. Mechanistic insight into the allosteric activation of a ubiquitin-conjugating enzyme by RING-type ubiquitin ligases. Proc Natl Acad Sci U S A. 2005 Dec 27;102(52):18890-5.
117. Parikh SS, Mol CD, Slupphaug G, Bharati S, Krokan HE, Tainer JA. Base excision repair initiation revealed by crystal structures and binding kinetics of human uracil-DNA glycosylase with DNA. Embo j. 1998 Sep 01;17(17):5214-26.
118. Parsons JL, Dianov GL. Co-ordination of base excision repair and genome stability. DNA Repair (Amst). [Research Support, Non-U.S. Gov't

Review]. 2013 May 1;12(5):326-33.
119. Parsons JL, Dianova, II, Allinson SL, Dianov GL. DNA polymerase beta promotes recruitment of DNA ligase III alpha-XRCC1 to sites of base excision repair. Biochemistry. 2005 Aug 09;44(31):10613-9.
120. Parsons JL, Dianova, II, Allinson SL, Dianov GL. Poly(ADP-ribose) polymerase-1 protects excessive DNA strand breaks from deterioration during repair in human cell extracts. Febs J. 2005 Apr;272(8):2012-21.
121. Parsons JL, Dianova, II, Khoronenkova SV, Edelmann MJ, Kessler BM, Dianov GL. USP47 is a deubiquitylating enzyme that regulates base excision repair by controlling steady-state levels of DNA polymerase beta. Mol Cell. [Research Support, Non-U.S. Gov't]. 2011 Mar 4;41(5):609-15.
122. Parsons JL, Dianova II, Dianov GL. APE1 is the major 3'-phosphoglycolate activity in human cell extracts. Nucleic Acids Research. 2004 07/06

04/30/received

06/09/revised

06/09/accepted;32(12):3531-6.
123. Parsons JL, Elder RH. DNA N-glycosylase deficient mice: a tale of redundancy. Mutat Res. 2003 Oct 29;531(1-2):165-75.
124. Parsons JL, Khoronenkova SV, Dianova, II, Ternette N, Kessler BM, Datta PK, et al. Phosphorylation of PNKP by ATM prevents its proteasomal degradation and enhances resistance to oxidative stress. Nucleic Acids Res. [Research Support, N.I.H., Extramural

Research Support, Non-U.S. Gov't

Research Support, U.S. Gov't, Non-P.H.S.]. 2012 Dec;40(22):11404-15.
125. Parsons JL, Tait PS, Finch D, Dianova, II, Allinson SL, Dianov GL. CHIP-mediated degradation and DNA damage-dependent stabilization regulate base excision repair proteins. Mol Cell. 2008 Feb 29;29(4):477-87.
126. Parsons JL, Tait PS, Finch D, Dianova II, Edelmann MJ, Khoronenkova SV, et al. Ubiquitin ligase ARF-BP1/Mule modulates base excision repair. 2009 2009-10-21.
127. Pickart CM. Mechanisms underlying ubiquitination. Annu Rev Biochem. 2001;70:503-33.

128. Podlutsky AJ, Dianova, II, Podust VN, Bohr VA, Dianov GL. Human DNA polymerase beta initiates DNA synthesis during long-patch repair of reduced AP sites in DNA. Embo j. 2001 Mar 15;20(6):1477-82.
129. Powell SN, Kachnic LA. Roles of BRCA1 and BRCA2 in homologous recombination, DNA replication fidelity and the cellular response to ionizing radiation. Oncogene. 2003 Sep 1;22(37):5784-91.
130. Prasad A, Wallace SS, Pederson DS. Initiation of Base Excision Repair of Oxidative Lesions in Nucleosomes by the Human, Bifunctional DNA Glycosylase NTH1. Molecular and Cellular Biology. 2007 10/08

05/04/received

06/18/revised

09/26/accepted;27(24):8442-53.
131. Preston BD, Singer B, Loeb LA. Mutagenic potential of O4-methylthymine in vivo determined by an enzymatic approach to site-specific mutagenesis. Proc Natl Acad Sci U S A. 1986 Nov;83(22):8501-5.
132. Puebla-Osorio N, Lacey DB, Alt FW, Zhu C. Early embryonic lethality due to targeted inactivation of DNA ligase III. Mol Cell Biol. 2006 May;26(10):3935-41.
133. Ran Y, Zhang J, Liu LL, Pan ZY, Nie Y, Zhang HY, et al. Autoubiquitination of TRIM26 links TBK1 to NEMO in RLR-mediated innate antiviral immune response. J Mol Cell Biol. 2016 Feb;8(1):31-43.
134. Rastogi RP, Richa, Kumar A, Tyagi MB, Sinha RP. Molecular mechanisms of ultraviolet radiation-induced DNA damage and repair. J Nucleic Acids. 2010;2010:592980.
135. Riley PA. Free radicals in biology: oxidative stress and the effects of ionizing radiation. Int J Radiat Biol. 1994 Jan;65(1):27-33.
136. Rydberg B, Lindahl T. Nonenzymatic methylation of DNA by the intracellular methyl group donor S-adenosyl-L-methionine is a potentially mutagenic reaction. Embo j. 1982;1(2):211-6.
137. S.A M, Lord CJ, Ashworth A. Therapeutic Targeting of the DNA Mismatch Repair Pathway. 2010 2010-11-01.
138. Saleh-Gohari N, Helleday T. Conservative homologous recombination preferentially repairs DNA double-strand breaks in the S phase of the cell cycle in human cells. Nucleic Acids Research. 2004;32(12):3683-8.
139. Schrader M, Fahimi HD. Peroxisomes and oxidative stress. Biochim Biophys Acta. 2006 Dec;1763(12):1755-66.
140. Schröfelbauer B, Yu Q, Zeitlin SG, Landau NR. Human Immunodeficiency Virus Type 1 Vpr Induces the Degradation of the UNG and SMUG Uracil-DNA Glycosylases. Journal of Virology. 2005 05/04/received

05/25/accepted;79(17):10978-87.
141. Schumacher F-R, Wilson G, Day CL. The N-Terminal Extension of UBE2E Ubiquitin-Conjugating Enzymes Limits Chain Assembly. Journal of Molecular Biology. 2013 11/15/;425(22):4099-111.
142. Selvaraju K, Mazurkiewicz M, Wang X, Gullbo J, Linder S, D'Arcy P. Inhibition of proteasome deubiquitinase activity: a strategy to overcome resistance to conventional proteasome inhibitors? Drug Resistance Updates. 2015 7//;21–22:20-9.
143. Shapiro R, Danzig M. Acidic hydrolysis of deoxycytidine and deoxyuridine derivatives. General mechanism of deoxyribonucleoside hydrolysis. Biochemistry. 1972 1972/01/01;11(1):23-9.
144. Shen JC, Rideout WM, Jones PA. The rate of hydrolytic deamination of 5-methylcytosine in double-stranded DNA. Nucleic Acids Research. 1994;22(6):972-6.
145. Singh NP, McCoy MT, Tice RR, Schneider EL. A simple technique for quantitation of low levels of DNA damage in individual cells. Exp Cell Res. 1988 Mar;175(1):184-91.
146. Sobol RW, Horton JK, Kuhn R, Gu H, Singhal RK, Prasad R, et al. Requirement of mammalian DNA polymerase-beta in base-excision repair. Nature. 1996 Jan 11;379(6561):183-6.
147. Sun B, Latham KA, Dodson ML, Lloyd RS. Studies on the catalytic mechanism of five DNA glycosylases. Probing for enzyme-DNA imino intermediates. J Biol Chem. 1995 Aug 18;270(33):19501-8.
148. Swenberg JA, Lu K, Moeller BC, Gao L, Upton PB, Nakamura J, et al. Endogenous versus exogenous DNA adducts: their role in carcinogenesis, epidemiology, and risk assessment. Toxicol Sci. 2011 Mar;120 Suppl 1:S130-45.
149. Takao M, Kanno S, Kobayashi K, Zhang QM, Yonei S, van der Horst GT, et al. A back-up glycosylase in Nth1 knock-out mice is a functional Nei (endonuclease VIII) homologue. J Biol Chem. 2002 Nov 1;277(44):42205-13.
150. Tanaka H, Fujita N, Sugimoto R, Urawa N, Horiike S, Kobayashi Y, et al. Hepatic oxidative DNA damage is associated with increased risk for hepatocellular carcinoma in chronic hepatitis C. British Journal of Cancer. 2008 2008-01-29;98(3):580-6.
151. Tebbs RS, Flannery ML, Meneses JJ, Hartmann A, Tucker JD, Thompson LH, et al. Requirement for the Xrcc1 DNA base excision repair gene during early mouse development. Dev Biol. 1999 Apr 15;208(2):513-29.
152. Tell G, Quadrifoglio F, Tiribelli C, Kelley MR. The Many Functions of APE1/Ref-1: Not Only a DNA Repair Enzyme. Antioxid Redox Signal2009. p. 601-19.
153. Thayer MM, Ahern H, Xing D, Cunningham RP, Tainer JA. Novel DNA binding motifs in the DNA repair enzyme endonuclease III crystal structure. Embo j. 1995 Aug 15;14(16):4108-20.

154. Thrower JS, Hoffman L, Rechsteiner M, Pickart CM. Recognition of the polyubiquitin proteolytic signal. The EMBO Journal. [10.1093/emboj/19.1.94]. 2000;19(1):94.
155. Torre LA, Bray F, Siegel RL, Ferlay J, Lortet-Tieulent J, Jemal A. Global cancer statistics, 2012. CA Cancer J Clin. 2015 Mar;65(2):87-108.
156. Trzeciak AR, Nyaga SG, Jaruga P, Lohani A, Dizdaroglu M, Evans MK. Cellular repair of oxidatively induced DNA base lesions is defective in prostate cancer cell lines, PC-3 and DU-145. Carcinogenesis. 2004 Aug;25(8):1359-70.
157. Tsutsumi M, Masutani M, Nozaki T, Kusuoka O, Tsujiuchi T, Nakagama H, et al. Increased susceptibility of poly(ADP-ribose) polymerase-1 knockout mice to nitrosamine carcinogenicity. Carcinogenesis. 2001;22(1):1-3.
158. Tulard A, Hoffschir F, de Boisferon FH, Luccioni C, Bravard A. Persistent oxidative stress after ionizing radiation is involved in inherited radiosensitivity. Free Radic Biol Med. 2003 Jul 1;35(1):68-77.
159. Valavanidis A, Vlachogianni T, Fiotakis C. 8-hydroxy-2' -deoxyguanosine (8-OHdG): A critical biomarker of oxidative stress and carcinogenesis. J Environ Sci Health C Environ Carcinog Ecotoxicol Rev. 2009 Apr;27(2):120-39.
160. Venkatesan K, Rual J-F, Vazquez A, Stelzl U, Lemmens I, Hirozane-Kishikawa T, et al. An empirical framework for binary interactome mapping. Nat Meth. [Article]. 2009 01//print;6(1):83-90.
161. Versteeg Gijs A, Rajsbaum R, Sánchez-Aparicio Maria T, Maestre Ana M, Valdiviezo J, Shi M, et al. The E3-Ligase TRIM Family of Proteins Regulates Signaling Pathways Triggered by Innate Immune Pattern-Recognition Receptors. Immunity. 2013 2013/02/21/;38(2):384-98.
162. Vidal AE, Boiteux S, Hickson ID, Radicella JP. XRCC1 coordinates the initial and late stages of DNA abasic site repair through protein-protein interactions. Embo j. 2001 Nov 15;20(22):6530-9.
163. Vidal AE, Hickson ID, Boiteux S, Radicella JP. Mechanism of stimulation of the DNA glycosylase activity of hOGG1 by the major human AP endonuclease: bypass of the AP lyase activity step. Nucleic Acids Res. 2001 Mar 15;29(6):1285-92.
164. Walczak H, Iwai K, Dikic I. Generation and physiological roles of linear ubiquitin chains. BMC Biology. 2012 2012//;10(1):23.
165. Wallace SS. Biological consequences of free radical-damaged DNA bases. Free radical biology & medicine. 2002 Jul 1;33(1):1-14.
166. Wallace SS. Base excision repair: A critical player in many games. DNA repair. 2014 04/26;19:14-26.
167. Wang P, Zhao W, Zhao K, Zhang L, Gao C. TRIM26 negatively regulates interferon-beta production and antiviral response through polyubiquitination and degradation of nuclear IRF3. PLoS pathogens. 2015 Mar;11(3):e1004726.
168. Wang P, Zhao W, Zhao K, Zhang L, Gao C. TRIM26 Negatively Regulates Interferon-β Production and Antiviral Response through Polyubiquitination and Degradation of Nuclear IRF3. PLoS Pathogens. 2015 03/12

07/06/received

02/04/accepted;11(3):e1004726.
169. Wang Y, He D, Yang L, Wen B, Dai J, Zhang Q, et al. TRIM26 functions as a novel tumor suppressor of hepatocellular carcinoma and its downregulation contributes to worse prognosis. Biochem Biophys Res Commun. 2015 Jul 31;463(3):458-65.
170. Waters LS, Minesinger BK, Wiltrout ME, D'Souza S, Woodruff RV, Walker GC. Eukaryotic Translesion Polymerases and Their Roles and Regulation in DNA Damage Tolerance. Microbiol Mol Biol Rev2009. p. 134-54.
171. Waters TR, Gallinari P, Jiricny J, Swann PF. Human thymine DNA glycosylase binds to apurinic sites in DNA but is displaced by human apurinic endonuclease 1. J Biol Chem. 1999 Jan 01;274(1):67-74.
172. Watson JD, Crick FH. Molecular structure of nucleic acids. A structure for deoxyribose nucleic acid. 1953. Rev Invest Clin. 2003 Mar-Apr;55(2):108-9.
173. Weinfeld M, Mani RS, Abdou I, Aceytuno RD, Glover JN. Tidying up loose ends: the role of polynucleotide kinase/phosphatase in DNA strand break repair. Trends Biochem Sci. 2011 May;36(5):262-71.
174. Wenzel DM, Lissounov A, Brzovic PS, Klevit RE. UBCH7 reactivity profile reveals parkin and HHARI to be RING/HECT hybrids. Nature. 2011 2011//;474.
175. Weren RD, Ligtenberg MJ, Kets CM, de Voer RM, Verwiel ET, Spruijt L, et al. A germline homozygous mutation in the base-excision repair gene NTHL1 causes adenomatous polyposis and colorectal cancer. Nat Genet. 2015 Jun;47(6):668-71.
176. Wiederhold L, Leppard JB, Kedar P, Karimi-Busheri F, Rasouli-Nia A, Weinfeld M, et al. AP endonuclease-independent DNA base excision repair in human cells. Mol Cell. 2004 Jul 23;15(2):209-20.
177. Wilson D, Barksy D. The major human abasic endonuclease: formation, consequences and repair of abasic lesions in DNA. 2001 10 May 2001;485(4):283–307.
178. Wilson SH, Kunkel TA. Passing the baton in base excision repair. Nat Struct Biol. 2000 Mar;7(3):176-8.
179. Woodhouse BC, Dianova, II, Parsons JL, Dianov GL. Poly(ADP-ribose) polymerase-1 modulates DNA repair capacity and prevents formation of DNA double strand breaks. DNA Repair (Amst). 2008 Jun 01;7(6):932-40.

180. Xanthoudakis S, Miao GG, Curran T. The redox and DNA-repair activities of Ref-1 are encoded by nonoverlapping domains. Proc Natl Acad Sci U S A. 1994 Jan 4;91(1):23-7.
181. Xanthoudakis S, Smeyne RJ, Wallace JD, Curran T. The redox/DNA repair protein, Ref-1, is essential for early embryonic development in mice. Proc Natl Acad Sci U S A. 1996 Aug 20;93(17):8919-23.
182. Xiao TZ, Suh Y, Longley BJ. MAGE proteins regulate KRAB zinc finger transcription factors and KAP1 E3 ligase activity. Archives of Biochemistry and Biophysics. 2014 12/1/;563:136-44.
183. Yakovchuk P, Protozanova E, Frank-Kamenetskii MD. Base-stacking and base-pairing contributions into thermal stability of the DNA double helix. Nucleic Acids Res. 2006;34(2):564-74.
184. Yang N, Chaudhry MA, Wallace SS. Base excision repair by hNTH1 and hOGG1: a two edged sword in the processing of DNA damage in gamma-irradiated human cells. DNA Repair (Amst). 2006 Jan 5;5(1):43-51.
185. Yang N, Galick H, Wallace SS. Attempted base excision repair of ionizing radiation damage in human lymphoblastoid cells produces lethal and mutagenic double strand breaks. DNA Repair (Amst). 2004 Oct 5;3(10):1323-34.
186. Yau R, Rape M. The increasing complexity of the ubiquitin code. Nat Cell Biol. [Review]. 2016 06//print;18(6):579-86.
187. Ye Y, Rape M. Building ubiquitin chains: E2 enzymes at work. Nat Rev Mol Cell Biol. 2009 2009//;10.
188. Yi J, Huang D, Li X, Jiang G, Dong J, Liu Y. TRIM26 acts as a tumor suppressor in non-small-cell lung cancer. INTERNATIONAL JOURNAL OF CLINICAL AND EXPERIMENTAL PATHOLOGY. 2016;9(6):6385-90.
189. Zeng W, Sun L, Jiang X, Chen X, Hou F, Adhikari A, et al. Reconstitution of the RIG-I Pathway Reveals a Signaling Role of Unanchored Polyubiquitin Chains in Innate Immunity. Cell. 2010 4/16/;141(2):315-30.
190. Zharkov DO, Rosenquist TA, Gerchman SE, Grollman AP. Substrate Specificity and Reaction Mechanism of Murine 8-Oxoguanine-DNA Glycosylase. Journal of Biological Chemistry. 2000;275(37):28607-17.

Chapter 9 - Appendix

1. MASCOT search results showing the protein sequence coverage (**in bold red**, 19%) of TRIM26, following mass spectrometry analysis of the chromatography fraction containing ubiquitylated NTH1, following the final ion exchange chromatography stage during the purification stage

MATRIX SCIENCE **MASCOT Search Results**

Protein View: Q12899

Tripartite motif-containing protein 26 OS=Homo sapiens GN=TRIM26 PE=2 SV=1

Database: UniHumanReviewed
Score: 62
Nominal mass (M_r): 62925
Calculated pI: 4.98

Sequence similarity is available as an NCBI BLAST search of Q12899 against nr.

Search parameters

MS data file: 14015_fraction_25.mgf
Enzyme: Trypsin: cuts C-term side of KR unless next residue is P.
Fixed modifications: Carbamidomethyl (C)
Variable modifications: Oxidation (M)

Protein sequence coverage: 19%

Matched peptides shown in ***bold red***.

```
   1 MATSAPLRSL EEEVTCSICL DYLRDPVTID CGHVFCRSCT TDVRPISGSR
  51 PVCPLCKKPF KKENIRPVWQ LASLVENIER LKVDKGRQPG EVTREQQDAK
 101 LCERHREKLH YYCEDDGKLL CVMCRESREH RPHTAVLMEK AAQPHREKIL
 151 NHLSTLRRDR DKIQGFQAKG EADILAALKK LQDQRQYIVA EFEQGHQFLR
 201 EREEHLLEQL AKLEQELTEG REKFKSRGVG ELARLALVIS ELEGKAQQPA
 251 AELMQDTRDF LNRYPRKKFW VGKPIARVVK KKTGEFSDKL LSLQRGLREF
 301 QGKLLRDLEY KTVSVTLDPQ SASGYLQLSE DWKCVTYTSL YKSAYLHPQQ
 351 FDCEPGVLGS KGFTWGKVYW EVEVEREGWS EDEEEGDEEE EGEEEEEEEE
 401 AGYGDGYDDW ETDEDEESLG DEEEEEEEEE EEVLESCMVG VARDSVKRKG
 451 DLSLRPEDGV WALRLSSSGI WANTSPEAEL FPALRPRRVG IALDYEGGTV
 501 TFTNAESQEL IYTFTATFTR RLVPFLWLKW PGTRLLLRP
```

Unformatted sequence string: 539 residues (for pasting into other applications).

Sort peptides by ◉ Residue Number ○ Increasing Mass ○ Decreasing Mass

Show predicted peptides also

Query	Start – End	Observed	Mr(expt)	Mr(calc)	ppm	M	Score	Expect	Rank	U	Peptide
623	109 – 118	433.8485	1298.5237	1298.5237	-0.032	0	20	0.0093	1	U	K.LHYYCEDDGK.L
100	163 – 169	396.2239	790.4333	790.4337	-0.51	0	15	0.05	1	U	K.IQGFQAK.G
515	235 – 245	586.3510	1170.6875	1170.6860	1.29	0	20	0.045	1	U	R.LALVISELEGK.A
725	246 – 258	729.8534	1457.6923	1457.6933	-0.62	0	12	0.076	1	U	K.AQQPAAELMQDTR.D
726	246 – 258	486.9054	1457.6944	1457.6933	0.77	0	19	0.016	1	U	K.AQQPAAELMQDTR.D
24	259 – 263	332.6742	663.3339	663.3340	-0.19	0	27	0.019	1		R.DFLNR.Y
419	269 – 277	358.5463	1072.6171	1072.6182	-1.03	0	7	0.23	1	U	K.FWVGKPIAR.V
67	290 – 295	365.2340	728.4534	728.4545	-1.43	0	37	0.002	1	U	K.LLSLQR.G
25	307 – 311	334.1682	666.3218	666.3224	-0.94	0	13	0.21	1	U	R.DLEYK.T
488	334 – 342	567.7783	1133.5420	1133.5427	-0.64	0	22	0.0086	1	U	K.CVTYTSLYK.S
858	343 – 361	711.6739	2131.9998	2131.9997	0.069	0	5	0.34	1	U	K.SAYLHPQQFDCEPGVLGSK.G
49	362 – 367	348.1791	694.3437	694.3439	-0.29	0	16	0.032	1	U	K.GFTWGK.V
6	535 – 539	306.2154	610.4162	610.4166	-0.63	0	18	0.042	5	U	R.LLLRP.-

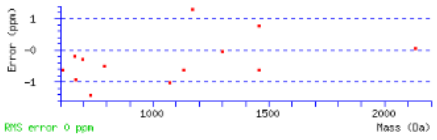

2. Chromatogram following sequencing of the pET28-NTH1-K42, 48, 52, 67R plasmid DNA using the Sanger Source Bioscience sequencing service (Nottingham, UK). The mutated lysine residues have been highlighted in yellow.

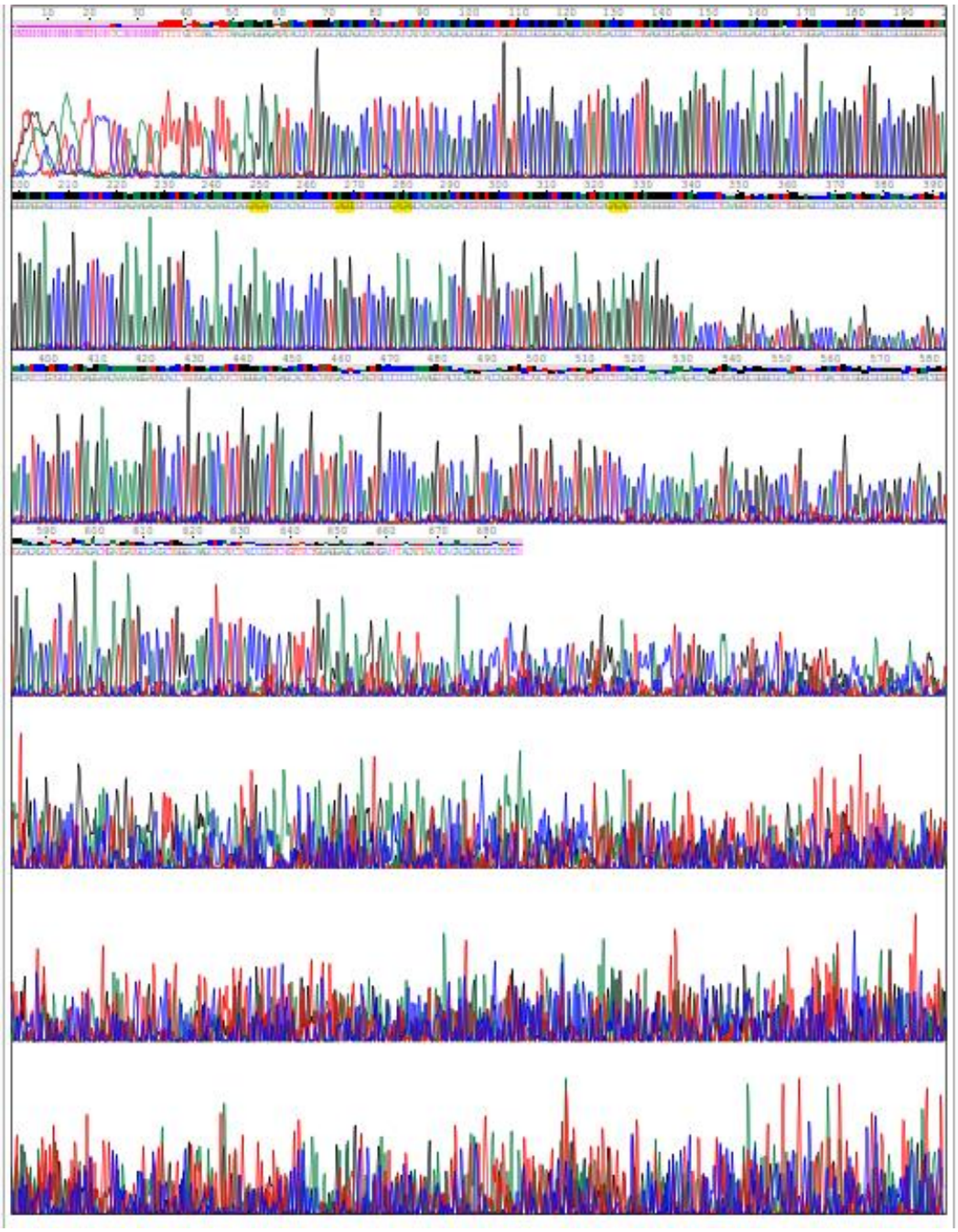

3. Chromatogram following sequencing of the pET28-NTH1-K48, 52R plasmid DNA using the Sanger Source Bioscience sequencing service (Nottingham, UK). The mutated lysine residues have been highlighted in yellow.

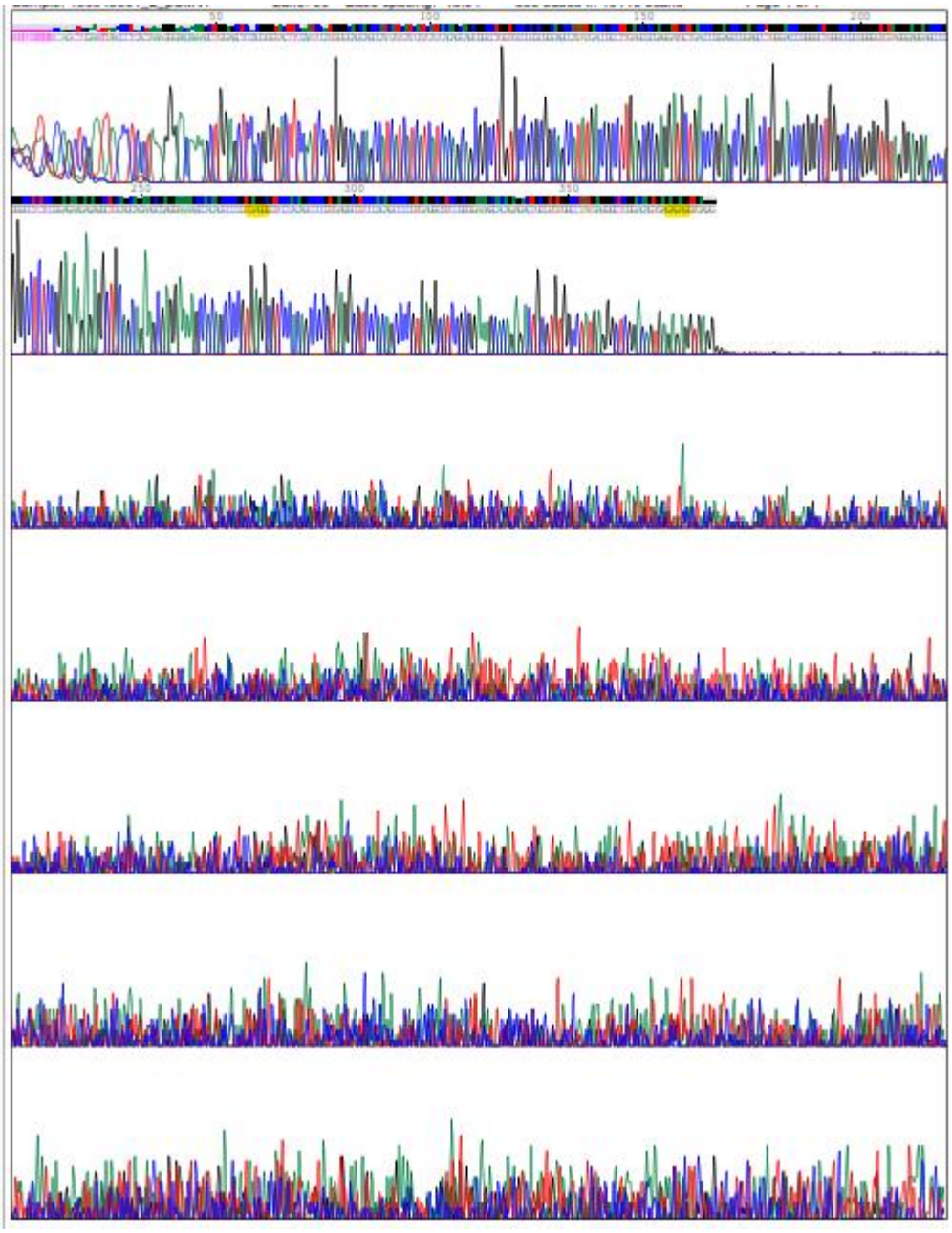

4. Chromatogram following sequencing of the pET28-NTH1-K48R plasmid DNA using the Sanger Source Bioscience sequencing service (Nottingham, UK). The mutated lysine residues have been highlighted in yellow.

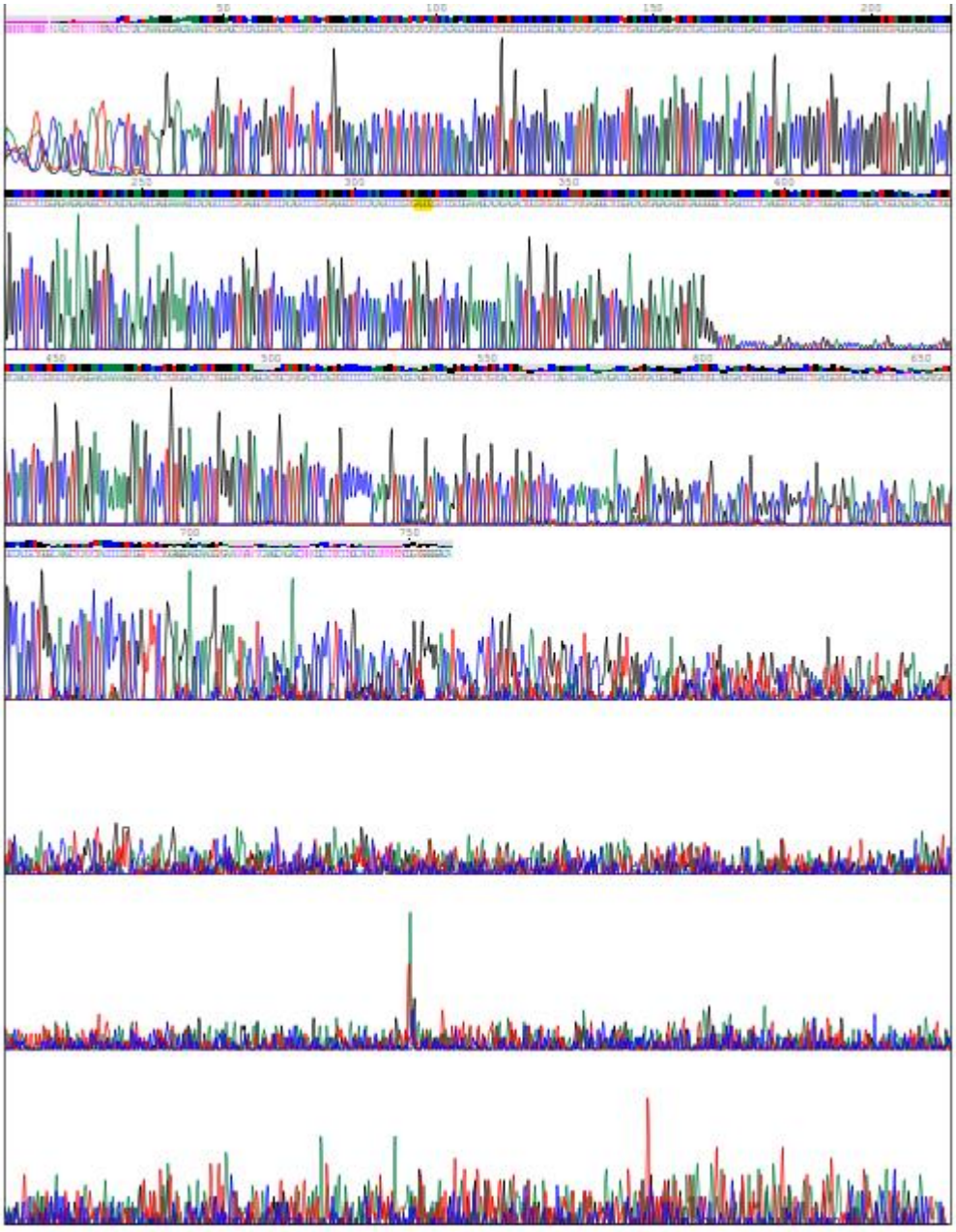

5. Chromatogram following sequencing of the pET28-NTH1-K42R plasmid DNA using the Sanger Source Bioscience sequencing service (Nottingham, UK). The mutated lysine residue has been highlighted in yellow.

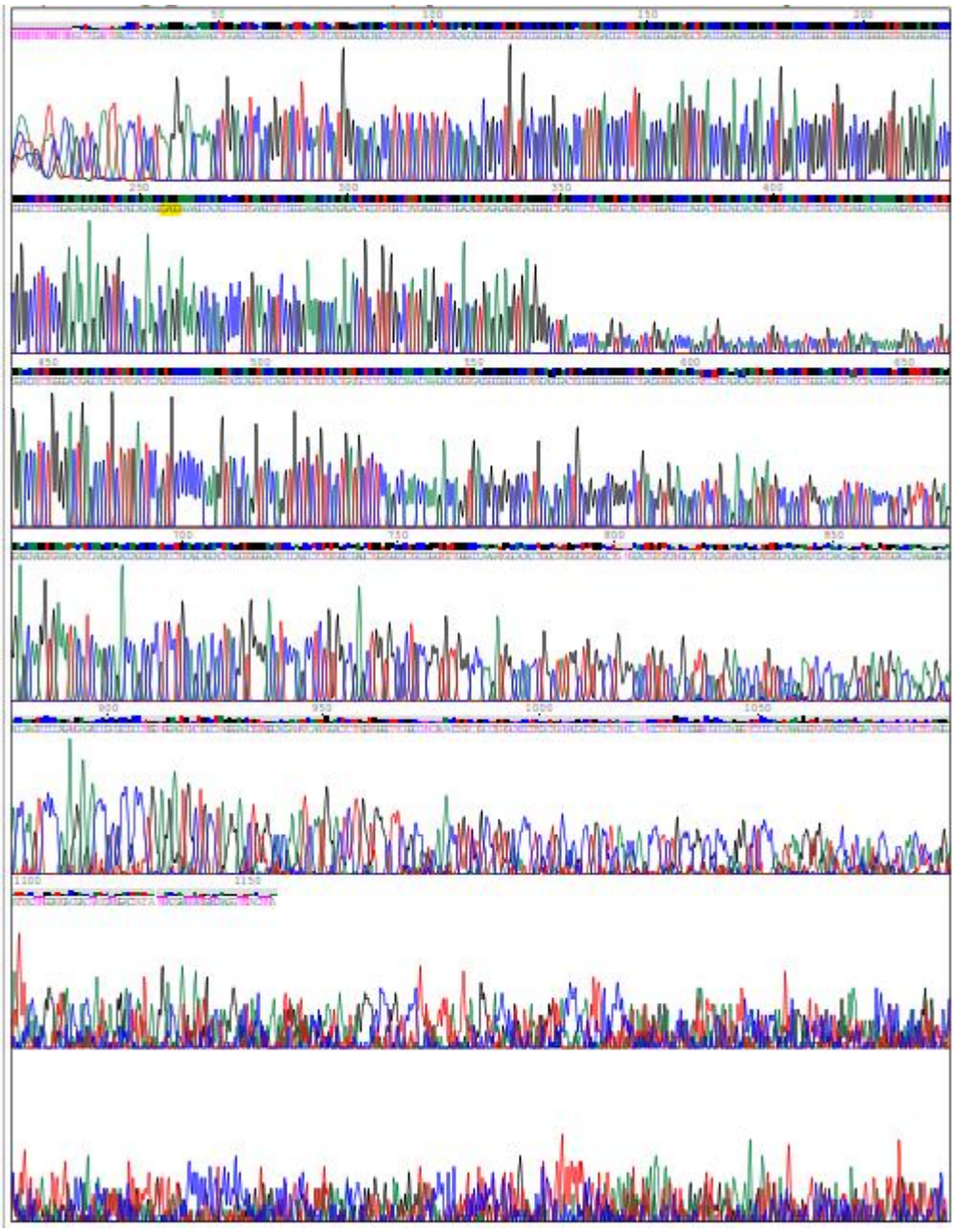

6. Chromatogram following sequencing of the pET28-NTH1-K67R plasmid DNA using the Sanger Source Bioscience sequencing service (Nottingham, UK). The mutated lysine residue has been highlighted in yellow.

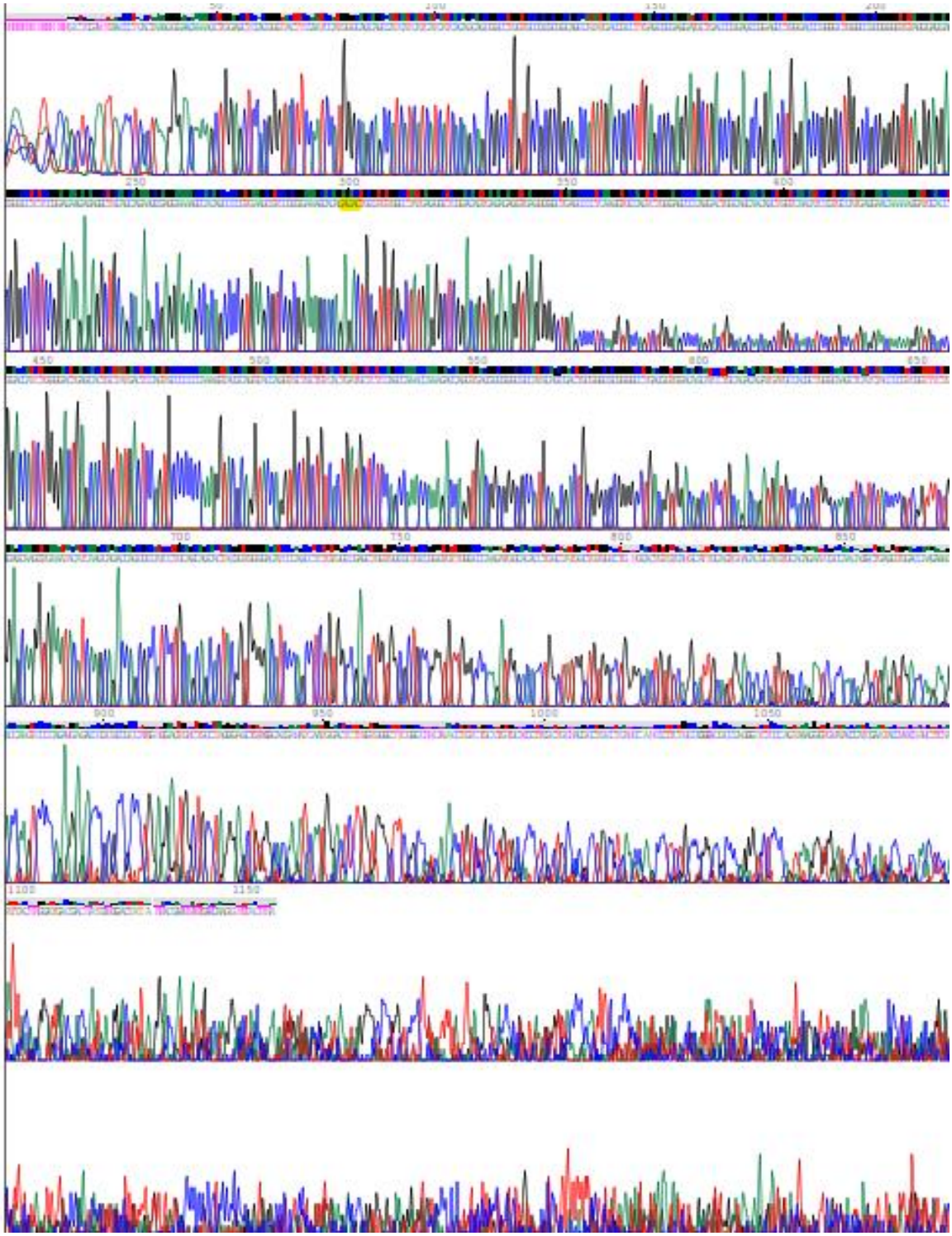

7. Chromatogram following sequencing of the pET28-NTH1-K42R plasmid DNA using the Sanger Source Bioscience sequencing service (Nottingham, UK). The mutated lysine residue has been highlighted in yellow.

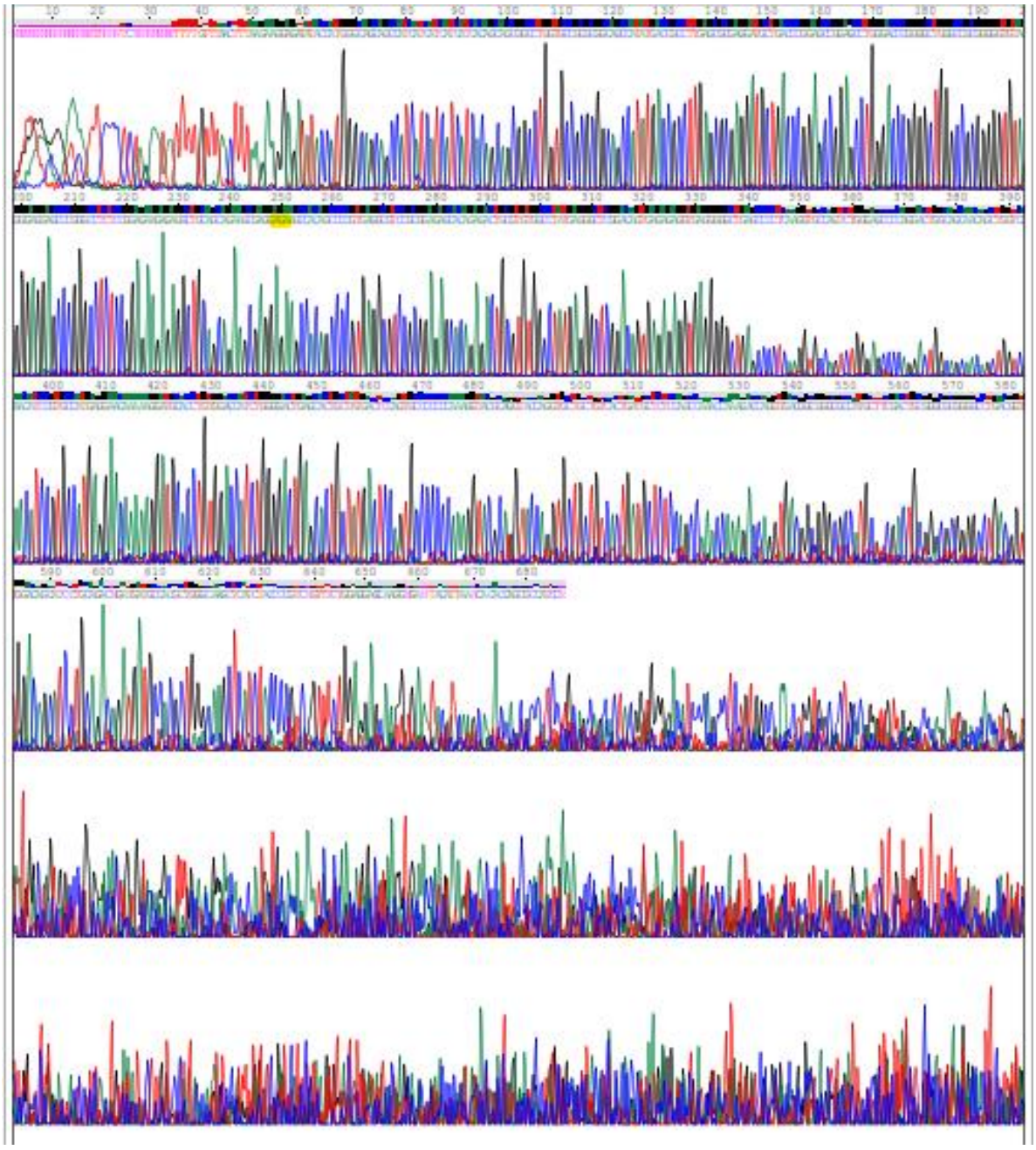

8. Chromatogram following sequencing of the pET28-NTH1-D239Y plasmid DNA using the Sanger Source Bioscience sequencing service (Nottingham, UK). The mutated lysine residue has been highlighted in yellow.

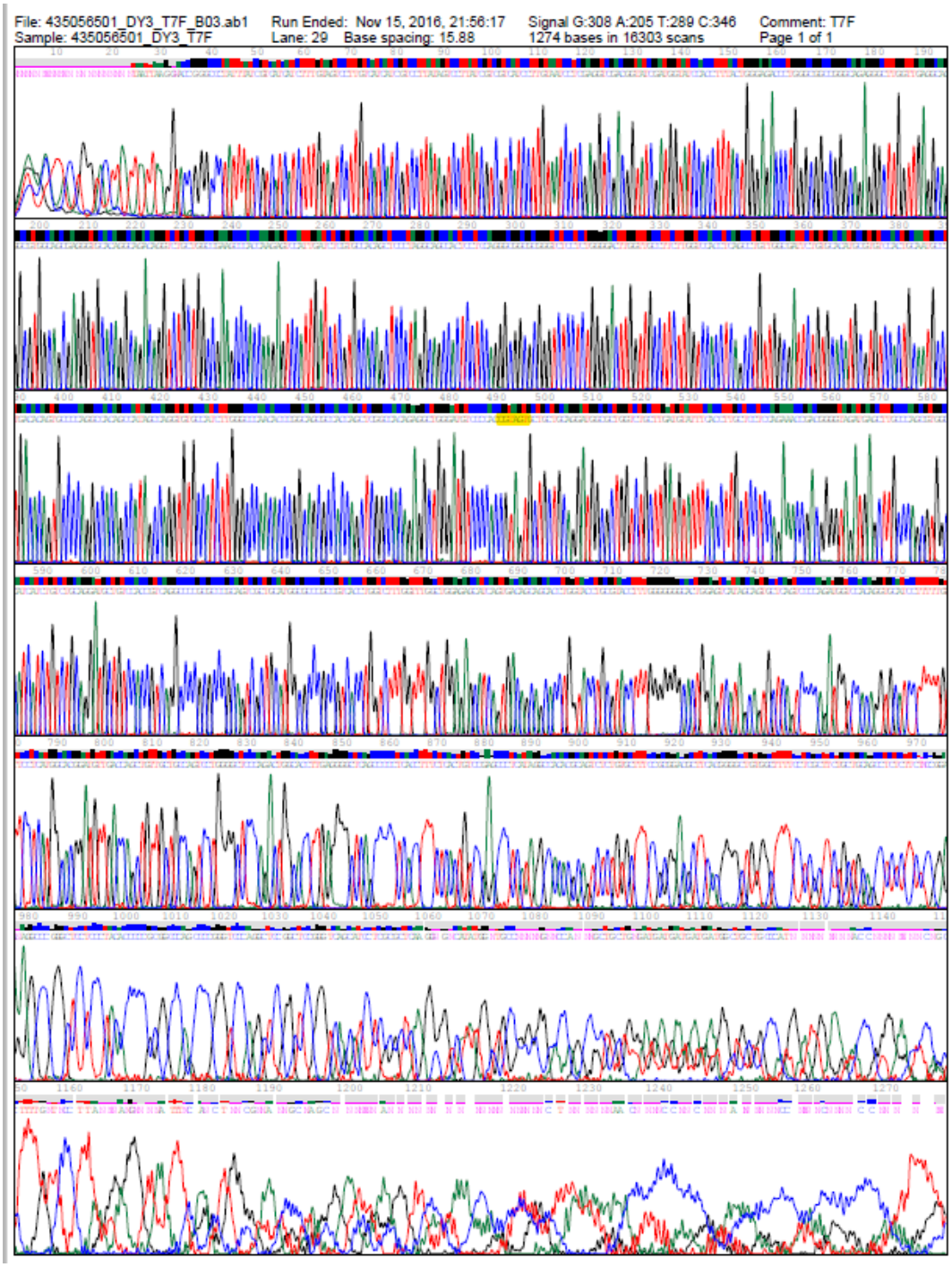

9. Chromatogram following sequencing of the pCMV-3Tag-TRIM26 plasmid DNA using the Sanger Source Bioscience sequencing service (Nottingham, UK).

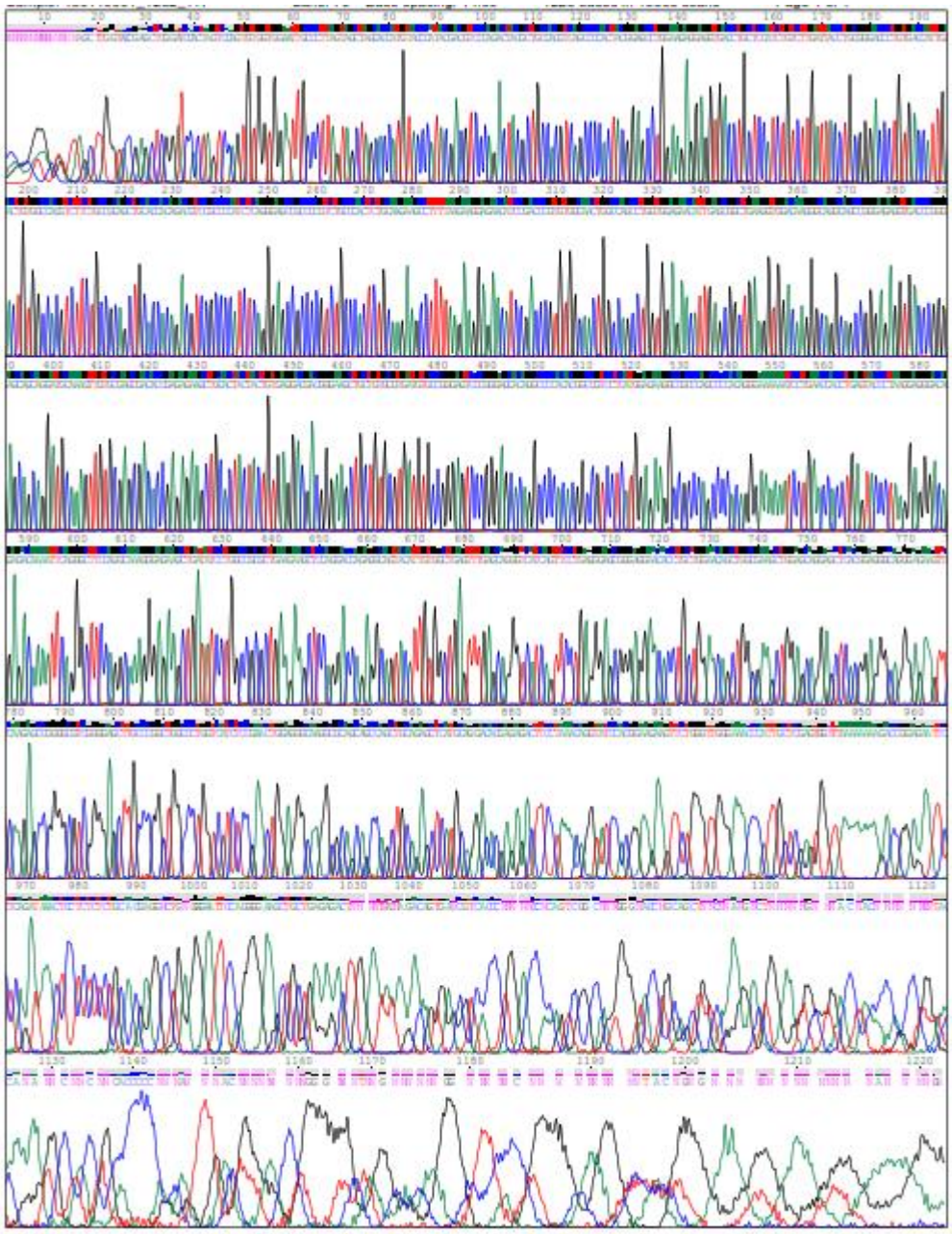

10. Mycoplasma test results confirming that the negative for HCT116 +/+ cells used within this investigation were mycoplasma negative. Mycoplasma testing was performed as part of an in-house service at the North-West Cancer Research Centre. The results for the HCT116$^{p53+/+}$ cells used throughout this research project have been highlighted in yellow.

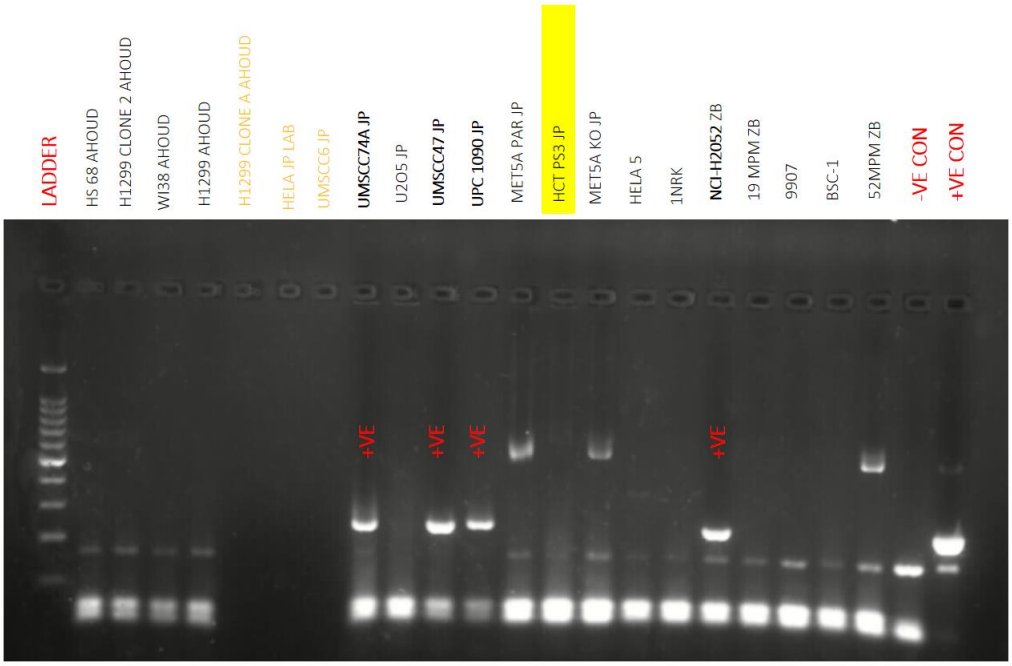

CHAPTER 10 - ABBREVIATIONS

5'Drp	5'-deoxyribosephosphate
8-oxoG	8-oxo-7,8-dihydrogaunine
A	adenine
AGC	automatic gain control
APE1	AP endonuclease 1
Bcl-2	B-cell lymphoma 2
BER	Base excision repair
C	cytosine
CHIP	carboxyl terminus of Hsc70 interacting protein
CPDs	*cyclobutane pyrimidine dimers*
CSA	Cockayne syndrome complementation group A
CSB	Cockayne syndrome complementation group B
Cul	Cullin
DDB	DNA binding protein
DDB1	DNA damage binding protein 1
DMEM	Dulbeccos Modified Eagle Medium
DNA	deoxyribose nucleic acid
DNA-PKcs	DNA protein kinase catalytic subunit
DSBs	Double strand breaks
ERCC1	excision repair cross-complementation group 1
FaPy	formamidopyrimidine
FBS	% fetal bovine serum
FDR	false discovery rate
FEN1	flap endonuclease
G	guanine
GGR	global genome repair
Gy	gray
H2O2	hydrogen peroxide
HA	hemagglutinin
HCT116p53 +/+	human colon carcinoma cells
HECT	homologous to E6-AP carboxyl terminus
HhH	Helix-hairpin-helix glycosylases
HIV	human immunodeficiency virus
HNPCC	hereditary non-polyposis colorectal carcinoma
HR	*homologous recombination*
HR23B	homologous recombinational repair group 23B;
JPDB	JPDB buffer (50 mM Tris HCl pH8, 50 mM KCl, 1mM EDTA, 10 % glycerol)
LB	lysogeny broth
LET	linear energy transfer
LIC	ligation-independent cloning
Lys	lysine
MMR	mismatch repair pathway
MPG	N-methylpurine DNA glycosylase

MPG	3-methyl-purine glycosylase
Mrna	messenger RNA
MS	Mass spectrometry
Mule	ARF-BP1/HectH9
MUTY	A/G mismatch specific adenine glycosylase
NEIL	endonuclease VII-like proteins
NEIL	endonuclease VIII-like protein 1
NF-Kb	nuclear factor κB
NHEJ	*nonhomologous end-joining*
NTH1	human endonuclease III
O2.-	superoxide anion
OD	optical density
OGG1	8-OxoG DNA glycosylase 1
OH	*Hydroxyl radicals*
PARP	poly (ADP-ribose) polymerase
PCNA	proliferating cell nuclear antigen
PCNA	proliferating cell nuclear antigen
PNKP	polynucleotide kinase phosphatase
Pol	Polymerase
PTM	post-translational modifcation
PVDF	Immobilon-FL polyvinylidene diflouride
RBR	RING between RING
RIG-1	retinoic acid inducible gene 1
RING	really interesting new gene
RNA	RiboNucleic Acid
RNAPII	RNA polymerase II
ROS	reactive oxygen species
RPA	replication protein A
SAM	S-adenosylmethionine
SDS-PAGE	Sodium dodecyl sulphate polyacrylamide gel electrophoresis
SSBs	Single strand breaks
STRAP	serine-threonine kinase receptor associated protein
T	thymine
TAE	Tris-acetate-EDTA
TCR	transcription-coupled repair
TDG	thymine DNA glycosylase
TFIID	transcription factor IID
TFIIH	transcription factor IIH
TFIIS	transcription initiation factor IIS
Tg	*Thymine glycol*
TRIM	tripartite motif containing 26
U	uracil
U2OS	human female osteosarcoma cells
UDG	Uracil DNA glycosylases
UPP	ubiquitin proteosome pathway

UV	Ultraviolet light
WT	wild type
XP	xeroderma pigmentosum (groups A–G).
XRCC	X-ray cross complementing protein